Electrostatic Interaction Between Macromolecules and Mixed Lipid Membranes

Thesis Submitted for the Degree
Doctor of Philosophy

by

Daniel Harries

Submitted to the Hebrew University Senate
in the year
2001

This work was carried out under the supervision of

Professor Avinoam Ben-Shaul

Acknowledgments

I would like to thank Professor Avinoam Ben-Shaul for his support and guidance. As a scientist and teacher he was a source of inspiration to me.

I thank Professor William Gelbart for his friendly advice and for often acting as my "advisor at a distance".

Special thanks go to Dr. Sylvio May with whom most of my work presented here was shared. I thank him for his teachings.

Thanks also go to Professor Joachim Rädler for a fruitful collaboration.

I thank Dr. Stella Park for our collaboration, but more importantly for being a good friend.

It is also a great pleasure to thank those who have always been supportive of me: Profs. Victoria Buch, Micha Asscher and David Andelman.

Thanks to my parents for all their encouragement and for being the first to answer my questions.

Abstract

This work focuses on the theoretical study of the electrostatic interaction between charged rigid macromolecules and lipid membranes. Many biologically relevant molecules and molecular aggregates carry charge, ranging from proteins, polynucleotides (e.g., DNA) to lipid membranes. The interaction between these macromolecules enables many processes inside living cells and organisms to be carried out. These include protein-DNA binding, the adsorption of peripheral proteins onto cell membranes and condensation of DNA in cell nuclei or viral capsids. The complex nature of these systems stems from the large number of relevant degrees of freedom.

As an introduction, we discuss in Chapter 1 the essential molecular components of the macromolecular, multi-component, complex systems considered later. First, electrolyte solutions are discussed together with the mean-field ("Poisson-Boltzmann") theoretical approach, used to deal with them throughout this work. Then, we present a short overview of the macromolecules that are studied later in this work. These include lipid aggregates, DNA and proteins. We also present some of their physical properties.

We next turn to study the DNA-lipid interaction in ordered composite phases that are spontaneously formed in aqueous solutions upon mixing DNA and mixed cationic and neutral ("helper") lipid vesicles. It has previously been found that these complexes may serve as efficient vectors for gene delivery into living cells. Substantial experimental effort has been made to characterize these phases, in the hope that they might serve in gene therapy. In chapters 2 and 3 we present a general statistical thermodynamic formulation that we have developed to account for the relative stability of various competing structures of complexes formed by DNA and mixed membranes. Chapter 2 deals with one specific ordered complex, whos structure has been accurately determined experimentally. This is the lamellar L_{α}^{C} phase, that may form when mixing lipids that tend to form planar membranes and DNA in an aqueous solution. Our model includes the electrostatic degrees of freedom, taking into account the mixing (and demixing) of the mobile salt ions, as well as the charged and uncharged lipids in the (mixed) membrane.

An important achievement presented in this work is devising and subsequently solving numerically the appropriate free energy functional, leading to a modified Poisson-Boltzmann (PB) equation with special boundary conditions, taking into account the possibility of charged lipids to demix in the presence of a charged macroion. We thus show the importance of lipid demixing in the vicinity of oppositely charged DNA, tending towards charge matching. Qualitative and quantitative predictions are presented concerning importance of the charge mod-

ulations in the lamellar complexes in determining the structure and stability of the condensed phase.

Underlying the association of DNA and cationic membranes and the stability of the complexes formed, is the entropy gain associated with the release of the partially bound counterions from the vicinity of the macromolecules into the bulk solution. The extent of this "counterion release" was determined directly by conductivity measurements, and in parallel, was calculated by us based on PB theory. The model calculations agree well with experiment revealing, for instance, that maximal (essentially) complete release of counterions takes place at the isoelectric point, i.e., when the fixed negative (DNA) and positive (cationic lipid) charges in the complex are equal. At this point the complex formation free energy is nearly purely entropic, i.e., entirely due to counterion release.

Using the same model, the experimentally observed phase behavior of the system is also accounted for. A simple analytical model is presented, reconfirming many of the important results of the more complex model.

In Chapter 3, we add the contribution of membrane elasticity, another important degree of freedom, to the electrostatic and mixing free energy contributions. Thus, yet more complex and rich phase behavior is accounted for. One example is the experimentally observed formation of the hexagonal H_{II}^{C} phase upon softening of the lipid membrane involved in forming the L_{α}^{C} complex. Several phase diagrams are presented, differing in the spontaneous curvature and bending moduli of the constituent layers. The principles governing the formation of the different phases are elucidated. We also show how all the relevant degrees of freedom (electrostatic, mixing and elasticity) could all be combined and solved self-consistently in one free energy functional. Consequently, we find that the lipid layers in the L_{α}^{C} complexes may bend around the DNA "rods" in order to achieve better electrostatic matching. This, we suggest, may explain the registry between DNA monolayers in different "galleries" in the lamellar complex.

In Chapter 4, we turn to discuss the way charged peripheral proteins, another class of rigid macromolecules, interact with lipid membranes. The coverage dependent adsorption free energy is determined, again including electrostatic and mixing contributions to the free energy. The importance of these degrees of freedom, as well as the electrostatic interaction between adsorbed proteins is demonstrated through the adsorption isotherms. Some common principles to the ones discussed in chapters 2 and 3 emerge here: the tendency towards charge matching on the membrane and protein, and the consequent membrane polarization. We find that the lipid mobility influences the binding free energy and adsorption isotherms most substantially when the charge density on the membrane is much lower than that on the protein (which is the biologically most relevant

case). We also show how membrane charges are typically over compensated by protein-charges. Finally, we argue that lipid-protein domains may be enhanced by non-ideal lipid mixing contributions.

Chapter 5 concludes with a short summary.

Contents

1 Introduction **1**

1.1 Prelude . . . 1
1.2 Electrolyte solutions . . . 3
1.2.1 Mean field variational approach . . . 4
1.2.2 Alternative approaches . . . 6
1.3 Lipids . . . 7
1.3.1 Structure . . . 7
1.3.2 Self-assembled phases . . . 9
1.3.3 Elastic deformations . . . 11
1.3.4 Frustration . . . 12
1.3.5 Charged membranes . . . 13
1.3.6 Mixed charged membranes . . . 14
1.4 DNA . . . 15
1.4.1 Structure . . . 15
1.4.2 Persistence length . . . 17
1.4.3 Counterion distribution . . . 19
1.4.4 DNA-DNA interaction and condensation . . . 22
1.4.5 Gene therapy and gene delivery . . . 23
1.5 Proteins . . . 24
1.5.1 Structure . . . 24
1.5.2 Peripheral proteins . . . 25
1.6 Charged macromolecule interaction . . . 27
1.7 Overview . . . 28

2 Lamellar DNA-Lipid Complexes **31**

2.1 Introduction . . . 31
2.2 Theory . . . 35
2.2.1 Model . . . 35
2.2.2 Free energies . . . 37
2.2.3 Phase behavior . . . 41

2.2.4 Counterion release 46
2.3 Results and Analysis 47
2.3.1 Complex structure and stability 48
2.3.2 Phase evolution 53
2.3.3 Extent of ion release 57
2.4 Discussion and summary 59
2.4.1 A simple box model 60
2.4.2 Other models 63
2.4.3 Concluding remarks 65

3 From Lamellar to Hexagonal Complexes 67
3.1 Introduction 67
3.2 Theory 71
3.2.1 Phases 72
3.2.2 Degrees of freedom 75
3.2.3 Free energies 76
3.3 Results and discussion 85
3.3.1 Electrostatics of the $\mathbf{H_{II}^C}$ and $\mathbf{L_\alpha^C}$ phases 86
3.3.2 The corrugated $\mathbf{L_\alpha^C}$ complex 90
3.3.3 The $\mathbf{L_\alpha} \rightarrow \mathbf{H_{II}}$ transition 96
3.3.4 Phase Diagrams 97
3.4 Concluding remarks 107

4 Adsorption of proteins on mixed membranes 109
4.1 Introduction 109
4.2 Theory 112
4.2.1 Adsorption free energy 112
4.2.2 Adsorption isotherms 117
4.3 Results and Discussion 119
4.3.1 Adsorption of a single protein 120
4.3.2 Protein lateral interactions and adsorption isotherms . . . 123
4.3.3 Surface overcharging 127
128
4.3.5 Non-ideal Mixing 131
4.4 Concluding Remarks 134
4.4.1 Other theoretical models 134
4.4.2 Conclusions 136

5 Postlude 139

A Solving the Poisson–Boltzmann Equation for two parallel cylinders 143

A.1 Introduction 143

A.2 Method of solution 145

A.3 Results and discussion 147

B Numerical method for solving the Poisson–Boltzmann Equation 153

References 155

Chapter 1

Introduction

1.1 Prelude

This dissertation is concerned with the theoretical study of the electrostatic interaction between charged biological macromolecules. Charge is carried by many such molecules ranging from proteins and polynucleotides (e.g., DNA) to lipid membranes. The interaction between these macromolecules are at the base of many biological processes, such as protein-DNA binding, the adsorption of peripheral proteins onto cell membranes and the condensation of DNA in cell nuclei or viral capsids.

More specifically, we shall consider systems where one of the interacting "macromolecules" is a charged lipid membrane, while the other is a *rigid* macromolecule such as DNA or protein. A lipid membrane, strictly speaking, is a molecular aggregate or colloid. However, it is often useful to consider it as a macro-body or macromolecule, since its integrity is generally kept even when interacting with other macromolecules. Albeit, lipid aggregates bear some unique features that are absent from other, more generic, macromolecules or colloids. Perhaps most important is the fact that the lipid membrane is fluid. Therefore, e.g., a mixed membrane, composed of charged and uncharged lipids, may be regarded as a two dimensional fluid mixture. Consequently, it may respond to the presence of another (charged) macromolecule by locally varying its chemical composition, hence modulating its surface charge density (polarization). Furthermore, being elastic with respect to curvature and area deformations, the membrane may undergo, e.g., curvature modulations in the vicinity of the interacting macromolecule.

Two particular types of systems will be in the lime light. In the first, an overall positively charged lipid membrane interacts with (negatively charged) DNA. This will be the focus of Chap.2 and Chap.3. Upon the interaction of these

two macromolecules, ordered composite phases are spontaneously formed. These complexes have attracted a large volume of interest, due to their potential of being vectors for gene delivery, as a first stage in gene transfection, in the design of gene therapeutics. In the second, a globular, overall (positively) charged, peripheral protein interacts with a (negatively) charged membrane. The importance of the interaction of peripheral proteins with lipid biological cell membranes can not be over stressed, since this type of interaction is the first stage of many trafficking and signaling processes across such membranes. This will be the topic of Chap.4. Further complexity is added to these systems due to the the fact that these charged macromolecules are always accompanied by their small counterions, and are generally found in aqueous solutions where salt is also present in fair amounts (e.g. the human serum has a salt concentration of $\sim 0.1M$).

A first glance at these systems of interacting particles display almost ominous complexity. How can we set about understanding systems with so many degrees of freedom? A closer look reveals that, as in assembling a jigsaw puzzle, a knowledge of the properties of the individual building blocks aids in forming the complete picture. Imagine a musical instrument performing as part of a symphonic orchestra: it is part of a highly complex, music generating, system. Even so, each instrument keeps its special sound and quality even when playing in concert. Similarly, the basic characteristics of each component (molecule) in the system is not generally lost even when interacting with other components. For example, DNA interacting with membranes will still possess its stiffness and propensity to form ordered, liquid crystalline phases, while the membrane will tend to form lyotropic phases reminiscent of the ones it would form in the absence of DNA. What remains, is to understand the reciprocity between the different components, and how it effects the resulting phases that are observed. The lipid membrane can be regarded as a scaffolding for the assembly of DNA, while DNA may be regarded as a non-homogeneous field to which the membrane lipids (charged and uncharged) responds. Based on our (prior) knowledge of the individual components, we are in search of a theoretical model that will account, self-consistently, for the most important degrees of freedom in the combined interacting system and the important coupling between these degrees of freedom. That is the aim of this work.

Understanding some of these underlying principles, and the ability to predict the outcome of the self-assembly in these systems of interacting macromolecules, should give a possible starting point for the design of synthetic, biologically non-occurring materials, such as drugs relaying on proteinomimetic strategies (see e.g. Kasher *et al.* (1999) and references therein) or lipid-based potential gene delivery agents in gene therapy. Although this field is in its early stages, and many of

the mechanisms and interactions are not yet fully understood, the uncovered potential is well appreciated.

We therefore start with describing the basic components in the complex systems considered later. We first discuss electrolyte solutions and the mean-field ("Poisson-Boltzmann") theoretical approach, used to deal with them throughout this work. Then, we present a short overview of the macromolecules that are studied later in this work (namely: Lipids aggregates, DNA and proteins) and their physical properties, will be given. The intent is not to give any kind of comprehensive review of the wealth of knowledge concerning these topics, but rather to serve as an introductory basis for the later chapters.

1.2 Electrolyte solutions

Aqueous electrolyte solution are all around us: a simple glass of tap water already contains many ions. Even when completely purified or distilled, water always contains ions that originate in the dissociation of water itself: $H_2O \rightleftharpoons H^+ + OH^-$, a reaction which has an equilibrium constant of $K_a = [H^+][OH^-] = 10^{-14}M^2$. If only electrostatic forces are considered, one would expect such solutions to be unstable. The ions should either collapse into a crystal (if the solution is neutral), or otherwise repel each other and "explode" (Landau & Lifshitz, 1960). In fact, the enthalpy of solvation of most common univalent salts from the solid crystal state is slightly positive (on the order of 10 $KJ\,mole^{-1}$). It is the translational entropy which opposes the electrostatic attraction and keeps the ions in solution from collapsing. The excluded volume of the ions also contributes to the repulsion between ions, but is often negligible compared to the other two contributions. Water is a good solvent for salts, because its high dielectric constant renders the solvation enthalpy only slightly positive, while the enthalpy is much larger for solvation in low dielectric solvents. This allows the entropy to dominate and enable solvation (up to the level of saturation).

It has been shown that such simple considerations are sufficient in explaining the existence of a (first order) phase transition which is experimentally observed in salt solutions. In fact the theoretical treatment of the transition between an electrolyte-dilute to an electrolyte-dense phase goes back to Debye and Hückel (Debye & Hückel, 1923; Debye & Hückel, 1924). Since that time more experimental evidence and theoretical work has revealed that these systems of electrolytes possess special peculiarities (Fisher & Levin, 1993; Fisher, 1994; McGahay & M.Tomozawa, 1989; Weingärtner *et al.*, 1992; Japas & Sengers, 1990). These are mainly due to the long range nature of the electrostatic potential. It has long been known that it is impossible to use some of the standard tools of statistical

mechanics in combating electrolyte solutions. For instance, it is impossible to derive a virial expansion even for very dilute electrolyte solutions (Hill, 1960). Moreover, the properties of electrolyte solutions seem to possess mean field-like critical exponents while defying the results based on renormalization-group theory, which yield Ising-like critical exponents. This behavior has been attributed to the fact that fluctuation-neglecting mean-field theory is appropriate in describing systems in which the range of interaction is greater than the range dominated by fluctuations. It was found that electrolyte solutions may have a lower and upper consulate points such that there is a transition between Ising-like (fluctuation dominated) and mean field-like (long range potential) behaviors (Fisher & Levin, 1993).

The theoretical treatment of electrolyte solutions and of macromolecules in salt solutions goes back to the early years of the 20th century with the work of Debye and Hückel (1923) and Gouy and Chapman (Gouy, 1910; Chapman, 1913), and continued with the celebrated work of Verwey and Overbeek (1948). A charged isolated (dry) macromolecule is always accompanied by its counterions, so that it is electrostatically neutral. Once solvated in water, the mobile counterions, as well as any other ions present in solution, have a choice: they can either bind to the macroion and gain electrostatic energy, or else diffuse into solution thus gaining translational entropy. At equilibrium compromise is achieved, the density of counterions remaining close to the macroion being determined by its charge density, shape and the salt concentration in solution. These ideas are incorporated in the Derjaguin-Landau-Verwey-Overbeek (DLVO) model, which assumes that the electrostatic double layer formed near charged surfaces, together with another important class of forces, the van der Waals interactions, govern colloid stability (Verwey & Overbeek, 1948; Derjaguin *et al.*, 1987; Evans & Wennerström, 1994).

Next we present one particular mean-field-based theoretical approach for determining the ion density (hence the free energy) in a solution containing charged macromolecules or colloids. This approach will be used throughout this work to obtain self consistent solutions for the distribution of ions in and around special macromolecular assemblies.

1.2.1 Mean field variational approach

Consider an aqueous solution of volume V, containing 1:1 electrolyte at a temperature T. Each pair of ions, seperated by a distance r in the solution, each with an elementray charge $\pm e$, interact via a Coulomb interaction of magnitude $e^2/4\pi\epsilon r$ (within mks convention, and with a negative sign for an anion interacting

with a cation - positive otherwise); $\epsilon = \epsilon_0\epsilon_r$, and ϵ_r is the dielectric constant of the solution (for water we shall assume $\epsilon_r = 78$), while ϵ_0 is the permittivity of vacuum. This volume is in contact with a bulk solution of (similar) positive and negative ions, each at a concentration n_0. The electrostatic cumulative potential emanating from these ions, and any other *stationary* charged object in solution (such as large macromolecules) at a point $\vec{r}$ is $\varphi(\vec{r})$. The local concentrations of positive and negative *mobile* ions (denoted by $n_+(\vec{r})$ and $n_-(\vec{r})$ respectively) depend on φ, and should be found self-consistently. The mobile ions move in the field they themselves are affecting, so as to minimize the system free energy.

Using a mean field approach, neglecting all correlation between mobile ions, the charging free energy functional of the system for any particular choice of the distribution $n_\pm$ is:

$$\mathcal{F}\left[n_+, n_-, \varphi(n_+, n_-)\right] = k_B T \int_V \left[n_+ \ln \frac{n_+}{n_0} + n_- \ln \frac{n_-}{n_0} - (n_+ + n_- + 2n_0) \right] \mathrm{d}v + \int_V \frac{\epsilon}{2} (\nabla\varphi)^2 \, \mathrm{d}v \tag{1.1}$$

The first term on the right-hand side of this equation accounts for the translational ("mixing") entropy of the mobile ions in the volume V, relative to their entropy in the bulk solution, with $n_+ = n_- = n_0$. The second term is the electrostatic energy (in the mks convention) (Verwey & Overbeek, 1948); k_B is Boltzmann's constant.

Taking the first variation of $\mathcal{F}$ with respect to n_+ and n_-, yields for the distribution of mobile ions the usual Boltzmann distribution, $n_\pm = n_0 \exp(\mp\psi)$, where $\psi = e\varphi/k_B T$ is the scaled dimensionless electrostatic potential and e is the elementary charge. Upon substitution into Poisson's equation the non-linear "Poisson Boltzmann" (PB) equation is derived,

$$\nabla^2\psi = \kappa^2 \sinh\psi \tag{1.2}$$

where $\kappa^{-1} = (\epsilon_0\epsilon_r k_B T/2n_0e^2)^{1/2} \equiv l_D$ is the Debye length.[1] This differential equation must then be solved with appropriate boundary conditions.

Using this approach it is also possible to obtain modified PB equations with special boundary conditions. This is done by constructing an appropriate functional $\mathcal{F}$, and deriving the free energy variationally from it. For a detailed discussion of this approach and some applications see (Levine, 1939; Reiner & Radke,

[1]The Debye length can be considered as the screening length of an electrolyte solution of concentration n_0. A result of the linearized version of the PB equation (valid when the potential ψ is small throughout the solution) is that the maximal density ("ionic atmosphere") of counterions is situated at a distance l_D from any central ion.

1990; Honig & Nicholls, 1995; Borukhov *et al.*, 1995; Borukhov *et al.*, 1997; Fogolari & Briggs, 1997) and references therein. The proof that the free energy for the system is indeed derived from a variation of $\mathcal{F}$, is a subtle point also discussed in the above references.

We will utilize this approach when we consider macromolecular assemblies of DNA and lipids, and also when addressing the adsorption of proteins on lipid membranes. We will thus be able to include additional terms to the free energy, such as membrane curvature and lipid translational entropy, in a self consistent manner.

Shortcomings of PB theory

The limitations of PB (mean-field) theory stem from its primary simplifying neglect of mobile ion correlations. When these become important, the theory may give quantitatively, as well as qualitatively, wrong results. the validity of the PB theory for treating the interaction between charged surfaces and colloidal particles has been examined by various authors based on comparisons to either non-mean-field (integral equation) or computer simulation studies ((Linse & Jönsson, 1982; Wennerström *et al.*, 1982; Das *et al.*, 1995; Deserno *et al.*, 2000); for reviews see Andelman (1995) and Vlachy (1999)). The conclusion from these studies is that PB theory is adequate for aqueous solutions containing monovalent electrolyte for salt concentrations not exceeding $\sim 0.1M$, and surfaces bearing a potential of only a few k_BT/e. The aqueous solutions considered in the present work fulfill this condition.

An important case where counterion correlations must be taken into account is when considering the attraction that is observed between macromolecules baring the same charge (see Sec. 1.4.4). PB theory *always* predicts repulsion between such charged objects (Neu, 1999; Sader & Chan, 1999b; Sader & Chan, 1999a; Langmuir, 1938; Harries, 1998; Stankovich & Carnie, 1996; Ohnishi *et al.*, 1960). It will therefore inevitably fail to reproduce this attractive force. It is also clear that when dealing with polyvalent salt ions in solution or with ions with large excluded volume (or dense solutions) correlations are expected to play an important role, and special care should be taken in dealing (theoretically) with these (Borukhov *et al.*, 1997; Borukhov, 1999).

1.2.2 Alternative approaches

When PB theory is inadequate in dealing with electrolyte solutions, there are alternative theoretical tools for combating the systems. Using the integral equation approach, some intrinsically non mean-field phenomena were reproduced. These

include the attraction between two charged colloidal particles (see e.g., (Sánches-Sánches & Lozada-Cassou, 1992; Marčelja, 1992) and cited references), and an apparent "charge inversion" of charged surfaces, due to an excess of accumulated ions close to the surface (Kékicheff *et al.*, 1993; Greberg & Kjellander, 1998). The approach has been compared with results from Monte-Carlo simulations and found to be satisfactory in these cases (Greberg *et al.*, 1997).

Recently another approach has been pursued by Netz and Orland (1999; 2000). In this approach, the Poisson-Boltzmann equation is obtained as the saddle-point of the field-theoretic action, and the effects of counter-ion fluctuations are included by a loop-wise expansion around this saddle point.

Another approach that has been utilized is computer simulations based on Monte Carlo, Brownian Dynamics, or molecular dynamics. Such simulations have been successful in predicting attractions between macroions (Lyubartsev & Nordenskiold, 1995; Grønbech-Jensen *et al.*, 1997). The main difficulty with this approach is that the long range of the electrostatic forces requires special methods to account for the boundary conditions of the simulation cell, and for summing over all interactions between ions ad infinitum.

Other combined approaches whereby the short range interaction between ions are added to the PB free energy have also been used to account for the effect of ion hydration on the potential around charged surfaces (Marčelja, 1997; Burak & Andelman, 2000).

1.3 Lipids

1.3.1 Structure

Lipids are a set of biomolecules which are defined by biochemists as substances that are insoluble in water and can be extracted from living cells by organic solvents of low polarity. In fact, in this work, we shall only consider one type of lipids: the fats or glycerides – carboxylic esters derived from glycerol (Morrison & Boyd, 1992; Alberts *et al.*, 1994). The fats, and in particular the phosphoglycerids or phospholipids, are important, since they are a major constituent in all biological membranes, separating and compartmentalizing their interior from the outside world, and defining internal organelles inside cells, which have specific defined functions (Stryer, 1988). The phospholipids contain two acyl groups (usually containing between 14 to 24 carbon atoms) connected to the glycerol group. A third ester linkage is made to a phosphate group. The fatty acid chains may be saturated or unsaturated. The configuration of the double bond in the unsaturated chains is almost always *cis*. This has a marked effect on the packing

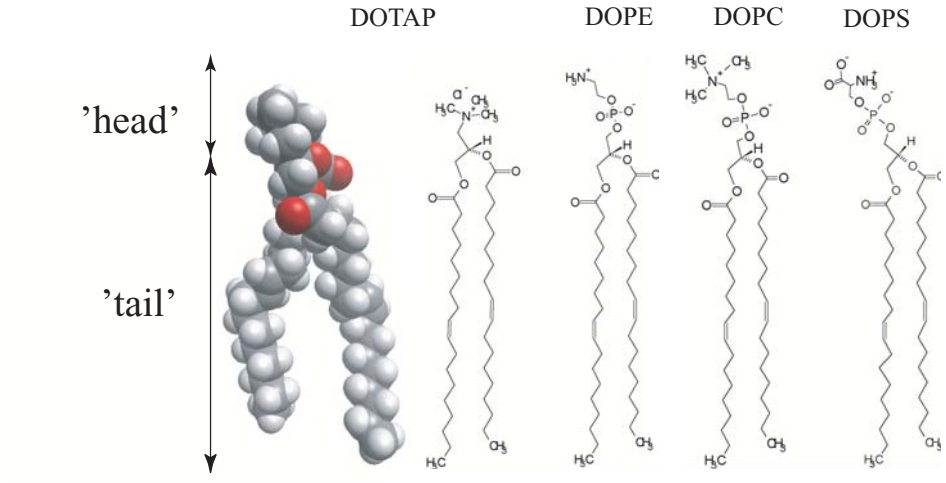

Figure 1.1: Schematic illustration of four lipids: Positively charged DOTAP, neutral (zwitterionic) DOPE and DOPC, and negatively charged DOPS. For DOTAP, a space filling mode of one typical configuration is also shown.

of lipid chains in biological membranes, thus enabling control over the fluidity of the membranes through changes in composition.

Phospholipids are *amphiphilic* in their nature, implying their dual propensity: they all possess a hydrophilic ("water-loving") "head" moiety, attached to a hydrophobic ("water-dreading") "tail" consisting of the fatty acid residues (Tanford, 1980; Israelachvili, 1992). Structures of three such phospholipids of the type mentioned later in this work, are shown in Fig. 1.1: DOPC (dioleoylphosphatidylcholin), DOPE (dioleoylphosphatidylethanolamine) and DOPS (di oleoylphosphatidylserine).

All three share the same "tail" unit, but have very different headgroups that are either negatively charged (DOPS) or zwitterionic (DOPC and DOPE). The size of the "head" unit is also very different: larger in DOPC than in DOPE, due to the presence of the bulky cholin group. Note however, that the van der Waals excluded volume of the lipid headgroup alone is often misleading, since the tight binding of water molecules from solution to the headgroup, or electrostatic headgroup-headgroup repulsion, often enlarge its effective size significantly.

Many synthetic fats have also been devised, in a way that they share some features with the naturally derived ones, but are also in some way unique. One example is DOTAP (dioleoyltrimethylammonium propane), which possesses a (naturally uncommon) positively charged headgroup.

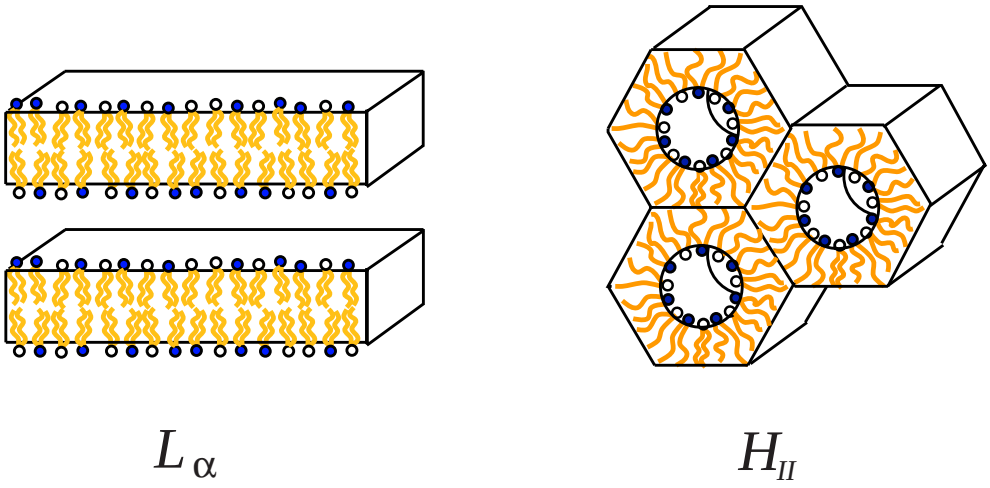

Figure 1.2: Illustration of two lipid phases: the multilamellar, L_α, phase and the inverted hexagonal phase, H_{II}. In both cases the lipids are a mixture of two species differing in their headgroup properties.

1.3.2 Self-assembled phases

In aqueous solutions, lipid molecules tend to self-assemble into aggregates of a well defined geometry. The hydrocarbon tails of the lipids huddle together to form an oily bulk, while the hydrophilic headgroups tend to reside at the interface, intervening between the chains and the engulfing water solution. The stability of these aggregates is due to the (effective) attractive forces between hydrocarbon tails that appear in order to minimize the unfavorable water-hydrocarbon interfacial area. This effective interaction is the "hydrophobic interaction". Many lipid packing geometries satisfy the hydrophobic effect. These range from blob-like, roughly spherical micelles, through elongated micelles, lamellar lipid bilayers (membranes) to inverted hexagonal structures. Fig. 1.2 schematically illustrates two of the aggregation geometries which lead to formation of ordered phases. The fluid lamellar (smectic-like) L_α phase and the inverted hexagonal H_{II} phase will be referred to extensively in this work. The phases formed depend sensitively on the lipid concentration in solution and are therefore classified as lyotrophic[2].

It is often convenient to describe the shapes of the lipid aggregates in terms of the two principal curvatures of the water–hydrocarbon interface, $c_1 = 1/R_1$ and $c_2 = 1/R_2$, and the interfacial surface area available to a lipid molecule, a. For example, in a perfectly planar lipid bilayer, $c_1 = c_2 = 0$; for a spherical micelle, $c_1 = c_2 = 1/R$, where R is the radius of the hydrophobic blob. On the other hand, for the inverted hexagonal structure of the H_{II} phase, $c_1 = 0$ while $c_2 = -1/R$;

[2]These are materials in which liquid crystalline properties appear induced by the presence of a solvent, with mesophases depending on solvent concentration.

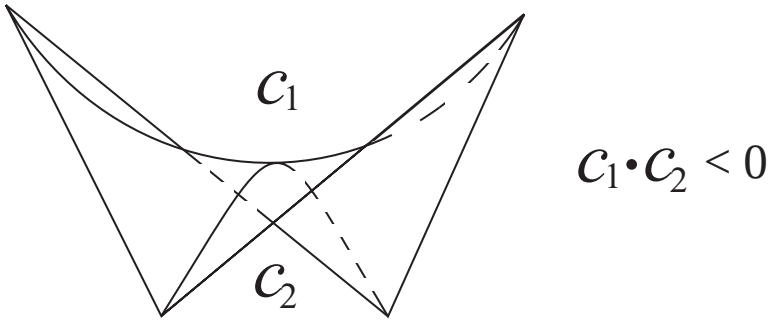

Figure 1.3: Illustration of a saddle-like geometry, for which $c_1 c_2 < 0$.

here R is the radius of the "water tubes". We adopt here the convention that surfaces that are curved *away* from the tail region possess a *negative* curvature. For a saddle-like geometry, illustrated in Fig. 1.3, for which the two principle cuvatures are oppositly curved, we find $c_1 c_2 < 0$.

The geometry that the lipid phases will adopt in solution is dictated by the balance of lateral forces (and torques) operating on a lipid molecule in the aggregate. This in turn is intimately related to the chemical structure of the lipid and also to the conditions in the embedding solution. Fig. 1.4 illustrates the different contributing forces: in the headgroup region an overall repulsive interaction due to a combination of steric (excluded volume), electrostatic, hydrational and possibly (attractive) hydrogen-bonding, acting between headgroups, tend to increase a. Acting against this tendency is the water–oil like interfacial tension, which acts to minimize the exposure of the hydrocarbon aggregate interior to water. The lipid tails inside the hydrophobic core are highly constrained by the requirement for a uniform liquid like, tightly packed bulk. This in turn, results from an attractive (van der Waals) cohesive force between tails on the one hand, and the requirement for connectivity between tail chain segments and between tails and the (interface bound-) headgroup. Consequently the conformational freedom of the chains is lowered with respect to a single ("free") chain. The entropy loss associated with this tight packing is responsible for a significant repulsion between chains, which depends on the curvature and surface areas (Ben-Shaul, 1995).

Simple geometrical consideration of a single lipid leads to the qualitative conclusion that amphiphiles with a very small headgroup and large tail volume will result in negatively curved aggregates, while lipids with large headgroups and rather short tails will prefer to pack in aggregates of positive curvature (Israelachvili *et al.*, 1977). Phospholipids are often intermediate between these two cases, preferentially packing into planar bilayer.

Ultimately, the preferred geometry is the one that minimizes the free energy of the system, and all the geometrical parameters (including the area per molecule

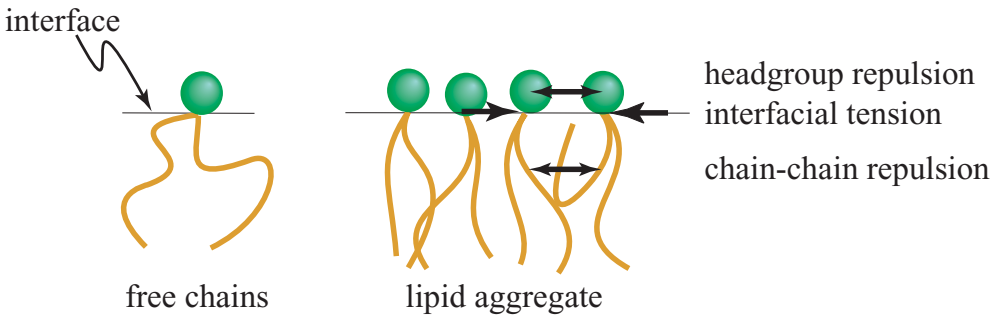

Figure 1.4: The geometry of lipid aggregation is determined by a balance of forces, acting in the headgroup, interface and tail regions. A free isolated chain is also shown for reference.

a) are a result of this minimization. To a good approximation, the free energy of a lipid molecule in an aggregate may be written as a sum of three contributions:

$$f_l = f_t + f_s + f_h \tag{1.3}$$

These stem, respectively, from the hydrocarbon chains, the surface free energy and headgroups' interaction. The interfacial term, f_s, may be expressed most simply as $f_s = \gamma a$, with γ denoting the effective surface tension of the interface. Theoretical predictions for f_h are more complex. They involve models including electrostatic calculations (based, e.g., on PB theory) for charged headgroups, hard core repulsion estimates, and phenomenological expressions (Andelman, 1995; Lekkerkerker, 1989; Israelachvili, 1992; Ben-Shaul & Gelbart, 1994). On the mean-field level, a successful, rather comprehensive treatment has been given to the expression for f_t (Ben-Shaul, 1995; Ben-Shaul & Gelbart, 1994). This was done through examining the probability distribution function of a single chain in the mean-field of its neighboring chains, subject to the geometrical packing constraints. Other, mostly phenomenological expressions have also been suggested and utilized. Note, that these expressions are all local, intimately depending on the geometrical packing constraints.

1.3.3 Elastic deformations

A useful approach to analyzing the free energy of lipid phases has been to describe the free energy of a lipid layer in terms of its elastic properties. In general, three modes of elastic deformation are possible for a lipid layer. The first is lateral stretching (dilation). The second is a bending elastic energy.[3] The third is the

[3]The energy associated with deformations involving stretching are usually much larger than the bending, and will therefore be ignored throughout this work.

Gaussian (elliptic or hyperbolic type) curvature.[4] The curvature elastic energy per lipid molecule, f^{el} for small bending deformations of a lipid monolayer can be expanded up to quadratic terms in the curvature:

$$f^{el} = a\frac{k}{2}(c_1 + c_2 - c_0)^2 \tag{1.4}$$

where c_0 is the *spontaneous curvature*, a local propensity of the monolayer that depends on membrane composition and structure of the lipids forming it, and k is the elastic bending modulus (Helfrich, 1973). In the case that the lipid phase has a cylindrical or lamellar symmetry (such as the H_{II} and L_α phases), the elastic energy becomes: $f^{el} = (ak/2)(c - c_0)^2$.

1.3.4 Frustration

Formation of stable lipid phases often involves a certain amount of "frustration" energy. For example, a symmetric lipid membrane, is composed of two monolayers, each with the same intrinsic spontaneous curvature c_0. Since in a bilayer these monolayers are facing and touching each other (to avoid exposure of tails to the water), they cannot both accommodate this spontaneous curvature, c_0 (unless it happens to be $c_0 = 0$). The resulting aggregate is necessarily frustrated, in the sense that any curvature will be suppressed, and a compromising uncurved membrane results (see Fig. 1.5). If the unfavorable frustration energy becomes large enough, the membrane may no longer be the most stable packing structure for these lipids. For instance, if a monolayer has a negative spontaneous curvature, the inverted hexagonal, H_{II}, phase may form, thus relieving some or all of the frustration associated with bending. However, this structure is not altogether rid of frustration. Although the monolayers propensity to form negatively curved interfaces is satisfied, the constraint of filling the hydrocarbon interior of the lipid chains involves another form of frustration. In the hydrophobic interstices the lipid chains must stretch in order to fulfill the packing constraint (namely, uniform chain segment density). This stretching is associated with a loss of configurational entropy (Seddon, 1990; Seddon & Templer, 1995; May *et al.*, 1997; Kozlov *et al.*, 1994). We shall address this point in more detail in Chap. 3, where we discuss phase transitions between lipid–containing phases.

[4] Due to the Gauss-Bonnet theorem, which states that the integral of Gaussian curvature is a topological invariant, and since all phases considered in this work have the same number of membrane pieces and the same number of handles, we shall not consider this term further in comparing lipid phases.

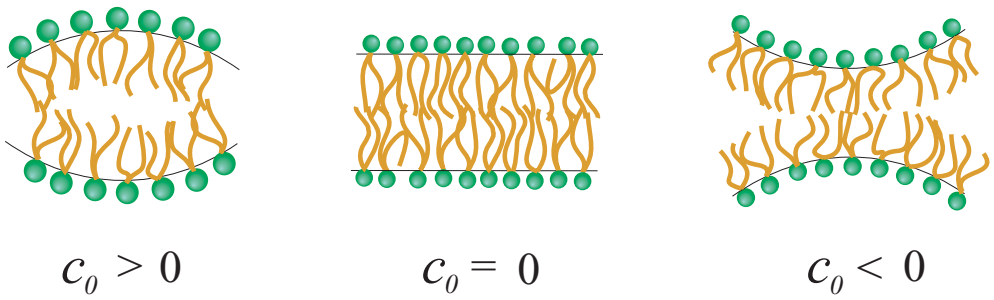

Figure 1.5: Illustration of three types of lipid monolayers, with (left to right) positive, zero and negative spontaneous curvatures. In a lipid bilayer all but the one with zero spontaneous curvature will pay a certain frustration energy penalty.

1.3.5 Charged membranes

Lipid membranes often carry a net charge on their surface. This charge may originate from a dissociation of a counterion (or proton) into solution, or from the adsorption of a (polyvalent) ion from solution. Most biological membranes are negatively charged, with around 10 % of their lipids being charged. The most simple model of such a planar membrane is to consider an infinite planar dielectric slab of low dielectric, ϵ_{oil}, and thickness t with charges smeared on its surface, with a constant charge density σ, immersed in an aqueous solution of dielectric ϵ_w, and a salt concentration corresponding to l_D. It is often possible to ignore the fact that the two membrane interfaces are charged (the *decoupling limit*) as long as $\epsilon_{oil}/\epsilon_w \ll t/l_D$. For this scenario, the PB equation can be solved exactly (Andelman, 1995).

One limit is the result of the linearized version of the PB equation (the "Debye-Hückel approximation") for the potential, valid when the surface potential is low (or l_D is small), for a 1:1 electrolyte solution,

$$\psi = -\frac{2}{\kappa l_{GC}} e^{-\kappa z} \tag{1.5}$$

where z is the distance away from the surface, $l_D = \kappa^{-1}$ is the Debye length, and $l_{GC} = e/2\pi l_B|\sigma|$ is the so called *Gouy Chapman length*, which is related to the distance between charges on the surface. Here we also introduce the Bjerrum length, l_B. The Bjerrum length is the distance at which the interaction between two elementary bare charges is k_BT; in the mks convention $l_B = e^2/4\pi\epsilon k_BT$. For water at room temperature $l_B \approx 7.14$Å. In limit for which Eq. 1.5 is derived, the diffusive layer of ions near the membrane surface is characterized by a thickness l_D. In other limit, corresponding to the case of no added electrolyte (or high surface potential), the potential away from the surface is:

$$\psi = -2\ln(z + l_{GC}) \tag{1.6}$$

In this limit, the thickness of the diffusive counterion layer is characterized by l_{GC}. Here, the cumulative amount of counterions per unit area, from the surface and up to a distance l_{GC} from it, is $-\sigma/2$. In both limits, it is clear that counterions have a strong tendency to reside close to the membrane. This result reflects the infinite 2D nature of the charged plane considered, and the strong consequent potential. As we shall see, dimensionality is crucial for maintaining a diffuse layer around the macroion: for the 1D cylindrical geometry the layer may be much less compact, or even non existent (see Sec. 1.4.3). For "0D" objects such as charged colloidal spheres, the diffuse layer is weaker still, and only a renormalization type effect can appear (Alexander *et al.*, 1984; Borukhov, 1999).

The membranes bending constant, k, is largely affected by the fact that the membrane is charged. We shall return to this point in Chap. 3, where we show how using the variational approach mentioned in Sec. 1.2.1, we can account for this change is a self consistent way.

1.3.6 Mixed charged membranes

Typical biological membranes are primarily composed of phospholipids of many types. These can have a variety of attached chains and headgroups, both charged and uncharged, the former being charged according to the pH and salt conditions in solution. The question of how a membrane, possessing headgroups that can ionize, will be charged under certain pH and salt conditions, has been previously addressed (Ninham & Parsegian, 1971). Within PB theory, this corresponds to solving the equation with a special ("charge regulation") boundary condition. Furthermore, since the the lipids are in the fluid state, they can migrate laterally in the membrane. Thus the membrane lipids can respond to the field of, e.g., externally interacting charged macromolecules, or to elastic deformations, by varying their *local* composition. This migration and hence demixing is entropically unfavorable, yet a substantial segregation is often found to lower the total free energy of the system. This may correspond to a segregation of charges around an oppositely charged macroion, or to a more favorable local composition of lipids that will match some (e.g., constrained) curvature. One example where this effect can be rather large is the adhesion-induced phase separation and reorganization in a the interaction of (oppositely charged) membranes (Nardi *et al.*, 1998). More generally, the membrane elastic and electrostatic degrees of freedom are coupled. For example, it was found that for a mixed, self-adjusting (annealed) membrane, an electrostatic coupling between the inplane distribution and the membrane curvature produces an added effective interaction which stabilizes modulated phases (Andelman, 1995; Guttman & Andelman, 1993).

In the following chapters we shall return extensively to the effect of lipid mobility in mixed (charged and uncharged lipid) membranes. We will show how the variational approach introduced in Sec 1.2.1 can be used to derive special boundary conditions for the PB equation. Solving this equation will lead to self consistent results for the local lipid composition and the electrostatic (charging) free energy of the system. These will be shown to be a consequence of the intimate coupling between the different local membrane properties, such as elasticity and electrostatics.

1.4 DNA

1.4.1 Structure

DNA (deoxyribonucleic acid) is a semiflexible polymer made of deoxyribonucleotide units that form a chain through a *polyester* backbone. Together with RNA (ribonucleic acid), the two make up a class of biopolymers called polynucleotides. It is these molecules that are responsible for carrying the genetic information of biological, living, organisms.

Formally, the ester is derived from phosphoric acid and a sugar (deoxyribose). Attached to each sugar is one of 4 heterocyclic bases. The bases involved in forming DNA are: adenine (A) and guanine (G) (derivatives of purine) and thymine (T) and cytosine (C) (derivatives of pyrimidine), as shown in Fig. 1.6. A sugar–base unit is called a *nucleoside* and a base–sugar-phosphoric acid unit is called a *nucleotide*.

The unique properties of DNA are mainly a result of its fascinating secondary structure. This, in turn, was elucidated by J.D. Watson and F.H.C. Crick (1953), using X-ray diffraction measurements, for a certain form of DNA named B-DNA. They found that DNA is made up of two polynucleotide chains wound about each other to form a double helix with a radius of $R_D \sim 10$Å, often also referred to as double stranded (ds-) DNA. The chains are held together at intervals by hydrogen bonds, spanning between bases on apposed strands. It was also found that A was always bonded to T, and G is always bonded to C. In this sense, the two strands are complimentary. This specificity is a result of steric restrictions dictated by the periodic nature of the DNA backbone. The genetic code is therefore embedded in the exact sequence of matching base pairs along the polyester chain (for a more comprehensive discussion see, e.g., Stryer (1988), Morrison and Boyd (1992)). Each of the two helixes is right handed, and contains about 10.5 paired nucleotide units or "base pairs" (bp's) per turn. As shown in Fig. 1.7, the pitch of B-DNA is 34Å. The distance between two bp's along the chain's length is therefore

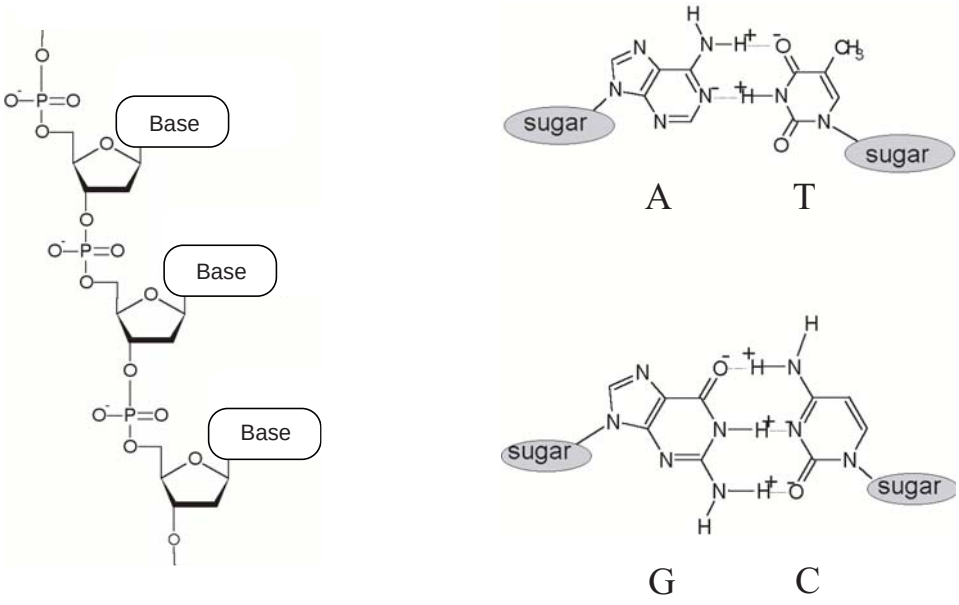

Figure 1.6: Elements of DNA: (left) one strand of DNA is composed of the phosphate sugar backbone which can carry four types of bases; (right) the four bases possible in DNA molecules: Adenine (A), Thymine (T), Guanine (G) and Cytosine (C). These bases form specific pairs (AT and GC) between two complimentary strands.

$\sim$ 3.4Å. Since there are two phosphate groups (which are negatively charged in aqueous solution) associated with each bp, the average distance between two charges along the DNA helical axis is $l \approx 1.7$Å, making DNA one of the most highly charged polyelectrolytes in nature. The DNA bases face the inner side of the helix, whereas the (charged) phosphate and deoxyribose units are on the outside. The planes of the bases are almost perpendicular to the helix axes, while the planes of the sugars are nearly at right angles to the those of the bases.

To this point DNA has been treated as a homogeneous polymer whose properties are uniform throughout. However, DNA has only such uniform properties if its sequence is *random*. Specific base sequences give rise to considerable deviations from these (see e.g., Olson *at al.* (1995) and references therein). For example G-C rich stretches of DNA may develop a spontaneous, non-zero curvature and even twist. In nature, this deviation is used to form *recognition sites* along the DNA molecule, which mark specific places along the DNA for interaction with other biomolecules such as proteins (see Sec. 1.5). However, in all further discussion we shall limit ourselves to the more simple case of random (or close to random) B-DNA. In addition, the nature of the solution and the environment in which the DNA molecule resides, also affect its structure, e.g., through association with other molecules or dehydration. Since the discovery of B-DNA, other forms (isomers) have been identified (e.g., Z- and A-DNA). These

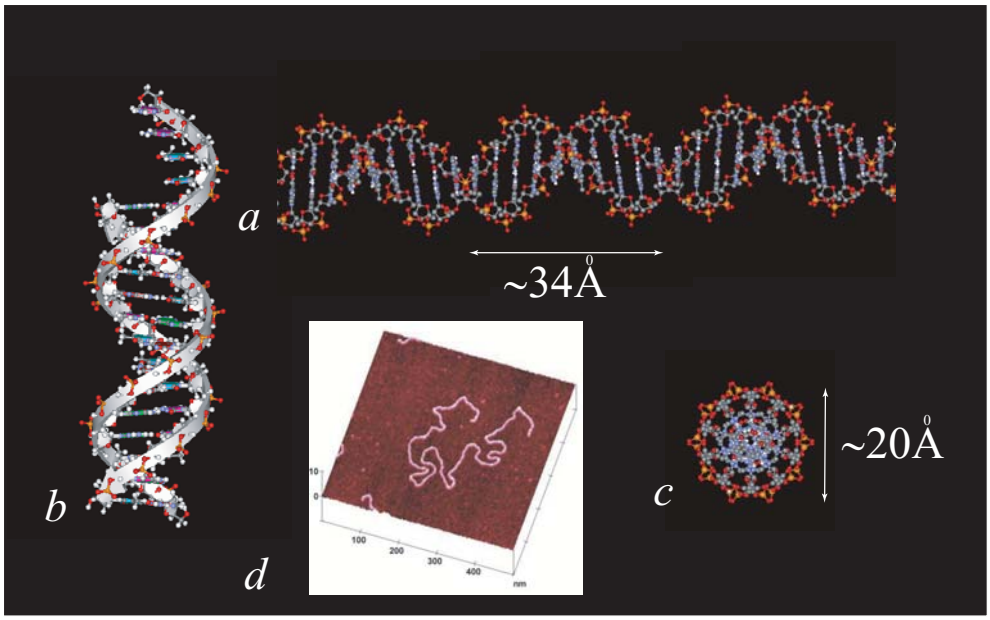

Figure 1.7: Views of B-DNA: a) a stick and ball type representation of a ds-DNA molecule. the pitch of the DNA helix is shown to be ≅ 34Å. b)Ribbon representation of B-DNA showing its double helix nature. c) A "top view" of B-DNA, with a diameter ≅ 20Å/ d) An AFM image of a single DNA molecule adsorbed on a lysine functionalized mica surface. [coordinates for B-DNA: the protein data bank, AFM image: from the Cambridge university department of pharmacology http://www.phar.cam.ac.uk/RI/lots.html]

have rather different molecular parameters from B-DNA (Alberts *et al.*, 1994; Stryer, 1988).

1.4.2 Persistence length

The physical properties of DNA are a direct consequence of their (chemical) structure. One such property is the high stiffness of the DNA molecule. This is reflected in the *persistence length* that the DNA molecule displays. The persistence length may be considered as a measure of the distance over which a polymer chain is still kept straight, and segments along its length are still correlated. Conversely, it may be regarded as the distance beyond which thermal fluctuations erase orientational correlations.

More precisely, let us denote by ϑ the angle between two (unit) vectors, $\vec{u_1}$ and $\vec{u_2}$, tangent to the axis of the DNA molecule (or other polymer) and separated by a distance s along the molecule contour line (see Fig. 1.8). Assuming an invariance in the elastic properties along the polymer chain, the avarage of the cosine of ϑ over all vectors, $\vec{u_1}$ and $\vec{u_2}$, seperated a distance s apart (reflecting also the thermodynamic ensamble avarage) may written, at least for s sufficiently

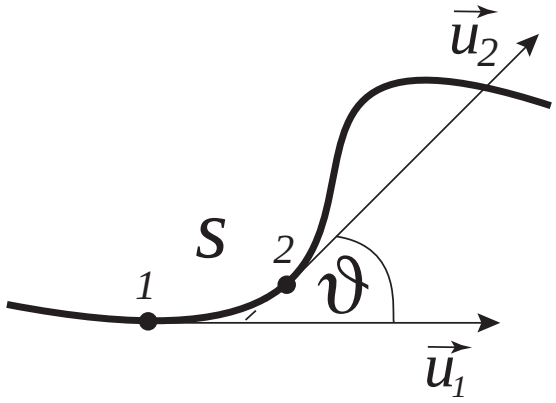

Figure 1.8: Illustration of a semi-flexible polymer chain with two tangent (unit) vectors $\vec{u}_1$ and $\vec{u}_2$ at two points seperated by a distance s along the chain, forming an angle ϑ between them.

large, as

$$\langle \cos \vartheta(s) \rangle = e^{-s/l_p} \tag{1.7}$$

where l_p defines the persistence length for a polymer. For a simple synthetic polymer, such as polystyrene, $l_p \approx 1.0 - 1.4$Å. In contrast, for ds-DNA one finds $l_p \approx 50$nm (approximately 150 bp's)(Grosberg & Khokhlov, 1994). This property of the DNA molecule can be seen, at least approximately, in the inset of Fig. 1.7. This atomic force microscopy (AFM) image of a single DNA molecule adsorbed on a mica surface functionalized with (positively charged) lysine clearly shows that the distance between bends in the DNA molecule is of the order of 50nm, not much different than l_p of DNA in solution.

What is the source of rigidity in DNA ? For a neutral polymer, the persistence length is directly proportional to its bending rigidity: the farther fluctuations are endured, the more rigid the polymer. In ds-DNA, the interaction between stacked bases forms a molecule that is hard to bend along its axis. In contrast, single stranded DNA – lacking the ordered stacks of the ds-DNA double helix supported by hydrogen bonds – has a persistence length of only a few Å. However, ds-DNA is also a highly charged molecule, and it is usually solvated in an aqueous salt solution (such as the interior of living cells). For a polyelectrolyte with a large persistence length, such as DNA, the Odijk-Skolnik-Fixman theory (Odijk, 1977; Skolnick & Fixman, 1977) can be used to estimate the influence of the electrostatic interaction between charges along the chain, on the rigidity of the molecule. The theory predicts that at short distances (shorter than about $10 - 20$Å for DNA) the electrostatic influence on the rigidity is negligible. However, at distances larger than this, the persistence length becomes significantly larger, due to long

range electrostatic forces. The contribution to the persistence length due to the presence of salt in solution, Δl_p, may be estimated in terms of the screening length, l_D (Sec. 1.2), to be $\Delta l_p = l_B l_D^2/4l^2$. For double stranded DNA in a salt solution of about 0.1M, $\Delta l_p \approx$ 5nm. It can therefore be expected that the salinity of double stranded DNA solutions (even for simple salts) will change the persistence length to some degree. Indeed, experimental numbers for l_p vary quite significantly.

1.4.3 Counterion distribution

In many cases, and throughout this work, it is adequate to consider DNA strands to be infinitely long rigid rods with negative charges uniformly distributed over its surface. In doing this, we ignore any edge effects, and any effects associated with their flexibility; in particular curvature fluctuations and undulation forces (Podgornik *et al.*, 1989; Podgornik *et al.*, 1994; Strey *et al.*, 1997), and also the possibility for *specific* interactions and sequence recognition between DNA strands (Kornyshev & Leikin, 2001). We also ignore the groove structure and the discrete distribution of phosphate charges. Although this picture provides a reasonable approximation for the electrostatic potential several Å's away from the charged surface, (Wagner *et al.*, 1997), it may quantitatively fail at the immediate vicinity of the surface (Kornyshev & Leikin, 2001). Albeit, this approximation is often useful in view of the fact that the DNA persistence length, l_p, is much larger than the (axial) separation between neighboring charges, l, and DNA radius R_D.

For a charged cylinder, the PB equation has been solved both for (either analytically or numerically) the case of added salt, and for salt-free solutions(see, e.g., (Lifson & Katchalsky, 1954; Hill, 1955; Oosawa, 1970)). We cite here only the result for high salt concentration, where the PB equation may be linearized, with the resulting potential at a distance r from the rod axis:

$$\psi(r) = AK_0(\kappa r) \tag{1.8}$$

where K_0 is the zero order modified Bessel function of the second kind, and A is a constant related to the surface charge density (Brenner & Parsegian, 1974). For small r, there is no screening from counterions, and the potential behaves like that of a bare cylinder (logarithmic). For large r, the potential tends to fall off exponentially, due to the screening of the cylinder surface by counterions in the diffuse layer. This notion of some layer of counterions which stays close to the cylinder surface led to the notion of "counterion condensation".

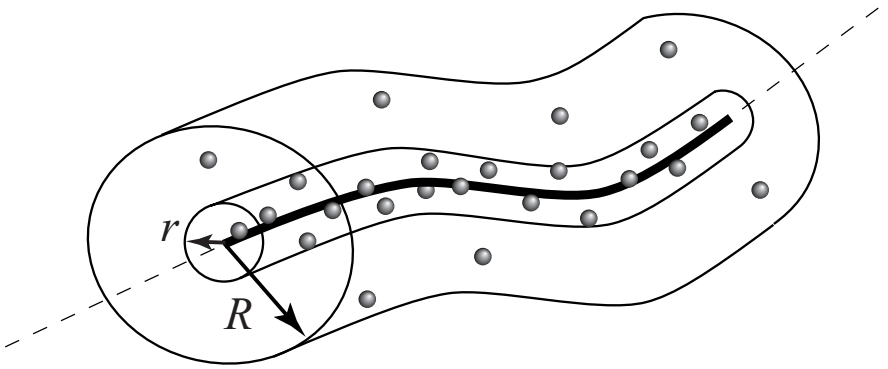

Figure 1.9: Schematic of the model used by Oosawa in considering charged rigid polyelectrolytes. A layer of adsorbed counterions resides in a cylindrical volume of radius r around the polymer, while the rest are far from the charged polymer within a cylindrical cell of radius R

Counterion Condensation

Oosawa and Manning independently proposed a simple model to explain some experimental results, pertaining to the anomalously low activity coefficient of counterion in solutions containing DNA (or any rigid polyelectrolyte), even at low salt concentrations (Oosawa, 1970; Manning, 1978; Manning, 1969). They have considered a unit length of an almost straight segment of a rigid (semiflexible) polyelectrolyte, solvated in a (salt free) solution. The polymer is confined to a cell of volume $V = \pi R^2$ (we may assume that within this simple, Wigner-Seitz like, model $2R$ is the average distance between two polymers in solution). There are N (fixed) charges on this segment, and therefore N (univalent) counterions. These counterions are assumed to be in one of two "states". As schematically illustrated in Fig. 1.9, N_b are bound ions, constrained to move in a small (cylindrical) volume, $v = \pi r^2$, around the polymer, due to electrostatic attraction. The remaining, mobile, ions $N - N_b$ are free to move in a larger cylindrical volume, $V - v$, thus gaining translational entropy. The equilibrium density of ions in these two states is found by equating the chemical potential in the two regions, with the result:

$$\frac{N_b}{v} = \frac{N - N_b}{V - v} \exp(-e\Delta\varphi/k_B T) \tag{1.9}$$

where e is the elementary charge, and $\Delta\varphi$ is the potential difference between a charged ion in the "bound" and "free" states. In the above equation the simplifying assumption is made that a counterion can only reside at a distance r (bound), or R (unbound), away from the polymer. Denoting the fraction of free ions by $X_f = (N - N_b)/N$, and the ratio of the proximal volume to the overall volume by $\Phi = v/V$, Eq. 1.9 may also be written as:

$$\ln \frac{1 - X_f}{X_f} = \ln \frac{\Phi}{1 - \Phi} - \frac{e\Delta\varphi}{k_B T} \tag{1.10}$$

Since N_b ions are bound, the polymer effective (net) charge as seen from outside the proximal cell is $N - N_b = NX_f$. The potential difference may be approximated by that of a simple cylinder, $\Delta\varphi = 2(X_f e/\epsilon l)\ln(R/r)$. Here we have used $l = 1/N$, so that X_f/l is simply the net charge on the polymer. Using this expression for $\Delta\varphi$, Eq. 1.10 becomes:

$$\ln\frac{1-X_f}{X_f} = \ln\frac{\Phi}{1-\Phi} + X_f\lambda_{om}\ln\frac{1}{\Phi} \tag{1.11}$$

where $\lambda_{om} = e^2/\epsilon k_B T l = l_B/l$ is the "Oosawa-Manning" parameter, and l is the distance between two charges along the polymer. Now, looking at the behavior at infinite dilution, i.e. $\Phi \to 0$, Eq. 1.11 is:

$$\ln\frac{1-X_f}{X_f} = (1 - X_f\lambda_{om})\ln\Phi \tag{1.12}$$

In the limit $\Phi \to 0$, this equation implies different behaviors, depending on whether λ_{om} is smaller or larger than 1 (Oosawa, 1970). For $\lambda_{om} < 1$ we find $X_f \to 1$. On the other hand, for $\lambda_{om} > 1$, the degree of dissociation is some number in the range $0 < X_f < 1$. This may be considered a form of condensation. When charges on the polymer are closer than l_B apart, a condensed layer of counterions appears close to the polymer. The translational entropy never wins over their electrostatic binding energy. A simple qualitative explanation to the condensation may be given as follows. If the distance between two fixed charges is such that they interact with an energy much larger than $k_B T$, the gain in energy from relieving this positive contribution to the free energy (through the binding of a counterion) is larger than the possible translational entropic gain of the same counterion. Some ions therefore may be expected to reside close to the DNA molecule, sufficient to create an effective "renormalized" l such that $l_{eff} \equiv l/X_f \to l_B$.

This notion of "counterion condensation" has been extended to many other cases, such as for solutions containing added salt and to the interaction of two DNA molecules (Manning & Ray, 1998; Ray & Manning, 1994). Though there may be some merits to the two-state model of Oosawa and Maning, it seems that the predicted results based on this oversimplified picture are often quantitatively and sometimes even qualitatively wrong. The theory has therefore been under a fair amount of scrutiny and criticism (Stigter, 1995; Deserno *et al.*, 2000; LeBret & Zimm, 1984). In particular it has been suggested that the only consistent method for evaluation of the counterion atmosphere around DNA is (on the mean-field level) PB theory. Even so, it may be useful to bear this model in mind when speaking about DNA, for which $\lambda_{om} > 1$ ($l \approx 1.7$Å), in the sense that DNA in aqueous solutions has many (potentially mobile) counterions bound in close proximity.

1.4.4 DNA-DNA interaction and condensation

DNA strands are negatively charged, and therefore it seems reasonable to assume that they will repel each other. This in fact the result that is always obtained within PB theory (see e.g., the studies involving some approximations (Brenner & Parsegian, 1974)).

In App. A, a numerical method for solving the PB equation is presented. This method will later be used to solve for other systems, with more elaborate boundary conditions (Harries, 1998).

In spite of the expected repulsion between DNA strands, inside living cells (be they the simple *prokaryots* which lack a nucleus or the more highly evolved *eukaryots*) and viruses, DNA in always found to be highly compact. It is amazing to think that several meters of DNA are packed inside practically every human cell ! This compactisation is achieved in cells by positively charged peptides and polyamines (such as spermine and spermidine) and proteins (particularly Histones) (Stryer, 1988). It has been shown that DNA undergoes an abrupt transition to a densely packed form in the presence of a wide range of condensing agents. These include multivalent cations, neutral and charged polymers and alcohols (for recent reviews see Bloomfield (1991; 1992) and Bloomfield (1996)). In all these cases, strong forces, either electrostatic or "depletion" type forces (see e.g., (Israelachvili, 1992)) overcome the repulsion between strands (Park, 1999; Rau & Parsegian, 1992).

DNA is known to form a multitude of phases when condensed. Some of these mesophases reflect the elongated aspect ratio of DNA, akin to the phases observed in (other) liquid crystalline phases. Other phases also reflect the helical nature of the DNA helix, forming twisted (or even double twisted) phases (for reviews see (Livolant & Leforestier, 1996; Podgornik *et al.*, 1998; Gelbart *et al.*, 2000)).

Some 30 years ago, Oosawa proposed that correlated fluctuations in the counterion density around macroions could lead to van der Waals like attractions between the two macroions (Oosawa, 1970; Oosawa, 1968). This is one important case where correlations between mobile ions must be included to get the correct effect (see Sec. 1.2.1). Computer simulations helped in assessing the ability of mobile multivalent ions to cause attraction between like-charged macroions. Since that time, another alternative mechanism was suggested as the cause of attraction between macromolecules, namely a Wigner-crystal type attraction (Rouzina & Bloomfield, 1996; Grønbech-Jensen *et al.*, 1997; Shklovskii, 1999). According to this mechanism, ions firmly (electrostatically) bound to one macroion may attract a similar, correlated array on another macroion. This will again lead to attraction. An important difference between the two mechanisms, is that the former is based on thermal fluctuations, and therefore the resulting attraction

between macroions becomes stronger the higher the temperature. In contrast, for the latter, the attraction results from correlated bound counterions. Therefore, the lower the temperature, the stronger the binding of the ions, and the attraction between macromolecules is reinforced. A crossover between these two regimes may therefore be expected (Oosawa, 1970; Grønbech-Jensen *et al.*, 1997; Lau *et al.*, 2001).

1.4.5 Gene therapy and gene delivery

An individual gene in a living cell is a stretch of DNA that, in most cases, acts as a blueprint for making a specific protein. In its sequence is coded the sequence of amino acids composing the protein. If a particular gene is mutated, its protein product may not be made at all, or may work poorly or even too aggressively. This flaw may disturb vital functions of cells and tissues, and thereby cause symptoms of disease. Scientists have long been enchanted by the possibility that they could replace, silence, or otherwise manipulate defective genes by putting foreign DNA into them, thus achieving "transfection" – the delivery of functional genes to cells. During the 1960's, investigators established that a principle obstacle to the uptake of DNA by cells was that in aqueous solutions of the kind found in cells, the molecule is negatively charged. This means it tends to be repelled from the membranes of cells, since they are also negatively charged.

Many strategies for gene delivery in gene therapy have been proposed and studied (Friedmann, 1997). One of these employed modified viruses to shuttle DNA into human cells. The modified virus with its cargo of DNA invades cells, as a normal virus would, then releases the "healthy" gene, which is then transferred to the nucleus. Though modified viruses are effective at transferring genes into cells, their therapeutic use has encountered some difficulties. A major limitation is that a patient may generate an immune response to the virus, thereby destroying the virus itself or possibly killing the infected cells before the therapeutic gene has had a chance to help a patient.

A wide variety of non-viral strategies to gene delivery have also been proposed (Felgner, 1997). All use a positively charged agent to complex DNA. These include mineral calcium phosphate, and organic polymers such as DEAE-dextran. The tight complex formed is then taken up by the cells. Papahadjopoulos and Nicoloau, independently managed to achieve transfection by mixing DNA with liposomes. Felgner later proposed using mixed, cationic and neutral liposomes, instead of the naturally abundant negatively charged lipid membranes (Felgner *et al.*, 1987; Felgner & Ringold, 1989). This, it was hoped, would make the liposomes interact more easily with DNA, as well as with the cell surface. It was

found that stable DNA-lipid complexes ("lipoplexes") were formed. These complexes have been shown to efficiently transfect cultured cells. Their clinical use is however hampered, mainly by the toxicity of the synthetic lipids used. Therefore, a substantial effort has been made to increase the efficiency of transfection, while lowering the toxicity of these potential agents. An important step in devising more efficient complexes, is understanding the relationship between the structure, composition and function (i.e., the transfection efficiency) of the complexes, so as to later direct the synthesis of DNA-lipid complexes towards the desired structures. We shall return to this point in Chaps. 2 and 3, where we discuss the theoretical basis for the structure–composition relationship experimentally found in these complexes.

1.5 Proteins

1.5.1 Structure

Proteins are found in all living cells. They are responsible for forming and maintaining the shape of cells and the complete organisms, and for coordinating their functions. They are a major component of muscle, tendons, nerves, enzymes, antibodies and hormones (Stryer, 1988; Alberts *et al.*, 1994).

Proteins are polyamids, whose monomers are derived from $\alpha-$amino carboxylic acids. Fig 1.10 shows how the amino acid residues are joined by amide (peptide) linkages. To every third atom on the chain, a (generally different) side chain is attached. A single protein may contain hundreds to thousands of amino acid units. By convention, if under a molecular weight of 10,000 Daltons a polyamide is named a *peptide*. Twenty kinds of amino acids are commonly found in proteins, and these determine which side group can be attached to the peptide chain. The number of different combination, each constituting a different possible protein, are huge. Some of these side chains contain basic groups, such as lysine (Lys) or arginine (Arg), and are therefore positively charged at pH=7. Others are acidic; aspartic (Asp) and glutamic (Glu) acids, see Fig. 1.11. Histidine (His) is also a basic amino acid, but may be considered neutral at pH=7. In general every side chain has specific propensities. In 1951 Linus Pauling and Robert Corey proposed, based on x-ray data and molecular models, two polypeptide structures: the α helix and the β pleated sheet. Stabilized by hydrogen bonds between the NH and CO groups of the main chain, the α helix forms a rodlike structure. Conversely, the β pleated sheet forms a sheetlike structure in which the polypeptide chains are almost extended. Which of these "secondary structures" that are ultimately formed, and how they arrange into superstructures, depends

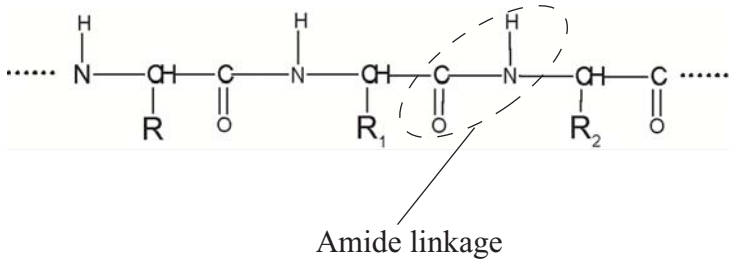

Figure 1.10: Chemical formula representation of a protein backbone made of amino acids with different side chains, connecter through an amide bond. The $R_i's$ denote the amino acid "side chains".

on the particular sequence of acids in the heteropolymer. The tertiary structure of a protein forms when different structural motifs are folded together, sometimes with turns and loops between them, sometimes with di-sulphide bonds, and sometimes from several polypeptide chains joining together (Stryer, 1988). Predicting this intricate folded structure, which confers the specific activity of a protein, on the basis of the order of amino acids alone, has been the focus of much scientific research.

It is possible to divide proteins into two broad classes: *fibrous* and *globular* proteins (Morrison & Boyd, 1992). Fibrous proteins are long and threadlike, and tend to bundle into fibers by strong intermolecular forces (such as hydrogen bonds) all along their length. On the other hand, globular proteins spontaneously fold into compact units that often approach spheroidal shapes. The specific sequence of amino acids along the polymer dictates the final shape. Hydrophilic residues, such as charged groups, in general, line the outer surface of the protein, so as to achieve better contact with the surrounding water molecules. The hydrophobic parts tend to be turned inwards, facing each other.

1.5.2 Peripheral proteins

According to their function, proteins interact with a wide range of other macromolecules, such as other proteins, nucleic acids, and lipid membranes. The proteins that are found to be intimately associated with biological membranes can be classified as being either *peripheral* (associating with the membrane through a lipid anchor or by adsorption) or *integral* (partially or completely embedded in the membrane), according to how strongly they are found to be bound to the lipid membrane. The function of these proteins is most often related to signaling and trafficking across the membranes, or to anchoring or docking of other molecules to the membrane surface, such as proteins from the intercellular matrix. Integral proteins are almost always found to span or penetrate the lipid membrane,

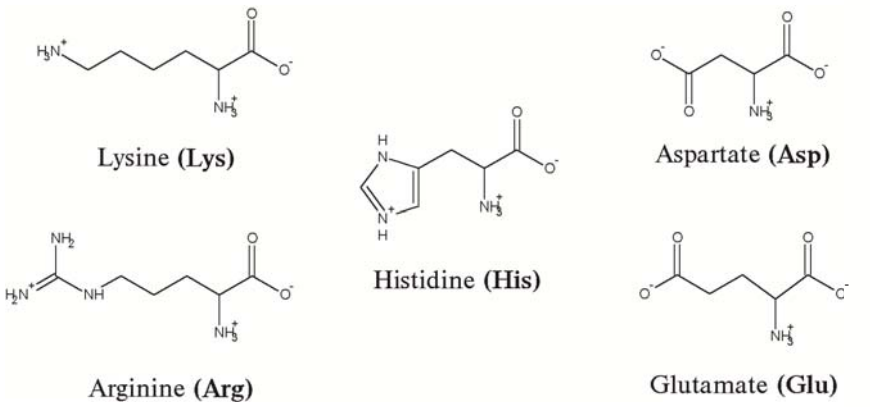

Figure 1.11: Chemical structure of the "basic" amino acids : lysine, arginine and histidine, and of the "acidic" amino acids:Aspartate and Glutamate.

and interact extensively with the hydrocarbon chains of the membrane lipids. Peripheral proteins are bound to membranes mainly through electrostatic forces and also through hydrogen bonding. Therefore, the binding of these proteins depends strongly on the ionic strength: it becomes weaker the more salt is added. In general peripheral proteins are globular. Since most biological membranes are negatively charged, the peripheral proteins interacting with it are generally either positively charged on their surface, or they are roughly speaking, positively charged on one hemisphere, the one proximal to the apposed membrane (while the other may be almost neutral or negatively charged).

An example of one well studied peripheral, water soluble protein is cytochrome *c*. The protein is roughly spherical, with a diameter of 34 Å. It serves as an electrontransferring protein and contains a heme prosthetic group. Cytochrome *c* carries electrons from cytochrome reductase, the second of three proton-pumping complexes in the mitochondrial based respiratory system chain, to cytochrome oxidase, the third of these membrane based pumps. The highly charged cytochrome *c* possesses clusters of lysine side chains around the heme crevice on one hemisphere of the protein. This array of positive charges on the face of cytochrome *c* is central to the recognition and binding of the reductase and oxidase, which are negatively charged. Moreover, the proper membrane association of cytochrome *c*, which is essential to its function and activity as an electrontransferring protein, has been shown to require the presence of acidic phospholipids. The exact mechanism of the binding and adsorption of this protein to the membrane has also been studied (Rytömaa & Kinnunen, 1996; Stryer, 1988; Alberts *et al.*, 1994). Furthermore, it has been shown that cytochrome *c* could cause lipid segregation and induce lateral phase separation in the membrane it adsorbs onto (Boggs *et al.*, 1977; Birrell & Griffith, 1976). We shall return to discuss the adsorption

of peripheral proteins onto membranes in Chap. 4.

In following chapters we will only be modeling peripheral proteins at the most elementary level: we will consider them to be spherical objects of low dielectric constant with (positive) charges smeared on their surface.

1.6 Charged macromolecule interaction

Before plunging into the realm of oppositely charged macromolecular interactions, it is useful to note why they should interact at all. When separated, each charged macroion in solution is surrounded by a diffuse layer of spatially confined counterions. Why then do they attract each other to form complexes ? Upon approach the fixed macroion charges partially (sometimes fully) neutralize each other, allowing the release of mobile counterions into the bulk solution, thereby increasing their translational entropy. This implies that macroion association in solution is, to a large extent, an "entropically driven" process, which was named *"counterion release"* (Record *et al.*, 1978). Yet, the actual contribution of the counterion entropy to the association free energy depends on the detailed geometries and charge distributions of the separated and bound macroions, as well as on the salt concentration in solution (Record *et al.*, 1978; Sharp *et al.*, 1995; Palkar & Lenhoff, 1994; Sens & Joanny, 2000).

Counterion release has been studied extensively in the context of "biomacromolecular" association processes (such as the binding of proteins to DNA) which can be described in terms of chemical equilibrium theory (Record *et al.*, 1978; Sharp *et al.*, 1995). The "condensed" counterions are treated as bound ligands. The number of released ions upon association of the two macromolecules may be inferred (experimentally) from the salt dependence of the standard reaction free energy. The theoretical interpretation of these results relies on structural and thermodynamic-electrostatic models for calculating the number of "bound" ions. More generally, the phenomenon of counterion release is relevant to any system of oppositely charged macroions, for instance complexes involving high molecular weight polyelectrolytes (Khokhlov *et al.*, 1993; Dautzbenberg, 1997).

This underlying mechanism of association was also used to describe the interaction between two oppositely charged planar surfaces with a surface charge density of $\sigma_1 < 0$ and $\sigma_2 > 0$, a distance h apart. Using linear PB theory, the electrostatic "disjoining pressure" between two such surfaces was shown to be (Parsegian & Gingell, 1972):

$$P(h) = \frac{8\pi}{\epsilon} \frac{(\sigma_1^2 + \sigma_2^2 - 2|\sigma_1|\sigma_2 \cosh \kappa h)}{(2 \sinh \kappa h)^2} \tag{1.13}$$

For large h, the interaction is attractive, due to the continuous release of counterions from the volume between the two surfaces. For all cases where $|\sigma_1| \neq \sigma_2$, repulsion appears for small h. This is caused by the confinement of counterions (which must remain in the gap to provide local charge neutrality) and the subsequent loss of entropy (Parsegian & Gingell, 1972; Nardi *et al.*, 1998). An important consequence of this is that attraction will be observed for all h, only if the two surfaces exactly neutralize each other.

Later, in Chap. 2, we shall return to this point, arguing that the association of DNA and charged lipid membranes can unambiguously be attributed to the release of counterions, both theoretically and experimentally. We will show that maximal ion release is associated with the special point of *isoelectricity*, i.e., when the number of fixed charges on both macroions is equal.

1.7 Overview

Each of the molecular components surveyed in this introduction has unique properties. These will manifest themselves in the macromolecular assemblies we are about to examine. In Chap. 2 we will consider a system of DNA interacting with mixed, charged and neutral, planar lipid membranes, to form a specific type of composite phases, elucidated and named the L_α^C phase. We will present a theoretical model that will include all relevant degrees of freedom self-consistently. The model will be shown to account for all experimental observations for the system. In particular we will stress the importance of the membrane fluidity and the mobility of lipids in the membrane plane. Another point we will address is the role of counterion release in the formation of these composite phases. We will show how the theoretical model correctly predicts the experimental results.

In Chap. 3 we will extend the model discussed in Chap. 2 to include another important degree of freedom, namely the membrane's ability to bend around DNA molecules. When lipid bilayers are allowed to bend, i.e., when they are relatively "soft" with respect to bending deformations, the resulting complexes may display a corrugate membrane in an L_α-like complex, or even bring about a transition to yet another phase, the H_{II}^C phase, reminiscent of the pure lipid H_{II} phase. We will demonstrate the important coupling between local curvature and electrostatic properties, which add to the stability of the complexes by further lowering the complexe's free energy.

In Chap. 4 we utilize similar theoretical tools to model a system of peripheral proteins interacting with an oppositely charged membrane. Again, we will argue, that membranes fluidity is an important degree of freedom, fundamental in modeling this system. We will also emphasize the important role of lateral

protein-protein interaction.

A short summary will follow in Chap. 5.

Chapter 2

Lamellar DNA-Lipid Complexes

2.1 Introduction

In this chapter we examine a most compelling example of macroion association, involving the formation of composite phases upon mixing DNA and liposomes composed of a binary (cationic and neutral) lipid mixture.[1] As discussed in Sec. 1.4.5, the interest in the complexes formed was inspired by the search for liposomal vectors that can serve as gene delivery vehicles, i.e., in the targeting of extracellular DNA into cell nuclei (Felgner *et al.*, 1987; Felgner & Ringold, 1989; Felgner *et al.*, 1996; Gershon *et al.*, 1993; Gustafsson *et al.*, 1995; Lasic *et al.*, 1997; Zuidam & Barenholz, 1997; Meidan *et al.*, 2000; Hui *et al.*, 1996; Mok & Cullis, 1997). Fundamental electrostatic issues arise immediately when examining these phases, because of the strong interactions between the DNA and the cationic lipids used to complex it.

In a series of studies Rädler *et al.* (Rädler *et al.*, 1997; Rädler *et al.*, 1998; Salditt *et al.*, 1997; Koltover, 1998) reported the existence of highly novel DNA-cationic liposome complexes (also named "lipoplexes" (Felgner & Ringold, 1989)), as determined by high resolution synchrotron X-ray diffraction and optical microscopy. In particular, one type of complexes was shown to consist of multi-layer, lamellar, smectic-like stacks of mixed bilayers, each consisting of a mixture of the charged cationic lipid (CL), e.g., DOTAP and neutral ("helper", HL) lipid, e.g, DOPC (see Sec.1.3), with monolayers of DNA strands intercalated within the intervening water gaps, see Fig. 2.1. The DNA strands within each gallery are parallel to each other, exhibiting a definite repeat distance d. While d depends on the CL/DNA and CL/HL concentration ratios, the spacing between two apposed

[1] The results presented in this chapter were previously reported in Harries *et al.* (1998) and Wagner *et al.* (1997).

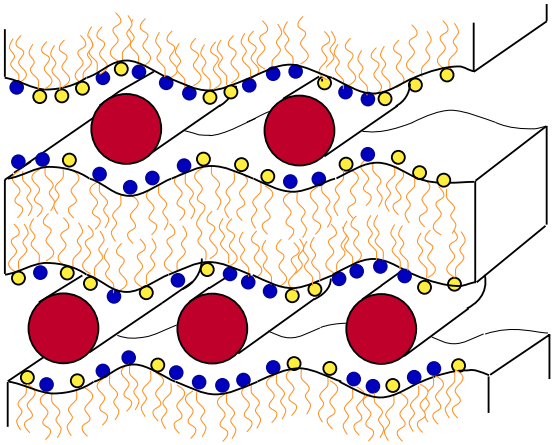

Figure 2.1: Schematic illustration of the lamellar (L_α^C) lipid-DNA complex.

lipid monolayers is nearly constant, $h \approx$ 26Å, corresponding to the diameter of a double stranded B-DNA ($2R_D \approx 20$ Å) surrounded by a thin hydration shell. This lamellar (also named the L_α^C or "sandwich") complex, is stabilized by the electrostatic attraction between the negatively charged DNA and the cationic lipid bilayer. Without DNA the lamellar lipid phase (L_α, see Sec. 1.3) is unstable owing to the strong electrostatic repulsion between the charged bilayers.

Quite different equilibrium ordered phase morphologies were found to arise for other choices of HL. In the case of DOPE (see Sec.1.3), or lecithin, for example, inverted hexagonal ("honeycomb" or H_{II}^C) organization of the lipid, with single strands of ds-DNA in aqueous solution regions, were found to form (Felgner *et al.*, 1987; Tarahovsky *et al.*, 1996; Koltover *et al.*, 1998). The H_{II}^C structure may be regarded as an ordinary inverse-hexagonal (H_{II}) lipid phase with DNA strands intercalated within its water tubes. Here too, the diameter of the water tubes is just slightly larger than the diameter of the DNA "rods". The presence of DNA is crucial for stabilizing the hexagonal structure. Without it, strong electrostatic repulsions will generally drive the lipids to organize in planar bilayers. In fact, the "raw lipid materials" from which hexagonal complexes are formed are liposomes, namely, lipid bilayers.

Metastable intermediates, and in particular the "Spaghetti" structures, have also been reported, in which each (possibly supercoiled) DNA strand is coated by a cylindrical bilayer of the CL/HL lipid mixture (Sternberg *et al.*, 1994; Sternberg, 1996). Both these honeycomb and spaghetti-like structures were previously investigated theoretically (May & Ben-Shaul, 1997; Dan, 1998).

Experimental studies show that the two ordered complex structures show a different type of interaction with living cells. A correlation was found between the structure of the lipoplexes formed and the transfection efficiency. (The structure

formed was in turn dependent on the specific choice and relative amount of HL, CL and DNA.) For example, the H_{II}^{C} complex was found generally to be a more potent vector than L_{α}^{C} (Lin *et al.*, 2000). However, the operation mechanism is not entirely clear (Hui *et al.*, 1996; Zuidam *et al.*, 1999; Meidan *et al.*, 2000). Understanding how to control and manipulate the formation of specific phases should aid in the design of more potent lipid based gene delivery vectors.

In this chapter we treat in detail the electrostatics and self-assembly characteristics of the multi-bilayer lamellar stacks of intercalated DNA: the L_{α}^{C} structures, see Fig. 2.1. In Sec. 2.2, we address them within the general context of the statistical thermodynamics of aqueous solutions of DNA and mixtures of neutral and cationic lipids. Mobile counterions are described by the nonlinear Poisson-Boltzmann (PB) equation, which is solved numerically. In the theoretical model presented in this chapter we neglect elastic deformations of the DNA strands and bilayers, treating them as a rigid macromolecule. This is appropriate for bilayers composed of monolayers with small spontaneous curvature, (see Sec. 1.4, 1.3 and Chap. 3). On the other hand, we explicitly allow for the possibility of spatial inhomogeneities in the membrane surface charge density, in response to interactions with the cationic DNA. This effect will be shown to be significant, reflecting the "extra" degree of freedom associated with cationic lipids in *mixed-fluid*, bilayers. Thus, we wish to account for the variation in charge density of the charged lipid headgroups on the membrane surface in the direction normal to the DNA strands, in a way which depends on the distribution of counterions (electrostatic potential), which in turn depends on the charge at the surface. In solving the PB equation, then, we need to treat the (Gauss law) boundary conditions at the membrane surface in a fully self-consistent way to account for this redistribution of charges. We do so in Sec. 2.3 using the variational approach outlined in Sec 1.2. We thus derive the appropriate boundary condition for the membrane surface, which is then solved self-consistently within PB theory. Results are presented for a wide range of DNA-DNA spacings, overall lipid composition, and added salt concentrations.

Generally, we find that lipid mobility favors optimal (local) charge matching of the apposed DNA and lipid membrane. This is the state in which a maximal number of mobile counterions are expelled from the gap, implying a maximal gain of free energy (see Sec. 1.6). However, the tendency for charge matching (hence migration of lipid molecules to/from the interaction zone) is opposed by the unfavorable lipid demixing entropy loss associated with it. This tendency of charged lipids to segregate in the vicinity of the rigid charged macromolecule has gained some experimental support through nuclear magnetic resonance (NMR) studies (Mitrakos & Macdonald, 1996). We shall see that the lipid composi-

tion profile within the bilayers is determined by a delicate balance between the electrostatic and mixing entropy contributions to the free energy of the complex.

Equipped with the free energies of the CL-DNA complex and its separate components, we proceed to determine the phase evolution of the system. To this end we solve the thermodynamic equations which express equilibrium between the L_α^C complex and, alternately, excess DNA and excess lipid. In this way we establish how DNA-DNA spacings d vary with the ratio ρ of charged lipid to DNA, for each of several different lipid compositions (ratio of neutral to cationic lipid). In agreement with experiment we find that for a lipid mixture of given composition, the spacings are constant throughout the low ρ range where the complex coexists with excess DNA. In the high ρ range, where the complex coexists with excess lipid, the spacings are nearly constant as well. Throughout the "single-phase" region, however, where all the DNA and lipids are accommodated by the complex, the DNA-DNA spacings increase linearly with ρ, as implied by material conservation and confirmed by experiment. This region is found to include the (very) special – "*isoelectric*" – point at which the total charges carried by DNA and lipid are equal. At the isoelectric point the free energy of the complex is minimal. We show, both theoretically and experimentally that the isoelectric point is associated with maximal counterion release (see Sec. 1.6). The association of DNA and lipid is thus shown to be (almost solely) driven by the gain of entropy resulting from the release of counterions.

All of the above results can be qualitatively accounted for by a simple "box" model described in Sec. 2.4, in which the electrostatic effects enter only via the "excess charge" which measures the extent of deviation from the isoelectric point. In this way one can understand the constancy of DNA-DNA spacings at low and high ρ, i.e., at *large* deviations from the isoelectric point, directly in terms of the mutual repulsions between like-charged DNA strands or lipid bilayer surfaces, respectively. We include in this final section, a brief account of the theory of the L_α^C complex presented independently by Bruinsma (1997), who interprets the observed structural evolution (d vs. ρ) via approximate analytical solution of the nonlinear PB theory. His analysis of the free energy (which is restricted to low cationic lipid contents) is based on a physical picture which is quite similar to ours; his conclusions regarding the phase evolution of the system are somewhat different. We also discuss there the quite different approach suggested by Dan (1996; 1997), who – in contrast – ascribes the preferred d spacing at low ρ to a competition between short-range electrostatic repulsions and longer-ranged DNA-DNA attractions mediated by the elastic deformation of the bilayer membranes.

2.2 Theory

In this section we outline our model for calculating the free energy of the L_α^C complex, and derive the thermodynamic relationships dictating the complex structure and phase behavior in lipid-DNA solutions, as a function of the overall lipid to DNA ratio and the CL/HL lipid composition.

2.2.1 Model

Ignoring edge effects, we shall treat the complex as an infinite periodic lamellar array consisting of alternating lipid bilayers and DNA monolayers, as schematically illustrated in Fig.2.1. The DNA strands are assumed to be infinite, parallel and equi-distant rigid rods thus forming a one-dimensional (1D) lattice.

As noted in the previous section, the existence of a well defined inter-axis distance d (which depends on lipid composition and lipid to DNA ratio) has been unequivocally confirmed by X-ray diffraction studies (Rädler *et al.*, 1997). Theoretical support for this finding will be given in the following sections. The naked DNA strands in solution will be treated as infinite cylindrical rods and the liposomal membranes as perfectly planar infinite bilayers.

Modeling DNA strands as infinite rigid rods was discussed in Sec. 1.4. Here, the approximation is justified in view of the fact that the DNA persistence length ($l_p \approx 500$Å) is significantly larger than all the other relevant length scales in the L_α^C complex; namely, the DNA radius $R_D \approx 10$Å, the inter-axial distance $d \approx 20 - 70$Å, the thickness of the inter-bilayer water gap $h \approx 25$Å, the bilayer thickness $w \approx 30$Å, and the average linear dimension of a lipid head group $a^{1/2}$, where $a \approx 70$Å^2 is the average cross sectional area per lipid molecule in the membrane. It should be noted that any curvature fluctuation of an individual DNA strand within the monolayer implies a change in d extending over a distance of order l_p. From the calculations presented in the next section it will become apparent that such changes involve an electrostatic free energy penalty of many k_BT's, indicating that curvature and inter-axis fluctuations in the complex are quite unlikely.

In general, the DNA lattice may induce membrane curvature modulations (with a maximal amplitude of A_0), as schematically illustrated in Figs. 2.1 and 2.2. However, an assumption that will be made throughout this chapter, that the lipid bilayers are perfectly planar, i.e., $A_0 = 0$, and their thickness, w, is constant and independent of their lipid composition. For lipid bilayers of high bending rigidity (Helfrich, 1973) the modulations are expected to play a minor role in determining the complex stability. On the other hand, when "soft" bilayers are involved in complex formation, these curvature modulations may become increas-

ingly important, possibly leading to structural phase transformations involving, say, the inverted hexagonal/honeycomb states mentioned in Sec. 2.1 (Koltover *et al.*, 1998). We return to this point in the next chapter, where we will consider the elastic degree of freedom, both within the L_α^C phase, and in the transition to the honeycomb (H_{II}^C) phase. The assumption of constant w is justified for bilayers whose CL and HL components are of similar chain length. This is the case for the neutral lipids DOPC and DOPE, as well as the cationic lipid DOTAP, mixtures of which are known to form lamellar complexes with DNA (Rädler *et al.*, 1997; Rädler *et al.*, 1998; Salditt *et al.*, 1997; Koltover, 1998). The extension of our model to cases where w varies with the lipid composition is, in principle, straightforward.

The negative charges on the DNA surface are densely spaced, see Sec. 1.4; the average spacing between these charges along the axis of B-DNA is $l = 1.7$Å. We shall assume that these charges form a continuous and uniform charge distribution over the DNA surface which will be regarded as a perfect cylindrical envelope. This approximation is supported by numerical studies revealing that the electrostatic potential around the DNA surface is no different from that produced by a continuous charge distribution, except for a narrow region in its immediate vicinity (Wagner *et al.*, 1997). In all our calculations we shall use $R_D = 10$Å for the radius of this cylinder, implying a uniform charge density $\sigma^- = e/2\pi R_D l \approx 0.15\ \mathrm{Cm}^{-2}$, corresponding, approximately, to one elementary charge, e, per 110Å^2.

We shall also assume that the CL and HL constituting the membrane are ideally mixed. In the free bilayer this implies, on average, a uniform and continuous charge distribution. The charge density is $\sigma^+ = e\phi/a$, where ϕ is the mole fraction of the cationic lipids and a is the average area per lipid head group. On the other hand, in the bilayers of the complex we shall allow for spatial modulations of the cationic charges, while assuming that ideal mixing applies *locally*. In all calculations we shall use $a = 70\text{Å}^2$ (implying $\sigma^- = \sigma^+$ when $\phi \approx 0.65$) for both lipid components, in both the free and the complexed bilayer.

Finally, the naked DNA, the free lipid bilayer and the lipid-DNA complex will be treated as macroscopic phases, i.e., we ignore the free energy contributions associated with their overall translational and rotational degrees of freedom. These free energies are on the order of $1k_BT$ per particle, much less than their "internal" (electrostatic and mixing) free energies.

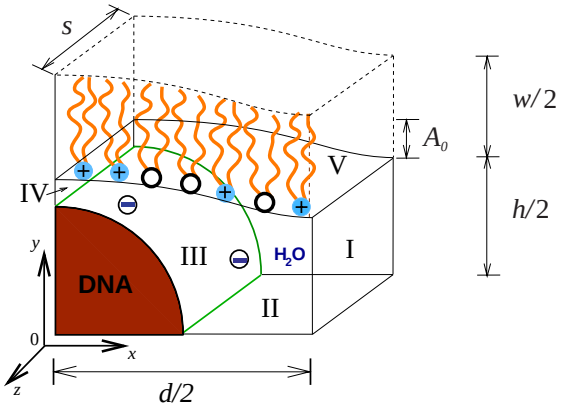

Figure 2.2: Schematic representation of one quarter of the complex's unit cell. The Poisson-Boltzmann equation is solved in the aqueous interior subject to boundary conditions appropriate for surfaces I – V, (see text).

2.2.2 Free energies

We define a unit cell of a complex as a box of dimensions $d \times b \times s$, where d is the distance, along the x axis, between two neighboring DNA strands, $b = h + w$ is the distance between two bilayer midplanes along the y axis, and s is the "depth" of the unit cell along the z (the DNA axis) direction. Since the complex is translationally invariant along the z axis the calculation of its free energy is a 2D problem, and the choice of s is arbitrary, Fig. 2.2.[2] Unless stated otherwise, our numerical results will be reported for $s = 1$Å. For the numerical evaluation of the complex free energy it is convenient to consider only one quarter of a unit cell, as shown in Fig. 2.2. Note, that in this cell the region accessible to water and ions is limited by the membrane and DNA strands.

Formation free energy

Let $f_C = f(\phi, d, h)$ denote the (charging) free energy of one unit cell of the complex, where $\phi = \phi_C$ is the average mole fraction of the cationic lipid in the complex. Alternatively, we may interpret f_C as the free energy of a DNA strand (of length s), when incorporated in a complex characterized by ϕ_C, d, h plus the free energy of a complexed bilayer segment containing $n = 2s \times d/a$ lipid molecules. In the limit $d \to \infty, h \to \infty$ the complex disintegrates into well separated DNA and lipid bilayer. Thus, $f_C = f(\phi, d \to \infty, h \to \infty) =$

[2] We stress here that all solutions to the PB equation throughout the whole of this work are purely 2D in nature. No modulation along the remaining axis are considered. This makes s an irrelevant parameter for most purpouses. We define it here soley for cases where different calculation used diferent s values as standards. The reader will be explicetly warned when the value s is changed.

$f_D + f_B(\phi) = f_D + d\tilde{f}_B(\phi)$. Here f_D is the free energy of a naked DNA rod of length s and $f_B(\phi)$ is the free energy of a bare bilayer segment of area $s \times d$; $\tilde{f}_B(\phi) = f_B(\phi)/d$. Henceforth, all energies denoted as are the free energy per unit length of a strip of width s. ($f_B/n = (a/2s)\tilde{f}_B$ is the free energy per lipid molecule in the bilayer.) The difference

$$\Delta f_C(\phi, d, h) = f_C(\phi, d, h) - f_D - d\tilde{f}_B(\phi) \tag{2.1}$$

is the free energy change associated with complex formation from its separate, DNA and lipid bilayer, components. A complex characterized by ϕ, d and h is thermodynamically stable only if the formation free energy is negative, $\Delta f_C < 0$. We now turn to a more detailed discussion of the terms appearing on the right hand side of Eq. 2.1.

Complex

As we do not allow for curvature or thickness modulations of the lipid layers, f_C involves only two contributions: the electrostatic (charging) free energy of the complex and the (in-plane) lipid mixing entropy. The negatively charged DNA grid can induce a spatial *modulation* (or "polarization") of the cationic lipid charges (along the x axis), so as to minimize the electrostatic *energy* of the system. However, this tendency is opposed by the lipid *"demixing" entropy* penalty associated with any deviation from a uniform distribution. Thus, the extent of lipid demixing (charge modulation) is governed by a delicate interplay between these two opposing tendencies; the electrostatic and lipid mixing contributions to the complex free energy are strongly coupled. Thus, the lipid composition profile $\eta(x)$, the electrostatic potential in the complex interior $\varphi(x, y)$, and the actual value of the complex's free energy, $f_C(\phi, d, h)$, must be determined by minimizing the *total* free energy functional, which includes both the mixing and electrostatic terms, namely (using the mks convention),

$$\begin{aligned} f_C &= \left(\frac{k_B T}{e}\right)^2 \int_v \frac{\epsilon}{2}(\nabla\psi)^2 \, \mathrm{d}v \\ &+ k_B T \int_v \left[n_+ \ln \frac{n_+}{n_0} + n_- \ln \frac{n_-}{n_0} - (n_+ + n_- - 2n_0) \right] \mathrm{d}v \\ &+ \frac{k_B T}{a} \int_{S_V} \left[\eta \ln \frac{\eta}{\phi} + (1-\eta) \ln \frac{1-\eta}{1-\phi} \right] \mathrm{d}S. \end{aligned} \tag{2.2}$$

The first term on the right hand side of this equation is the electrostatic energy; $\psi = e\varphi/k_B T$ is the scaled (dimensionless) electrostatic potential, and $\epsilon = \epsilon_0 \epsilon_r$ where ϵ_r is the dielectric constant of the solution and ϵ_0 is the permittivity

of vacuum (Verwey & Overbeek, 1948). The integration is over the volume of the unit cell. We use $\epsilon_r = 78$ for the aqueous regions.

The second term accounts for the translational ("mixing") entropy of the mobile ions in the complex interior, relative to their entropy in the bulk solution, with $n_+ = n_- = n_0$; $n_\pm = n_\pm(x, y)$ denoting the local concentrations of mobile ions in the complex. (We assume a 1:1 electrolyte solution.) The last term accounts for the mixing entropy (penalty) of the charged and neutral lipids in the membrane plane, relative to their entropy in the (ideally, evenly mixed) uncharged membrane. The integration is over the membrane surface, (surface V in Fig. 2.2). Locally, i.e., at any x, the lipids are assumed to be ideally mixed, with $\eta = \eta(x)$ denoting the local mole fraction of the charged lipid. (Recall that the average area per lipid in the membrane is assumed to be independent of the lipid composition.)

Note that the free energy functional in Eq. 2.2, which we shall treat as the total free energy of the system, does not include any contribution from the inner (hydrophobic) regions of the membrane and the protein. Namely, we disregard the dielectric properties of these regions, treating them as decoupled from those of the electrolyte solution (and charged surfaces). Formally, this decoupling is equivalent to setting $\epsilon = \epsilon_{int} = 0$ within the hydrophobic regions (i.e., in the interior of the DNA and the lipid membrane). Qualitatively one expects that because any molecular polarization within the hydrophobic regions provides the system with an additional degree of freedom, the interaction free energy between the particles will be lower for all $\epsilon_{int} > 1$. In fact, as has been shown in Sec. 1.3.5 the effect of setting $\epsilon_{int} = 0$ can be estimated, and for the case discussed here, the system is indeed in the decoupled regime. Detailed numerical studies, based on solving the PB equation in the electrolyte solution and the Laplace equation within the (charge-free) hydrophobic regions corroborate this notion. Yet, the magnitude of these effects for $\epsilon_{int} \approx 2$ (as appropriate for hydrophobic media) are negligibly small for all relevant interparticle separations (Carnie *et al.*, 1994; Carnie & Chan, 1993).

The local lipid composition must satisfy the *conservation constraint*

$$\phi = \frac{\int_{S_V} \eta \, \mathrm{d}S}{\int_{S_V} \mathrm{d}S} \tag{2.3}$$

where ϕ is the mean mole fraction of the charged lipid in the complex.

Functional minimization of f_C with respect to n_+, n_- and η, subject to the conservation constraint, Eq. 2.3, yields the following results. For the mobile ion distributions one finds the usual Boltzmann distributions, $n_\pm = n_0 exp(\mp\psi)$, which upon substitution into Poisson's equation yield the PB equation,

$$\nabla^2 \psi = \kappa^2 \sinh \psi, \tag{2.4}$$

where $\kappa^{-1} = (\epsilon_0 \epsilon_r k_B T / 2 n_0 e^2)^{1/2} \equiv l_D$ is the Debye length.

For $\sigma^+(x) = e\eta(x)/a$, the local charge density on the membrane, we obtain

$$\eta = \frac{e^{-(\psi+\lambda)}}{(1-\phi)/\phi + e^{-(\psi+\lambda)}} = -\beta \nabla\psi \cdot \hat{\mathbf{n}} \tag{2.5}$$

where $\beta = a\epsilon k_B T/e^2$, and λ is the Lagrange multiplier conjugate to the charge conservation constraint, Eq. 2.3, and $\hat{\mathbf{n}}$ is the unit vector normal to the boundary (pointing into the dielectric medium). The second equality in Eq. 2.5 is Gauss' law, relating the local surface charge density at x to the electrostatic potential at the membrane surface. This equation represents one of the boundary conditions (boundary V in Fig. 2.2) on the electrostatic potential and must be solved simultaneously, and self-consistently, with the PB equation, Eq. 2.4. A similar type of boundary condition appears in the "charge regulation" model for the electrostatic interaction between colloidal particles involving ionizable surface groups (Ninham & Parsegian, 1971; Carnie & Chan, 1993; Carnie *et al.*, 1994). In these systems, the equilibrium surface charge is adjustable, and determined self-consistently by the interplay between the chemical dissociation reaction and the electrostatic interaction between the charged surfaces. Note that for our model of the L_α^C complex Eqs. 2.4, 2.5 are 2D. Equations reminiscent of these were derived for other systems using a similar approach, as noted in Sec. 1.2.1.

The other boundary conditions, pertaining to domain boundaries I-IV in Fig. 2.2, are less intricate. At the DNA surface (domain boundary III), the boundary condition is that of constant charge density, $-\nabla\psi\cdot\hat{\mathbf{n}} = e\sigma^-/\epsilon_0\epsilon_r k_B T$. For domain boundaries I, II and IV we have, by symmetry, $\partial\psi/\partial x\,|_I = 0$, $\partial\psi/\partial y\,|_{II} = 0$, $\partial\psi/\partial x\,|_{IV} = 0$. The numerical procedure for solving the PB equation (Carnie *et al.*, 1994; Stankovich & Carnie, 1996; Houstis *et al.*, 1985) and for evaluating λ, ψ and the free energy of the complex is outlined in Appendix B.

Bare bilayer, naked DNA

The free energy of the bare bilayer is a sum of mixing and electrostatic contributions, $f_B = f_B^m + f_B^{es}$, both depending on the lipid composition ϕ. (By symmetry, at equilibrium, the bilayer is planar and the lipid compositions in its two monolayers are identical.) The mixing entropy contribution (per unit length of a bilayer strip of width s) is

$$\tilde{f}_B^m = (2s/a) k_B T \; [\phi \ln\phi + (1-\phi)\ln(1-\phi)] \tag{2.6}$$

For $\tilde{f}_B^{es}$ we can use a closed form expression for the electrostatic free energy of a charged planar surface (Lekkerkerker, 1989):

$$\tilde{f}_B^{es} = 2\,(2s/a)\,k_B T\,\phi\,\left[\frac{1-q}{p} + \ln\,(p+q)\right] \tag{2.7}$$

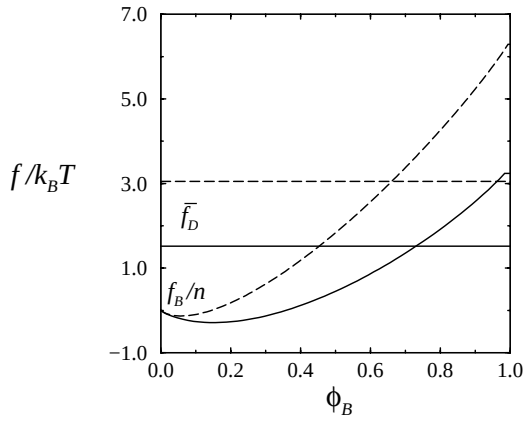

Figure 2.3: The free energy per molecule in the bare lipid bilayer (of area $a = 70\text{Å}^2$ per molecule) as a function of the cationic lipid mole fraction. Also shown is the charging energy $\bar{f}_D = af_D/2\pi R_D s$ of a naked DNA of surface area a. The solid and dashed curves correspond to l_D =10Å and 50Å, respectively

with $p = 2\,\phi\, l_B\, \pi/(\kappa\, a)$ and $q = \sqrt{p^2+1}$; $l_B \equiv e^2/(4\,\pi\,\epsilon\,k_BT)$ is the Bjerrum length (see Sec. 1.2). Note that, with the identification of $l_{GC} \equiv e/2\pi\sigma l_B$ as the Gouy-Chapman length ($\sigma = e\phi/a$), and $l_D \equiv \kappa^{-1}$ as the Debye length, p is recognized to be the ratio of fundamental lengths, $p = l_D/l_{GC}$.

In Fig. 2.3 we show the bilayer free energy per molecule, $f_B/n = (f_B^m + f_B^{es})/n$, as a function of the lipid composition, ϕ_B, for two values of the Debye length, $l_D = 50$ and 10Å. It should be noted that the electrostatic (charging) energy is a monotonically increasing function of ϕ_B; the shallow minimum of f_B at small ϕ_B is due to the lipid entropy contribution, $\tilde{f}_B^m$, (whose minimum is at $\phi_B = 1/2$). Also shown in this figure is (the constant) energy for charging a naked DNA of length $a/2\pi R_D$, corresponding to a DNA surface area of $a = 70\ \text{Å}^2$. This energy is calculated by the numerical solution of the PB equation for an isolated charged cylinder in aqueous electrolyte solution. The results shown in Fig. 2.3 will later be used for calculating the lipoplex formation free energy and the phase diagram of the system.

2.2.3 Phase behavior

Consider an aqueous solution containing DNA strands of total length sD, N^+ cationic lipids and N^0 neutral (helper) lipids; $N^+ + N^0 = N$. The total length of DNA associated in complexes will be denoted as sD_C. In general, the total length of DNA in the system, sD will be equal or larger than sD_C. Note that D_C is also the number of unit cells in the complex. The length distribution of the DNA strands is irrelevant as both the naked DNA and the complex are treated

as (immobile) macroscopic phases.

As the concentration of monomeric lipids in solution is generally negligible, we can safely assume that all lipids are organized in bilayers which, in both the free and complexed states, are assumed to be planar. We find it convenient to express the total bilayer area, $A = Na$, in the form $A = sL$, so that L is the total "length" of the bilayer, if regarded as a strip of width s. We shall use $L_C = \chi L$ and $L_B = (1-\chi)L$ to denote the total length of the complexed and free bilayer, respectively. Note that $L_C = dD_C$ where d is the distance between DNA strands in the complex. Also, using N_C^+ to denote the number of cationic lipids in the complex, we define $L_C^+ = (a/s)N_C^+$. Similarly, we define $L_B^+ = (a/s)N_B^+$, $L_C^0 = (a/s)N_C^0$, $L_B^0 = (a/s)N_B^0$ and $L_C^+ + L_B^+ = L^+, L_C^0 + L_B^0 = L^0$.[3] The mole fractions of cationic lipid in the complexed and free bilayer are given by $\phi_C = N_C^+/N_C = L_C^+/L_C$ and $\phi_B = N_B^+/N_B$, respectively. These two lipid compositions are generally different, but related to each other by the conservation condition ("lever rule"):

$$\chi\phi_C + (1-\chi)\phi_B = \bar{\phi} \tag{2.8}$$

where $\bar{\phi} \equiv N^+/N = L^+/L$ is the overall mole fraction of cationic lipid in solution.

Finally, we introduce the (dimensionless) quantity

$$\rho = N^+/(sD/l) = (\bar{\phi}L/D)(l/a) \tag{2.9}$$

expressing the ratio between the total number of immobile (or surface) positive (i.e., lipid) charges and negative (DNA) charges in the system. Of particular interest is the *"isoelectric point"*, $\rho = 1$. Experiment shows, (at least for $\bar{\phi} \approx 0.5$) that at this point all the lipids and DNA in solution are involved in complex formation (Rädler *et al.*, 1997). In the next section we shall show that this result holds for a wide range of lipid compositions $\bar{\phi}$ and, furthermore, that the isoelectric point corresponds to the minimum of the complex free energy f_C.

Experiment also shows that upon increasing the overall lipid to DNA ratio (L/D), at constant lipid composition $(\bar{\phi})$, the system evolves through three distinct regimes (see Fig. 2.4):

i) When L/D (equivalently $\rho \propto L/D$) is small the system is bi-phasic; the solution contains lipid-DNA complexes which coexist with excess, naked, DNA. Thus, in this regime, $D > D_C$ whereas $L_C = L$ (no free bilayer). The DNA-DNA distance in the complex is constant, $d = d_1(\bar{\phi})$, independent of ρ as long as

[3] Note that most of the variables introduced here represent the same quantity in the differnt phases: Complex, free DNA and bare lipid Bilayer membarnes. Experimentaly, we are in command of only the overall compositional degree of freedom, in our notation these will be $\bar{\phi}$, the total mole fraction of charged lipids in solution ρ, the lipid to DNA charge ratio. The rest is determined through thermodynamic equilibrium.

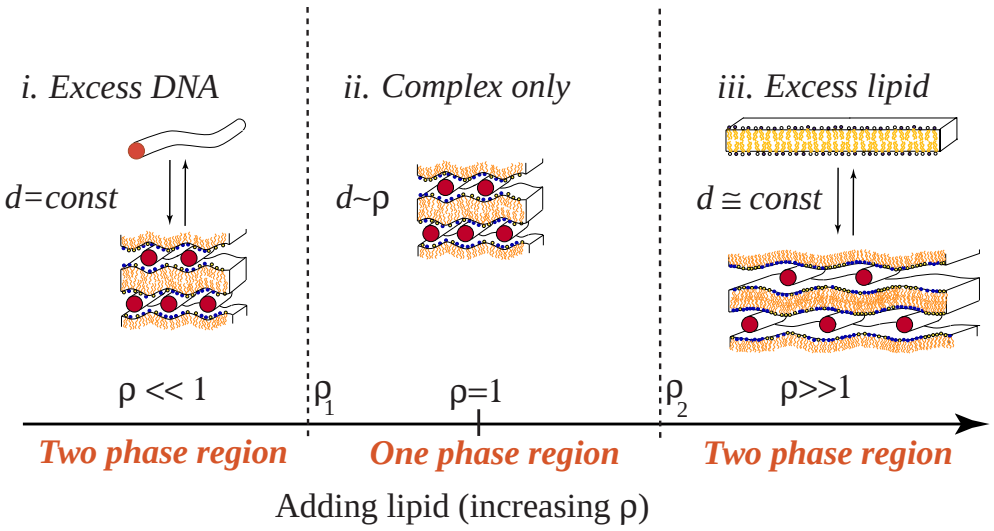

Figure 2.4: Schematic illustration of the phase evolution of L_α^C complexes (see text for details).

$\rho \leq \rho_1(\bar{\phi})$ which marks the onset of the next region. Once $\rho = \rho_1$ all the DNA is complexed so that $D_C = D = L/d_1$ and hence, from Eq. 2.9, $\rho_1 = \bar{\phi} d_1 (l/a)$. In general $\rho_1 < 1$.

ii) Between ρ_1 and a certain $\rho_2 = \rho_2(\bar{\phi}) > 1$ the system is one-phasic: all the DNA and lipid are involved in complex formation. Thus, $L_C = L$, $D_C = D$, and hence $d = L/D = (a/l)(\rho/\bar{\phi})$ increases linearly with the lipid/DNA ratio; from d_1 at ρ_1, through $d_I = d_I(\bar{\phi}) = (a/l)/\bar{\phi}$ at the isoelectric point ($\rho = 1$), to $d_2 = d_2(\bar{\phi})$ at $\rho_2(\bar{\phi}) = \bar{\phi} d_2 (l/a)$, which marks the onset of the third region. In general, $\rho_2 > 1$. Upon increasing ρ beyond the isoelectric point $\rho = 1$, the added lipids are first accommodated by the complexes, thereby d increases, and the condensates become "positively overcharged".

iii) For large L/D ($\rho > \rho_2$) the system is again bi-phasic, containing complexes which coexist with an excess bilayer phase; $D_C = D, L_C < L$. In this region the system possesses an extra thermodynamic degree of freedom, namely, the lipid composition of the complex, ϕ_C, (or, equivalently, ϕ_B which is related to ϕ_C by Eq. 2.8). Thus, unlike in region (i), ϕ_C (hence ϕ_B) need not be equal to $\bar{\phi}$. In other words, for any $\bar{\phi}$ and L/D, the system will adjust *both* d and ϕ_C so as to minimize its total free energy. Indeed, we shall see that in the excess bilayer regime both ϕ_C (hence ϕ_B) and d vary with ρ. It should be noted, however, that experimentally, $d \approx d_2(\bar{\phi})$ appears to be independent of ρ in region (iii). This result will be discussed in more detail in the next section.

In principle, the system may also exhibit three-phase (complex/bilayer/DNA) coexistence as well as bilayer/DNA coexistence (see Chap. 3). However, these conditions correspond to very narrow regions of the phase diagram (low ϕ values)

where the complexes are either unstable or only marginally stable. We shall thus focus on the three stage scenario outlined above.

Our analysis involves three possible phases: free DNA, free bilayer and complex. The first two may be regarded as incompressible condensed phases. On the other hand, the complex is "compressible" because both the DNA-DNA spacing, d, and the inter-bilayer spacing, h, may vary with $\bar{\phi}$ and L/D. However, both experiment and our calculations (next section) show that in general only d varies significantly with $\bar{\phi}$ and L/D, whereas h is essentially constant, $h \approx h^*$. In other words, for most ϕ_C and d, the complex free energy $f_C(\phi_C, d, h)$ has a narrow and deep minimum at h^*. In Sec. 2.3.1 we show how this minimum is a result of two opposing forces: the electrostatic and the short range hydration or other forces associated with excluded volume. Thus, we can safely treat $f_C = f_C(\phi_C, d) = f_C(\phi_C, d, h = h^*)$ as a function of only two variables.

For given $\bar{\phi}$ and L/D (and given l_D) the number and nature of the phases in solution are determined by the minimum of the total free energy

$$F = (D - D_C)f_D + D_C f_C(\phi_C, d) + (L - dD_C)\tilde{f}_B(\phi_B) \tag{2.10}$$

with respect D_C, d and ϕ_C, (ϕ_B depends on these three variables through Eq. 2.8).[4]

Setting $D_C = L/d, \phi_C = \bar{\phi}$ in Eq. 2.10 and minimizing F with respect to d, we find the equilibrium condition for region (i),

$$f_C(\bar{\phi}, d) - d\left(\frac{\partial f_C}{\partial d}\right)_{\bar{\phi}} - f_D = \left(\frac{\partial (f_C/d)}{\partial (1/d)}\right)_{\bar{\phi}} - f_D = 0 \tag{2.11}$$

This equation determines the equilibrium inter-axis distance in the complex, $d = d_1(\bar{\phi})$, in the presence of excess free-DNA. Based on this equation we anticipate that d_1 will be smaller than the "optimal" value, $d^* = d^*(\bar{\phi})$, corresponding to the minimum of $f_C(\bar{\phi}, d)$. This follows from the fact that the free energy of a DNA strand in a stable complex must be lower than in solution and hence $f_D - f_C(d, \bar{\phi}) > 0$, which means $(\partial f_C/\partial d)_{d=d_1} < 0$. Physically, the "overcrowding" ($d_1 < d^*$) of DNA strands in the complex results from the partial release of mobile counterions into solution upon bringing more DNA charges into contact with the cationic lipid charges. When $d = d_1$ this osmotic-like pressure of the DNA to enter the complex is balanced by DNA-DNA repulsion within the complex (the latter increases as d decreases).

In region (ii), where all the DNA and lipids are associated in complexes $F = Df_C(d, \bar{\phi})$ and $d = L/D$ increases *linearly* with the lipid to DNA ratio.

[4]Note, that contrary to what may be inferred from Eq. 2.10, the scenarios considered in this chapter will never include a free phase coexistence. We shall return to this point in the next chapter, where we show that theoretically a three phase coexistence is possible, it is experimentally hard to obtain.

(The linear increase reflects our assumption that the bilayer is planar and laterally incompressible.) At some point within this region, generally very close to $\rho = 1$, the complex free energy is minimal (i.e., $d_I(\bar{\phi}) \simeq d^*(\bar{\phi})$). The uptake of bilayer into the complex continues beyond this point, as long as the added lipids enjoy lower free energy in the complex as compared to that in the free bilayer. Eventually, at some $d = d_2(\bar{\phi}) > d^*$ (and $\rho = \rho_2(\bar{\phi}) > 1$) inter-bilayer repulsion becomes sufficiently large to forbid further accommodation of bilayer in the complex, marking the onset of region (iii). To support this qualitative description let us first consider the hypothetical case of *"blocked lipid exchange"* where $\phi_B = \phi_C = \bar{\phi}$. (This limit could perhaps be realized experimentally, as a transient state, if the rate of lipid exchange is small compared to that of complex formation.) Setting $D_C = D, \phi_C = \phi_B$ in Eq. 2.10 and minimizing F with respect to d we find,

$$\left(\frac{\partial f_C}{\partial d}\right)_{\bar{\phi}} - \tilde{f}_B(\bar{\phi}) = 0 \tag{2.12}$$

which determines $d_2 \equiv \hat{d}_2(\bar{\phi})$ for the case of blocked exchange. For this special case, let $\hat{\rho}_2(\bar{\phi})$ denote the value of ρ at the boundary between regions (ii) and (iii), corresponding to $\chi = dD/L = 1$ in Eq. 2.8. From Eq. 2.12 it follows that $d = \hat{d}_2(\bar{\phi})$ is constant throughout region (iii) ($\rho > \hat{\rho}_2(\bar{\phi})$, or $1 > \chi > 0$). Since $\hat{d}_2(\bar{\phi})$ is also the maximal d in region (ii) it follows that $\hat{\rho}_2(\bar{\phi}) = \bar{\phi}\hat{d}_2(l/a)$. Finally, since the bilayer charging energy, $\tilde{f}_B(\bar{\phi})$, is positive, it follows from Eq. 2.12 that $\hat{d}_2 > d^*$.

In the more general case of *free lipid exchange* the values of d, ϕ_C and ϕ_B in the bilayer-complex coexistence region are determined by the equilibrium conditions $(\partial F/\partial d) = 0$ and $(\partial F/\partial \phi_C) = 0$.[5] Noting that in this region $D_C = D$ and $(dD/L)\phi_C + (1 - dD/L)\phi_B = \bar{\phi}$ (see Eq. 2.8), we obtain,

$$\left(\frac{\partial f_C}{\partial \phi_C}\right)_d = d\frac{\mathrm{d}\tilde{f}_B}{\mathrm{d}\phi_B} \tag{2.13}$$

$$\left(\frac{\partial f_C}{\partial d}\right)_{\phi_C} - \tilde{f}_B(\phi_B) = (\phi_C - \phi_B)\frac{\mathrm{d}\tilde{f}_B}{\mathrm{d}\phi_B} \tag{2.14}$$

We could rewrite the last two equations in a slightly different form in terms of $\tilde{f}_C \equiv f_C/d$, the free energy per unit length of the complex, instead of, f_C, the

[5]Do not let the large number of introduced variables mislead you. In fact, when the system if bi-phasic containing complexes coexisting with free bilayers, there are only three variables that completely define the state of the two phases. These are d and ϕ_C for the complex phase, and ϕ_B for the free bilayer. The lipid to DNA charge ratio in the complex phase is simply related to d and ϕ_C through $dl\phi_C/a$. Furthermore, the free energies of type $\tilde{f}$ that appear in all the coexistence equations are *per unit length* of the complex.

free energy per unit cell. Then, *if* d were constant ("incompressible complex"), Eqs. 2.13, 2.14 would reduce to the familiar 'common tangent construction' for $\tilde{f}_C$ and $\tilde{f}_B$, representing the coexistence conditions of two incompressible binary mixtures. If this were the case we would also find that ϕ_C and ϕ_B are independent of χ. However, since the complexes are not incompressible, both d and ϕ_C (and hence also ϕ_B) may vary with χ, as will be shown in the next section.

2.2.4 Counterion release

Consider again an aqueous salt solution of volume V at temperature T, containing double stranded DNA of total length sD and $N = N^+ + N^0$ lipid molecules. We denote the concentration of fixed negative (DNA) charges in the system as $M^- = sD/lV$. Thus, $\bar{\phi} = N^+/N$ and $\rho = N^+/VM^-$.

Let m_+^C and m_-^C denote the excess numbers of counterions within a unit cell relative to the bulk solution. Thus,

$$m_\pm^C = s \iint \mathrm{d}x\,\mathrm{d}y\ \left[n_\pm^C(x,y) - n_0\right] \tag{2.15}$$

where $n_\pm^C(x,y)$ denote the local concentrations of counterions within the complex. The integration extends over the cross-sectional area, $d \times h$, of the unit cell; $h \approx 26$Å denoting the distance between apposed bilayer surfaces. We calculate the local ion concentrations using $n_\pm^C = n_0 \exp(\mp e\psi/k_BT)$, where $\psi = \psi(x,y)$ is the electrical potential. Again, for given ρ, $\bar{\phi}$ and n_0 we obtain ψ by solving, numerically, the nonlinear PB equation for the unit cell parameters.

For an isolated lipid bilayer, charge neutrality implies that the surface excess number of counterions is $m^B = 2sd\int \mathrm{d}y\,[n_+^B(y) + n_-^B(y) - 2n_0] = 2sd\bar{\phi}/a$; for monolayer area equal to that in a unit cell. The excess number of counterions around a DNA segment of length s is $m^D = s/l$. The number of counterions released into solution upon complex formation is $\Delta m = (m^D - m_+^C) + (m^B - m_-^C) = (1 + 2db\bar{\phi}/a) - (m_+^C + m_-^C) = 2(1 - m_+^C)$, per unit cell. (The last equality reflects charge neutralization, $m^D + m_-^C = m^B + m_+^C$.) The corresponding (small) change in free ion concentration is $2\Delta n_0 = K\Delta m$ where K is the number of unit cells, per unit volume. As an operational definition of the extent of counterion release we use the quantity

$$\xi = \frac{2\Delta n_0}{(N^+/V) + M^-} = 1 - \frac{K(m_+^C + m_-^C)}{(N^+/V) + M^-} \tag{2.16}$$

The first expression for ξ is measurable while the second can be calculated using PB theory (and the thermodynamic coexistence equations), enabling comparison of theory with experiment.

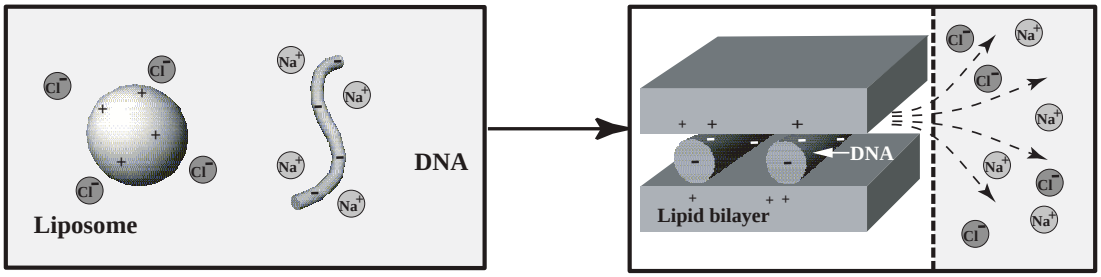

Figure 2.5: Schematic illustration of cationic liposomes and DNA condensing into a lamellar lipid-DNA complex. Counterions are released into the excess water phase

In the following section, we present ξ as a function of ρ for a low salt solution (4mM NaCl, corresponding to a Debye screening length of $l_D = 50$Å) containing DNA and an equimolar ($\bar{\phi} = 0.5$) CL/HL mixture. The phase boundaries, ρ_1 and ρ_2, were determined, as described in the previous section, by solving the thermodynamic coexistence equations. It can be shown theoretically that ξ exhibits different functional dependencies on ρ in the three regimes of the phase diagram. When the system is monophasic ($\rho_1 \leq \rho \leq \rho_2$), $K = D/V$ and hence $\xi = 1 - l(m_+^C + m_-^C)/[s(1+\rho)]$. This expression is also valid for $\rho > \rho_2$, i.e., when complexes coexist with an excess bilayer phase, implying a linear decrease of ξ with $1/\rho$ in the limit $\rho \to \infty$. When $\rho < \rho_1$, i.e., when complexes coexist with naked DNA, $K = N^+a/2d_1s\bar{\phi} = lN^+/s\rho_1$ and hence $\xi = 1 - l(m_+^{1,C} + m_-^{1,C})/s(\rho_1(1+1/\rho))$, implying $\xi \sim \rho$ as $\rho \to 0$.

In the next section, these theoretical predictions will be compared directly with experimental results (Wagner *et al.*, 2000). The experiment is schematically illustrated in Fig. 2.5. CL-DNA complexes were formed spontaneously upon mixing cationic vesicles and DNA. At high lipid-DNA concentrations the complexes are well above micron size and could easily be separated from the aqueous phase by centrifugation and filtration. Subsequently the number of released counterions was determined by the increase in conductivity of the supernatant. The concentration of free DNA in the supernatant was also measured by optical absorption. The experiments were carried out for 4mM NaCl solutions, enabling direct comparison with theory.[6]

2.3 Results and Analysis

Following the discussion in the previous section, we shall first present and analyze the numerical results for the free energy and structure of an isolated DNA-lipid

[6]The full experimental detail can be found in (Wagner *et al.*, 2000)

complex and then discuss the phase behavior of the solution. Finally, we will present the theoretical results for the extent of counterion release, and compare them with the experimental results. Comparison with detailed published data for L_α^C complexes will be presented for several systems, all composed of a solution containing a mixture of cationic (DOTAP) and nonionic helper (DOPC or DOPE) lipids for several values of $\bar{\phi}$, and linear (either λ-phage or plasmid) DNA, without added salt (Rädler *et al.*, 1997; Rädler *et al.*, 1998; Koltover, 1998). The bulk concentration of mobile ions in this system is low, but unknown exactly (as it is volume dependent). Thus, in most calculations we have used $n_0 \approx 4 \times 10^{-3} M$, corresponding to a Debye length $l_D = 50$Å. Very similar properties and phase behavior of the complex were found for larger values of l_D. Partial results will also be presented for $l_D = 10$Å, corresponding to physiological salt concentrations ($n_0 \approx 0.1M$). These calculations were also found to be in agreement with experimental results where salt was added to solution (Rädler *et al.*, 1998; Koltover, 1998). In all the calculations reported below we have used $R_D = 10$Å for the DNA radius and $a = 70$Å^2 for the average area per (both cationic and neutral) lipid head group.

2.3.1 Complex structure and stability

The electrostatic (charging) free energy per unit cell of the complex, f_C, is shown as a function of d for several values of ϕ_C in Fig. 2.6, (for $s = 1$Å$, l_D = 50$Å). Similarly, Fig. 2.7 shows f_C as a function of ϕ_C for several values of d.

All the results shown in Figs. 2.6 and 2.7 were obtained using $h = h^* = 26$Å, corresponding to a minimal distance of 3Å between the DNA and bilayer surfaces. This is the value of h^* observed experimentally for the L_α^C complex by Rädler *et al.* (1997). It should be noted, however, that h^* is larger than the minimal value of the inter-bilayer spacing, $h_{min} = 2R_D = 20$Å. In fact, for most values of ϕ_C, our calculations show that the electrostatic free energy of the complex decreases monotonically as h decreases, including the region $h^* > h > h_{min}$. Thus, we treat $h^* \approx 26$Å as the effective range of a "hard-wall" potential, representing the short range repulsive forces arising from hydration, protrusion and other excluded volume interactions (Israelachvili, 1992; Israelachvili & Wennerström, 1990). Subject to this condition we find that for all ϕ_C larger than ≈ 0.2 the minimum in $f_C(\phi_C, d, h)$ is always at $h = h^*$, regardless of d. For very low values of ϕ_C (less than 0.2) we find, for low d's, that the optimal value of h increases as d decreases, as demonstrated for $\phi_C = 0.15$ in the inset to Fig. 2.6. Note, however, that for these low ϕ_C's the minimum of f_C occurs at large d^*'s where, again, $h = h^*$. More generally, our conclusions regarding the complex structure

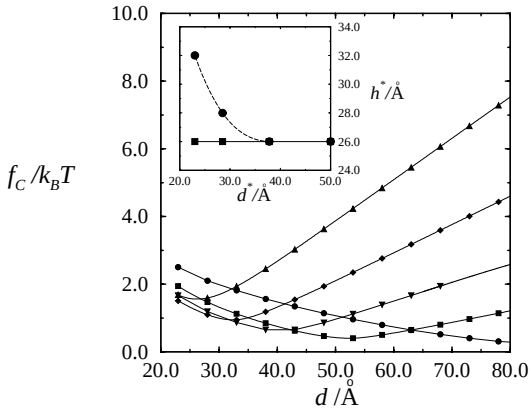

Figure 2.6: The free energy per unit cell of the complex as a function of the DNA-DNA spacing, for several different mole fractions of the cationic lipid: $\phi_C = 0.23(\bullet), 0.39(\blacksquare), 0.50(\blacktriangledown), 0.62(\blacklozenge), 0.78(\blacktriangle)$. The inset shows the optimal inter-bilayer distance, h^*, vs. the optimal DNA-DNA spacing, d^*, for a low lipid composition, $\phi_C = 0.15(\bullet)$. For all ϕ_C larger than ≈ 0.2 h^* is constant ($\blacksquare$).

and stability, as well as the phase behavior of the system are not sensitive to small variations in h^*.

In Fig. 2.6 we see that the optimal DNA spacing in the complex, d^*, is a decreasing function of ϕ_C. Similarly, Fig. 2.7 shows that the optimal complex composition ϕ_C^* is a decreasing function of the DNA-DNA distance.

Qualitatively, these results are easily understood. The minima in the electrostatic free energy are expected to occur when the fixed negative charges on the DNA surface are balanced by the same number of positive charges on the bilayer surface, i.e., at the isoelectric point. At this point the complex will remain electrically neutral even if all the mobile ions in its interior would be released into the bulk solution, thus increasing their translational entropy and consequently lowering the free energy of the system. Of course, some counterions will always remain within the complex water gaps, as dictated by the bulk value of their chemical potentials. However, the concentrations of these mobile ions will be much smaller than in the diffuse layers near the surfaces of the *non*-complexed DNA and membrane. Now, the total charge on the bilayer surface is proportional to $d \times \phi_C$ whereas the total charge on the DNA surface is constant. Thus, at the *isoelectric point* $d = d_I(\phi_C) = (a/l)/\phi_C$, explaining the decrease of $d_I \simeq d^*$ with ϕ_C. The inset to Fig. 2.7 shows how d_I and d^* vary with ϕ_C. The two curves are essentially identical, confirming that *the complex free energy is, indeed, minimal at the isoelectric point where counterion release is maximal.* Thus, hereafter, we set $d_I \equiv d^*$.

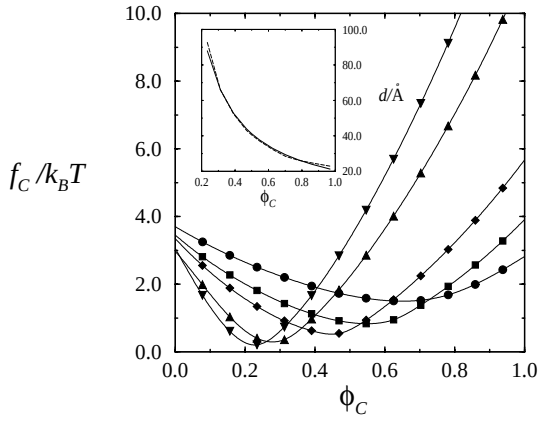

Figure 2.7: The free energy per unit cell of the complex, as a function of the lipid composition, for several values of the DNA-DNA spacing: $d = 23(\bullet), 33(\blacksquare), 43(\blacklozenge), 73(\blacktriangle), 93(\blacktriangledown)$Å. The inset shows how the optimal spacing, d^* (dashed line) and isoelectric spacing, d_I (solid line) vary with the lipid composition in the complex, revealing that d^* and d_I are essentially identical.

Figs. 2.6, 2.7 reveal also that the minimum value of the complex free energy $f_C^* \equiv f_C(\phi_C, d^*(\phi_C))$ varies rather weakly with ϕ_C. More generally, we note that upon changing ϕ_C (or d) the complex can change its d (or ϕ_C), i.e., "cross" to a neighboring free energy curve, without significantly changing its free energy. This ability of the complex, to change its composition (and d) at minimal free energy cost, is manifested when complexes coexist with an excess bilayer phase, in which case ϕ_C and ϕ_B are determined by the minimum of F (rather than f_C), as will be demonstrated in Sec. 2.3.2.

From the results in Fig. 2.6 it follows that inter-axis fluctuations, $\Delta d = [\langle (d - d^*)^2 \rangle]^{1/2}$, in a complex of a given lipid composition are expected to be quite small. The free energy cost of displacing a DNA strand of (minimal) length $l_p = 500$Å by a small distance $d - d^*$ from its equilibrium position is $\delta f_C \approx 2l_p[f_C(\phi, d) - f_C(\phi, d^*)]$. Our calculations show that for, say, $|d - d^*| \sim 1$Å and $\phi_C = 0.5$, this implies δf_C on the order of $\sim 100 k_B T$, indicating a negligible Δd.

When $d < d^*$ there is a net, negative, surface charge on the complex "walls". To ensure electrical neutrality, negative mobile ions must be brought from the bulk solution into the confines of the complex, thus increasing the free energy of the system. As d decreases the excess concentration of positive counterions increases, for two reasons: the increase of the excess surface charge and the decrease of the inner complex volume. The concomitant increase in the free energy of the complex, and hence the effective DNA-DNA repulsion, is due to the excess charging energy of the DNA surfaces, and the increased osmotic pressure

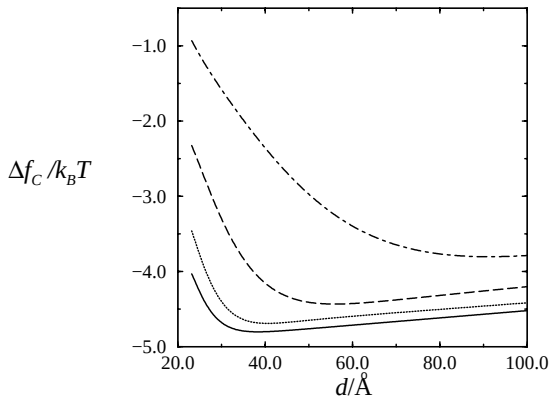

Figure 2.8: The formation free energy of the complex, as a function of d, for several values of the lipid composition, ϕ_C: 0.3 (dot-dashed line), 0.5 (dashed), 0.7 (dotted), 0.9 (full).

of the counterions within the complex interior. (A simple electrostatic model accounting for this behavior will be described in Sec. 2.4.)

Similarly, as d increases above d^* negative mobile ions must be brought into the complex in order to balance the excess positive charge on the (lipid bilayer) surfaces. However, unlike in the $d < d^*$ regime where counterion confinement depends strongly on d, in this region counterion confinement is mainly due to the finite bilayer spacing h. Since h is constant, f_C is expected to increase *linearly* with d (in the large d regime), as indeed observed in Fig. 2.6. The rate of this increase, i.e., $\partial f_C/\partial d$, is proportional to the electrostatic free energy per unit area of the bilayer in the complex. This free energy is a sum of the bilayer charging energy, which increases with ϕ_C (see below), and the inter-bilayer repulsion energy. For most values of ϕ_C considered here the complex conditions are those of the "Gouy-Chapman regime" (Andelman, 1995) where the inter-bilayer interaction energy is independent of the surface charge density. Thus, the ϕ_C dependence of the asymptotic slope of f_C in Fig. 2.6 is mostly due to the charging energy of the lipid monolayers.

These notions are confirmed in Fig. 2.8, which shows the formation free energy of the complex, Δf_C, as a function of d for several values of ϕ_C. Note from Eq. 2.1 that this quantity, which represents the net stabilization energy of the complex, is obtained from f_C after subtracting the charging energy of the non-complexed DNA and bilayer. Thus, the steep variation of Δf_C at small values of d is dominated by the strong DNA-DNA repulsion (counterion confinement) in this regime. Similarly, the increase of Δf_C at high d's ($d \gg d^*$), is due, almost exclusively, to inter-bilayer repulsion. From the discussion above it follows that

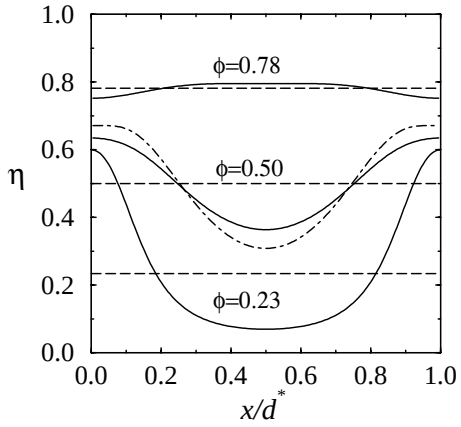

Figure 2.9: Spatial modulations of the cationic lipid charge within a unit cell of the complex. The local charge density profile, $\eta(x)$ (between two neighboring DNA strands), is shown (full lines) for complexes of three lipid compositions: $\phi_C = 0.23, 0.50, 0.78$. All complexes are at their isoelectric value, $d^* \approx 89$, 41, 26 Å respectively. The horizontal (dashed) lines correspond to uniform charge densities. The dash-dotted line, corresponding to $\phi_C = 0.5$, shows the charge density profile in a (hypothetical) complex where charge modulation (lipid demixing) does not involve any entropy penalty. Note that in all but the highest ϕ_C case, cationic lipid is pushed out from in between the DNA positions.

in this region $\partial \Delta f_C / \partial d$ should be nearly independent of ϕ_C, as confirmed by Fig. 2.8.

From the results in Fig. 2.8 we also conclude that stable complexes ($\Delta f_C < 0$) can be formed for a wide range of lipid compositions. The complex stabilization energies are on the order of a few $k_B T$'s per unit cell. For a "mesoscopic" complex, containing DNA strands of total length on the order of, say, $1\mu m$ this implies a total stabilization energy of order $10^4 k_B T$.

In the previous section we have emphasized the fact that the lateral distribution of the cationic lipid charges in the complex need not be uniform. Indeed we find that the actual charge distribution is polarized, reflecting a compromise between the tendency to minimize the electrostatic energy on the one hand, and the unavoidable demixing entropy penalty on the other. The extent of spatial charge modulations in the complex is demonstrated in Fig. 2.9. The figure shows the variation of the local charge density $\eta(x)$ between two neighboring DNA strands, for complexes of three lipid compositions (high, low and equi-molar $\phi_C = \langle \eta(x) \rangle$), all at their isoelectric (i.e., optimal) value of d.

When ϕ_C is low, d^* is necessarily large. To effectively screen the negative DNA charges, cationic lipids must be displaced over a relatively large distance, resulting in a dramatic charge modulation. On the other hand, when ϕ_C is large, d is small, and the charge segregation is rather weak. In fact, in this case some of

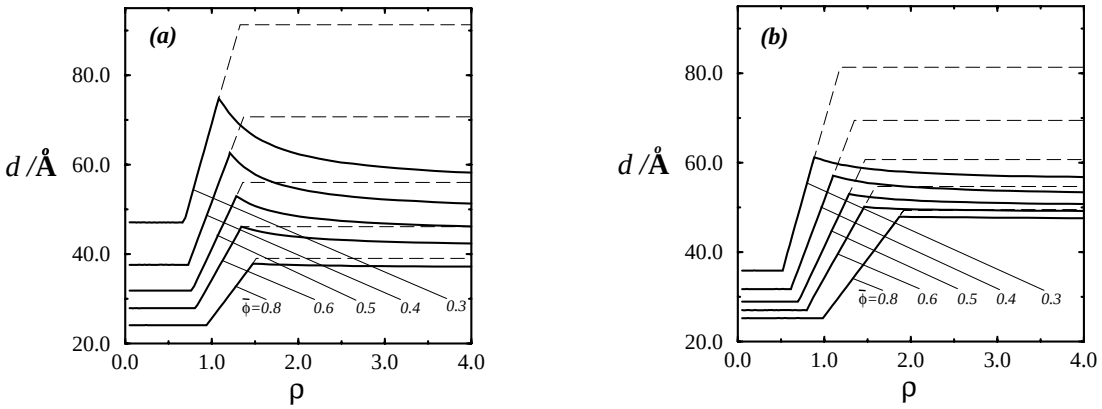

Figure 2.10: The DNA-DNA spacing d in the complex, as a function of the charged-lipid to DNA ratio ρ, for several lipid compositions: $\bar{\phi} = 0.3,\ 0.4,\ 0.5,\ 0.6,\ 0.8$ (solid lines). For each value of $\bar{\phi}$, the dashed curve describes the variations in d for the case of blocked lipid exchange. (a): $l_D = 50$Å. (b): $l_D = 10$Å.

the charged lipids are shifted from the immediate vicinity of the DNA towards the center of the unit cell, as their optimal local concentration near the DNA strands is lower than ϕ_C. (Recall, the charge density on the DNA surface corresponds to one elementary charge per ≈ 110 Å^2. The average charge density on the bilayer surface is ϕ_C/a which, for $\phi_C = 0.78$, corresponds to one elementary charge per ≈ 90Å^2.) Intermediate, though substantial charge modulation is found for the equi-molar lipid mixture, $\phi_C = 0.5$. For this system we also show, for comparison, the charge density profile in the hypothetical case that lipid segregation does not involve a demixing entropy penalty. (Namely, we artificially ignore the lipid mixing entropy contribution to f_C. The PB equation is then solved subject to the condition of constant electrical potential on the bilayer surfaces, as if they were conducting sheets.) As expected, the charge modulation in this system is still more dramatic than in the "real" complex. In all these cases, a clear tendency for charge matching (thus maximal counterion release) opposed to some degree by the lipid demixing penalty is observed.

2.3.2 Phase evolution

In Figs. 2.10a,b we show how d, the DNA-DNA spacing in the complex, varies with $\rho = \bar{\phi}(l/a)L/D$, the (scaled) charged-lipid to DNA ratio in solution. The $d - \rho$ plots in Fig. 2.10a were calculated for a solution of low salt content, $l_D = 50$Å, and several different lipid compositions $\bar{\phi}$. Similar calculations are shown in Fig. 2.10b for $l_D = 10$Å.

These calculations provide the most critical test of our model since d is an experimentally measurable quantity. The experimental $d - \rho$ data points (adapted

from (Rädler *et al.*, 1997; Koltover, 1998)), which were obtained for solutions of ($\bar{\phi} = 0.5\,0.3\,0.7$) and without added salt, are shown in Fig. 2.11a,b. Also shown in this figure are the theoretical curves corresponding to $l_D = 50$Å for $\bar{\phi} = 0.3, 0.4, 0.5, 0.6, 0.8$ (for $\bar{\phi} = 0.5$ we also present curves corresponding to $l_D = 10$Å). The low-salt ($l_D = 50$Å) results show reasonable agreement with the experimental data. There is, however, a systematic difference, particularly in the large ρ regime (region *iii*). In this region the experimental results for d are generally intermediate between the theoretical prediction for the *free lipid exchange* condition and the *blocked lipid exchange* case. A possible explanation is that the experimental conditions are also intermediate between these two (theoretical) conditions considered. Also, there is some evidence that the DOTAP and DOPC lipids pair together in the membrane (the positively charged DOTAP binds to the negatively charged phosphate group on DOPC) (Bandyopadhyay *et al.*, 1999). This may lead to a necessarily smaller charge density modulation, since some of the charged lipids are bound to neutral lipids, so that their (local) charge density is at most $e/2a$ (already rather close to the charge density on DNA $\sigma^- \approx e/110\text{Å}^2$.

The $d-\rho$ "phase diagrams" in Figs. 2.10, 2.11 were calculated using Eq. 2.11 for region (i) (excess DNA), and Eqs. 2.13, 2.14 together with the lever-rule, Eq. 2.8, for region (iii) (excess bilayer). Eq. 2.11 yields $d_1 = d_1(\bar{\phi})$ for the complex-DNA coexistence region (i), $0 \leq \rho \leq \rho_1(\bar{\phi}) = \bar{\phi} d_1(l/a)$.

In the one phase (complex) region (ii), $d = L/D = (a/l)(\rho/\bar{\phi})$ varies linearly with ρ. The slope, $\partial d/\partial\rho$, in region (ii) is inversely proportional to the charged lipid mole fraction, $\bar{\phi}$.

For region (iii) the calculation is a little more complicated because of the additional, lipid composition degree of freedom. For each value of $\bar{\phi}$, the solution of Eqs. 2.13, 2.14, 2.8 yields d, ϕ_C, ϕ_B as a function of ρ in the complex-bilayer coexistence region (iii). The onset of this region is at $\rho_2 = \bar{\phi} d_2(\bar{\phi})(l/a)$. At this point all lipids are still complexed and hence $\chi = d_2 D/L = 1$ and $\phi_C = \bar{\phi}$, but $\phi_B \neq \bar{\phi}$. The inset to Fig. 2.11a shows how the (calculated) lipid compositions in the complex and free bilayer (in the "excess bilayer" regime) vary with the charged-lipid to DNA ratio. As shown in the figure (and in more detail in Fig. 2.12 below), we generally find that at point ρ_2, $\phi_B < \bar{\phi}$. As ρ increases (hence χ decreases) we find, for all values of $\bar{\phi}$, that d decreases monotonically, reaching the asymptotic value $d = d_\infty(\bar{\phi})$ as $\rho \to \infty$. In this limit we have $\chi \to 0$ and hence $\phi_B \to \bar{\phi}$, but now $\phi_C \neq \bar{\phi}$; in general we find that, asymptotically, $\phi_C > \bar{\phi}$. From Fig. 2.10 it is apparent that the change in d in region (iii), i.e., the difference $d_2 - d_\infty$ is generally small, essentially negligible for low l_D and/or large $\bar{\phi}$.

The dashed curves in Figs. 2.10 show, for comparison, how d varies with ρ

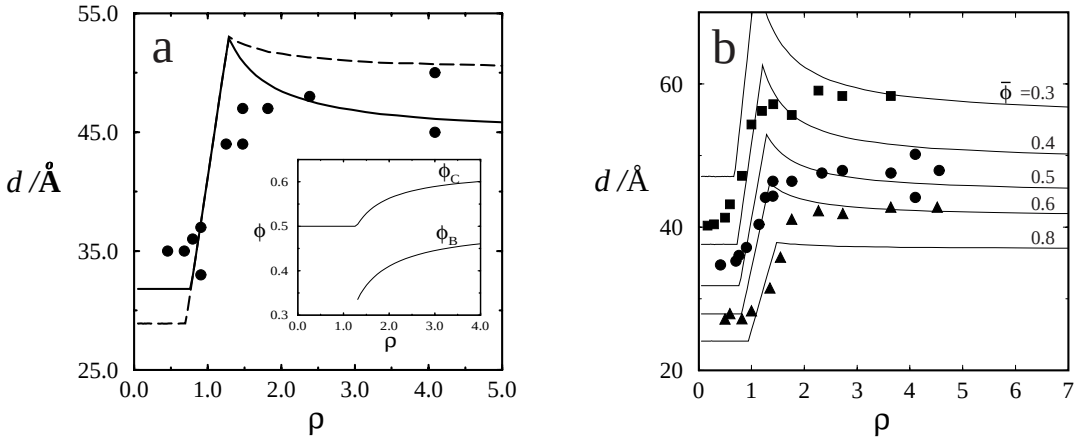

Figure 2.11: (a) The DNA-DNA spacing, d, as a function of charged lipid to DNA ratio, ρ, for $\bar{\phi} = 0.5$; $l_D = 50$Å (solid line), 10Å (dashed line). The dots are the experimental data of Rädler *et al* (1997). The inset shows the variation of lipid composition in the complex and free bilayer as a function of the charged lipid to DNA ratio, for $l_D = 50$Å. (b) DNA-DNA spacing as a function of ρ in series of theoretical and experimental results. The theoretical results correspond to (top to bottom) $\bar{\phi} = 0.3$, 0.4, 0.5, 0.6, 0.8; all results are for $l_D = 50$Å. The experimental results correspond to: $\bar{\phi} = 0.3(\blacksquare), 0.5(\bullet), 0.7(\blacktriangle)$ and for no added salt. [experimental results adapted from (Koltover, 1998)].

in the limit of "blocked lipid exchange". For this case, regardless of the value of $\bar{\phi}$, we see that the onset of region (iii) is postponed to a larger L/D ratio, corresponding to $\rho = \hat{\rho}_2 > \rho_2$ and consequently $d = \hat{d}_2 > d_2$. For this special case $d = \hat{d}_2$ in region (iii) is independent of ρ. The difference between the cases of "blocked" and "free" lipid exchange is particularly pronounced for small values of $\bar{\phi}$.

Qualitatively, the difference $\hat{d}_2(\bar{\phi}) - d_2(\bar{\phi}) > 0$, which reflects the role of lipid exchange between the complex and the free bilayer can be explained as follows. In the case of blocked exchange ($\phi_B = \phi_C = \bar{\phi}$) a free bilayer first appears when the increase in f_C upon adding lipids to the complex becomes larger than the electrostatic free energy of these lipids when organized in a free bilayer; see Eq. 2.12. This happens at $\rho = \hat{\rho}_2(\bar{\phi})$ and $d = \hat{d}_2(\bar{\phi})$. Suppose now that, at this point, we allow for lipid exchange between the complex and the bilayer. The bilayer (charging) energy can be significantly reduced by diluting its charges with neutral lipids which can be imported from the complex, thus making $\phi_B < \bar{\phi}$. This, in turn, implies an increase in the complex charge density, from $\bar{\phi}$ to $\phi_C > \bar{\phi}$. However, this change can be accommodated at a minimal free energy cost since, simultaneously, the complex can adjust (lower) its d, to ensure better electrostatic balance. The net result of this lipid-demixing process is an

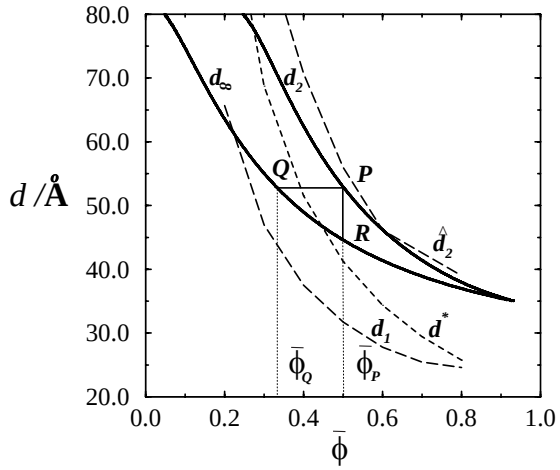

Figure 2.12: DNA-DNA distances in the complex at phase boundaries, as a function of the overall lipid composition in solution; d_2 and d_∞ represent, respectively, the inter-axial distance at the onset of complex-bilayer coexistence and in the limit of infinite excess of bilayer. $\hat{d}_2$ marks the onset of complex-bilayer coexistence for the case of blocked lipid exchange. Also shown are the DNA-DNA spacing at the isoelectric point (d^*), and at the limit of the complex-DNA coexistence region (d_1).

increase in the amount of free bilayer. Although imaginary, this process clearly accounts for the "earlier" appearance ($\rho_2 < \hat{\rho}_2$, $d_2(\bar{\phi}) < \hat{d}_2(\bar{\phi})$) of bare bilayer in a system where lipid exchange is free.

In Fig. 2.12 we show how d_2 and d_∞, the values of d at the boundaries of region (iii), $\chi = 1$ and $\chi = 0$, respectively, vary with the overall lipid composition $\bar{\phi}$. The figure also shows $d_1(\bar{\phi})$, the value of the inter-axis distance in the complex, at the phase boundary between regions (i) and (ii). Two additional curves, marked $d^*(\bar{\phi})$ and $\hat{d}_2(\bar{\phi})$, describe the interaxis distance at the isoelectric point and the boundary between regions (ii) and (iii) for the case of blocked lipid exchange, respectively.

The d_2 and d_∞ curves in Fig. 2.12 can be viewed as a "distillation diagram", prescribing the lipid compositions in complexes (of well defined d) and free bilayers, when these two phases coexist in solution. More explicitly, consider a pair of points, such as P and Q, one on the d_2 and the other on the d_∞ curves, both corresponding to the same value of d. Then, the projections of these points on the $\bar{\phi}$ axis, $\phi_C = \bar{\phi}_P$ and $\phi_B = \bar{\phi}_Q$, give the lipid compositions of the complex and free bilayer, for all values of $\bar{\phi}$ in the range $\phi_C \geq \bar{\phi} \geq \phi_B$, provided the inter-axis distance in the complex is d. This follows from the fact that, for this d, the points ϕ_B and ϕ_C represent the unique solution of the coexistence conditions Eqs. 2.13, 2.14. The relative amounts of lipid in the complex and the bilayer, are dictated by the "lever rule" $\chi\phi_C + (1-\chi)\phi_B = \bar{\phi}$. In particular, when $\chi = 1$ and hence $\phi_C = \bar{\phi}$ (and $d = d_2$, point P) ϕ_B is the bilayer composition at the

onset of region (iii); similarly, when $\chi = 0$ and hence $\phi_B = \bar{\phi}$ ($d = d_\infty$, point Q) ϕ_C is the asymptotic value of the complex composition. Experimentally it is of course easier to follow a vertical line, $\bar{\phi} = constant$, such as that between points P and R. Any point on this line dictates a given value of d and hence, as above, a pair of coexisting compositions ϕ_C, ϕ_B. Since $\bar{\phi}$ is known, one obtains χ using the lever rule, and then the lipid/DNA ratio from $\rho = d(\bar{\phi}/\chi)(l/a)$.

2.3.3 Extent of ion release

The experimental and theoretical results for ξ are shown in Fig. 2.13a. Theoretically, we find that $\xi \simeq 1$, i.e. complete counterion release, at the isoelectric point, $\rho = 1$. The experiments (Wagner *et al.*, 2000) show maximal release at a slightly larger value of ρ; the difference may be due to the finite size of the condensate and by other experimental uncertainties. The fractional release of counterions decreases monotonically on both sides of the isoelectric point. Within the one-phase region ($\rho_1 \leq \rho \leq \rho_2$) the decrease is linear, reflecting the negative ($\rho < 1$) and positive ($\rho > 1$) "overcharging" of the complex by fixed charges. For the system considered, the calculations yield $\rho_1 \simeq 0.77$ and $\rho_2 \simeq 1.3$. At both ρ_1 and ρ_2 there is a change in the slope of the ξ vs. ρ curve, corresponding to passages between the one- and two-phase regions. At ρ_1 the change in slope is hardly noticeable, both theoretically and experimentally. However, the complete complexation of DNA at ρ_1 is clearly reflected in Fig. 2.13b, which shows α, the fraction of free DNA in solution. The second phase boundary ($\rho = \rho_2$) is indicated, both experimentally and theoretically, by the change in slope of the ξ versus ρ curve.

In Fig. 2.14 we show how $\Delta f_C = \Delta E - T\Delta S$, the formation free energy of the L_α^C phase, per unit cell, varies with ρ, for $\bar{\phi} = 0.5$, and $n_0 = 4mM$. Here we have used $s = l = 1.7$Å, so that there is exactly one DNA charge in each unit cell. $-T\Delta S$ is the contribution to Δf_C from the entropy gain associated with the release of counterions, whereas ΔE is the change in the electrostatic energy (in which we include the very small contribution resulting from the lipid demixing entropy). The most striking result of these calculations is the large contribution of the counterion release entropy, reaching its absolute and relative maximum, ($-T\Delta S/\Delta f_C \approx 0.97, \Delta f_C \approx -7.5 k_B T$), at the isoelectric point, $\rho = 1$. Note that Δf_C is minimal at ρ slightly larger than 1; again, the moderate increase of Δf_C at larger ρ arises from the weak repulsion between the apposed cationic monolayers. The maximum of ΔS at isoelectricity is not surprising, because at this point electrical neutrality can be achieved by the fixed macroion charges. When ρ is less than 1 positive counterions must be present within the condensate. Since d,

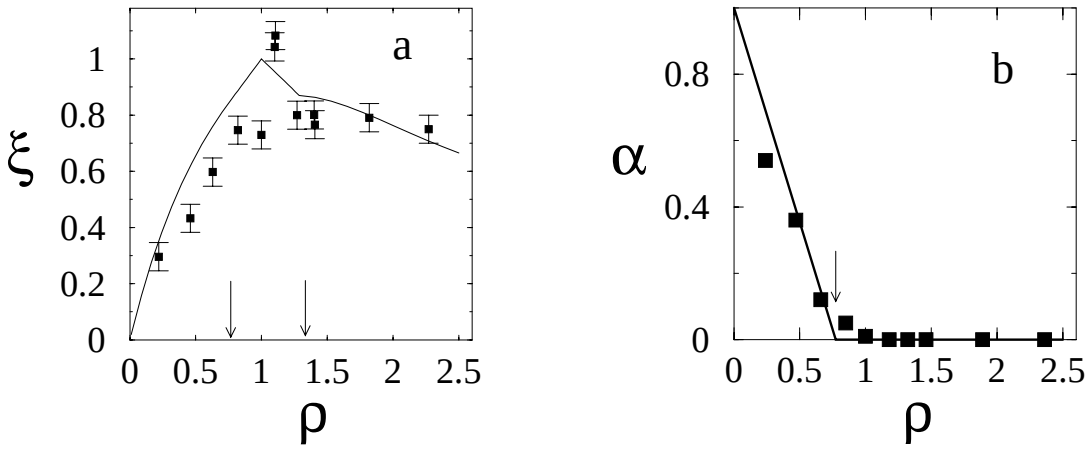

Figure 2.13: a) The fraction of counterions released upon complex formation as a function of the CL/DNA charge ratio, for an equimolar lipid mixture, $\bar{\phi} = 0.5$. The results from conductivity measurements are shown as solid squares. The solid curve is the theoretical prediction for the 4mM NaCl solution. The arrows mark the theoretical phase boundaries, ρ_1 and ρ_2. b) The fraction, α, of free DNA in solution, as determined by optical absorption at $260nm$ (squares) and the theoretical calculations (solid curve). The arrow marks ρ_1.

the distance between DNA strands, decreases with ρ, a larger number of highly confined counterions enter the complex as ρ decreases, explaining the steep rise in $T\Delta S$ on this side of the isoelectric point. Additional, negative, counterions also enter the complex when ρ increases beyond 1. Here, however, d increases while the spacing between the confining bilayer surfaces, h, is constant. Since h is comparable to the screening length of the isolated lipid layers the increase in $-T\Delta S$ in this regime is quite moderate.

Somewhat less expected is the small value of $|\Delta E|$, reaching its minimum at $\rho = 1$. This is because the electrostatic attraction between the DNA and lipid surfaces is largely compensated by the electrostatic repulsion between the apposed DNA and cationic lipid surfaces.

A qualitative estimate of the entropy gain associated with counterion release can be obtained as follows. Let $\bar{n}_+$ and $\bar{n}_-$ denote, respectively, the "effective" concentrations of counterions in the vicinity of the lipid bilayer and DNA surfaces prior to complexation. Now suppose, based on our calculations, that all counterions which are not needed for charge neutrality in the bound state are indeed released. For $\rho = 1$, this implies $\Delta S \approx 2k_B \ln(\bar{n}/n_0)$ where $\bar{n} = \sqrt{\bar{n}_+\bar{n}_-}$ is the mean "effective" concentration of counterions in the diffuse layers. Rather than estimating ΔS using $\bar{n}$, let us estimate $\bar{n}$ using the calculated value $T\Delta S = 7.5k_BT$. For $n_0 = 4mM$ this implies $\bar{n} \approx 0.17M$. Noting that the areas per fixed charge on the membrane and DNA surfaces are similar, $\approx 120\text{Å}^2$, we obtain $l_{eff} \approx 80\text{Å}$

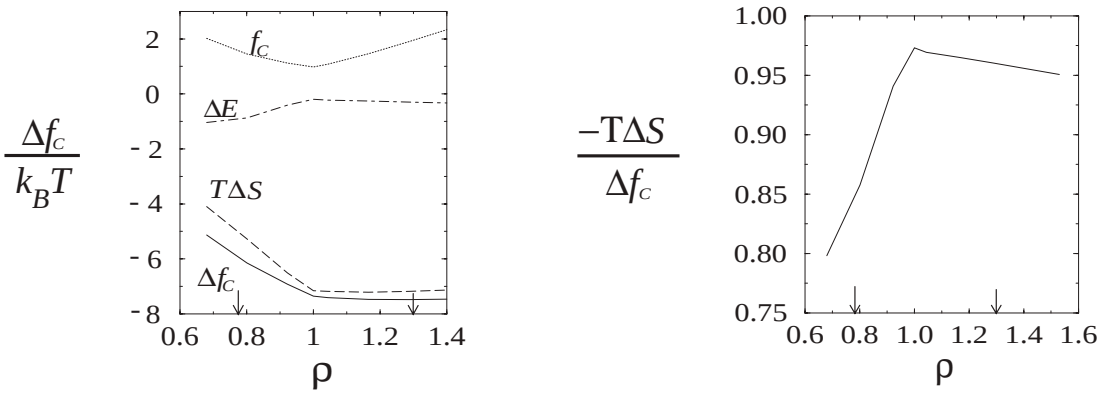

Figure 2.14: *Left*: Δf_C – the formation free energy of the L_α^C phase, per unit cell, as a function of the lipid/DNA charge ratio, ρ .$-T\Delta S$ and ΔE are the counterion entropy and electrostatic energy contributions, respectively. f_C is the charging free energy of the complex. *Right*: The relative contribution of the counterion entropy to the formation free energy. The arrows mark the phase boundaries.

for the "effective thickness" of the diffuse counterion layers. This value is comparable to the screening length of the, separated, charged surfaces, which should be on the order of the Debye length $l_D = 50$Å.

Our calculations reveal that the entropic contribution to the association free energy of the L_α^C complex is dominant, essentially complete at the isoelectric point. More generally, the entropic and energetic components of the complex formation free energy should depend sensitively on its geometry. It is expected, for instance, that the energetic contribution to the formation free energy of the hexagonal (H_{II}^C) CL-DNA phase is larger than that of the L_α^C phase, owing to the more favorable (concentric) configuration of the oppositely charged surfaces in this geometry (Koltover *et al.*, 1998; May *et al.*, 2000a; May & Ben-Shaul, 1997).

2.4 Discussion and summary

We have seen in the above that inter-bilayer repulsion in the complex is responsible for the fact that the amount of bilayer which the complex can accommodate is finite, resulting in the appearance of a free bilayer phase once ρ exceeds $\rho_2(\bar{\phi}) > 1$. Similarly, inter-DNA repulsion is responsible for the finite amount of DNA (in excess of that at the isoelectric point) which can be incorporated into the complex, resulting in the appearance of free DNA in solution when ρ falls below $\rho_1(\bar{\phi}) < 1$. In the previous section, based on numerical calculations of the complex free energy and the coexistence conditions, we have shown how $\rho_1(\bar{\phi})$, $d_1(\bar{\phi}) = \rho_1(\bar{\phi})(a/l\bar{\phi})$, $\rho_2(\bar{\phi})$ and $d_2(\bar{\phi}) = \rho_2(\bar{\phi})(a/l\bar{\phi})$ vary with $\bar{\phi}$. Now we provide a qualitative interpretation of these results, based on a simple "box" model of the

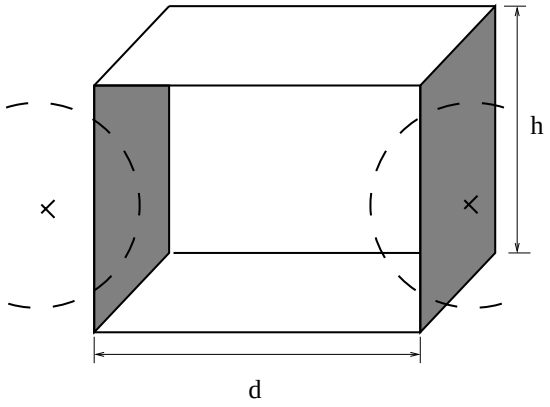

Figure 2.15: The complex unit cell used in the box model. The broken circles illustrate the DNA cross-section. In the model, these are the shaded surfaces.

complex. As we shall see, this model, though highly approximate, captures the essential physical principles governing the complex stability, and yields simple closed form expressions for d_1, d_2, ρ_1 and ρ_2.

2.4.1 A simple box model

The complex unit cell may be viewed as a box, bounded ("above and below") by two positively charged lipid bilayer "walls", and ("to the left and right") by two negatively charged DNA "walls". The third dimension of this box, along the DNA axis direction, is infinite.

The free energy of the complex reflects the charging energy of these walls, as well as the interactions between these charged surfaces (associated with the confinement of mobile ions to the complex "box"). Similar factors would dictate the complex free energy if the DNA surfaces were planar rather than curved, as shown in Fig. 2.15, which illustrates our box model. Of course, the finite curvature of real DNA surfaces is important for determining the numerical value of the complex free energy, but not the *qualitative* dependence of this quantity on such factors as the lipid charge density ($\bar{\phi}$) and the asymmetry (d/h ratio) of the unit cell . Thus, our first approximation is to replace the curved DNA surfaces by planar surfaces of height h, extending between the two planar bilayers. The distance between these walls will be denoted as d. (As indicated in Fig. 2.15 this d represents an intermediate value, smaller than the inter-axis separation and larger than the inter-surface spacing between neighboring DNA rods. An exact identification of d is irrelevant, as all our conclusions involve the ratio d/d^*.)

The complex free energy is minimal at the isoelectric point where the net charge on the complex walls is zero. Above the isoelectric point ($\rho > 1, d > d^*$)

the net charge on the complex walls is positive, with the excess, *uncompensated*, charge spread over the bilayer surfaces. Similarly, when $\rho < 1$, an excess negative charge is spread over the DNA surfaces. The complex free energy will be calculated based on two assumptions reflecting these notions. First, it will be assumed that the electrostatic free energy of the complex arises, completely, from the excess charging of the bilayer surfaces when $\rho > 1$ and from the excess charge on the DNA surfaces when $\rho < 1$. Second, to model the free energy between a pair of charged (e.g., bilayer) walls we shall treat them as infinite two-dimensional surfaces, in the regime where the Debye length (l_D) greatly exceeds the Gouy-Chapman length (l_{GC}). (More specifically, we shall consider the "Gouy-Chapman regime" where l_D is larger than l_{GC} as well as the spacing between the charged surfaces i.e., d and h)

For $\rho > 1$ the net charge density on the bilayer surfaces is $\sigma^+_{net} = (d\sigma^+ - h\sigma^-)/d = \sigma^+ - (h/d)\sigma^-$ where $\sigma^+ = e\bar{\phi}/a$ is the actual cationic surface charge density. Similarly, $\sigma^- = e/2hl$ is the charge density on the planar surface representing (one half of) the DNA envelope. In analogy to the bilayer composition we define $\bar{\phi}_D = (e/a)\sigma^- = a/2hl$ as the dimensionless charge density ("composition") of the DNA surface. (Recall, $l = 1.7$Å is the separation between charges along a DNA strand. Using also $a = 70\text{Å}^2$ and $h = 26$Å we find $\bar{\phi}_D \approx 0.8$.) The excess charge density on the bilayer surfaces is given by

$$\phi = \bar{\phi} - \frac{h}{d}\bar{\phi}_D = \bar{\phi}(1 - \frac{d^*}{d}) \qquad (\rho > 1) \tag{2.17}$$

Similarly, the excess charge density on the DNA surfaces is given by

$$\phi_D = \bar{\phi}_D - \frac{d}{h}\bar{\phi} = \bar{\phi}_D(1 - \frac{d}{d^*}) \qquad (\rho < 1) \tag{2.18}$$

For the electrostatic free energy of the complex, above the isoelectric point, we write

$$f_C = Ad(2\phi[\ln(D\phi) - 1] + B/h) \qquad (\rho > 1) \tag{2.19}$$

whereas below the isoelectric point

$$f_C = Ah(2\phi_D[\ln(D\phi_D) - 1] + B/d \qquad (\rho < 1) \tag{2.20}$$

where $A = 2sk_BT/a, D = 4\pi l_B/\kappa a$ and $B = \pi a/2l_B$ are constants; s denoting the (arbitrary) depth of the unit cell. The first term in Eq. 2.19 accounts for the excess charging energy of the bilayer surfaces (from 0 to ϕ) in the low salt (high l_D) limit, and follows from Eq. 2.3 for $p \approx q \gg 1$. The second term in this equation represents the electrostatic interaction between two equally charged surfaces, separated by a distance h, corresponding to the conditions defining the Gouy-Chapman regime ($h \gg (1/p\kappa) \equiv l_{GC}$). Eq. 2.20 is, similarly, the electrostatic

energy corresponding to excess (negative) charge on the DNA surfaces, whose area is proportional to h and whose separation is d.

To solve the coexistence conditions we also need the free energies of the bare bilayer and the naked DNA. The electrostatic free energy of the bilayer is given by the first term in Eq. 2.19, with the actual charge, $\bar{\phi}$, replacing the net charge ϕ; namely, $f_B = Ad(2\bar{\phi}[\ln(D\bar{\phi})-1])$. Our analysis of the bilayer-complex coexistence will be limited to the simpler case of "blocked lipid exchange". In this case the lipid mixing free energy in the free bilayer and the complex are identical and can thus be disregarded. For the charging energy of the naked DNA surfaces (which, for consistency, we treat as planar) we have $f_D = Ah(2\bar{\phi}_D[\ln(D\bar{\phi}_D) - 1]$.

Using the above expressions for f_C and f_B in the bilayer–complex coexistence condition, Eq. 2.12, we obtain

$$\ln\left(1 - \frac{d}{d^*}\right) + \frac{d^*}{d} + \frac{B}{2h\bar{\phi}_D} = 0 \qquad (\rho > 1) \qquad (2.21)$$

The solution of this equation, $d = \hat{d}_2(\bar{\phi})$, determines the value of d at the boundary between regions (ii) and (iii) for the case of blocked lipid exchange. Correspondingly, $\hat{\rho}_2(\bar{\phi}) = \bar{\phi}\hat{d}_2(\bar{\phi})(l/a)$.

Suppose first that $B = 0$, as would be the case if there were no repulsion between the charged bilayer surfaces in the complex. For this, hypothetical, case we find $\hat{d}_2(\bar{\phi}) \to \infty$. This result is consistent with the fact that, for all finite d, the effective charge on the complexed bilayer, ϕ, is smaller than that of the free bilayer, $\bar{\phi}$. Consequently, in the absence of inter-bilayer repulsion, the complex free energy is always lower than that of the free bilayer, which explains the unbound uptake of bilayer into the complex. We know, however, that $\hat{d}_2(\bar{\phi})$ is not much larger than d^* (see Fig. 2.10); i.e., bilayer repulsion is important. For $d^*/d \lesssim 1$ we find from Eq. 2.21,

$$\hat{d}_2 = d^*/(1 - \exp[-(1 + B/2h\bar{\phi})]) \qquad (\rho > 1) \qquad (2.22)$$

indicating that $\hat{d}_2(\bar{\phi})/d^*$ is a decreasing function of $\bar{\phi}$. For the molecular parameters used in our calculations we find $B/h \approx 0.6$. For $\bar{\phi} = 0.5$ this implies $\hat{d}_2/d^* \approx 1.25$, in surprisingly good agreement with the value obtained from our detailed calculations $\hat{d}_2/d^* \approx 1.3$.

Using the complex-DNA coexistence condition, Eq. 2.11, an equation similar to Eq. 2.21 can be derived for $d/d^* = d_1(\bar{\phi})/d^*$ in the region $\rho < 1$. Here, for $d/d^* \lesssim 1$, we find

$$d_1 = d^*(1 - \exp[-(1 + B\bar{\phi}/h\bar{\phi}_D^2)]) \qquad (\rho < 1) \qquad (2.23)$$

From this equation it follows that as $\bar{\phi}$ increases, $d_1 \to d^*$, in qualitative agreement with the results shown in Fig. 2.10. For the equi-molar system ($\bar{\phi} = 0.5$)

we find $d_1/d^* \approx 0.77$, which, perhaps fortuitously, is nearly identical to the result derived from our detailed calculations.

Considering the drastic approximations and assumptions involved in the formulation and solution of the simple box model we obviously do not expect that this model should confirm all our findings. For instance, we did not even try to include in this model the (important) effects of lipid charge modulations, nor to account for the more complicated case of free lipid exchange. Note also, that none of the above equations reflects the dependence of the phase boundaries on the salt concentration in the system, (which follows from the fact that the model was applied for the Gouy-Chapman regime, corresponding to low salt solutions). Nevertheless, as stated earlier, the simple box model does capture the basic features of the complex-DNA and complex-bilayer coexistence.

2.4.2 Other models

Bruinsma (1998), has independently discussed how the nonlinear Poisson-Boltzmann theory can account qualitatively for the features observed by Rädler *et al.* (1997) for the structural evolution of DNA-cationic lipid complexes as a function of charged-lipid to DNA ratio. Because he develops an analytical – rather than numerical – solution of the problem, he is constrained to introducing several simplifications (e.g., low surface charge densities, and no added salt) in addition to those discussed in our present work. Nevertheless, his model of the lipoplex is consistent with ours and provides a slightly different flavor to its interpretation. He too allows for spatial variation of the bilayer surface charge density, induced by interaction with the oppositely-charged DNA strands, and – while not solving explicitly for $\eta(x)$ – is careful to treat self-consistently the corresponding boundary condition for the electrostatic potential at this surface. Also in his treatment, two-phase coexistence between the L_α^C complex and excess DNA (low ρ) and excess lipid (high ρ) are identified by chemical potential relations equivalent to our Eqs.2.11-2.14. However, unlike in our model, where the naked DNA is treated as *a macroscopic phase* – embedded in a dilute aqueous *salt solution* – Bruinsma's expression for the free energy of DNA in solution is based on a cell-like model for the *pure counterion case* (Lifson & Katchalsky, 1954) which involves a $\ln \Phi$ term, with Φ denoting the volume fraction of the free DNA. This Φ dependence then enters the DNA-lipoplex equilibrium condition, implying a weak dependence of d on ρ at finite Φ (excess DNA, our region (i)). Around $\Phi = 0$, which is identified as the isoelectric point, d shows a singular dependence on Φ (equivalently ρ) increasing steeply from a low value to a higher one, the latter determined by lipoplex-bilayer coexistence. In other words, the isoelectric point is *unstable*

with respect to uptake of either DNA or bilayer. In our terminology this picture implies a sudden jump from d_1 to d_2, and $\rho_1 \equiv \rho^* \equiv \rho_2$, i.e., no one-phase (complex) region. This result is at variance with our findings. On the other hand Bruinsma's conclusion regarding region (iii) (excess bilayer) are similar to ours. He explains the constancy of DNA-DNA spacing at high ρ values in terms of the repulsive interaction between bilayers within the complex; this repulsion increases with the deviation from the isoelectric point and hence ultimately overwhelms the effect of counterion release which had been driving uptake of lipid bilayer. Recall that we had explained the uptake of DNA ($\rho < 1$) and bilayer ($\rho > 1$) in terms of the entropy gain of bound counterions (relative to their state in "free" DNA or "free" bilayer, respectively) as they move into the complex with significantly lower concentrations. See, for example, the excess charge densities defined by Eqs. 2.17, 2.18 in the "box "model, each of which is generally quite small compared to their "bare" values in the free macroions (DNA or liposome). This phenomenon appears still more dramatically in the approximate analytical work of Bruinsma's leading to the "isoelectric instability".

Dan (1996) has proposed a quite different explanation of the constancy of DNA spacings at low and high values of charge-lipid to DNA. Her argument is based on the idea that elastic deformation of the bilayer by its interaction with DNA gives rise to an effective attraction between the DNA strands. At high ρ values (i.e., low DNA content relative to lipid, at fixed neutral-to-cationic lipid ratio – note that Dan's ratio ρ is defined in a way which makes it inversely proportional to ours), all the DNA in solution is intercalated in the sandwich complexes, which in turn coexist with excess liposomes. Here the DNA spacing takes on its optimum value, d_o, reflecting directly the competition between these relatively long-ranged attractions (taken to vary linearly with d) and the exponentially-screened, electrostatic repulsions. Upon decreasing ρ – adding DNA, more and more of the "free" bilayer is bound, with the DNA spacing remaining constant at d_0. This regime persists down to ρ values which are low enough so that there is no longer any "free"/"excess" bilayer. Further decrease in ρ leads to a decrease in d spacing, because the strand-bilayer adsorption energy overwhelms the strand-strand repulsion. But, according to Dan, this drop in d is arrested by the onset of the isoelectric point, beyond which she argues that the DNA spacing will remain constant at a value equal to the average distance d_a between cationic lipid charges (or to the hard-core diameter of the DNA strands, if this quantity is larger than d_a). This scenario, then, is significantly different from the present one, and Bruinsma's, not only because of the central role ascribed to an effective attraction between intercalated DNA's, but also because it underplays the special nature of the isoelectric complex as one which tends to suck in both excess DNA

and cationic lipid bilayers because of the lower concentrations made available to bound counterions than in the "free" DNA and "free" liposomes, respectively.

2.4.3 Concluding remarks

Using an electrostatic model for the lipoplex and straightforward, though appropriately modified, thermodynamic expressions for phase equilibria, we were able to explain the structure and phase evolution in aqueous solutions containing DNA, neutral-cationic liposomes and L_α^C lipoplexes. Our treatment of these phenomena was based on the premise that the lipid bilayers in the complex are perfectly planar and of constant thickness, for all lipid compositions. This, of course, is an approximation, valid for lipid bilayers of high bending rigidity and small spontaneous curvature, consisting of lipids with similar chain lengths. On the other hand, for a lipid mixture whose (monolayer's) spontaneous curvature is negative (e.g. DOPE containing mixtures) the honeycomb (H_{II}^C) complex may be a more stable structure (Koltover *et al.*, 1998).

Quite generally, variations in the lipid composition imply variations in both the bending rigidity and the spontaneous curvature of the monolayers constituting a lipid membrane. In an L_α^C complex, for instance, softening the membrane would, most probably, involve curvature modulations of the lipid bilayers around the DNA strands. Correlated curvature modulations between stacked (lipoplex) bilayers may result in 3D order ("locking") of the DNA strands in the complex. If, by compositional variations, the lipid membranes change both their rigidity and spontaneous curvature, a structural phase transition may take place between one complex geometry and another (e.g. $L_\alpha^C \rightarrow H_{II}^C$). These scenarios are the topic of the next chapter.

Chapter 3

From Lamellar to Hexagonal Complexes

3.1 Introduction

In the previous chapter we considered, among other degrees of freedom, the important role of lipid mobility in stabilizing the L_α^C DNA-lipid complex. In this chapter we will examine another important degree of freedom, namely the lipid (bi/mono-)layer elasticity. We will study the way lipid mobility and elasticity are intimately coupled, so that it is the combination of the two that ultimately determines what will be the equilibrium state of the complex.[1]

Quite generally, the preferred equilibrium geometry of a DNA-lipid condensate is dictated by the surface charge density and the elastic properties of its constituent lipid layers. Both of these characteristics depend, in turn, on the nature and composition of the CL/HL mixture. Double stranded DNA, being a rather rigid molecule (of large persistence length, see Sec. 1.4), imposes constraints on the possible lipoplex geometries since it retains its essentially linear structure in all complexes. On the other hand, the lipid layers are soft self-assembled membranes which can adapt their structure so as to optimize the complexation geometry.

In Chap. 2, two specific ordered DNA-lipid phases were introduced, namely the L_α^C and H_{II}^C complexes. The structural differences between the L_α^C and H_{II}^C phases imply significant differences between the electrostatic (charging) energies and the lipid elastic energies of these two geometries. In the H_{II}^C phase each DNA molecule is surrounded by a highly ("negatively") curved lipid monolayer,

[1] Some of the results presented in this chapter were previously reported in May *et al.* (2000a). This chapter also contains some previously unpublished results.

of radius $R \approx$ 13Å (Koltover *et al.*, 1998). This, cylindrically concentric geometry provides efficient neutralization of the DNA charges by the cationic surface charges, especially at the *isoelectric point* where the total cationic charge exactly balances the total DNA charge (May & Ben-Shaul, 1997). On the other hand, the strongly bent lipid monolayer may inflict a significant curvature deformation energy penalty. The lower the bending rigidity of the monolayer, k, the smaller the deformation free energy price (see (Helfrich, 1973); see also Sec. 1.3). More favorable is the case where c_0, the spontaneous curvature of the monolayer, conforms to the curvature of the DNA rod, namely, $-c_0 \simeq 1/R_D$, (the minus sign signifying that the monolayer curvature is opposite to that of the DNA). Under these circumstances the hexagonal complexes are expected to be more stable than the lamellar ones. It must be noted, however, that charged lipids generally prefer the planar bilayer geometry ($c_0 \approx 0$), whereas the inverse-hexagonal geometry is preferred by (some) neutral lipids, e.g., DOPE. Thus, the stability of $\mathrm{H}_{\mathrm{II}}^{\mathrm{C}}$ complexes is expected to depend sensitively on lipid composition. Similar qualitative considerations imply that lipid mixtures characterized by a high bending stiffness ($k \gg k_B T$ where k_B is Boltzmann's constant and T the temperature) and/or small spontaneous curvature ($|c_0| \ll 1/R_D$) will favor the formation of the $\mathrm{L}_{\alpha}^{\mathrm{C}}$ phase (May & Ben-Shaul, 1997; Harries *et al.*, 1998; Koltover *et al.*, 1998). In this geometry charge matching is somewhat less efficient than in the hexagonal packing, yet the lower curvature energy overrides this difference.

These qualitative notions were elegantly corroborated by experiments in which the elastic properties of the lipid monolayers were controlled by changing the nature of the lipid mixture (Koltover *et al.*, 1998). The cationic lipid in these experiments, DOTAP (see Sec. 1.3), is characterized by a very small spontaneous curvature. Using mixed-lipid vesicles composed of DOTAP as the cationic lipid and DOPE as the helper lipid it was found that the preferred aggregation geometry is the $\mathrm{H}_{\mathrm{II}}^{\mathrm{C}}$ phase. On the other hand, the use of DOPC as the helper lipid promotes the formation of $\mathrm{L}_{\alpha}^{\mathrm{C}}$ complexes. These findings are consistent with the fact that pure DOPE self-organizes into an H_{II} phase, i.e., the spontaneous curvature of this lipid is negative, whereas DOPC molecules prefer the formation of planar bilayers. In these experiments one tunes the spontaneous curvature of the lipid layer by controlling the composition of the lipid mixture. Based on many experiments in microemulsion systems it is known that one can also control the bending rigidity of amphiphilic films. For example, by adding short chain alcohols to the mixture it is possible to reduce the bending rigidity by about one order of magnitude (Safinya *et al.*, 1989; Szleifer *et al.*, 1988). Indeed, the addition of hexanol to the DOTAP/DOPC-DNA system results in a clear, first order, $\mathrm{L}_{\alpha}^{\mathrm{C}} \rightarrow \mathrm{H}_{\mathrm{II}}^{\mathrm{C}}$ phase transition (Koltover *et al.*, 1998).

The qualitative considerations outlined above regarding the relative stabilities of different CL-DNA aggregates apply to one, given, CL/HL mixture composition. Furthermore, they are only valid if all lipids and DNA molecules participate in complex formation. Different considerations apply when the mixture is "non-stoichiometric". Taking into account that aqueous solutions containing DNA and two kinds of lipids are multicomponent systems they are expected to exhibit rich and complex phase behaviors.

For a given salt concentration (chemical potential) the aqueous solution can be treated as a large reservoir embedding the condensed phases (i.e., complexes, bare bilayers and naked DNA), allowing to count out the water and salt. This leaves us with three relevant chemical species (CL, HL, and DNA) which, by Gibbs' phase rule corresponds to (a maximum of) five thermodynamic degrees of freedom. Fixing the temperature, and assuming that the lipid layers are incompressible, (in all four lipid-containing phases), we eliminate two more degrees of freedom. Still, the phase rule implies that (up to) three condensed phases can coexist in solution, e.g., two kinds of complexes and uncomplexed DNA. The experimental observation of a first order $L_\alpha^C \rightarrow H_{II}^C$ transition (Koltover *et al.*, 1998), i.e., two coexisting phases, is in line with this conclusion. As we shall see these systems are also expected to exhibit three-phase equilibria.

Thus far, we modeled the lipid membranes in the L_α^C complex as perfectly planar slabs. However, this need not be the case. When the membranes are sufficiently soft (yet not soft enough to favor the H_{II}^C phase) or if one of the CL/HL has a propensity to form curved surfaces, the membrane may corrugate so as to optimize its contact with DNA (see Fig. 2.1). If the membrane is further softened, a transition may occur to the H_{II}^C phase. In this respect, the membrane corrugation in the L_α^C complex may be regarded as a delay of the onset of the $L_\alpha^C \rightarrow H_{II}^C$ transition.

Limited experimental evidence supports this notion. In cryo-transmission electron microscopy (cryo-TEM) studies of the L_α^C phase, spatial correlations were found between DNA strands in different galleries (Battersby *et al.*, 1998). In another series of X-ray studies, the corrugation and charge density modulation in an L_α^C-like complex, but in which the membranes are in the *gel* phase, were measured (Artzner *et al.*, 1998). The results show that these effects are significant. Further support for the possible formation of corrugations is gained from computer simulations of lipid-DNA complexes (Bandyopadhyay *et al.*, 1999) . Another possible consequence of membrane corrugation in the L_α^C phase is an induced locking between neighboring galleries. This follows the formation of "troughs" in a gallery, induced by the interaction of the membrane with DNA in adjacent galleries. This imposes "adsorption sites" for the DNA in the two neigh-

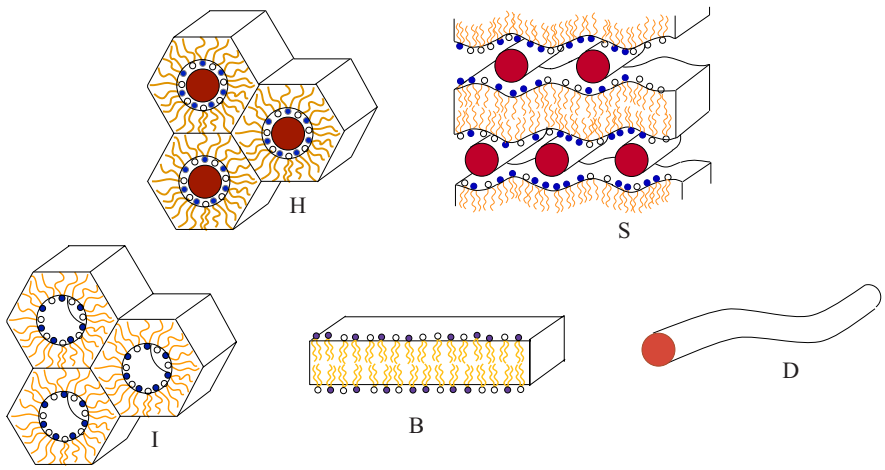

Figure 3.1: Schematic illustration of the five macroscopic phases included in our theoretical scheme. The phases denoted by H and S are the H_{II}^{C} and L_{α}^{C} complex structures, respectively. The symbols I and B mark the H_{II} and L_{α} phases, respectively. D represents uncomplexed DNA. The shaded regions correspond to the DNA cross sectional area. The lipid layers are mixed, consisting of cationic and uncharged (helper) lipids.

boring galleries - and so on. The formation of these troughs may thus correlate between the positions of DNA in different galleries. Furthermore, if the troughs are shallow, or absent altogether a mechanism for the formation of phases where DNA in different galleries are uncorrelated (elsewhere termed "sliding phases" (O'Hern & Lubensky, 1998; O'Hern *et al.*, 1999; Salditt *et al.*, 1997)) may form.

Our goal in this chapter is to analyze, theoretically, the major determinants of the phase behavior of lipid-DNA solutions. To this end we have studied in detail several representative systems, corresponding to lipid mixtures of different elastic characteristics. As we shall see, the phase behavior is relatively simple for "rigid" lipid layers which, in the absence of DNA, show strong propensity to form planar bilayers. Much richer and more complex phase diagrams, involving a multitude of transitions and coexistence regimes, are predicted for flexible and/or "curvature loving" lipid layers.

The phase diagrams presented in the following sections involve two levels of calculations. First, for a given type of lipid mixture we calculate, as a function of the lipid composition (CL ratio) and lipid/DNA ratio, the elastic, mixing and electrostatic charging free energies of all relevant structures, i.e., the H_{II}^{C} and (perfectly planar) L_{α}^{C} complexes, the bilayer and inverse-hexagonal lipid phases and the uncomplexed DNA, as illustrated in Fig. 3.1. (The symbols, H for H_{II}^{C} etc. are used for notational brevity.)

The electrostatic free energies are calculated based on the nonlinear Poisson-Boltzmann (PB) equation using methods described in Chap. 2 and elsewhere (May & Ben-Shaul, 1997; Harries *et al.*, 1998). The elastic terms are evaluated

using familiar expressions for the curvature and stretching deformations and simple models for the elastic constants of mixed lipid monolayers. Then, writing the total free energy of the solution as a weighted sum involving all possible phases, we determine the phase diagram by minimizing this free energy with respect to all relevant thermodynamic variables.

We will then turn to study the possibility of corrugations forming in the L_α^C complex. We shall show how, and to what extent, the geometry and free energy of the complex is affected through corrugations, and charge density modulations, and how these relate to the lipid composition degree of freedom. We will also discuss the stability of the corrugations with respect to the membrane thermal undulations, and show that for a certain range of compositions and elastic properties, a stable corrugated L_α^C phase is expected. We do this by extending the expression for the free energy functional for the L_α^C unit cell (Sec. 2.2) to also include an elastic contribution.

3.2 Theory

We consider an aqueous salt solution containing N^+ (monovalent) cationic lipids, N^0 helper lipids, and double stranded DNA of total charge $-eM$, Where $M \equiv sD/l$ and e is the elementary charge. The lipid and DNA molecules are distributed among the five possible structures shown in Fig. 3.1. We assume that all these structures, including the naked DNA, are large enough and can thus be treated as macroscopic phases. The total volume fraction of the condensed phases is assumed to be small, enabling us to treat the embedding solution as an infinite reservoir of (monovalent) salt of concentration $n_0^+ = n_0^- = n_0 = constant$. Under these assumptions the total volume of the solution is irrelevant for phase transitions involving the condensed phases.

At a given temperature, T, and salt concentration, n_0, our three component system (DNA, CL, HL) is specified by two composition variables,

$$\bar{\phi} = \frac{N^+}{N^+ + N^0} \quad , \quad \rho = \frac{N^+}{M} \tag{3.1}$$

Here $\bar{\phi}$ is the mole fraction of the cationic lipid in the original lipid mixture, and ρ is the ratio between the total number of cationic and DNA charges in the system. Equivalently, since all lipids, whether in pure lipid phases or DNA-lipid complexes, are organized in monolayers, we can regard ρ as the ratio between positive and negative *macroion charges* in the solution, (to distinguish from the mobile counterion charges).

The total free energy of the three component system $F = F(N^+, N^0, M; n_0, T)$ is a sum of terms corresponding to the various phases. Each term involves several

thermodynamic and structural degrees of freedom. The phase diagram of the system is determined by minimizing F with respect to these variables subject to material conservation conditions. In the two following subsections we first define the relevant degrees of freedom corresponding to the various phases, and then describe our model for calculating the free energy components of each phase. We end this section with a brief discussion of the approximations and assumptions employed in our theoretical model and their possible influence on our conclusions.

3.2.1 Phases

DNA

We treat the double stranded DNA as an infinitely long and straight rod, ignoring end effects as well as translational and conformational entropy contributions to its free energy. More specifically, as in Sec. 2.2, the DNA is treated as a rigid rod of radius $R_D = 10\,\text{Å}$, (corresponding to the surface of B-DNA), with uniform surface charge density $\sigma^- = -e/2\pi R_D l$. (We postpone discussing these, and other, approximations to the end of this section.) We shall assume that the dielectric constant inside the DNA rod is vanishingly small compared to that of the aqueous phase. The free energy of the DNA phase (D in the phase diagrams) is entirely due to the electrostatic charging energy of the rod in the given salt solution. Its contribution to F is $F_D = lM_D\hat{f}_D$ where lM_D is the length of uncomplexed DNA in solution and $\hat{f}_D$ is its charging free energy per unit length, (hereafter 1 Å). Note that for given n_0 and T, $\hat{f}_D$ is constant.

Lipid bilayer

We use N_B^+ and N_B^0 to denote the number of CL and HL molecules in the bilayer phase, respectively. (In the phase diagrams, and as subscripts, we replace L_α by B.) The two lipid species are assumed to be uniformly mixed, forming an ideal two-dimensional (2D) fluid mixture. We use the same cross-sectional area per molecule, $a = 70\,\text{Å}^2$, for both the CL and HL molecules.

The total number of molecules in the L_α phase is $N_B = N_B^+ + N_B^0$. Its composition, specified by $\phi_B = N_B^+/N_B$, is the only relevant intensive variable of the bilayer; ϕ_B determines the surface charge density, $\sigma_B = e\phi_B/a$, and the elastic properties of a given lipid mixture. The contribution of the bilayer phase to the total free energy F is $F_B = N_B f_B(\phi_B)$, with $f_B(\phi_B)$ denoting the free energy, per lipid molecule, in a bilayer of composition ϕ_B; f_B involves electrostatic (charging), elastic and mixing terms, all depending on ϕ_B. The hydrophobic lipid chain regions in the bilayer phase, as well as in all other phases, will be treated

as a medium of zero dielectric constant.

Inverse-hexagonal phase

We use N_I^+ and N_I^0 to denote the number of CL and HL molecules in the inverse-hexagonal lipid phase, H_{II}. (For notational brevity we use I = "inverse", rather than H_{II} as the subscript denoting this phase). The total number of lipids in this phase is $N_I = N_I^+ + N_I^0$, and its lipid composition is $\phi_I = N_I^+/N_I$. We assume that the radius of the water tubes, $R_I = 13$ Å, and the area per lipid molecule $a = 70$ Å^2 are constant, independent of ϕ_I, and hence of the cationic surface charge density. Note that we use the same area per molecule for both the planar and the inverse-hexagonal phases. This is a reasonable approximation provided this area, a, is measured at the so-called "pivotal surface", as discussed in more detail later in this section.

For the cylindrical symmetry of the H_{II} phase, the area per headgroup, a_{hg}, and the area at the pivotal surface (typically located just inside the hydrophobic region) a are related by,

$$a_{hg} = a\,(1 + \hat{h}\,c_I) = aR_I/(R_I + \hat{h}) \tag{3.2}$$

with $\hat{h}$ denoting the distance of the headgroup surface from the pivotal surface and $c_I = -1/(R_I + \hat{h})$ is the monolayer curvature at this surface. We adopt here the convention that the curvature of the inverse hexagonal phase is negative. In the calculations presented in the next section we shall use $\hat{h} = 6$ Å which, for $R_I = 13$ Å and $a = 70$Å^2, implies $a_{hg} = 47.9$Å^2.

Subject to the assumptions above the free energy of the H_{II} phase, $F_I = N_I f_I(\phi_I)$, depends on one intensive variable, ϕ_I. Like in the bilayer phase, the free energy per molecule, $f_I(\phi_I)$, is a sum of electrostatic, elastic and mixing contributions.

Lamellar Complexes

The L_α^C (or S = "sandwich") phase is an ordered smectic-like array, as schematically illustrated in Fig. 3.1. It is composed of N_S^+ cationic lipids, N_S^0 helper lipids, and M_S DNA charges. The lipid composition is specified by $\phi_S = N_S^+/N_S; N_S = N_S^+ + N_S^0$. The L_α^C phase is a periodic structure in the plane (x, y) perpendicular to the DNA axis (z), translationally invariant along z. Assuming that the lipid bilayers are perfectly planar, the structure of this phase is specified by the DNA-DNA repeat distance, d, the distance between apposed lipid surfaces, l, and the thickness of the lipid bilayers, w. Because the dielectric constant within the hydrophobic region is set equal to zero, w does not enter our model for the

electrostatic energy. (However, it still has a substantial effect on the boundary condition, in that it includes "image charges" in an explicit way.) The bilayer thickness affects the bilayer bending rigidity, yet this is already accounted for by our choice of the bending constant, k, (see below). Also, both experimentally (Rädler *et al.*, 1997) and theoretically (Chap. 2), it was shown that the thickness of the water gap, h, is essentially independent of ϕ_S, for all relevant compositions. Consistent with this finding we shall use $h = 2(R_D + \delta) = 26$ Å with $\delta = 3$ Å denoting the thickness of the thin hydration layer separating the lipid and DNA charges.

The free energy of the L_α^C phase, F_S, depends on two independent intensive variables; e.g., the mole fraction of charged lipid, ϕ_S, and the positive/negative charge ratio $\rho_S = N_S^+/M_S$. These composition variables also determine the only structural variable of the L_α^C phase, d; namely, $d = N_S a/2M_S l = (a/2l)\rho_S/\phi_S$. We can thus write $F_S = N_S f_S(d, \phi_S) = l M_S \hat{f}_S(d, \phi_S)$ where $f_S(d, \phi_S)$ is the free energy per lipid in the L_α^C phase. In the second equality $\hat{f}_S \equiv f_C/s$ is the free energy of the L_α^C phase, per unit length of DNA. We shall also refer to $\hat{f}_S$ as the free energy "per unit cell" of the complex. When corrugations are allowed in the L_α^C complex, $h(x)$ is no longer constant. Thus, generally, $d \neq l_M$ where l_M is the length of lipid membrane between two strands. We return to this point in Sec. 3.2.3.

Hexagonal Complexes

The H_{II}^C (or "honeycomb" = H) phase consists of N_H^+ cationic lipids, N_H^0 helper lipids, and M_H DNA charges. Its lipid composition is $\phi_H = N_H^+/N_H$ with $N_H = N_H^+ + N_H^0$ denoting the number of lipids in the hexagonal complex. The radius of curvature of the (strongly curved) lipid headgroup surface in the H_{II}^C phase, R_H, must be larger than the radius R_D of the DNA strands intercalated within the cylindrical water tubes. We thus set $R_H = R_D + \delta = 13$ Å with $\delta = 3$ Å denoting the thickness of the water layer intervening between the DNA and lipid charges. This choice is based on experimental observations (Koltover *et al.*, 1998). Note also that small δ ensures (at isoelectricity) efficient electrostatic charge balance (May & Ben-Shaul, 1997). Furthermore, as will be discussed in the next subsection, large δ, and hence large R_H, implies a high energetic penalty associated with the unfavorable stretching of lipid tails towards the interstitial axes within the hydrophobic core of the hexagonal phase (See Sec. 1.3 and also (Seddon & Templer, 1995; Turner & Gruner, 1992; Gawrisch *et al.*, 1992; Kozlov *et al.*, 1994; Leikin *et al.*, 1996)). Finally, note that to simplify the calculations we have set $R_I = R_H$. Thus, the areas per molecule in the pivotal and headgroup surfaces in the H_{II}^C complex are related by Eq. 3.2.

Assuming $R_H = constant$ the H_{II}^C phase is characterized by a single intensive variable: ϕ_H. The free energy of this phase is then $F_H = N_H f_H(\phi_H) = l M_H \hat{f}_H(\phi_H)$, where f_H is the free energy per lipid molecule, and $\hat{f}_H$ is the free energy per unit length of DNA. Note that $N_H/M_H = 2\pi R_H l/a_{hg} = 2\pi(R_D + \delta + \hat{h})l/a$, implying $\hat{f}_H = [2\pi(R_D + \delta + \hat{h})/a] f_H$.

3.2.2 Degrees of freedom

The DNA/CL/HL mixture can exhibit a variety of phase equilibria. One way to map the phase diagram of this system is to consider all possible two- and three-phase equilibria, solve the relevant coexistence equations and identify the phase boundaries by matching the chemical potentials of the pertaining components. We adopt here an alternative, computationally more efficient, route. Namely, we express the total free energy of the three component mixture, F, as a sum of contributions representing all possible phases, and minimize it with respect to all relevant variables. For every given lipid/DNA mixture the minimization yields the number and identity of the coexisting phases, their relative proportions, as well as their compositional and structural characteristics.

Explicitly, our free energy functional involves eleven "concentration" variables: four N_i^+'s ($i = B, I, S, H$), four N_i^0's, and three M_i's ($i = D, S, H$). All quantities appearing in F,

$$\begin{aligned} F &= N_H f_H(\phi_H) + N_S f_S(d, \phi_S) \\ &+ N_B f_B(\phi_B) + N_I f_I(\phi_I) + l\, M_D \hat{f}_D \end{aligned} \tag{3.3}$$

are functions of these variables, e.g., $N_H = N_H^+ + N_H^0$, $\phi_H = N_H^+/N_H$, etc. However, not all variables are independent. Furthermore, according to the phase rule there can be no more than three coexisting phases, implying that (following the minimization of F for a given mixture) some of the concentrations must vanish.

For a given mixture, characterized by the total numbers of molecules, M, N^+ and N^0, three of the eleven variables are eliminated by the material conservation conditions,

$$\begin{aligned} N^+ &= N_B^+ + N_I^+ + N_S^+ + N_H^+ \\ N^0 &= N_B^0 + N_I^0 + N_S^0 + N_H^0 \\ M &= M_D + M_S + M_H \end{aligned} \tag{3.4}$$

Yet another variable can be counted out because of the structural-compositional constraint imposed on the H_{II}^C phase,

$$N_H = [2\pi(R_D + \delta + \hat{h})l/a] M_H \tag{3.5}$$

Subject to these conditions F is now a function of seven independent variables. The thermodynamic state of a given lipid/DNA mixture (M, N^+, N^0) is determined by the global minimum of F in the multidimensional space defined by the seven composition variables. Note that specifying M, N^+ and N^0 is equivalent to specifying ρ and $\bar{\phi}$, (see Eq. 3.1), and one extensive variable which is irrelevant for determining the phase behavior of the mixture. Thus, the phase diagrams presented in the next section will be described in the $\rho, \bar{\phi}$ plane.

As a convenient reference point for calculating F we choose the state where all lipids reside in a planar bilayer and all DNA is uncomplexed. Relative to this state the free energy of the system is given by

$$\Delta F = F - N f_B(\bar{\phi}) - l\, M \hat{f}_D \tag{3.6}$$

When all lipids and DNA are associated in one phase, e.g., the lamellar complex, this free energy change may be regarded as the "formation" free energy of this phase.

3.2.3 Free energies

In this section we describe the various contributions to the free energy of the different phases, and their dependence on the relevant chemical compositions. In fact, for all phases except the naked DNA (D), the free energy is of the form

$$f_\zeta = f_\zeta^{es} + f_\zeta^{el} + f_\zeta^{mix} \qquad (\zeta = S, H, B, I) \tag{3.7}$$

where the three terms on the right hand side of this equation represent the electrostatic (charging) free energy, the elastic curvature energy, and the (2D) mixing entropy of the lipid layers, respectively. In the following we briefly discuss each of these contributions and its specific form in a given phase.

Elastic energy

Lipid bilayers and monolayers are elastic membranes which, at a certain free energy cost, can either be stretched, or bent (or both) with respect to their equilibrium state (Sec. 1.3;(Helfrich, 1973)). The energy penalty associated with curvature deformations is generally much smaller than that involved in area changes. For this reason we can treat the membranes as laterally incompressible. On the other hand we must account for the ability of cationic membranes to undergo curvature deformations under the strong electrostatic forces exerted by the highly charged and strongly curved DNA strands. Thus, in the presence of DNA in its immediate vicinity, a planar cationic lipid bilayer may re-assemble into inverse-hexagonal layers, enveloping the DNA strands. This rearrangement is most likely

to take place when the bilayer is composed of *monolayers* characterized by *negative spontaneous curvature*. When this propensity is strong enough, as is the case with pure DOPE systems, the inverse-hexagonal phase will appear even in the absence of DNA (Gawrisch *et al.*, 1992; Kozlov *et al.*, 1994; Chen & Rand, 1997). Otherwise, i.e., if the spontaneous curvature is not sufficiently negative, the monolayers assemble into a planar bilayer, paying the necessary but tolerable curvature frustration energy toll.

In mixed lipid layers the spontaneous curvature is a function of composition. For example, in the CL/HL mixture DOTAP/DOPE the spontaneous curvature becomes increasingly negative as the mole fraction of the helper lipid increases. Without DNA the bilayer will destabilize at a certain mole fraction of the helper lipid, undergoing a phase transition from the planar to the inverse hexagonal geometry. The addition of DNA to the mixture can promote the transition to take place at a considerably lower concentration of the helper lipid. These effects play a crucial role in determining the phase behavior of CL/HL/DNA system. We account for them using a simple model for the bending rigidity of mixed lipid layers.

The elastic energy of the lipid monolayers constituting the four lipid-containing phases illustrated in Fig. 3.1 will be expressed in the form

$$f^{el}(c,\phi) = a\frac{k}{2}(c - c_0(\phi))^2 + f_v \tag{3.8}$$

The first term in this equation represents the familiar elastic deformation energy, per molecule, in a cylindrically bent lipid monolayer (Helfrich, 1973). Here, k is the *bending modulus*, c_0 is the *spontaneous curvature* of the monolayer, c is the actual curvature and a the area per molecule. We use this expression for both the planar and inverse-hexagonal geometries, assuming that k, a and c_0 are the same for both curvatures. The second term corrects for the fact that in the inverse-hexagonal symmetry, not all molecules experience the same deformation. Those molecules whose hydrophobic tails point towards the hexagonal interstices (or "voids") of the hydrophobic core are more extensively stretched than those directed towards neighboring water tubes. Since not all lipid tails are equally stretched some of them are necessarily "frustrated", resulting in an average free energy penalty of f_v per molecule; see e.g.,(Kirk *et al.*, 1984; Seddon & Templer, 1995). It should be noted that a, c, c_0 and k are measured with respect to the "*pivotal* surface" where, upon cylindrical deformations the area per molecule stays constant, see e.g., (Gawrisch *et al.*, 1992; Kozlov *et al.*, 1994; Leikin *et al.*, 1996). For laterally incompressible lipid monolayers, as we assume to be the case here, the pivotal surface coincides with the *neutral* surface, where area and curvature deformations are, by definition, decoupled. Typically, the pivotal surface lies

inside the hydrophobic region, close to the hydrocarbon-water interface (Kozlov *et al.*, 1994; Leikin *et al.*, 1996).

In general, both k and c_0 depend of the lipid composition ϕ. In the calculations presented in the next section we shall assume that k is independent of ϕ, as is often the case for lipid molecules of similar chain length. For the dependence of the spontaneous curvature on ϕ we shall adopt the simple but adequate linear interpolation formula (May & Ben-Shaul, 1995; Andelman *et al.*, 1994),

$$c_0(\phi) = c_0^h + \phi(c_0^c - c_0^h) \tag{3.9}$$

where c_0^c and c_0^h are the spontaneous curvatures of the cationic and helper lipids, respectively.

Eqs. 3.8 and 3.9 will be used for all four lipid-containing phases considered in this work. Clearly, for the two lamellar phases $f_v = 0$. The curvatures of the lipid-containing phases are $c = c_B = c_S = 0$, $c_I = c_H = -1/(R_D + \delta + \hat{h}) = -1/19$ Å (recall $R_D = 10$ Å, $\delta = 3$ Å, and $\hat{h} = 6$ Å). In the calculations reported in the next section we shall consider several different lipid mixtures, corresponding to different sets of the elastic constants k, c_0^h and f_v.

Finally, it should be noted that the bending rigidity of charged lipid layers is a sum of contributions of different origins, including entropic (conformational) repulsions between the hydrocarbon tails as well as steric and electrostatic repulsions between headgroups. In Eq. 3.8 we include all contributions to the elastic energy except the electrostatic one. When electrostatic-curvature effects are small, they can be accounted for through an additional contribution to the bending rigidity k, i.e., to the first term in Eq. 3.8. Usually, this contribution is derived from the second order term in the curvature expansion of the PB electrostatic energy (Lekkerkerker, 1989). However, the surfaces in the H_{II} and H_{II}^C phases are not only highly curved but also *closed*. Furthermore, for the same lipid mixture, the cationic charge densities in the hexagonal phases are different from those in the planar phases (May, 1996). Thus, instead of treating the changes in electrostatic energy based on low order curvature expansions, we use the full nonlinear PB solution for all geometries.

Mixing entropy

As in other phase separation phenomena, when two or more lipid-containing phases coexist in solution their CL/HL compositions are generally different, implying different mixing entropies. Following Chap. 2 and previous studies (May & Ben-Shaul, 1997) we shall assume that the monolayers in the L_α, H_{II} and H_{II}^C phases are ideal 2D mixtures. Their mixing free energy is thus given by

$$f^{mix}/k_BT = \phi \ln \phi + (1-\phi)\ln(1-\phi) \tag{3.10}$$

The presence of DNA strands in the L_α^C phase induces a nonuniform distribution of the two lipid components. The *deviations* from ideal mixing in this phase are taken into account in the electrostatic free energy, f_S^{es}. For the uniform mixing entropy of this phase we use Eq. 3.10.

Electrostatics

The gain in electrostatic free energy is the driving force for the mutual condensation of DNA and cationic vesicles to form an ordered, composite, phase. The major contribution to this free energy change is the entropy gain associated with the release of "partially bound" counterions into the bulk solution (Harries *et al.*, 1998; Bruinsma, 1998). Before the association of the oppositely charged macroions (DNA and cationic lipid vesicles) each macroion is surrounded by a diffuse layer of "partially bound" counterions. In the condensed CL-DNA phase most of these counterions are no longer needed for charge neutrality and can thus be released.

The electrostatic free energy depends on the surface charge densities of the separated macroions, the structure and composition of the condensed phases, and the salt concentration in solution. The electrostatic free energies of the various structures are calculated based on the nonlinear PB equation. Although the PB approach involves some inherent approximations (see below), it was shown to adequately predict the principal structural and phase characteristics of both the H_{II}^C phase (May & Ben-Shaul, 1997) and the L_α^C phase (Chap. 2). Here we use the same algorithms for calculating the electrostatic free energy components of the many-phase system. All our PB calculations apply to symmetric 1:1 electrolyte solutions.

According to PB theory the electrostatic (charging) free energy of any surface, or group of surfaces, in solution can be expressed in the form (Verwey & Overbeek, 1948),

$$\begin{aligned} F^{es} &= \frac{1}{2}\int_S \sigma\varphi \mathrm{d}s \\ &+ k_B T n_0 \int_V [\psi \sinh\psi - 2\cosh\psi + 2]\,\mathrm{d}v \end{aligned} \tag{3.11}$$

The first integral extends over all the charged surfaces (S), where σ denotes the local surface charge density and φ is the corresponding (surface) electrostatic potential. The second integration is over the volume (V) of the electrolyte solution; $\psi = e\varphi/k_BT$ is the reduced electrostatic potential. In writing Eq. 3.11 it is assumed that the dielectric constant inside the DNA and lipid membrane is vanishingly small compared to the aqueous solution.

To obtain ψ we solve the PB equation, Eq. 2.4. In all calculations in this chapter we have used $n_0 = n_0^+ = n_0^- = 4mM$ for the salt concentration, corresponding to $l_D = 50$ Å.

The solutions of the PB equation depend on the specific boundary conditions for the system considered. We shall now briefly describe the boundary conditions appropriate for the five structures illustrated in Fig. 3.1, and the corresponding free energies. Additional details are given in Chap. 2 (see also Harries *et al.* (1998) and May & Ben-Shaul (1997)).

$\mathbf{L}_\alpha$: The existence of a low dielectric hydrophobic region between the two bilayer surfaces allows treating them as separate, electrostatically decoupled, cationic surfaces (see discussion in Sec. 1.3.5). The PB equation of a charged planar surface is one-dimensional: $d^2\psi/dz^2 = \kappa^2 \sinh\psi$, with z denoting the distance from the charged surface. The boundary conditions are $\psi' = d\psi/dz = 0$ at $z \to \infty$ and $\psi' = -4\pi\phi_B l_B/a$ at the charged surface. Upon substituting the solution for ψ into Eq. 3.11 one obtains the well known expression for the free energy per molecule (Sec. 2.2),

$$\frac{f_B^{es}(\phi_B)}{k_B T} = 2\phi_B \left[\frac{1-q}{p} + \ln(p+q)\right] \tag{3.12}$$

Unfortunately, this is the only geometry for which the PB equation can be solved analytically.

$\mathbf{H_{II}}, \mathbf{H_{II}^C}, \mathbf{D}$: In all these three geometries the charged surfaces are cylindrically symmetric. Thus the PB equation is again one-dimensional, involving only the radial coordinate r. Using ψ' for $d\psi/dr$ etc, the PB equation reads $\psi'' + \psi'/r = \kappa^2 \sinh\psi$.

The boundary conditions for an isolated DNA rod (D phase) are: $\psi' = 0$ at $r = \infty$, and $\psi'(R_D) = 2l_B/R_D l$ at the surface of the rod,

For the $\mathrm{H_{II}}$ phase the PB equation is solved within the inner aqueous cylinders. The boundary conditions are $\psi'(0) = 0$ and $\psi'(R_I) = 4\pi\phi_I l_B/a_{hg}$; $R_I = R_D + \delta$.

Intercalating the DNA rods within the water tubes of the $\mathrm{H_{II}}$ phase we obtain the geometry of the $\mathrm{H_{II}^C}$ phase. The electrostatic problem here consists of two concentric, oppositely charged, surfaces. The PB equation is solved for the aqueous region between the two surfaces, $R_D \le r \le R_H$. The boundary conditions are: $\psi'(R_D) = 2l_B/R_D l$ at the DNA surface, and $\psi'(R_H) = 4\pi\phi_H l_B/a_{hg}$ at the lipid surface. Recall that we use $R_H = R_I = R_D + \delta$.

The PB equation for this geometry has been solved numerically for different values of the surface charge densities and the radius of the outer (lipid) cylinder. These solutions reveal that the electrostatic free energy is always minimal at, or very near, the isoelectric point, where the surface charges are equal in magnitude and opposite in sign. At this point, for surface spacings δ, typical of the $\mathrm{H_{II}^C}$ phase

(several Å), most counterions in excess of the bulk concentration are released from the cylindrical aqueous gap into the bulk solution, resulting in maximal entropy gain of these mobile ions. Because there are very few counterions in the gap, the two concentric surfaces can be treated as constituting a cylindrical capacitor (May & Ben-Shaul, 1997). In the next section we show that, at the isoelectric point, this model yields very good agreement with the numerical solutions of the PB equation. Away from the isoelectric point we use the PB equation to approximate the increase in the electrostatic free energy, as discussed in the next section.

Planar $\mathbf{L_\alpha^C}$: The PB equation for the unit cell of the planar L_α^C phase is solved (self-consistently) with the same boundary conditions outlined in Sec. 2.2.

Corrugated $\mathbf{L_\alpha^C}$ complexes: Further complexity arises when we consider elastic deformations in the L_α^C complex (depicted in Fig. 2.1). Following the notation in Sec. 2.2 and Sec. 3.2.3, we write the corrugated complex free energy $f_C = s\,\hat{f}_S$ as a sum of the electrostatic (charging) free energy of the complex, the (in-plane) lipid mixing entropy, and the elastic deformation energy. Here however, the presence of the DNA molecules may induce both charge density modulations and spatial membrane corrugation. The electrostatic, mixing and elastic degrees of freedom are thus intimately coupled. Consequently, the lipid composition profile $\eta(x)$, the spatial complex corrugation $h(x)$, the electrostatic potential in the complex interior $\varphi(x,y)$, and the actual value of the complex's free energy, $f_C(\phi, l_M, h)$, must be determined by minimizing the *total* free energy functional, which includes the mixing, elastic and electrostatic terms, namely,

$$\begin{aligned} f_C &= \int_v \frac{\epsilon}{2}(\nabla\psi)^2 \mathrm{d}v \\ &+ k_B T \int_v n_+ \ln\frac{n_+}{n_0} + n_- \ln\frac{n_-}{n_0} - (n_+ + n_- - 2n_0)\mathrm{d}v \\ &+ \frac{k_B T}{a}\int_{S_V}\left[\eta\ln\frac{\eta}{\phi} + (1-\eta)\ln\frac{1-\eta}{1-\phi}\right]\mathrm{d}S \\ &+ \frac{1}{2}\int_{S_V} k(c - c_0(\eta))^2 \mathrm{d}s. \end{aligned} \tag{3.13}$$

Note that due to corrugation in the complex, $h = h(x)$ may change with the position along the x axis. Also note that the complex free energy is now dependent on the *length* of membrane between two DNA strands, l_M (generally, $l_M \geq d$) rather than on the DNA-DNA distance d.

The first term on the right hand side of Eq. 3.13 is the electrostatic energy. The second term accounts for the translational ("mixing") entropy of the mobile ions in the complex interior, relative to their entropy in the bulk solution. The

third term accounts for the mixing entropy of the charged and neutral lipids in the membrane plane. The integration is over the membrane surface, (surface V in Fig. 2.2). Locally, i.e., at any x, the lipids are assumed to be ideally mixed, with $\eta = \eta(x)$ denoting the local mole fraction of the charged lipid. (Recall that the average area per lipid in the membrane is assumed to be independent of the lipid composition.) The last term in the free energy is the elastic deformation energy in a (locally) cylindrically bent lipid monolayer. For the dependence of the spontaneous curvature on η we use Eq. 3.9. The local lipid composition must satisfy the conservation constraint, Eq. 2.3

Functional minimization of f_C with respect to n_+, n_- and η (for a certain, predefined $h(x)$) subject to the conservation constraint, Eq. 2.3, yields for the mobile ion distributions the usual Boltzmann distributions, which upon substitution into Poisson's equation yield the PB equation, Eq. 2.4.

For $\sigma^+(x) = e\eta(x)/a$, the local charge density on the membrane, we obtain, for a given membrane spatial profile $h(x)$

$$\ln \frac{\phi(1-\eta)}{\eta(1-\phi)} - \psi - \lambda = k \left\{ c - \left[c_0^c \, \eta + c_0^h (1-\eta) \right] \right\} (c_0^c - c_0^h), \tag{3.14}$$

where λ is the Lagrange multiplier conjugate to the charge conservation constraint, Eq. 2.3. Using Gauss' equation, we relate the local surface charge density at x to the electrostatic potential at the membrane surface, Eq. 2.5. These equations represent the boundary condition on the electrostatic potential for boundary V in Fig. 2.2 and must be solved simultaneously, and self-consistently, with PB equation, Eq. 2.4. The other boundary conditions, pertaining to domain boundaries I-IV in Fig. 2.2, are as in Sec. 2.2.

In order to find the equilibrium configuration (i.e., both the spatial corrugations and lateral distribution of lipids in a membrane), for a given amount of DNA and lipid, a stationary point in $f_C^\star[\{h(x)\}]$, the free energy functional of the complex for a set of *predefined* h, must be found, so that $f_C = \min_{\{h\}} f_C^\star[h(x)]$. In the following we restrict h to be of the form:

$$h = \frac{1}{2} A_0 \cos(2\pi x/d) + h_0 \tag{3.15}$$

where in this study we take $h_0 = h(x=0) - A_0 = 26\text{Å}$ and A_0 determines the amplitude of corrugation. We shall therefore neglect all possible shorter wave lengths contributions to h. The numerical procedure for solving the PB equation (Carnie *et al.*, 1994; Stankovich & Carnie, 1996; Houstis *et al.*, 1985) and for evaluating λ, ψ and the free energy of the complex is outlined in App. B. In determining the value for A_0, we calculate the free energy of a unit cell with a specified l_M and ϕ, for a set of different A_0's (which were in all incremented by

0.5Å between calculations). The corrugation with the lowest free energy was then chosen as the equilibrium structure for those l_M and ϕ.

Membrane corrugation stability: Throughout our discussion we have assumed that the complexes bear a constant and well defined unit cell. We allowed for variations in the shape and size of this predefined unit cell, but, in effect, assumed an infinitely large "nematic" field, responsible for aligning DNA molecules in a certain preferred direction (at least on the length scale of the persistence length). Thus, we assume that a 2D ordered array of DNA strands form in each gallery. The possible registry and locking *between* galleries, and formation of a 3D liquid crystal, manifests itself in our model, only through the membrane corrugations, which we assume are repeated throughout the complex. However, even when membrane corrugation is expected, it may prove to be unstable with respect to the thermal undulations of the membrane. In these cases we can expect neighboring galleries to loose their registry, and the complex will behave as a set of decoupled layers of 2D crystals. To find the onset of melting in the 3D liquid crystal, we shall follow the ideal gas analogy of Helfrich and Servuss in determining the steric interaction in the lamellar phase of lipids (Sornette & Ostrowsky, 1994; Helfrich & Servuss, 1984). In terms of the Monge representation, $u(x,z)$ gives the vertical displacement of the surface from a plane reference state. We consider an undulating membrane of area L_d^2, for which the the fluctuations in the membrane displacement $\langle u^2 \rangle_{L_d}^{1/2}$ is on the order of the (average) extent of membrane corrugation A_0, i.e., $\langle u^2 \rangle_{L_d}^{1/2} \approx A_0$. When $L_d \approx d$ we should expect the onset of decoupling between galleries. For a tensionless membrane,

$$\langle u^2 \rangle^{1/2} = \sqrt{\frac{k_B T}{4\pi^3 k}} L_d \tag{3.16}$$

We can therefore expect to find registry between galleries, only if

$$A_0 \gtrsim \sqrt{\frac{k_B T}{4\pi^3 k}} d \tag{3.17}$$

In the next section we will show how this condition is indeed satisfied for certain choices of parameters governing the membrane profile.

Molecular free energies

The free energies per lipid molecule in the four lipid-containing phases were already described in Eq. 3.7. They include contributions from the electrostatic, elastic and mixing contributions. We reiterate these expressions for each phase

to emphasize their dependence on the different variables:

$$\begin{aligned} f_H(\phi_H) &= f^{el}(c_H, \phi_H) + f_H^{es}(\phi_H) + f^{mix}(\phi_H) \\ f_S(d, \phi_S) &= f^{el}(0, \phi_S) + f_S^{es}(d, \phi_S) + f^{mix}(\phi_S) \\ f_B(\phi_B) &= f^{el}(0, \phi_B) + f_B^{es}(\phi_B) + f^{mix}(\phi_B) \\ f_I(\phi_I) &= f^{el}(c_I, \phi_I) + f_I^{es}(\phi_I) + f^{mix}(\phi_I) \end{aligned} \tag{3.18}$$

Using these expressions in Eqs. 3.3 and 3.6 we can calculate the formation free energy, ΔF, for *any* specific partitioning of the DNA and lipids (both cationic and uncharged) among the different phases. Minimizing ΔF with respect to the seven concentration variables in this expression we obtain the number, nature and compositions of the phases corresponding to a system with given ρ and $\bar{\phi}$.

Approximations of the model

The systems modeled in the present study are very complex, both with respect to the number of relevant degrees of freedom and the variety of contributions to their free energies. Thus, the theoretical analysis of their phase behavior necessarily involves quite a few assumptions and approximations. Let us briefly review the most important approximations and their possible consequences.

The model involves several simplifying assumptions pertaining to structure of the phases considered. For instance, treating a double stranded DNA as a rigid cylindrical rod with negative charges uniformly distributed over its surface we ignore the groove structure and the discrete distribution of phosphate charges as has been discusses in Chaps. 1,2. Ignoring the molecular structure of water, the finite size of the counterions, and using the continuous, mean-field, PB approach to calculate the electrostatic energies of these complexes are additional approximations. Still, using this approach to calculate the phase structure and phase behavior of lamellar complexes we obtained good agreement with experiment. This agreement may be attributed to the fact that some features of the model are robust, e.g., the occurrence of the free energy minimum at the isoelectric point.

Here, the same structural and electrostatic free energy assumptions are used consistently to analyze phase transitions between phases of markedly different symmetries, e.g, the H_{II}^C and L_α^C phases. Even though we use approximate theories, the resulting phase behaviors are quite complex, and strongly dependent on the elastic and electrostatic properties of the lipid mixture. Although our theoretical model does not include all possible free energy contributions, it certainly captures the chief features of the relevant phase diagrams. It may fail to predict

the exact locations of phase boundaries, but not the nature of the phases and phase transitions observed, which is our main goal in this work.

One can also argue, for instance, that PB theory is inappropriate for considering the counterion distributions within the narrow aqueous confines of the lamellar or hexagonal complexes. Yet, our calculations reveal that whenever these structures appear in solution their net fixed charge is generally very small, i.e., the complexes are nearly isoelectric. Consequently, the counterion concentration within the narrow aqueous regions is typically small, in which case PB theory provides an adequate approximation, (subject of course to the approximations used to describe the structure of the charged surfaces).

Our model involves various other approximations. For example, we ignore conformational entropy contributions associated with the (very small) flexibility of double stranded DNA or the curvature fluctuations of the lipid layers. Yet, these contributions are negligible compared to the electrostatic or elastic free energy differences between the various phases. (For instance, the conformational entropy of DNA is of order 1 k_BT per DNA persistence length ($l_p \approx 500$Å) whereas the electrostatic and elastic energies are of order 1 k_BT per 1Å).

Assuming ideal mixing of the lipids in the various phases (except the L_α^C), as well as our simple model for the spontaneous curvature of the mixed lipid layers, represent additional approximations. On the other hand it should be remembered that uncertainties are also involved in the values of the elastic constants of even the best studied lipid systems. Albeit, it is clear that lipids preferring the hexagonal symmetry must have very different spontaneous curvatures from those which self-assemble into lipid bilayers. The model calculations presented in the next section aim to account for qualitative differences on this level, rather than those resulting from small variations of the elastic constants.

3.3 Results and discussion

The most interesting and relevant phases in lipid-DNA mixtures are of course the lipoplexes. Our model accounts for the two most important structures, namely, the H_{II}^C and L_α^C phases. In both phases the DNA and lipid layers are tightly associated, yet the complexation geometries are qualitatively different. These differences imply different electrostatic stabilization energies and different dependencies on the elastic properties of the lipid layers and their composition.

The goal of the forthcoming analysis is to provide a theoretical scheme for predicting the conditions favoring one lipoplex phase over the other or, possibly, the coexistence of both structures. The term 'conditions' refers here to the elastic properties of the lipid monolayers on the one hand, and the relative amounts of

HL, CL and DNA in solution, i.e., ρ and $\bar{\phi}$, on the other.

As we shall see below, the phase diagrams of CL/HL/DNA mixtures may exhibit rather complex behaviors, involving a variety of phase transitions and coexistence regimes. To assist the interpretation of these phase diagrams we begin the discussion with two preparatory subsections. In the first we compare the electrostatic free energies of the two complex phases, as a function of lipid composition and lipid/DNA ratio. The second subsection is concerned with the effects of electrostatic interactions on the relative stabilities of the pure lipid phases, L_α and H_{II}. We then discuss the effect of membrane corrugations on the L_α^C complex stability, before discussing the phase behavior of CL/HL/DNA mixtures.

All the calculations presented below were carried out for $n_0 = 4mM$, ($l_D = 50$ Å). Similar phase behaviors correspond to lower salt concentrations. Significant differences are expected only at very high salt contents, that is, when the Debye length becomes considerably smaller than the dimension of a typical lipoplex unit cell. In this limit, however, the complexes become unstable.

3.3.1 Electrostatics of the H_{II}^C and L_α^C phases

In our phase diagram calculations the radius of the lipid headgroup surfaces in the H_{II}^C phase is kept fixed at $R_H = R_D + \delta = 13$ Å. It is instructive however to examine how the electrostatic free energy of this structure varies with δ and ϕ_H. In Fig. 3.2 the electrostatic free energy per hexagonal unit cell, $\hat{f}_H^{es}$, is shown as a function of ϕ_H for four values of the water gap thickness; $\delta = 0.5, 3.0, 8.5$ and 15.0 Å. (The lowest value of δ is unrealistic, as we must allow for at least a minimal water layer, which we set equal to $\delta = 3$ Å. It is shown only for comparison.) Note that

$$\hat{f}_H^{es}(\phi_H) = 2\pi[(R_D + \delta + \hat{h})/a] f_H^{es}(\phi_H) \tag{3.19}$$

where f_H^{es} is the electrostatic energy per lipid molecule in the H_{II}^C phase. For $R_D + \delta + \hat{h} = 19$ Å and $a = 70$ Å^2 we have $\hat{f}_H^{es}/f_H^{es} \simeq 1.7$ Å^{-1}.

For all δ we find that the free energy $\hat{f}_H^{es}(\phi_H)$ is minimal at, or very near, the isoelectric point. At this point ϕ_H is given by

$$\phi_H^\star = \frac{a}{2\pi(R_D + \delta + \hat{h})l} \tag{3.20}$$

as marked by the vertical dotted lines in Fig. 3.2. The minima of $\hat{f}_H^{es}$ are more pronounced and occur closer to the isoelectric point for the smaller values of δ.

The dashed curve in Fig. 3.2 denotes the electrostatic energy according to the capacitor model mentioned in the previous section. This is the free energy of a

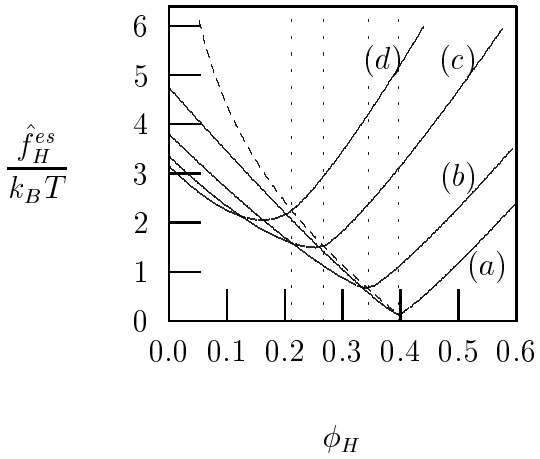

Figure 3.2: The electrostatic free energy, $\hat{f}_H^{es}$, of the H_{II}^C complex per hexagonal unit cell (of length 1Å) for $\delta = 0.5$Å (a), $\delta = 3.0$Å (b), $\delta = 8.5$Å (c), and $\delta = 15.0$Å (d). The dotted lines indicate the compositions, $\phi_H^\star$, for which the H_{II}^C structure is isoelectrical. The dashed curve corresponds to the free energy, $\hat{f}^{cap}(\phi_H = \phi_H^\star)$, according to the capacitor model, as given in Eq. 3.21.

concentric cylindrical capacitor, composed of an inner surface of radius $R_D = 10$Å and an outer surface of radius $R_H = R_D + \delta$, with water as the dielectric medium. The charge densities on these two surfaces are $-e/2\pi l R_D$ and $e\phi_H/2\pi l(R_D + \delta)$, respectively. The charging energy, per 1 Å, of this capacitor is

$$\frac{\hat{f}_H^{cap}}{k_BT} = \frac{l_B}{l^2} \ln \frac{R_D + \delta}{R_D} \tag{3.21}$$

with $\delta = a/2\pi l\phi_H - (R_D + \hat{h})$.

For $\delta \ll l_D$ (recall $l_D = 50$ Å) the minimum in the PB free energy exactly coincides with the simple capacitor model (curves (a) and (b) in Fig. 3.2), indicating that the surface charges are not screened by counterions. Namely, all the excess (diffuse layer) counterions have been expelled into the bulk solution. The capacitor model becomes less adequate as δ approaches l_D. Correspondingly, the minimum of $\hat{f}_H^{es}$ is shifted from $\phi_H^\star$ to $\phi_H < \phi_H^\star$, i.e., to a lower charge density of the outer surface, thus reducing the charging energy. The minimum of $\hat{f}_H^{es}$ increases, reflecting the less efficient charge neutralization associated with the increasing value of δ.

Unfortunately, the simple capacitor model is valid only at the isoelectric point. For $\phi_H \neq \phi_H^\star$ we need the PB equation to calculate the electrostatic energy. When the surfaces are not equally charged, counterions must be present in the aqueous gap to ensure electrical neutrality. As mentioned in Sec. 1.6, the reduced entropy of these counterions results in a repulsive interaction (disjoining pressure) between the apposed surfaces (Ninham & Parsegian, 1971). To a good approximation this

energy is equal to the capacitor energy plus the excess charging energy of the lipid surface (when $\phi_H > \phi_H^\star$) or the DNA surface (when $\phi_H < \phi_H^\star$), i.e., the charging energy of the relevant surface by the amount of charge $\phi_H - \phi_H^\star$.

Hereafter, when referring to the H_{II}^C phase we shall consistently use $\delta = R_H - R_D = 3$ Å. In addition to being the electrostatically most favorable configuration this δ also corresponds to minimal chain stretching (frustration) energy in the inverse-hexagonal symmetry. The isoelectric point corresponding to $\delta = 3$ Å, $\hat{h} = 6$ Å and $a = 70\text{Å}^2$ occurs at $\phi_H = \phi_H^\star = 0.345$.

Let us now compare the electrostatic energies per unit cell in the H_{II}^C and L_α^C complexes. In analogy to $\hat{f}_H^{es}$ in Eq. 3.19 we define $\hat{f}_S^{es}$ as the the electrostatic free energy per 1 Å of the L_α^C unit cell,

$$\hat{f}_S^{es}(\phi_S) = (2d/a) f_S^{es}(\phi_S) \tag{3.22}$$

where $2d/a = N_S/(lM_S) = \rho_S/l\phi_S$.

In Fig. 3.3 we show $\hat{f}_S^{es}$ as a function of the fraction of charged lipid in the complex, ϕ_S, for several values of the DNA-DNA spacing d (Chap. 2). Also shown, (broken curve), is the electrostatic free energy of the H_{II}^C phase for $\delta = 3$ Å, (curve (b) in Fig. 3.2). The curves marked (a)-(d) in Fig. 3.3 correspond to lamellar complexes containing exactly the same number of lipids per unit cell as those marked (a)-(d), respectively, in Fig. 3.2, which describes the hexagonal complexes.

As for the H_{II}^C phase, for all values of d, the minima of $\hat{f}_S^{es}$ occur at the isoelectric point ($\phi_S = \phi_S^\star = a/2ld$) or its immediate vicinity. However, unlike in the H_{II}^C phase, where the minima vary markedly with the unit cell dimensions (i.e., δ), the minima of $\hat{f}_S^{es}$ are nearly equal for all d. The reason for that is the ability of the CL/HL lipid layers in the L_α^C complex to polarize their charge density ("demix" the lipid distribution) so as to achieve close contact with the DNA charges. The demixing entropy penalty associated with this charge modulation is very small compared to the gain in electrostatic energy.

Two important conclusions can be derived from the results shown in Fig. 3.3. First, the L_α^C complex can respond to changes in lipid composition by varying the DNA-DNA distance, maintaining its electrostatic energy close to its minimum. Second, the global minimum of the electrostatic free energy of the H_{II}^C phase is lower than that of the L_α^C phase. The difference is a direct consequence of the different complex geometries. In the H_{II}^C phase *all* lipid charges are close to the DNA charges. On the other hand, in the L_α^C phase only *a fraction* of the cationic lipids are close to the DNA strands, the rest are necessarily farther away, contributing less efficiently to charge neutralization.

From Fig. 3.3 it is also apparent that the "electrostatic dominance" of the H_{II}^C

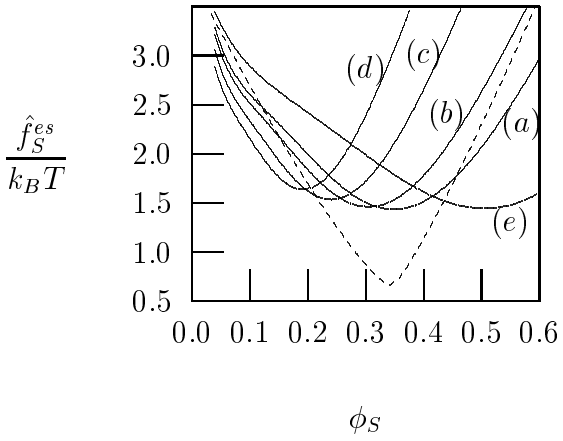

Figure 3.3: The electrostatic free energy of the L_α^C complex per unit cell (of length 1 Å), as a function of the CL mole fraction, ϕ_S. The solid curves correspond to five representative values of the DNA-DNA spacing: $d = 51.8$ Å (a), $d = 59.7$ Å (b), $d = 77.0$ Å (c), $d = 97.4$ Å (d), and $d = 35.0$ Å (e). (The minimal value of d is $d = 2R_D + \delta = 23$ Å.) For comparison we also show (broken curve) the electrostatic energy of the hexagonal complex, $\hat{f}_H^{es}(\phi_H)$, for $\delta = 3$ Å (curve (b) in Fig. 3.2). Note that a given d implies a given number of lipid molecules in the L_α^C complex. The solid curve (b) and the broken curve correspond to the same number of molecules (per unit DNA length) in the lamellar and hexagonal complexes, respectively.

complex is limited to a finite range of compositions around its isoelectric point. Consider first the two curves marked (b) in Figs. 3.2 and 3.3, the former is shown again (dashed curve) in Fig. 3.3. Both curves correspond to the same number of lipids per unit cell. Thus, the difference between these two curves represents the free energy change associated with the complete transformation of an H_{II}^C unit cell into a L_α^C unit cell, containing the same number of lipids at the same composition, $\phi = \phi_H = \phi_S$. Comparing $\hat{f}_H^{es}$ with $\hat{f}_S^{es}$ we find that, *electrostatically*, this complete transition is favorable only for $\phi < 0.15$ (where curve (b) crosses the broken line). Recall however that the lamellar complexes can lower their free energy by adjusting their DNA-DNA spacing, and hence the number of lipid molecules in the unit cell. From Fig. 3.3 we conclude that when this additional degree of freedom is taken into account (i.e., allowing the lamellar complex to shift from one d curve to another) the electrostatic preference of the hexagonal complex is limited to a considerably smaller range of lipid compositions. It should be noted however that these considerations ignore the important effects of membrane elasticity which may either narrow or widen the regime over which one phase is more favorable than the other. They also ignore the important role of other phases in the system.

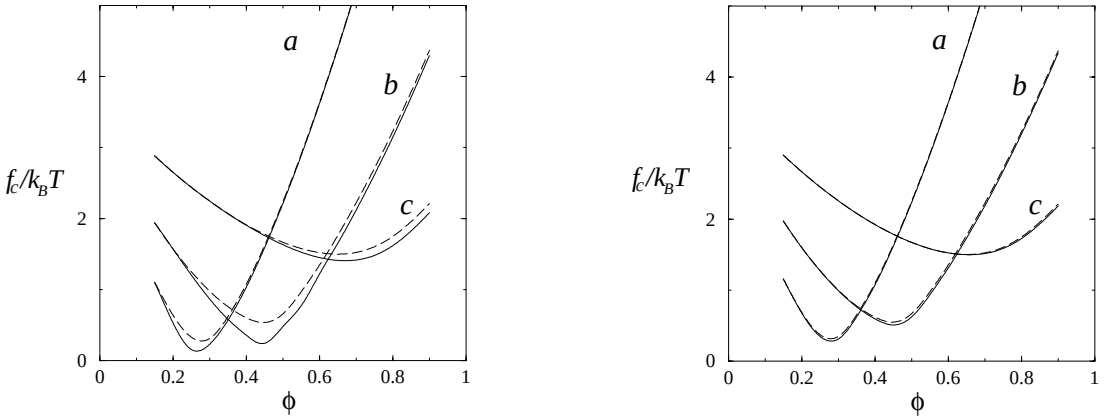

Figure 3.4: Left: Complex free energy as a function ϕ for $l_M = 73$ Å(a),43 Å(b),23 Å(c) for $k = 1k_BT$ and $c_0^h = c_0^c = 0$. Right: Complex free energy as a function ϕ for $l_M =$ 73 Å(a),43 Å(b),23 Å(c) for $k = 10k_BT$ and $c_0^h = 1/100$ Å, $c_0^c = 0$. The full line corresponds to the corrugated complex, while the dashed line to the fully planar one. For all curves, $s = 1$Å.

3.3.2 The corrugated $\mathbf{L}_\alpha^\mathbf{C}$ complex

Free energy

The effect of membrane corrugation on the complex free energy is greatest when the membrane rigidity is small. In this case, the membrane can adjust its geometry to fit the apposed DNA molecule, achieving better electrostatic contact, at a relatively small elastic energy cost. Fig. 3.4(left) shows the complex free energy f_C as a function of membrane composition ϕ, for a soft membrane whose (monolayer) bending modulus for both lipids is $k = 1k_BT$, and spontaneous curvature of the HL and CL are $c_0^h = c_0^c = 0$. Results are shown for three values of complexed membrane length l_M; for all results in this section we set $s = 1$Å. f_c is shown as a function of membrane composition ϕ, for three values of l_M. Also shown is the complex free energy corresponding to a system where the membrane is kept planar.

As has previously been shown, in all cases a minimum in the free energy is seen, corresponding closely to the isoelectric point of the complex. Moreover, The difference between a complex with relaxed (corrugated) membranes, and a complex with constrained (uncorrugated-planar) membrane is also largest at the isoelectric point in all cases. Close to the isoelectric point most of the counterions are already released into the bulk solution. Therefore, further gain in free energy can only be achieved by better charge and spatial matching of the apposed surfaces, in order to optimize the electrostatic interaction energy. Thus, at the isoelectric point the effect of corrugation (i.e., better fitting of apposed surfaces)

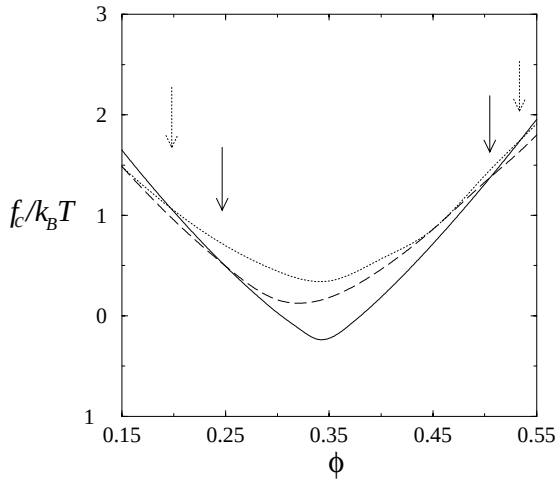

Figure 3.5: L_α^C complex free energy as a function ϕ for $l_M = 58$Å for the case of allowed corrugations (dashed) and suppressed corrugations (dotted). Also shown is the free energy of the hexagonal complex for the same amount of lipid (full line). In all cases $k = 1k_BT$ and $c_0^h = c_0^c = 0$. The arrows mark the points of intersection between the free energy of the lamellar and hexagonal complexes.

on the complex free energy is most substantial. The largest gain in free energy due to corrugations is $\approx 0.25k_BT$. The gain from this added degree of freedom for a unit cell of $s = l_p$ is therefore rather large ($\approx 125k_BT$) .

When more rigid membranes form complexes, the gain in electrostatic energy is expected to be much smaller, since the penalty for bending is large. The membranes bend only slightly, and consequently the free energy is not changed substantially. This can be seen in Fig. 3.4(right) which shows the complex free energy for membranes with $k = 10k_BT$, as a function of membrane composition $\phi = \phi_S$, for three values of l_M. In this case, $c_0^h = 1/100$ Å, $c_0^c = 0$ (modeling a mixture of e.g., DOPC and DOTAP). Here, the gain in free energy following corrugation is only on the order of $5k_BT$ for a unit cell of length $s = l_p$. Similar results were obtained for membranes where the bending rigidity was $k = 10k_BT$ and $c_0^c = 0$, as before, but with $c_0^h = -1/25$ Å (close to the elastic constants measured for DOPE (Gawrisch *et al.*, 1992; Kozlov *et al.*, 1994; Chen & Rand, 1997)).

Allowing for L_α^C complex corrugation adds somewhat to its stability as compared with the H_{II}^C phase. Fig. 3.5 shows the complex free energy as a function of membrane composition, ϕ, for soft lipid membranes ($k = 1k_BT$) and $l_M = 58$Å. We also show the free energy of a complex where corrugations are suppressed, and the membranes are flat. In addition, the free energy of the H_{II}^C phase, for the same number of lipids as in the L_α^C is shown. Since, in general, the spatial corrugations lower the free energy of the lamellar complex, we can expect spatial

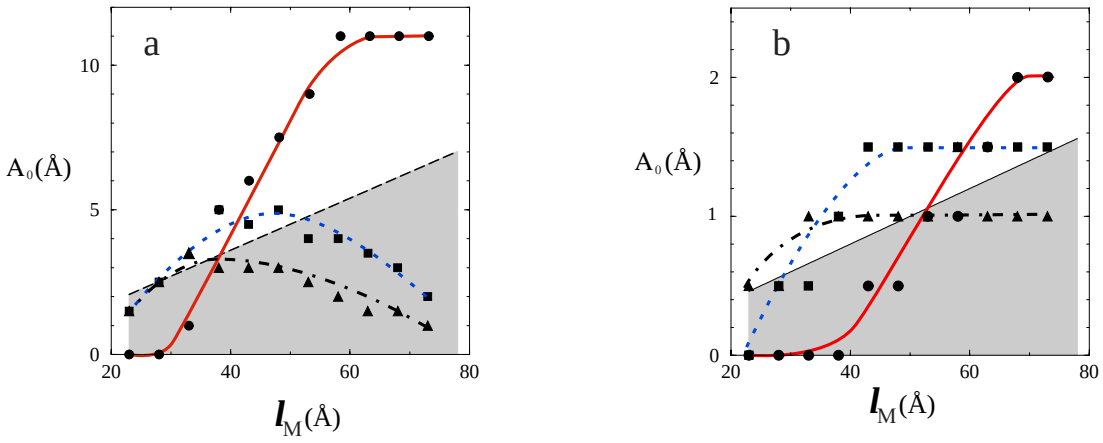

Figure 3.6: (a) A_0 as a function of l_M for $\phi = 0.25$ (full), 0.5 (dotted),0.7 (dash-dotted) for $k = 1k_BT$ and $c_0^h = c_0^c = 0$. The unshaded area corresponds to Eq. 3.17. (b) A_0 as a function l_M for $\phi = 0.25$ (full), 0.5 (dotted), 0.7 (dash-dotted). $k = 10k_BT$, $c_0^h = 1/100$Å and $c_0^c = 0$ The unshaded area corresponds to Eq. 3.17. In all cases, the calculated values are designated by full symbols. The lines are guides for the eye.

modulations to play a role in stabilizing the L_α^C phase with respect to the H_{II}^C phase. This is reflected in the positions at which the free energy curves for the L_α^C and H_{II}^C cross when corrugations are allowed, and when they are forbidden. We see that the region along ϕ in which the hexagonal complex is more stable than the lamellar one is narrower for the corrugated complex. We expect the phase boundary to follow this trend as well. The region where the hexagonal complex will be found is expected to be smaller.

Corrugation amplitude

The free energy was determined for for several systems as described in Sec. 3.2.3. We first consider a soft membrane, $k = 1k_BT$, with $c_0^h = c_0^c = 0$. The extent of corrugation at equilibrium, A_0, as a function l_M for several values of ϕ is shown in Fig. 3.6a. The unshaded area corresponds to the range given by Eq. 3.17.

The maximal corrugation occurs for membranes of low ϕ. When the membrane is of low charge, the proper matching of the DNA molecule and membrane becomes more important for obtaining maximal counterion release. This matching can be achieved both by charge density modulations and by corrugations. Therefore, we expect that if the cost of bending is not too great, the highest modulation will be observed for the membrane of lower ϕ. In all cases a maximum in the corrugation can be observed at a certain l_M. This l_M closely (but not exactly) matches the isoelectric point. At the isoelectric point, the proper release of counterions to solution ultimately depends on the geometrical fit between macroions. It is also clear from Fig. 3.6a that a substantial corrugation

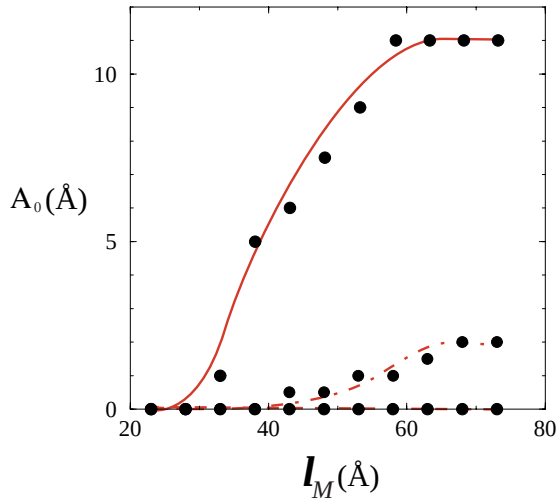

Figure 3.7: A_0 as a function l_M for $\phi = 0.25$. The three curves correspond to: $k = 1k_BT$, $c_0^h = c_0^c = 0$ (solid line); $k = 10k_BT$, $c_0^h = 1/100$Å and $c_0^c = 0$ (dot dashed); $k = 10k_BT$, $c_0^h = -1/25$Å and $c_0^c = 0$ (dashed). In all cases, the calculated values are designated by full symbols. The lines are guides for the eye.

is expected for only a limited *range* of l_M's, for which the corrugation is higher than the expected membrane thermal undulations.

We next consider a more rigid membrane, $k = 10k_BT$, and with $c_0^h = 1/100$Å and $c_0^c = 0$. Fig. 3.6b shows the extent of corrugation, A_0, as a function l_M for the same values of ϕ as shown in Fig. 3.6a. Again, the unshaded area corresponds to the inequality in Eq. 3.17. As expected, for all values of ϕ, A_0 is smaller than for the soft membranes. The maxima are somewhat shifted to higher l_M values. This is easily understood. Since k is substantially higher, the elastic deformation energy cost is higher. When l_M is larger, the (average) curvature is smaller for a certain A_0. It follows that the membranes can deform at a relatively low energy cost only when l_M is large. Again, it can be seen that even when the membranes are stiff, stable corrugations may persist for a certain l_M range. This is due to the fact that *both* the thermal undulations *and* the corrugations are smaller for membranes of higher k. Both these effects cancel each other out to a large extent.

A clear demonstration of the importance of the elastic contribution to the modulation is a comparison of three different membranes all with the same $\phi = 0.25$. In Fig. 3.7 three membrane types are compared, a soft membrane ($k = 1k_BT$, $c_0^h = c_0^c = 0$), a membrane with two lipid types of (nearly) vanishing spontaneous curvature ($k = 10k_BT$, $c_0^h = 1/100$Å and $c_0^c = 0$) and a membrane with a HL characterized by a high negative spontaneous curvature ($k = 10k_BT$, $c_0^h = -1/25$Å and $c_0^c = 0$).

Since the membranes corresponding to the three cases in Fig. 3.7 bear a rather small charge density ($\phi = 0.25$), the effect of the uncharged lipid species is con-

siderable. For membranes of a small bending rigidity - the modulation will be large, as expected. More complex is the case where the bending rigidity is non negligible ($k = 10k_BT$). In this case there is a pivotal role to the spontaneous curvature of the lipid species. As can be seen, in the case where the HL has a high negative curvature ($c_0^h = -1/25$Å) the corrugation is suppressed completely (for $\phi = 0.25$) while it is substantial ($A_0 \approx 2$Å) when the HL has a spontaneous curvature of $c_0^h = 1/100$Å. The qualitative reason is as follows. Since charged lipids tend to migrate towards the interaction zone with the DNA, the uncharged lipids are expelled to the region outside the interaction zone. However, the monolayer area outside the interaction zone is of *positive* curvature, so that placing a HL with a negative spontaneous curvature in that region is unfavorable. Ultimately, the system tends to suppresses corrugations when the spontaneous curvature of the HL is highly negative, and the bending rigidity is substantial.

Charge density modulations

As has been shown in Chap. 2, charge density modulations can contribute substantially to lowering the complex's free energy. Here, charge and curvature modulations are strongly coupled to each other. This is because each lipid species has combined elastic (bending and spontaneous curvature) and an electrostatic (charged or uncharged) properties. At equilibrium, the lipid arrangement (corrugation and charge density modulation) will be determined by the optimum of the free energy.

Fig. 3.8a shows the charge density modulation η as a function of the x coordinate between two adjacent DNA molecules in the same gallery for a rather small DNA-DNA distance, $l_M = 28$ Å, and $\phi = 0.7$ (very close to the isoelectric point). The modulations are shown for three different membranes, corresponding to the ones in the previous section. In general the trend towards charge matching on the DNA and membrane is observed ($\sigma^- \approx 0.6$) at the point of closest approach between the membrane and DNA molecules (i.e., at $x = 0$ and $x \approx 28$ Å). At this distance the effect of the electrostatic interaction is strongest. Thus, charge matching of apposed layers is most effective at this point, enabling a maximal number of counterions to be released from the gap.

The charge density modulation is largest when the membranes are most soft, which also corresponds to the case of largest corrugation. In this case the importance of charge matching (hence lowering of the disjoining pressure) is greatest, since the membrane is wrapped more tightly around the DNA ($A_0 \approx 2.5$ Å for the soft membranes vs. $A_0 \approx 0.5$ Å for the stiff membranes).

More intricate is the case for complexes formed of rather stiff membranes ($k = 10k_BT$), and where in addition the uncharged lipid molecules have a posi-

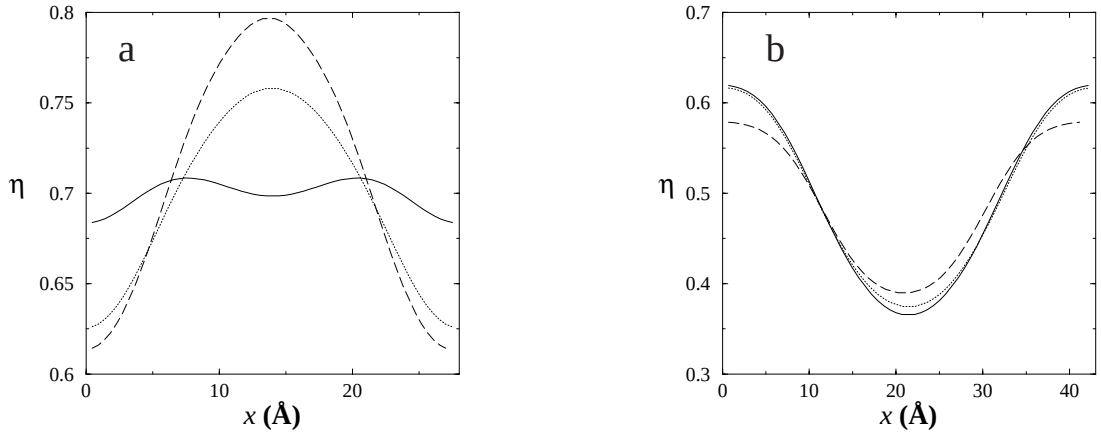

Figure 3.8: (a) η as a function of x for $\phi = 0.7$ and $l_M = 28$ Å. The three curves correspond to: $k = 1k_BT$, $c_0^h = c_0^c = 0$ (dashed); $k = 10k_BT$, $c_0^h = 1/100$ Å and $c_0^c = 0$ (solid); $k = 10k_BT$, $c_0^h = -1/25$ Å and $c_0^c = 0$ (dotted). (b) η as a function of x for $\phi = 0.5$and $l_M = 43$ Å. The three curves correspond to: $k = 1k_BT$, $c_0^h = c_0^c = 0$ (dashed); $k = 10k_BT$, $c_0^h = 1/100$Å and $c_0^c = 0$ (solid); $k = 10k_BT$, $c_0^h = -1/25$Å and $c_0^c = 0$ (dotted).

tive spontaneous curvature ($c_0^h = 1/100$ Å). For these, we find that the modulations do not come to a maximum at the point farthest from the interaction zone, i.e., at the midplane between DNA molecules (solid line in Fig. 3.8). In general, when membranes are stiff, the elastic contribution to the free energy becomes more dominant. Furthermore, in this case the uncharged lipid molecules possess a (rather low) positive spontaneous curvature, so that elastically it favours the midplane, away from the DNA. However, the same (neutral) lipid species also tends to be drawn *towards* the DNA molecule in order to achieve better electrostatic charge matching between the DNA and membrane (at a certaint elastic penalty). The optimum of the two contributions, electrostatic and elastic, which in this case work agains each other, tends to supress the charge density modulation. The results show that maximum charge density is found where the membrane is *most flat*, reflecting $c_0^c = 0$. The uncharged species resides both in the negatively curved region (i.e, favorable electrostatic interaction, unfavorable elastic penalty) and in the positively curved area close to the midplane (i.e., favorable elastic interaction, unfavorable electrostatic interaction).

When l_M is larger, the resulting modulation is somewhat less complex. Fig. 3.8b shows the charge density modulations for the same three membrane properties as before. This time $\phi = 0.5$ and $l_M = 43$ Å, closely corresponding to the isoelectric point.

The charge density modulations are smallest for soft membranes, where corrugations are also more prominent. Charge matching, again, plays an important

role in determining the charge density in the proximity of the DNA. Since the wrapping of membrane around DNA for a substantial length of x implies a larger interaction zone between DNA and lipid, a larger region is expected to fulfill the charge matching tendency, and thus the change in charge density is the smallest.

When the membranes are more rigid, i.e. $k = 10k_BT$, the spontaneous curvature of the HL becomes more important in determining the charge density modulations. Fig. 3.8b reviels that the modulations are largest for $c_0^h = 1/100$Å. For this case, both the electrostatic and elastic considerations to lowering the free energy coincide. While the helper lipid is expected to be (electrostaticaly) expelled from the interaction zone between DNA and lipid, it also has a (small) positive spontaneous curvature, which matches the curvature of the non-interacting region, i.e., close to the midplane.

3.3.3 The $L_\alpha \rightarrow H_{II}$ transition

The phase behavior of lipid-DNA mixtures is strongly affected by the intrinsic propensity of the lipids to form, in the absence of DNA, a particular lipid phase. Lipoplexes are often prepared using helper lipids, such as DOPE, which under physiological conditions form the H_{II} phase, (Gawrisch *et al.*, 1992; Kozlov *et al.*, 1994; Chen & Rand, 1997). These lipids are characterized by large, negative, spontaneous curvature. Adding to the mixture cationic lipids, or more generally lipids of small spontaneous curvature, will result in a first order transition to the bilayer (L_α) phase at some well defined composition.

The major characteristics of this transition are demonstrated in Fig. 3.9 for a CL/HL lipid mixture with the following elastic properties: $c_0^h = -1/25$ Å and $c_0^c = 0$ are the spontaneous curvatures of the helper and cationic lipids, respectively; $k = 10k_BT$ is the bending modulus of both HL and CL, $\hat{h} = 6$Å is the distance of the head group charges from the pivotal surface, and $f_v = 0.35k_BT$ is the stretching-frustration free energy of the inverse hexagonal phase. The elastic constants of the helper lipid correspond closely to those measured for DOPE and mixtures of DOPE with other lipids (Gawrisch *et al.*, 1992; Kozlov *et al.*, 1994; Chen & Rand, 1997).

The figure shows the free energies of the two phases, f_B and f_I, as a function of the CL mole fraction. The lipid compositions at the transition are determined by the common tangent construction. The free energies were calculated using Eqs. 3.18.

In the upper set of curves the free energies of the two phases include all the relevant (i.e., electrostatic, elastic and mixing) contributions. To emphasize the important role of the electrostatic free energy we also show the free energies

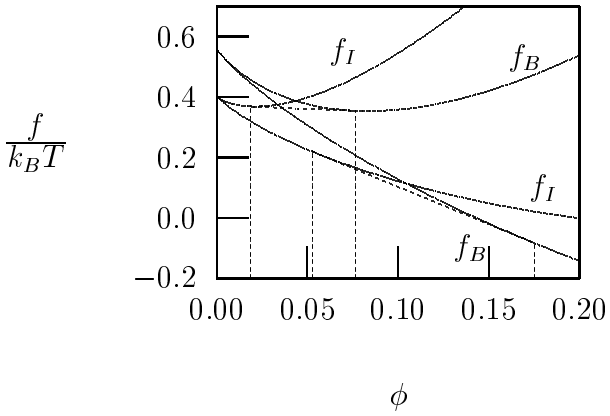

Figure 3.9: The free energies per lipid molecule, f_B and f_I in the lamellar (L_α) and inverse-hexagonal (H_{II}) phases, respectively, as a function of the lipid layer composition ϕ. The upper set of curves display the free energies per molecule as given in Eq. 3.18. In the lower set the electrostatic contributions to f_B and f_I are omitted (that is, only the elastic, interstitial, and mixing contributions are included). The common tangent construction and the coexisting compositions, ϕ_H and ϕ_B, are marked by broken lines. The free energies were calculated for lipid layers with $k = 10 k_B T$, $c_0^c = 0$, $c_0^h = -1/25$Å, $f_v = 0.35$, $h = 6$ Å, and $l_D = 50$ Å.

of these phases for a hypothetical, electrically neutral, mixture with the same elastic properties. (In other words, in this calculation we have omitted f^{es} from f). From these calculations it is apparent that the lipid charges enhance the $H_{II} \rightarrow L_\alpha$ transition. That is, the transitions sets in at a smaller value of ϕ. The origin of the electrostatic destabilization of the H_{II} phase is twofold. The mutual repulsion between cationic charges in the highly curved cylindrical tube and the strong confinement of the counterions within this tube.

3.3.4 Phase Diagrams

As in Sec. 3.3.2, we show in this section three representative lipid-DNA phase diagrams, corresponding to CL/HL mixtures of qualitatively different elastic characteristics, i.e., different sets of k, c_0^c and c_0^h.

In the first system both lipids prefer the planar monolayer curvature, ($c_0^h = c_0^c = 0$), and strongly resist curvature deformations (large k). The second system features the opposite limit, corresponding to very "soft" lipid monolayers, i.e., $k \simeq 0$. Besides the theoretical interest in this limit it should be noted that very soft lipid layers ($k \leq 1\, k_B T$) can be prepared, for example, by adding short chain alcohols to the lipid mixture (Safinya *et al.*, 1989; Koltover *et al.*, 1998; Szleifer *et al.*, 1988). These added molecules may also enter the hexagonal voids of the H_{II} phase and relieve the chain stretching energy, (i.e., $f_v \simeq 0$). Clearly, for

$k = 0$ the spontaneous curvature is irrelevant. Yet it should be noted that the phase behavior observed for $k = 0$ is essentially identical to the one calculated for $k \simeq 1\, k_B T$, $c_0^h = c_0^c = 0$, and $f_v = 0$. The third, perhaps the most interesting, case describes a lipid mixture in which the cationic lipid still prefers the planar monolayer, ($c_0^c = 0$), but the helper lipid, such as DOPE, prefers the inverse-hexagonal geometry, ($c_0^h = -(1/25)\ \text{Å}^{-1}$). The phase behaviors of the three systems are qualitatively different in both the nature of the lipoplex phases which appear in solution and the complexity of the phase diagrams. They represent a rather wide range of experimentally interesting systems.

The phase diagrams will be presented in the $\rho, \bar{\phi}$ plane, the two (experimentally controllable) intensive variables specifying the overall chemical composition of the mixture. For each point in the $\rho, \bar{\phi}$ plane, the number, nature, proportions and chemical compositions of the coexisting phases are determined by minimizing ΔF, (Eq. 3.6), with respect to the seven independent concentration variables defined by Eqs. 3.3, 3.4 and 3.5. The minimization is carried out numerically.

Rigid planar membranes

We first consider a lipid mixture where $c_0^h = c_0^c = 0$. For concreteness we set $k = 10\, k_B T$, a rather common value for many lipid monolayers (Lipowsky & Sackmann, 1995). For these elastic constants, no hexagonal phases appear in our calculated phase diagram. Thus, the value of f_v which further increases the free energy of these phases is irrelevant. (In fact, for $c_0 \equiv 0$, $f_v = 0.35\, k_B T$ and $\hat{h} = 6$ Å identical phase diagrams are obtained for all monolayers with $k \geq 2.5 k_B T$.) An experimental system with similar characteristics is the lipid mixture DOTAP/DOPC (DOPC) which exhibits only lamellar lipid and lipoplex phases (Rädler *et al.*, 1997; Rädler *et al.*, 1998). Lamellar complexes have also been observed using other lipid mixtures (Templeton *et al.*, 1997; Battersby *et al.*, 1998; Boukhnikachvili *et al.*, 1997).

The phase diagram of the system considered is shown in Fig. 3.10. The structural and thermodynamic characteristics of this, relatively simple, mixture have been analyzed in detail, both experimentally and theoretically (see Chap. 2). Below we briefly outline those features of the phase diagram which are relevant for the forthcoming discussion.

Upon increasing ρ at constant $\bar{\phi}$ the system evolves through three distinct stages, (except in the narrow regime $\rho \leq 0.1$). At low values of ρ, lamellar complexes coexist with an uncomplexed DNA phase. In this regime (SD in Fig. 3.10) the DNA-DNA distance is constant $d = d_1(\bar{\phi})$, ($d_1(\bar{\phi})$ increases with $\bar{\phi}$). Once ρ reaches a certain $\rho = \rho_1(\bar{\phi})$ all DNA and lipid become complexed and the system is monophasic. It remains monophasic as ρ increases until it reaches a second

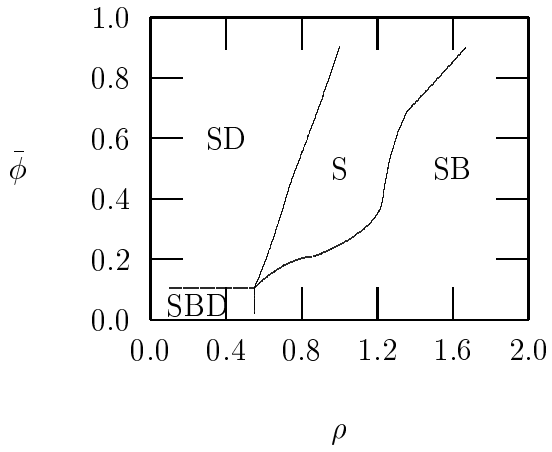

Figure 3.10: The phase diagram of a lipid-DNA mixture, for lipids which self-assemble into rigid planar membranes. The phase diagram was calculated for membranes characterized by $4\,k_BT < k < \infty$ and $c_0^h = c_0^c = 0$. The symbols S, B and D denote, respectively, the L_α^C, L_α, and uncomplexed (naked) DNA phases. (See Fig. 3.1.)

phase boundary, $\rho = \rho_2(\bar{\phi})$. Within the one phase region, which (except for $\rho \leq 0.2$) includes the isoelectric point ($\rho = 1$), d increases linearly with ρ. When $\rho > \rho_2$, ($d > d_2(\bar{\phi})$), the system is again biphasic, with complexes coexisting with an excess bilayer phase. It is important to note that in this (SB) regime, owing to the possibility of lipid exchange, the lipid compositions in the complex and bilayer are different, both depending on ρ. Also, d slowly decreases with ρ. ϕ_S, ϕ_B and d approach constant values at $\rho \gg 1$. In the context of this phase diagram, the role of the isoelectric point can be better understood. While the point $\rho = 1$ essentially always coincides with the minimum of the complex free energy, it does not mark a special or obvious point in the complete phase diagram. In fact it is not always even a one phase region (though it is for $\bar{\phi} > 0.3$).

The appearance of a small three phase region in the left-bottom (small $\bar{\phi}$, small ρ) corner of Fig. 3.10 is interesting theoretically, but of rather limited practical interest. This is because at very low lipid charge densities, around $\bar{\phi} \leq 0.15$, the electrostatic stabilization of the complexes is significantly reduced; the interbilayer spacing $h(\phi)$ begins to increase and the lamellar aggregates eventually disintegrate. Thus, our assumption that h is constant does not hold for very small values of $\bar{\phi}$, certainly not below $\bar{\phi} \approx 0.1$. Nevertheless, the existence of a small three phase region cannot entirely be ruled out. Let us therefore briefly explain its thermodynamic-energetic origin.

When ρ is small part of the DNA must be left uncomplexed. If all lipids were complexed $\phi_S = \bar{\phi}$ is necessarily small. Suppose momentarily that this is indeed the case, and that the complexes are essentially isoelectric. (Strongly "overcharged", i.e., not isoelectric, complexes are less stable.) Since ϕ_S is small

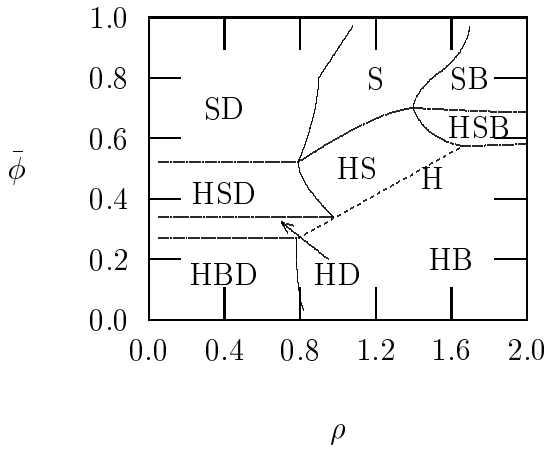

Figure 3.11: The Phase diagram of a lipid-DNA mixture, for lipids which self-assemble into very soft planar membranes. The phase diagram was calculated for membranes characterized by $k = 0$ and $f_v \equiv 0$. The symbols S, B, H and D, denote, respectively, the L_α^C, L_α, H_{II}^C and uncomplexed DNA phases. (See Fig. 3.1.) The straight dashed line marks the single (H_{II}^C) phase region.

d is large, implying poor DNA/lipid charge matching. The situation is improved if the cationic lipids concentrate in the vicinity of the DNA rods. Yet, this lipid segregation involves a nonzero demixing entropy penalty. As a result the middle regions of the L_α^C complex unit cell remains weakly charged implying an energy penalty due to the mutual repulsion of the two apposed monolayers in the complex. It is in fact this repulsion which drives the formation of a third, very weakly charged, bilayer phase.

Hexagonal lipid-DNA complexes appear in certain regions of the $\rho, \bar{\phi}$ plane as soon as k or f_v become sufficiently small, or when the mean spontaneous curvature becomes strongly negative. These two cases are discussed in the following sections.

Soft planar membranes

Although not very abundant some lipid membranes are characterized by small bending rigidities of only a few k_BT (Lipowsky & Sackmann, 1995). Moreover, the bending rigidity can be substantially reduced by adding short chain amphiphiles to the lipid mixture (Safinya *et al.*, 1989). Upon lowering k one expects the appearance of hexagonal lipoplex phases as indeed observed experimentally (Koltover *et al.*, 1998). Thus, our second phase diagram was calculated for the limiting case $k = 0$, (in which limit the value of c_0 is irrelevant). We have also set $f_v \equiv 0$. Qualitatively similar results were obtained with $k \approx 1\, k_BT$ and $c_0^c = c_0^h = 0$.

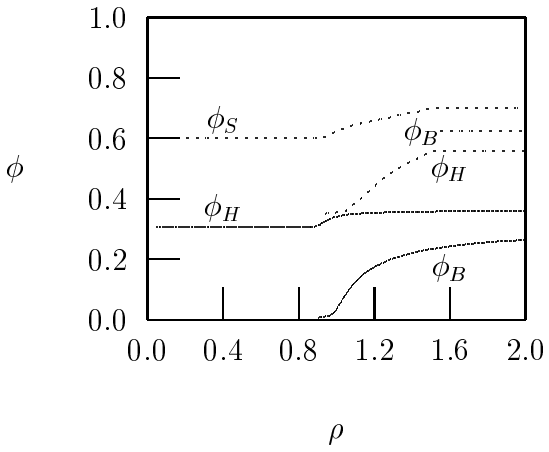

Figure 3.12: The change in the lipid compositions of coexisting phases upon increasing ρ at $\bar{\phi} = constant$ in the phase diagram shown in Fig. 3.11. Solid curves correspond to $\bar{\phi} = 0.31$ and dashed curves to $\bar{\phi} = 0.6$.

For "infinitely flexible" membranes the relative stability of the various possible phases is fully governed by electrostatics. Thus, for instance, owing to its higher charging energy the H_{II} phase is always less stable than the L_α phase. On the other hand, as shown in previous sections, the H_{II}^C phase is more stable than the L_α^C, but only for a certain range of lipid compositions. Thus, since the electrostatic free energies of the different structures show different dependencies on lipid (CL/HL) and lipid/DNA ratios, the phase diagram is determined by a rather complex interplay between electrostatic energies and chemical composition constraints.

The phase diagram for the system of interest here is shown in Fig. 3.11, revealing a plethora of phase boundaries and coexistence regimes. Despite its apparent complexity this phase diagram is not too difficult to explain.

Let us first point out some gross features of the phase diagram. When ρ is small there are not enough lipid molecules to complex all the DNA strands. Thus, on this side of the diagram we always find naked DNA (D) coexisting with either S-type (L_α^C) or H-type (H_{II}^C) complexes, or both. Similarly, at high values of ρ all DNA is already complexed, and the appearance of an excess lipid (here bilayer) phase is unavoidable. Also expected is the complete absence of an H_{II} phase. Whenever lipids are expelled from complexes they prefer the, electrostatically more favorable, bilayer (B) phase. We also note the existence of monophasic regions. The sandwich complex (S in the figure) persists over a range of ρ's (at high $\bar{\phi}$), reflecting the ability of this structure to tolerate changes in lipid composition by adjusting the DNA-DNA distance, d. Recall that we have not allowed a similar, structural, degree of freedom for the honeycomb structure (H).

That is, we have imposed the structural constraint $R_H = R_D + \delta = constant$. If all lipids and DNA are involved in H-complex formation this implies the linear relationship $\bar{\phi} = [a/2\pi(R_D + \delta + \hat{h})l]\rho$. Thus, the monophasic H phase regime shrinks to a straight line in the phase diagram, as indicated by the dashed curve in Fig. 3.11. Had we allowed δ to vary, the H phase line would expand somewhat, yielding a lens-shaped region.

In our discussion of the electrostatic properties of the L_α^C and H_{II}^C unit cells we have concluded that a single H_{II}^C phase becomes unstable with respect to a L_α^C phase once $\phi_H \leq 0.15$. When the possible appearance of other phases is taken into account, the H_{II}^C phase may lose its dominance at even higher values of ϕ_H. Indeed, in Fig. 3.11 we observe that the H phase line extends over the range $0.27 \leq \bar{\phi} \leq 0.57$, indicating that the H_{II}^C phase is partly dissolved, giving rise to the appearance of *two* additional phases, (B and D at low $\bar{\phi}$'s, B and S at high $\bar{\phi}$'s).

To interpret the more subtle features of the phase diagram it is important to bear in mind that whenever two (or three) lipid-containing phases are in equilibrium with each other, their lipid compositions are generally different. The compositional degrees of freedom allow the system to minimize its free energy by optimizing the lipid compositions of the possible phases. To demonstrate these notions let us follow the phase evolution of the system as we increase ρ, keeping $\bar{\phi} = constant$. Fig. 3.12 describes the changes in the lipid compositions of the evolving phases along two such lines, $\bar{\phi} = 0.31$ and $\bar{\phi} = 0.60$.

Along $\bar{\phi} = 0.31$ (solid lines in Fig. 3.12) we always find the H_{II}^C phase. From Fig. 3.3 we know that for $\bar{\phi} = \phi_H = 0.31$ the H_{II}^C complex is more stable than the alternative lipoplex phase, L_α^C. Thus, at low values of ρ all lipids are accommodated in hexagonal complexes (hence $\phi_H = \bar{\phi}$), coexisting with uncomplexed DNA, (region HD in Fig. 3.11). Upon increasing ρ a point is reached where all DNA and lipid are complexed. For $\bar{\phi} = 0.31$ this happens at $\rho = 2\pi m(R_D + \delta + \hat{h})l/a = 0.9$. This point lies on the H phase line in Fig. 3.11. Immediately beyond this point another, bilayer, phase begins to appear. Since the H_{II}^C complexes are most stable at isoelectricity, $\phi_H = \phi_H^\star = 0.345$, they tend to increase their CL content from 0.31 to 0.345. The presence of the extra, bilayer, phase allows them to do so by trading CL's for HL's with the bilayer, as clearly seen in Fig. 3.12. In fact, for $0.9 < \rho < 1$ nearly all charged lipid are used to increase ϕ_H towards $\phi_H^\star$, implying a very weakly charged coexisting L_α phase. Once the H_{II}^C phase has reached its optimal composition $\phi_H^\star$ (at about $\rho \approx 1$) it further takes up only a small fraction of cationic lipids to ensure the same chemical potential in both the L_α^C and H_{II}^C phases. Finally we note that the phase evolution scenario along $\bar{\phi} = 0.31$ is quite similar to the phase

progression observed in Fig. 3.10 (for most values of $\bar{\phi}$). Namely, a two phase (complex/DNA) region, followed by a one phase (complex) region and then again a two phase (complex/bilayer) region. The only difference is that the L_α^C complex is replaced here by the H_{II}^C complex. In Fig. 3.11 the one phase region shrinks to a line, because the hexagonal complex does not possess any structural degrees of freedom.

Richer phase evolution is encountered as ρ increases along the $\bar{\phi} = 0.6$ line, (dashed curves in Fig. 3.12). In this case the first complexes to form (i.e., at low values of ρ) are lamellar aggregates. This follows from the fact that at high CL concentrations the L_α^C phase is more stable than the H_{II}^C phase. From Fig. 3.3 we know that for $\bar{\phi} = \phi_S = 0.6$ the DNA-DNA distance in the lamellar complexes must be small, we find $d = 28$ Å. At $\rho \simeq 0.9$ all the DNA is complexed and only L_α^C aggregates are present in solution. For $\bar{\phi} = 0.6$ this single phase region (S in Fig. 3.11) is very narrow, ending at $\rho \simeq 0.95$. Within this region $d = \rho a/l\bar{\phi}$ increases linearly with ρ and $\phi_S = \bar{\phi} = 0.6$ is constant. From Fig. 3.3 we recall that as d increases (at constant ϕ) there should be a point where the H_{II}^C complex becomes more stable than the L_α^C complex. Thus, an $L_\alpha^C \rightarrow H_{II}^C$ transition should take place at a certain ρ, even if $\phi_S = \phi_H = \bar{\phi} = constant$. Owing to the fact that ϕ_S and ϕ_H need not be the same, the H_{II}^C phase appears already at a smaller value of ρ. The initial composition of the H_{II}^C phase is $\phi_H \simeq 0.35$. As ρ increases further within the HS coexistence region ($0.95 \leq \rho \leq 1.5$) both ϕ_H and ϕ_S increase, implying "overcharging" of the complexes by cationic lipids. Eventually, at $\rho \simeq 1.5$ the lipids prefer the formation of a separate bilayer phase (of composition $\bar{\phi} = 0.6$) rather than joining and continuing to overcharge the DNA-lipid complexes.

Koltover *et al.* (1998) have studied experimentally the phase progression along the isoelectric "dilution line" (lowering $\bar{\phi}$ at $\rho = 1$) in a system of soft lipids. Our calculations agree with their results.

Curvature-loving membranes

The last lipid mixture considered here is characterized by the elastic constants: $k = 10\, k_BT$, $c_0^c = 0$, $c_0^h = -1/25$ Å, and an interstitial energy of $f_v = 0.35\, k_BT$. In this system the helper lipid (such as DOPE) prefers the curvature of the H_{II} phase. Yet, because the cationic lipid prefers the planar geometry and because in the hexagonal geometry both lipids must pay the chain stretching penalty, f_v, the elastic energy difference $\Delta f^{el}(\phi) = f_I^{el}(\phi) - f_B^{el}(\phi) = f_H^{el}(\phi) - f_S^{el}(\phi)$ may be either positive or negative, depending on the lipid composition ϕ. (Recall that the elastic energies of the lamellar complexes is equal to that of the planar bilayer. Similarly the elastic energy is the same for both hexagonal phases.) More

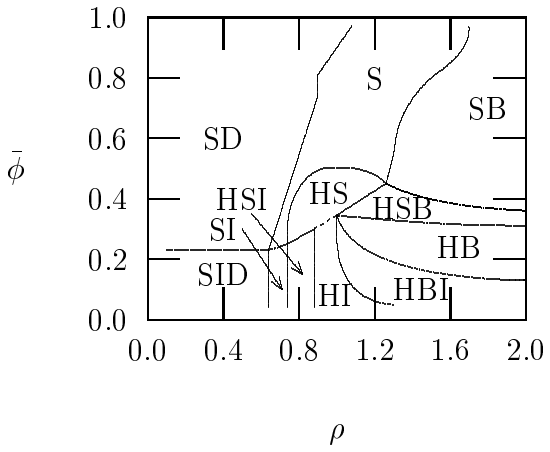

Figure 3.13: The phase diagram of a lipid-DNA mixture involving "curvature-loving" helper lipid, that is: $c_0^h = -1/25$ Å. The other elastic constants are $k = 10\, k_BT$, $f_v = 0.35$, $h = 6$ Å, and $c_0^c = 0$. The symbols S, H, B, I and D denote, respectively, the L_α^C, H_{II}, L_α, H_{II}^C, and uncomplexed (naked) DNA phases. The broken line marks the single H_{II}^C phase.

explicitly, using Eqs. 3.8 and 3.9

$$\begin{aligned} \Delta f^{el}(\phi) &= (ak/2)c_H[c_H - 2c_0(\phi)] + f_v \\ &\simeq 1.47\phi - 0.154 \end{aligned} \tag{3.23}$$

The second equality is obtained by substituting the values of the the elastic constants mentioned above as well as $a = 70$ Å^2 and $c_H = -1/(R_D + \delta + \hat{h}) = -1/19$ Å. From Eq. 3.23 it follows that, elastically, the planar geometry is preferred over the inverse-hexagonal geometry for all compositions exceeding $\phi \approx 0.1$. (The pure helper lipid, $\phi = 0$, indeed prefers the inverse-hexagonal geometry.) Recalling that the electrostatic energy of the H_{II} phase is always larger than that of the L_α phase, a DNA-free inverse-hexagonal is only expected to appear at very low values of ϕ.

On the other hand, around the isoelectric point of the H_{II}^C phase its electrostatic energy is lower than that of the L_α^C phase; i.e., $\Delta f^{es}(\phi) = f_H^{es}(\phi) - f_S^{es}(\phi) \leq 0$ around $\phi = \phi_H^\star \simeq 0.35$. From the results shown in Fig. 3.3 we find $\Delta f^{es}(\phi_H^\star) \simeq -0.5\, k_BT$, whereas from Eq. 3.23 $\Delta f^{el}(\phi_H^\star) \simeq 0.35$. Thus $\Delta f(\phi_H^\star) = \Delta f^{es}(\phi_H^\star) + \Delta f^{el}(\phi_H^\star) < 0$, indicating that just around $\phi_H^\star$ the hexagonal complexes are more stable than the lamellar ones. Yet, this situation quickly reverses as ϕ deviates from $\phi_H^\star$. Thus, around the isoelectric point, $\rho = 1$, where all DNA and lipid molecules tend to associate into complexes we should expect the appearance of H_{II}^C complexes when the total lipid composition, $\bar{\phi}$, is close to $\phi_H^\star$ and lamellar complexes at high values of $\bar{\phi}$. The CL-DNA complexes formed

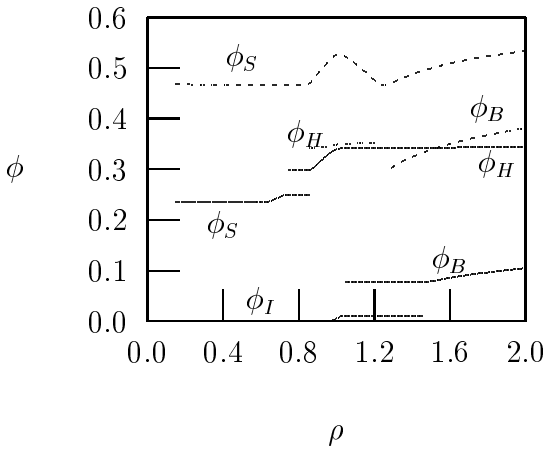

Figure 3.14: The change in the lipid compositions of coexisting phases upon increasing ρ at $\bar{\phi} = constant$ in the phase diagram shown in Fig. 3.13. Solid curves correspond to $\bar{\phi} = 0.16$ and dashed curves to $\bar{\phi} = 0.47$.

in other regions of the $\rho, \bar{\phi}$ diagram will be dictated by the optimal partitioning of the lipids between the various possible phases.

These qualitative considerations are corroborated by the phase diagram shown in Fig. 3.13. For example, in accordance with the above arguments, we note that the region over which all lipids and DNA are involved in the formation of a (single) H_{II}^C phase is extremely narrow, corresponding to the short dashed line (H) passing through $\rho = 1, \bar{\phi} = \phi_H^\star = 0.345$. The phase behavior around this point is also interpretable. As $\bar{\phi}$ increases (at $\rho \simeq 1$) a small region appears (HS) where lamellar and hexagonal complexes coexist in solution. In this region the H_{II}^C complexes maintain their optimal composition $\phi_H^\star = 0.345$ whereas the L_α^C complexes, whose energy is rather insensitive to lipid composition (Fig. 3.3), accommodate all other lipids. As we go in the opposite direction, i.e., lowering $\bar{\phi}$ (hence enriching the system with HL's) at $\rho \simeq 1$ we enter the HI regime where H_{II}^C complexes coexist with an H_{II} lipid phase. Here, again, the H_{II}^C phase maintains its optimal composition while the added helper lipids organize in their favorable hexagonal phase H_{II}. The H_{II} phase appears, as expected, in all the low $\bar{\phi}$ regions of the phase diagram.

In the high $\bar{\phi}$ regime ($\bar{\phi} \geq 0.5$) the lipid mixture is rich in CL molecules implying, by Eq. 3.23 and Fig. 3.2, that the L_α^C phase is more favorable than the H_{II}^C phase, both elastically and electrostatically. Similarly, the L_α phase is preferred over the H_{II} phase. Thus, for $\bar{\phi} \geq 0.5$, as ρ increases at constant $\bar{\phi}$, we observe the same phase progression, SD $\rightarrow$ S $\rightarrow$ SB, as we found in Fig. 3.10 (and in Fig. 3.11 for very large $\bar{\phi}$). Somewhat less obvious, yet not difficult to explain, is the phase behavior on the low ρ side of the phase diagram (say $\rho \leq 0.6$). In this

region there are not enough lipids to complex all the DNA. At high $\bar{\phi}$'s the L_α^C phase is more stable than the H_{II}^C phase and hence naked DNA (D) coexists with lamellar (S) complexes. For $\bar{\phi} \simeq 0.35$ the hexagonal complexes are more stable that the lamellar ones, yet the system prefers the lamellar complexes because, by increasing d, they enable complexation of larger amounts of DNA. Finally, at the bottom-left corner of the phase diagram (low ρ, low $\bar{\phi}$) we observe a three phase coexistence regime where lamellar complexes (S) coexist not only with an excess DNA phase (D), but also with an hexagonal lipid phase (I). The hexagonal lipid phase consists, essentially exclusively, of neutral helper lipids which not only prefer the hexagonal geometry but also do not contribute to the stability of the lamellar complexes. Thus, the lamellar complex phase is enriched by cationic lipids, as we shall see in Fig. 3.14 below.

More complex phase behavior is observed in the region $\rho \geq 0.7$, $\bar{\phi} \leq 0.5$ of the phase diagram, exhibiting the appearance of H_{II}^C complexes (H), coexisting with various other phases, depending on the exact lipid composition and lipid to DNA concentration ratio. The origin of this behavior is the delicate interplay between elastic and electrostatic contributions to the free energies of the L_α^C and H_{II}^C phases, and the ability of the H_{II} and L_α phases to serve as a lipid source (or "dump"). Some of the features characterizing the right-bottom "quarter" of the phase diagram have already been explained when we discussed the phase behavior around $\rho = 1$ and $\bar{\phi} = \phi_H^\star$. Additional aspects of this behavior become clearer when we follow the changes in lipid compositions of the various phases along $\bar{\phi} = constant$ lines.

In Fig. 3.14, we follow the phase progression along two, relatively low, $\bar{\phi} = constant$ lines; $\bar{\phi} = 0.16$ and 0.47. The $\bar{\phi} = 0.16$ line starts at the three phase, SID, region, where lamellar complexes of composition $\phi \simeq 0.23$, (i.e., their CL content is larger than the total CL percentage in the system), coexist with an hexagonal lipid phase composed of HL only ($\phi_I \approx 0$) and an excess DNA phase. At $\rho \simeq 0.6$ all the DNA is complexed. Then, over a narrow range of ρ, the added lipids continue to redistribute between the pure-HL hexagonal phase and the lamellar complexes whose CL content increases slightly to $\phi_S \simeq 0.25$. At $\rho \simeq 0.7$ hexagonal complexes coexist with the lamellar ones, the latter disappearing at $\rho \simeq 0.9$, where $\phi_H \simeq 0.3$. From $\rho \simeq 0.9$, ϕ_H increases linearly reaching its isoelectric value $\phi_H^\star = 0.345$ at $\rho = 1$. Beyond this point $\phi_H = \phi_H^\star$ stays essentially constant as ρ increases, i.e., all the DNA is packed in isoelectric H_{II}^C complexes. The excess lipids are arranged in one or two lipid phases. Just above $\rho = 1$, and as long as $\phi_I \leq 0.02$ the lipids organize in the H_{II} phase; $\phi_I = 0.02$ marks the onset of the $H_{II} \rightarrow L_\alpha$ transition, as shown in Fig. 3.9. At coexistence, the composition of the L_α phase is $\phi_B \simeq 0.07$, as dictated by the common tangent

construction. The $H_{II} \rightarrow L_\alpha$ transition is completed when $\rho \simeq 1.5$, from which point all the excess lipids go into bilayers. As $\rho \rightarrow \infty$, $\phi_B \rightarrow \bar{\phi} = 0.16$.

The phase progression along the $\bar{\phi} = 0.47$ line can be analyzed similarly. One point of special interest here is the reentrant transition S $\rightarrow$ HS $\rightarrow$ S which, for $\bar{\phi} = 0.47$, begins at $\rho \simeq 0.9$ (where the H$\equiv$ H_{II}^C phase appears) and ends at $\rho \simeq 1.2$ (where the H phase disappears).

To conclude, in a lipid DNA mixture containing curvature-loving helper lipids, hexagonal complexes are expected to be formed when the cationic lipid content is relatively low and the lipid to DNA ratio is high. In this region the system can optimally adjust the lipid composition of the complexes, expelling the rest of the lipids into excess lipid phases.

3.4 Concluding remarks

Following recent experiments (Koltover *et al.*, 1998) and qualitative theoretical predictions (May & Ben-Shaul (1997); Chap. 2) we have presented here a rather detailed analysis of the structural and thermodynamic characteristics of DNA/CL/HL mixtures. This analysis should be useful for the interpretation of future experimental studies and may be relevant for the design of a particular lipoplex geometry.

We have shown that the elastic properties of the lipid membranes used as the lipid source for DNA condensation play an important, albeit not exclusive, role in determining the preferred aggregation geometry of the lipoplex. Qualitatively, using mixed planar membranes (i.e., large vesicles) as the lipid source, the lamellar complex is the optimal structure provided the membranes are rigid. On the other hand, with soft, or "curvature frustrated membranes" as the lipid source the preferred aggregation geometry is generally provided by the inverse-hexagonal complex. By frustrated membranes we refer here to bilayers composed of monolayers characterized by negative spontaneous curvature, as is the case for instance with DOPE as the helper lipid. We have shown how "intermediates" in the form of a corrugated lamellar phase may also assemble when the membrane is soft, but not soft enough to stabilize hexagonal structures.

One must remember, however, that even more important than the elastic properties of the lipid membranes are the electrostatic interactions between the lipids and the DNA. Consequently, the preferred complexation geometry is generally dictated by a nontrivial interplay between the electrostatic and elastic contributions to the complex formation free energy. Since both contributions depend on the CL/HL composition different phases may be favored at different lipid compositions. Still, knowing the lipid composition and the way it affects

the relative stability of the lipid-DNA complex does not suffice to determine the nature, number and proportions of the different phases which appear in solution. This requires an additional, thermodynamic phase, calculation which takes into account all the relevant compositional and structural degrees of freedom of the various possible phases. Of particular importance in this context is the possibility of lipid exchange between different phases. As we have seen, under most conditions the CL/HL/DNA mixture splits into two or even three phases, involving different proportions of the three chemical species. When more than three components are present in solution the phase diagram will be even more complex.

Notwithstanding all these complexities our model calculations suggest that anticipating some gross features of the phase diagram corresponding to a given CL/HL/DNA mixture is not impossible. Namely, certain regions of the phase diagrams can always be predicted with considerable confidence; e.g., the "corners" of the $\rho, \bar{\phi}$ plane and the single phase regions. Intermediate regions can often be inferred by their bordering regions. Additional insights can be gained from our three "generic" phase diagrams. We believe that these qualitative conclusions are robust in the sense that they are valid despite the various approximations involved in our theoretical model.

Finally, it must be emphasized that our calculations are only valid for systems in true thermodynamic equilibrium. That is, we have assumed that the systems considered had enough time to exchange lipid molecules between the various possible phases, enabling the total free energy to reach its global minimum. Experimentally, this may not always be the case. Indeed, some experiments indicate the formation of complexes whose symmetries differ from the two basic structures considered here. At the same time, it is important to note that the observation of two or three coexisting structures is by no means an indication that the system is not already equilibrated.

Chapter 4

Adsorption of peripheral proteins on mixed charged membranes

4.1 Introduction

After discussing at some length the nature of the (electrostatic) DNA-lipid interactions, we now turn to study the interaction of charged peripheral proteins with mixed membranes (see Sec. 1.5).[1] As we shall see, some important features are common to the association of many rigid charged macromolecules with membranes. Such is the effect of lipid mobility on the lipid-macromolecule association energy, and also the effect of (electrostatic) interactions between charged macromolecules.

Much experimental and theoretical effort has been invested in the study of the adsorption of proteins onto charged lipid membranes since many biological processes, e.g., membrane activated enzymatic and signal transduction activity, occur at the membrane surface. This adsorption is also a primary step in other processes such as the formation of ion channels in cell membranes by self-assembled amphipathic peptides.

A large number of experimental studies based mainly on fluorescence labeling and NMR techniques reveal that the adsorption process may occur in several stages (Birrell & Griffith, 1976; Boggs *et al.*, 1977; Mayer *et al.*, 1983; Haverstick & Galser, 1989; Bazzi & Nelsestuen, 1990; Gawrisch *et al.*, 1993; Yang & Glaser, 1995; Rytömaa & Kinnunen, 1996; Carbone & Macdonald, 1996; Hinderliter *et al.*, 1998; Goldberg *et al.*, 1998; Krylov *et al.*, 2000; Bradley *et al.*, 1992; Denisov *et al.*, 1998). First, the negatively charged (basic) proteins bind to the

[1] The results presented in this chapter were previously reported in May *et al.* (2000b) and Harries *et al.* (2001).

mixed, acidic and neutral lipid membrane. The fluid nature of the lipid bilayer allows the lipid constituent which interact more favorably with the adsorbing protein (i.e, the acidic, positively charged component) to migrate laterally towards the protein's vicinity, thus modulating locally the lipid composition. Conversely, the less favorably interacting (neutral) lipids, migrate away from this area.

Experiments also show that in some cases, adsorbed proteins and the underlying anionic lipids may further colocalize into domains (or "rafts"). It was further shown that the radius of curvature of these domains was, in some cases, higher than that of the surrounding lipid. Domains were observed to bud and pinch off in the form of vesicles (Galla & Sackmann, 1975; Hartmann *et al.*, 1977; Bradley *et al.*, 1992). This process demonstrates the second mechanism by which a lipid bilayer can lower the interaction free energy: by stretching and bending the membrane can lower the interaction free energy with an adsorbing molecule.

The composition modulation in the underlying lipid bilayer due to lipid migration may be further enhanced by non-ideal lipid demixing. In general, such modulations also contribute to an unfavorable gradient-dependent term in the membrane free energy ("line-tension"). More explicitly, the non-ideal contribution to the membrane free energy may favor the segregation of adsorbed proteins, in order to satisfy the natural tendency of the two underlying lipid species to demix. Thus, the membrane can lower the free energy associated with "rims" of the lipid domains, minimizing them by coalescing smaller domains into larger ones, hence forming macroscopic lateral domains.

Retaining the main features of the model presented in Chaps. 2, 3, we consider a model system for the adsorption of basic globular proteins on a membrane containing varying proportions of acidic lipids. The protein is modeled as a rigid sphere of low dielectric constant, with positive charges uniformly smeared over its surface. This is a special case of the interaction between two, oppositely charged, unequal spheres, which has recently been investigated within PB theory for various boundary conditions on the spheres, accounting for constant charge density, constant potential and ionizable surface charges (Ninham & Parsegian, 1971; Carnie *et al.*, 1994; Warszyński & Adamczyk, 1997; Palkar & Lenhoff, 1994; McCormack *et al.*, 1995; Jönsson & Stahlberg, 1999). Lipid mobility is accounted for through the use of a free energy functional, similar to the one used in the previous chapters, which includes the relevant contributions. The lipid charge modulation (or "polarization") profile varies with the distance of the protein from the membrane surface. In general, the deviation of the local charge distribution from the average (say, uniform) distribution, increases as the protein approaches the surface, becoming most pronounced at the equilibrium distance.

Another important factor affecting the charge modulation profile, as well as

the adsorption free energy, is the lateral density of the adsorbed proteins, reflecting the combined effects of protein-membrane and protein-protein interactions. These interactions play a major role in determining the equilibrium density ("surface coverage") of proteins on the membrane, i.e., the adsorption isotherm; as dictated by the equality of the protein chemical potentials on the membrane surface and in the bulk solution.

The adsorption free energy and lipid distribution profiles are determined by a minimization of the free energy functional with respect to both the spatial distribution of the mobile counterions and the 2D distribution of the lipids in the membrane plane. The minimization results in the familiar nonlinear PB equation for the electrostatic potential in the system, supplemented by a special boundary condition on the electrostatic potential at the membrane surface. reflecting the requirement for a constant *electrochemical* potential of the membrane lipids.

As discussed in Chap. 2, our constant electrochemical potential boundary condition is as an intermediate case between the two familiar boundary conditions corresponding to surfaces of constant charge density and constant surface potential. As we shall see in the next section, in the (hypothetical) limit corresponding to infinite lipid demixing entropy, this special boundary condition reduces to the case of constant ("frozen") charge density. In the opposite (again, hypothetical) limit of zero demixing entropy penalty, the surface charges are fully mobile, as if the membrane were a conductor, implying constant surface potential. The validity of the PB theory for treating the interaction between charged surfaces and colloidal particles in aqueous salt solutions has been discussed in Sec. 1.2

Once the adsorption free energy has been evaluated as a function of protein density, and using an appropriate model for the configurational entropy of the adsorbed protein layer, one can calculate the chemical potential of the protein in the adsorbed state, and hence the adsorption isotherm. We shall adopt here a simple model for the configurational entropy of the adsorbed protein layer, resulting in a Langmuir-like adsorption equation, but with coverage dependent adsorption energy. Our main goal in presenting these isotherms is to demonstrate the important effects of lipid lateral mobility ("surface relaxation" or "annealing") and protein-protein interactions on the adsorption behavior of charged proteins on mixed fluid layers. As we will show, this degree of freedom influences the binding free energy and adsorption isotherms most substantially when the charge density on the membrane is much lower than that on the protein (which is the biologically most relevant case). Qualitatively, our conclusions should be relevant to a variety of adsorption processes involving charged macromolecules; e.g, oligonucleotides, colloidal particles or polyelectrolytes.

After presenting our model and results we will turn to comment in brief on

other models that have been suggested to account for some or all of the mentioned effects.

4.2 Theory

We model the proteins as positively charged spherical particles of radius $R_{\rm p}$, and the membrane surface as an incompressible 2D fluid mixture composed of acidic and neutral lipids, both of the same headgroup area, a. The headgroup of the acidic lipid carries a single negative charge. The membrane and proteins are embedded in an aqueous solution containing a symmetric 1:1 electrolyte of concentration n_0, corresponding to the Debye length l_D. The average charge density of the lipid membrane is $\bar{\sigma} = -\phi e/a$ where e is the elementary charge and ϕ is the (overall) mole fraction of charged lipids in the membrane. The positive charge is assumed to be uniformly distributed on the surface of the protein, with $\sigma_{\rm p}$ denoting the (fixed) surface charge density. One of the most relevant variables in our model is $X_{\rm c} = -\sigma_{\rm p}/\bar{\sigma}$, the ratio between the charge densities on the protein and membrane surfaces; $X_{\rm c} > 0$ to ensure opposite signs of the two macroion charges. For the purpose of presentation we find it convenient to introduce the quantity $\phi_{\rm p} = X_{\rm c}\phi$, expressing the "equivalent composition" of the protein surface. That is, if the protein surface is regarded as composed of (positively) charged and neutral groups, each of area a (identical to the lipid headgroup area), then $\phi_{\rm p}$ is the fraction of charged protein groups.

The equilibrium partitioning of proteins between the bulk solution and the adsorption layer is dictated by the equality of chemical potentials in these two phases. The chemical potential of the adsorbed proteins depends on their adsorption free energy and the 2D translational entropy, both depending on the lateral density of the adsorbed layer. We shall first consider the adsorption free energy and then describe our model for the protein chemical potential and adsorption isotherms.

4.2.1 Adsorption free energy

When the surface density of adsorbate is low, inter-protein interactions are weak, and the adsorption energy is nearly equal to that of an isolated protein. This is the limit in which lipid demixing or, more precisely, local composition modulations, are expected to be most important, especially at low surface charge densities (large $X_{\rm c}$). Protein-protein interactions become increasingly important upon increasing the lateral density of adsorbate. On the average, a given adsorbed protein is surrounded by a radially symmetric distribution of its neighbors. Based

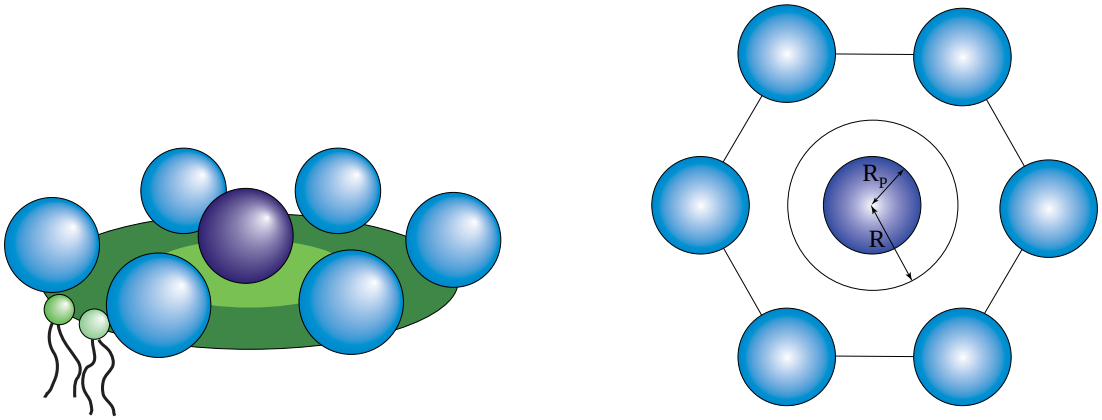

Figure 4.1: Schematic views of the Wigner Seitz cell: side (right) and top (left). The central protein (identical to all others in our model) is coloured uniquely for clarity.

on this notion we shall adopt a mean-field scheme whereby every adsorbed protein defines a cylindrical cell whose main axis (which passes through the protein's center) is normal to the membrane plane. Its projection on the membrane surface is a circular, Wigner-Seitz, cell of Radius R ($R > R_{\rm p}$) and area $A = \pi R^2$, as depicted in Fig. 4.1. Cell models of this kind have been used to describe a variety of electrostatic interaction phenomena in both two- and three-dimensional systems; e.g., the adsorption of divalent surfactants on solid surfaces (Ström *et al.*, 1999), the concentration polarization of colloidal particles at membrane surfaces (Jönsson & Jönsson, 1996), the ionic atmosphere around spherical micelles and other colloidal particles (Linse & Jönsson, 1982; Wennerström *et al.*, 1982), and the classical theory of Fuoss, Katchalsky and Lifson (1951; 1954) for calculating the electrostatic free energy of hexagonally packed (rigid) polyelectrolytes.

Based on the cell model scheme one can calculate the adsorption energy as a single particle property, with inter-protein interactions treated in a mean field approximation. At the cell limits we have the boundary condition $(\partial\varphi/\partial r)_R = 0$, where φ is the electrostatic potential and r is the radial coordinate, measuring the distance from the center of the protein in the x, y plane, parallel to the membrane surface; as described in Fig. 4.2. The minimal distance of the protein surface from the membrane plane, measured along the membrane normal axis (z) will be denoted by h. Any point within the cylinder defined by the circular Wigner-Seitz cell is specified by the three coordinates $\{r, z, \vartheta\}$, with ϑ denoting the azimuthal angle, see Fig. 4.2. By symmetry, $\eta = \eta(r, z)$ is independent of ϑ. Similarly, the lipid composition profile around a given protein is a function of r (and h), but is independent of ϑ.

The mean distance between adsorbed proteins, $2R$, is dictated by their 2D density, $\varrho \propto 1/A \propto 1/R^2$. Thus, the effects of protein lateral interactions on the

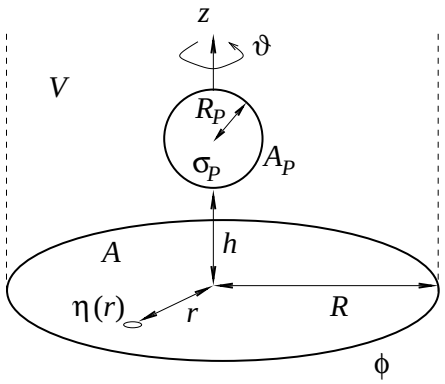

Figure 4.2: Schematic illustration of a spherical protein adsorbed on a mixed planar lipid membrane. The protein radius is R_p and its (uniform) surface charge density is σ_p. The minimal distance between the protein and membrane surfaces is h. A circular membrane region of radius R (and corresponding area $A = \pi R^2$) defines the basis of the cylindrical "cell" corresponding to one adsorbed protein. $\eta = \eta(r)$ is the locally varying mole fraction of charged lipid in the interaction zone.

adsorption free energy enter our model through the dependence on R of the electrostatic free energy per unit cell (or, per protein), F. Of course, this treatment is approximate, because it neglects the positional (both angular and radial) fluctuations of the protein 2D distribution. Note, however, that at very high surface densities the proteins tend to organize into a quasi-crystalline hexagonal lattice, as illustrated in Fig. 4.1. In this limit, where the lateral interactions are most pronounced, the main approximation corresponds to assuming that the nearest neighbor shell is perfectly circular rather than hexagonal. At low surface densities the lateral interactions and hence their effects on the adsorption energy, are rather weak. In particular, when $R \to \infty$ our model describes the adsorption of an isolated protein.

The adsorption free energy, per protein, is $\Delta F = F(h = h_\mathrm{eq}, \varrho) - F(h = \infty, \varrho = 0)$, where $F(h, \varrho)$ is the electrostatic (charging) energy of one protein and a membrane of surface area A (as defined by the cylindrical cell volume prescribed in Fig. 4.2) when the protein is at distance h from the membrane surface and surrounded by identical neighbors at distance $2R \propto \varrho^{-1/2}$; h_eq is the equilibrium distance of the protein, corresponding to the minimum value of F. The electrostatic potential, φ, the local lipid composition profile within the interaction zone, $\eta(r)$, and the electrostatic free energy, F, are all functions of h and depend, parametrically, on the the average lipid composition (ϕ), the size (R_p) and surface charge density (σ_p) of the protein, the salt concentration (n_0), and the linear dimension of the Wigner-Seitz cell, R. (Of course, $2R$ can be interpreted as the equilibrium distance between the adsorbed proteins only when

$h = h_{\rm eq}$.) We shall calculate F, φ, and $\eta(r)$ based on the nonlinear PB theory, thus neglecting the spatial correlations and finite sizes of the mobile salt ions. On the other hand, we shall explicitly account for protein-induced modulations in the lipid charge distribution, and protein-protein interactions. We shall assume that in the "unperturbed" membrane (i.e., when $h \to \infty$ or at $r \approx R$ when $R \to \infty$) the acidic and neutral lipids are mixed ideally.

As in the previous chapters, our starting point is the free energy functional for the electrostatic solution and the charged surfaces,

$$\begin{aligned}
\frac{F}{k_B T} &= \frac{1}{2}\epsilon\left(\frac{k_B T}{e^2}\right)\int_V (\nabla\psi)^2 \mathrm{d}v \\
&+ \int_V \left[n_+ \ln\frac{n_+}{n_0} + n_- \ln\frac{n_-}{n_0} - (n_+ + n_- - 2n_0)\right]\mathrm{d}v \\
&+ \frac{1}{a}\int_A \left[\eta \ln\frac{\eta}{\phi} + (1-\eta)\ln\frac{1-\eta}{1-\phi}\right]\,\mathrm{d}s \\
&+ \frac{1}{a}\int_A \tilde{\chi}\left[\eta(1-\eta) - \phi(1-\phi)\right]\,\mathrm{d}s \\
&+ \lambda\frac{1}{a}\int_A (\eta - \phi)\,\mathrm{d}s
\end{aligned} \tag{4.1}$$

The first term in the last equation is the electrostatic energy of the system, with the integration extending over the entire aqueous volume of the cylindrical region corresponding to our unit (Wigner-Seitz) cell, (including the volume "above" the protein). The second integral accounts for the translational ("mixing") entropy of the mobile ions (of local concentrations n_+ and n_-), relative to their entropy far away from the charged macromolecules where $n_+ = n_- = n_0$; within the interaction region $n_\pm = n_\pm(r, z)$. The third and fourth integrals, where $\eta = \eta(r) = -e\sigma(r)/a$, represent the 2D (non-ideal) demixing entropy of the lipid distribution; the integration extending over the membrane surface from $r = 0$ to $r = R$ ($\mathrm{d}s = 2\pi r\,\mathrm{d}r$). The (phenomenological, mean-field) interaction parameter $\tilde{\chi}$ accounts for a non-ideal mixing contribution to the free energy of the lipid molecules. Non-ideal lipid mixing is commonplace in biological membranes (Garidel *et al.*, 1997; Garidel & Blume, 2000; Garidel & Blume, 1998), resulting, for instance, from the different molecular structure of the lipid tails.

The last term in F has been added to the thermodynamic potential to account for the lipid charge conservation, namely, for the condition $\int_A \eta \mathrm{d}s = \phi A$. The Lagrange parameter, λ, expressing the chemical potential of the charged lipid is determined (following minimization of the system free energy) by the charge conservation condition. The approximations made here, such as setting $\epsilon = 0$

inside the macromolecule, has been extensively discussed in the previous chapters (see e.g., Sec. 1.3.5, Sec. 2.2.2).

The minimization of F with respect to the mobile ion distributions in the aqueous region, $n_{\pm}(r,z)$, and the mobile lipid charges in the membrane plane, $\eta(r)$, results in the familiar PB equation, Eq. 2.4, and a special boundary condition at the membrane surface. For $\tilde{\chi}=0$ this boundary condition is

$$\eta = \frac{\exp(\psi-\lambda)}{\frac{1-\phi}{\phi}+\exp(\psi-\lambda)} = \frac{l_D}{2p_0}\left(\frac{\partial\psi}{\partial z}\right)_{z=0}. \tag{4.2}$$

which should be solved self consistently with the PB equation. The second equality (where $p_0 = 2\pi l_B l_D/a$), relates the local lipid charge density and the normal derivative of the electrostatic potential at the membrane surface through Gauss' theorem.

Two additional boundary conditions on ψ are

$$\left(\frac{\partial\psi}{\partial n}\right)_{\rm p} = 2\frac{X_{\rm c}\,\phi\,p_0}{l_D}, \quad \left(\frac{\partial\psi}{\partial r}\right)_{r=R} = 0. \tag{4.3}$$

The first of these conditions fixes the normal derivative of the reduced potential at the surface of the protein, as implied by its uniform charge density $\sigma_{\rm p} = eX_{\rm c}\phi/a = e\phi_{\rm p}/a$. The second condition follows from our construction of the Wigner-Seitz cell.

Returning to Eq. 4.2 we note that for large R ($R \gg l_D$), i.e., low density of adsorbed proteins, the local lipid composition far away from the adsorption site should equal the unperturbed composition of the membrane, that is, $\eta \to \phi$. Similarly, the membrane potential ψ should equal the electrostatic potential corresponding to an unperturbed membrane, ψ_0; ($\psi_0 = -2\,\mathrm{arcsinh}(\phi p_0)$). From Eq. 4.2 we see that this implies $\lambda = \psi_0$. The limit just described corresponds to the adsorption of a single protein on a lipid membrane which is in contact with a lipid reservoir of composition ϕ and electrostatic potential ψ_0. It can be shown that the adsorption free energy energy in this system is, indeed, given by Eq. 4.1 with $\lambda = \psi_0$. The last term in Eq. 4.1 then becomes $\psi_0 \int_A (\eta-\phi)\,\mathrm{d}s/a$, expressing the change in the electrostatic energy of the reservoir, associated with the transfer of charged lipids into (or out of) the interaction zone.

The protein-induced lipid charge modulation is driven by the tendency of the membrane charges to provide optimal charge matching conditions between the membrane and protein surfaces. This tendency is opposed by the demixing entropy penalty. The actual, optimal, lipid composition profile reflects the compromise between these two conflicting tendencies. If no free energy price was involved in lipid demixing, the lipid charges could freely move on the membrane surface, lowering even further the electrostatic binding energy. This case, resembling a

conducting surface, corresponds to a constant surface potential $\psi(z=0)=\psi_0$. The free energy functional corresponding to this case is obtained by omitting the lipid demixing term in Eq. 4.1 and replacing the boundary condition in Eq. 4.2 by $\psi(z=0)=\psi_0$. In the opposite limit the lipids are forced to maintain a constant ("frozen") composition throughout the membrane, implying $\eta \equiv \phi$ in Eq. 4.1 and replacing Eq. 4.2 by $(l_D/2p_0)(\partial\psi/\partial z)_{z=0}=\phi$. This is the limit of a solid mixed membrane, appropriate for membranes below the chain melting temperature.

It will be interesting to compare the binding characteristics in the two limits above to the ones derived from our model. we do so in Sec. 4.3.1, where the adsorption free energies corresponding to constant-uniform lipid composition and constant membrane potential will be denoted as ΔF_ϕ and ΔF_ψ, respectively. We obviously expect that $\Delta F_\psi \leq \Delta F \leq \Delta F_\phi$ for all values of h and R. We will also briefly examine the effect of non-ideal mixing ($\tilde{\chi} \neq 0$) in the adsorption process (Sec. 4.3.5).

4.2.2 Adsorption isotherms

To examine the effects of lipid mobility and protein-protein interactions on the thermodynamics of protein binding to mixed lipid membranes, we shall present, in Sec. 4.3.2, several representative adsorption isotherms. Our main goal here is to compare adsorption isotherms calculated with, and without, these effects taken into account. Because there is no exact statistical-thermodynamic model for a layer of electrostatically interacting particles (nor for such particles in solution) we shall adopt here an approximate scheme, involving no adjustable parameters.

The finite size of the proteins and the strong electrostatic repulsions between them, in the adsorbed state, are explicitly taken into account in our calculation of ΔF. We shall not include in our model long range non-electrostatic (van der Waals) attractions between the proteins, as these may vary from one system to another and are generally weak compared to the electrostatic forces. Thus the "energetic" contribution to the (Helmholtz) free energy of the protein surface layer, $\mathcal{F}_s = \mathcal{E}_s - T\mathcal{S}_s$, is given by $\mathcal{E}_s = N_{\rm p}\Delta F$, with $N_{\rm p}$ denoting the number of adsorbed proteins and $\Delta F = \Delta F(h_{\rm eq}, R)$, the electrostatic adsorption energy, per protein. The configurational entropy of the adsorbed layer will be modeled using a 2D lattice gas model, whereby the membrane surface is regarded as a (say, hexagonal) array of N adsorption sites, each of which can accommodate, at most, one protein (thus accounting for excluded volume interactions). Using $\theta = N_{\rm p}/N$ to denote the fraction of occupied sites, the configurational entropy is given by the familiar expression, $\mathcal{S}_s = -Nk_B[\theta\ln\theta + (1-\theta)\ln(1-\theta)]$. Thus,

$$\mathcal{F}_s = N\ \{\theta\Delta F(\theta; h_{\rm eq}) + k_B T\,[\theta\ln\theta + (1-\theta)\ln(1-\theta)]\} \qquad (4.4)$$

The explicit dependence of ΔF on θ has been indicated to emphasize that unlike in simple Langmuir adsorption, the adsorption energy here depends on surface coverage.

We still need to define the size of the adsorption cell and hence the value of θ corresponding to a given surface density of proteins. Quite generally, we can set $\theta = \alpha_c(R_\mathrm{p}/R)^2$ where R_p is the radius of the protein sphere and R the radius of the Wigner-Seitz cell defining the area (πR^2) per protein on the membrane surface. The parameter α_c ($\alpha_c > 1$), expresses the extent to which the "actual" cell size exceeds the projected area (πR_p^2) of the bare protein. For a given experimental system it may be determined based on the saturation coverage of this system. We shall simply use $\alpha_c = 1$.

Using Eq. 4.4 the chemical potential of the adsorbed proteins, $\mu_s = (\partial \mathcal{F}_s/\partial N_\mathrm{p}) = \partial(\mathcal{F}_s/N)/\partial\theta)$, is given by

$$\mu_s = \Delta F + \theta\left(\frac{\partial \Delta F}{\partial \theta}\right) + k_B T \ln\left(\frac{\theta}{1-\theta}\right) \tag{4.5}$$

Recalling that the adsorption energy, ΔF, is measured with respect to the charging energy of the separated macroions, the energetic term in the chemical potential of the free proteins in solution is zero. The configurational entropy contribution to this chemical potential can be derived based on a 3D lattice model description, analogous to the one used for the adsorbed layer, yielding $\mu_f = k_B T \ln[c/(1-c)]$ for the chemical potential of the proteins in the bulk solution, with c denoting their volume fraction in this phase. Because we ignore inter-protein interactions in solution we shall only consider the dilute solution limit, implying $\mu_f = k_B T \ln c$.

Comparing the chemical potentials of the protein in the adsorbed and free states we obtain a Langmuir-like adsorption equation

$$\theta = \frac{K(\theta)c}{1 + K(\theta)c}, \tag{4.6}$$

with the caveat that the binding constant depends on surface coverage,

$$K = \exp\left\{ -\left[\frac{\Delta F + \theta(\partial \Delta F/\partial\theta)}{k_B T}\right]\right\} \tag{4.7}$$

It should be mentioned that coverage dependent adsorption constants have previously been presented to describe the effect of lateral interaction between adsorbates. Such are the Davies (Davies, 1958) and Frumkin (Adamson, 1990) isotherms, which are suitable for systems where adsorbates surface mixing entropy is non-ideal. Note, that here the adsorbed proteins interact weakly inter-surface distances larger than $\approx l_D$, but interact strongly when $R - R_\mathrm{p} \lesssim l_D$. Furthermore,

since the lipids are free to defuse in the membrane plane, thus optimizing the interaction energy with the adsorbate, we use a the complete form of $\Delta f(\theta)$ in our equation. We note, that Heimburg *et al.* (1999) have also considered coverage dependent adsorption constants. Their expression for $K(\theta)$ takes into account excluded volume and other, non-electrostatic, interactions between the adsorbed proteins, but not the direct electrostatic interactions.

4.3 Results and Discussion

The interaction between two planar and parallel surfaces, uniformly and oppositely charged with *exactly* the same charge density, is attractive (see Sec. 1.6). This is no longer the case when the charge densities of the two surfaces are not equal. In such cases, a certain fraction of the counterions must remain within the gap between the surfaces. Consequently, the interaction between the surfaces, which can be attractive at large surface separations becomes repulsive at close approach, owing to the increasing osmotic pressure of the remaining counterions. This short range repulsion is stronger the larger the "charge mismatch" between the surfaces (Parsegian & Gingell, 1972; Lau & Pincus, 1999).

As already demonstrated in Chaps. 2,3, qualitatively similar effects prevail, though to a lesser extent, when one or both surfaces are curved. For example, according to PB theory, when a charged sphere approaches an oppositely charged planar surface (of different but fixed charge density) the interaction turns repulsive only at very small distances. When lipid demixing (surface charge redistribution) is allowed, the interaction (according to PB theory) may be attractive at all distances. This scenario may prevail in the adsorption of charged proteins on mixed lipid membranes containing oppositely charged lipid molecules. In the terminology of the previous section, it is possible that ΔF_ϕ and ΔF (and even more so, ΔF_ψ) will differ not only in magnitude but also in sign. The differences are expected to depend sensitively on the charge density ratio $X_\mathrm{c} = -\sigma_\mathrm{p}/\bar{\sigma}$, becoming pronounced for large X_c and small $\bar{\sigma}$. Note, however, that our PB calculations which do not take into account the finite size of the ions and water molecules, are not applicable for distances shorter than $h_\mathrm{min} \approx 3$ Å, corresponding to the range of strong hydration repulsion. In the following discussion we present calculations of $\Delta F(h)$ and $\eta(r)$ as a function of h/l_D, extending to separations as small as $h/l_D = 0.1$. Clearly, our calculations are only relevant for $h > h_\mathrm{min}$.

We shall begin the discussion with a comparison of the adsorption characteristics of an isolated protein ($R \gg R_\mathrm{p} + l_D$) on "frozen" and fluid ("annealing") membrane. We shall then consider the effects of protein crowding on the binding behavior and their reflection in adsorption isotherms. We shall then present a

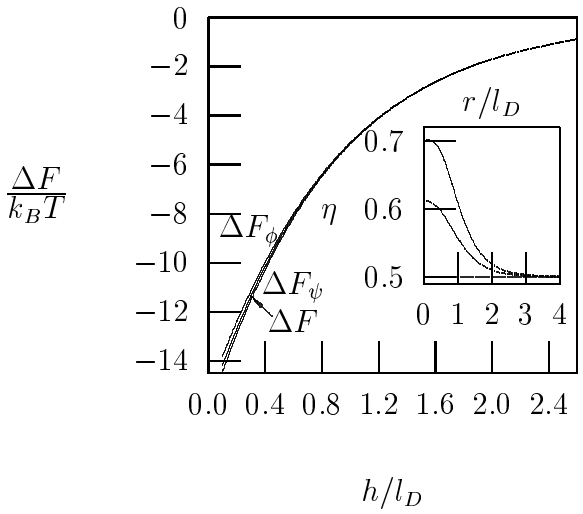

Figure 4.3: Adsorption free energies, ΔF_ψ, ΔF, and ΔF_ϕ, as a function of the protein-membrane distance, h, for $l_D = 10\,\text{Å}$, $R_\text{p} = l_D$, $a = 65\,\text{Å}^2$, $\phi = 0.5$, $X_\text{c} = 1.0$ and $\tilde{\chi} = 0$. The inset shows at $h/l_D = 0.3$ the local composition profile, $\eta(r)$, for membranes with constant surface potential (upper curve), a mixed fluid membrane (middle curve), and a frozen lipid distribution (lower, horizontal, curve).

simple, analytical, model for the adsorption of an isolated protein. We will conclude with a brief discussion of protein adsorption on non-ideally mixed ($\tilde{\chi} \neq 0$) membranes.

In all the calculations presented below we shall use the same set of values for: the cross-sectional area per lipid, $a = 65\,\text{Å}^2$; the Debye length, $l_D = 10\,\text{Å}$; and the radius of the protein sphere, $R_\text{p} = l_D = 10\,\text{Å}$. Numerical solutions of the PB equation are derived using the methods described in App. B.

4.3.1 Adsorption of a single protein

Equal surface charge densities

Our first set of calculations is presented for a lipid membrane where half of the lipids are acidic and the rest are neutral, i.e., $\phi = 0.5$, corresponding to one negative charge per $130\,\text{Å}^2$ of membrane surface. The protein charge density matches exactly the membrane charge density, i.e., $X_\text{c} = 1.0$, corresponding to a protein carrying about 10 positive charges, uniformly smeared on its surface.

Fig. 4.3 shows the adsorption free energies ΔF_ψ, ΔF, and ΔF_ϕ as a function of the membrane-protein distance, h.

Although, as expected, $\Delta F_\psi < \Delta F < \Delta F_\phi$, the adsorption free energies corresponding to the three cases considered are hardly discernible. This appears

reasonable in view of the fact that the average charge density of the membrane matches the one on the protein surface. Nevertheless, as indicated by the charge modulation profiles shown in the inset of Fig. 4.3, the extent of charged lipid recruitment to the immediate vicinity of the protein is non-negligible. (Recall that the calculations shown in Fig. 4.3 are only relevant for $h > h_{\min}$.)

A qualitative argument explaining why the substantial variations in local lipid composition are not reflected to the same extent in the binding free energy curves can be given as follows. As the protein approaches the membrane surface, the charged lipids in its immediate vicinity are essentially neutralized, thus lowering the electrostatic potential in the contact zone. When the lipids are mobile, they tend to diffuse from the surroundings towards the interaction zone, attempting to restore a uniform electrostatic potential throughout the membrane. The gain in electrostatic energy by the stronger adsorption is largely offset by the entropy loss associated with the concomitant transport of counterions into the confines of the interaction region. Later in this section we present a simple model (based on linear PB theory and the constant potential boundary condition on the membrane) that accounts for this mechanism.

Highly charged membrane, weakly charged protein

Our next representative case corresponds to a membrane where most lipids are acidic, $\phi = 0.8$, adsorbing a relatively weakly charged protein with $\phi_{\rm p} = 0.3$ ($X_{\rm c} = 0.375$). The adsorption free energies and charge modulation profiles for the three types of adsorbing membranes are shown in Fig. 4.4.

As expected, because the protein is weakly charged, the magnitude of the adsorption free energy is considerably smaller than in the previous case. However, the distinction between the three different types of membranes is completely lost; all three ΔF's are essentially identical. Nevertheless, noticeable, though small, differences appear again in the charge modulation profiles. Our calculation thus suggests that the adsorption energy of weakly charged proteins on highly charged membranes is not affected appreciably by the degree of lipid demixing. For small values of h/l_D charged lipids are depleted from the center of the interaction zone but concentrate at its rim, resulting in a non-monotonic composition profile.

Highly charged proteins on weakly charged membranes

The case of greatest biological relevance is that of highly charged basic proteins interacting with weakly charged acidic membranes. This is also the type of systems where the effects of lipid charge modulation effects are most pronounced.

The adsorption free energies, ΔF_ψ, ΔF, and ΔF_ϕ, for a system characterized

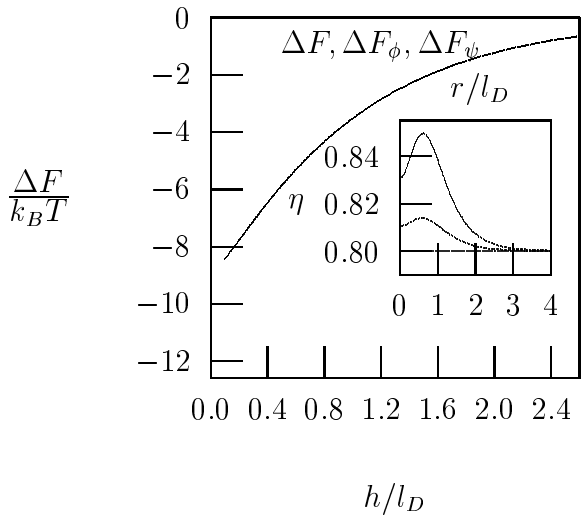

Figure 4.4: Adsorption free energies as a function of the protein-membrane distance, h, for $l_D = 10$ Å, $R_\mathrm{p} = l_D$, $a = 65$ Å^2, $\phi = 0.8$, $X_\mathrm{c} = 0.375$ $\tilde{\chi} = 0$. All adsorption free energies (ΔF_ψ, ΔF, and ΔF_ϕ) are essentially equal. The inset shows at $h/l_D = 0.3$ the local composition profile, $\eta(r)$, for membranes with constant surface potential (upper curve), a mixed fluid membrane (middle curve), and a frozen lipid distribution (lower, horizontal, curve).

by $\phi = 0.2$ and $X_\mathrm{c} = 3.5$ ($\phi_\mathrm{p} = 0.7$), are presented in Fig. 4.5. The inset shows the lipid composition profiles corresponding to the three types of adsorbing membranes for $\eta(r)$ at $h/l_D = 0.3$.

In this case the effects of lipid mobility are apparent in both the adsorption free energy and the composition profile. The magnitude of the binding free energy on a membrane of uniform, frozen, lipid composition ($\eta \equiv \phi$) is considerably smaller than that on a fluid membrane. We also note that ΔF_ϕ shows a minimum at some very small (albeit unrealistic) value of h/l_D, reflecting the osmotic pressure due to counterion confinement in the contact region. This minimum disappears when lipid demixing is allowed to take place, as charged lipids move towards the interaction zone so as to achieve charge matching, concomitantly releasing the confined counterions into the bulk solution. The tendency for charge matching is clearly visible in the inset of Fig. 4.5. The demixing entropy penalty associated with this process is reflected in the difference (of order 1 $k_B T$) between ΔF and ΔF_ψ. In this case, in contrast to the two previous cases considered, the diffusion of charged lipids into the interaction zone is accompanied by counterion release and concomitant gain in binding free energy.

Increasing the charge mismatch between the protein and the membrane surface lowers the adsorption energy and may result in the appearance of a minimum in the energy-distance curve at relatively large separations. This behavior is il-

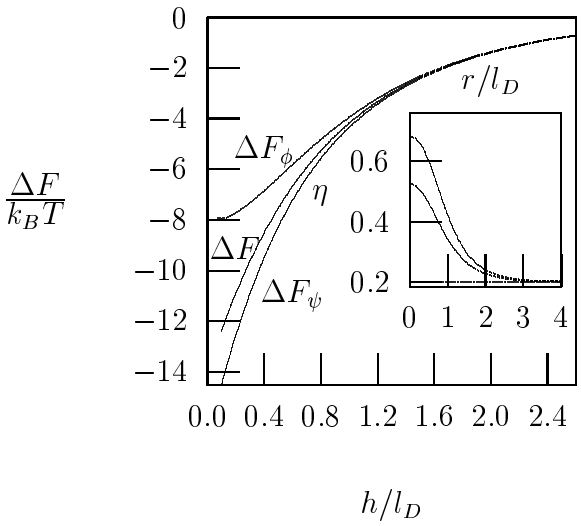

Figure 4.5: Adsorption free energies, ΔF_ψ, ΔF, and ΔF_ϕ, as a function of the protein-membrane distance, h, for $l_D = 10\text{Å}$, $R_\mathrm{p} = l_D$, $a = 65\text{Å}^2$, $\phi = 0.2$, $X_\mathrm{c} = 3.5$ ($\phi_\mathrm{p} = 0.7$), $\tilde{\chi} = 0$. The inset shows at $h/l_D = 0.3$ the local composition profile, $\eta(r)$, for membranes with constant surface potential (upper curve), a mixed fluid membrane (middle curve), and a frozen lipid distribution (lower, horizontal, curve).

lustrated in Fig. 4.6 for a protein with a relatively small surface charge ($\phi_\mathrm{p} = 0.2$, corresponding to four elementary charges on the surface of our protein sphere) and membranes containing a small fraction of acidic lipid. The figure shows ΔF and ΔF_ϕ for membranes of composition $\phi = 0.05$ and $\phi = 0.01$.

For $\phi = 0.05$ we find the same qualitative behavior as that found for larger surface charge densities (Fig. 4.5). The magnitude of the binding energy is smaller, because the charge densities are smaller. For the membrane containing only one percent of charged lipids the interaction is weak and attractive at large distances, turning repulsive at $h \sim l_D$. In this case, because of the very low "background" concentration of acidic lipids, importing these lipids into the interaction zone implies a severe demixing entropy penalty, which the system is reluctant to pay. Consequently, the binding energy remains small in both the fluid and frozen membranes.

4.3.2 Protein lateral interactions and adsorption isotherms

Two important effects come into play when charged proteins begin to crowd on the surface of a (relatively weakly) charged mixed membrane. First, they compete in recruiting charged lipids into their immediate vicinity. (In the opposite case, i.e., when the membrane charge density is larger than that of the protein, the adsorbed proteins compete in recruiting neutral lipids.) Second, lateral inter-protein

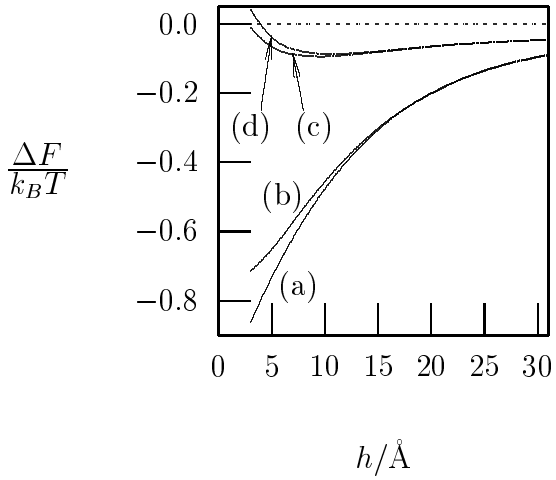

Figure 4.6: The protein adsorption energy ΔF as a function of the protein-membrane distance h for $\phi_{\rm p} = 0.2$. Curves (a) and (b) correspond to $\phi = 0.05$. Curves (c) and (d) correspond to $\phi = 0.01$. For curves (a) and (c), the lipids are mobile whereas for curves (b) and (d) the local membrane composition $\eta = \phi$ is fixed.

repulsion becomes significant, resulting in smaller adsorption free energies. The magnitude of these effects depends sensitively on the protein-membrane charge ratio and, of course, the degree of surface coverage $\theta = (R_{\rm p}/R)^2$.

In Fig. 4.7 we show how the lipid composition profile in the vicinity of an adsorbed protein, $\eta(r)$, depends on the average distance between the adsorbed proteins. (Recall that $2R$ is the distance between adjacent protein centers; the smallest distance between their charged surfaces is $2(R - R_{\rm p})$.) Calculated composition profiles are shown for basic proteins of two different surface charge densities, $\phi_{\rm p} = 0.7$ and $\phi_{\rm p} = 0.2$, interacting with a mixed membrane containing $\phi = 0.2$ acidic lipids. When $\phi_{\rm p} = \phi = 0.2$ ("charge matching") the extent of charge modulation, $\eta(r) - \phi$, is small, and mainly apparent at large inter-protein separations.

Pronounced lipid composition modulations are expected, and observed, for large R, especially when the surface charge density of the protein is significantly larger than that of the membrane, as seen for $\phi_{\rm p} = 0.7, \phi = 0.2$ and for $R = 60$ Å in Fig. 4.7. In this case charged lipids accumulate in the immediate vicinity of the protein, thereby reducing the charged lipid concentration at larger distances, $r \sim R$. The accumulation of charged lipids near the protein is somewhat smaller when $R = 31$ Å, yet their depletion from the "central region", $r \sim R$, becomes more pronounced. The charge modulations are rather weak when the proteins are densely packed ($R = 13$ Å in Fig. 4.7). In this limit the driving force for lipid polarization is diminished because the charged lipids in between neighboring proteins favorably interact with both of them.

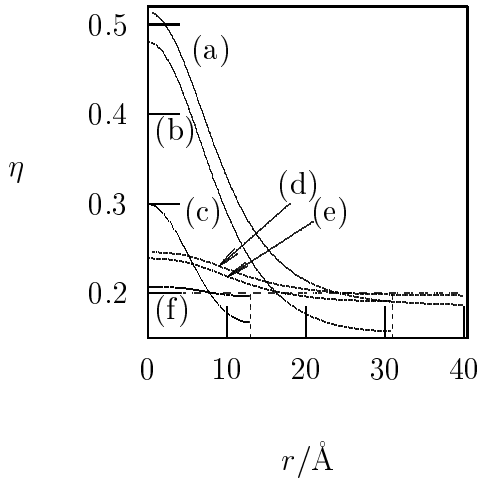

Figure 4.7: The local membrane composition, $\eta(r)$, for $\phi_{\rm p} = 0.7$, $\phi = 0.2$, $\tilde{\chi} = 0$ and $R = 60$ Å (a), $R = 31$ Å (b), and $R = 13$ Å (c). Curves (d), (e), and (f) correspond to $\phi_{\rm p} = \phi = 0.2$, for the same values of R as above. In all cases $h = h_{\rm eq} = 3$ Å.

Finally, in Fig. 4.8 we compile a series of calculations demonstrating the effects of lipid mobility and protein-protein interactions on the adsorption free energy, and how they are reflected in the adsorption isotherms, as calculated using Eqs. 4.6 and 4.7. The two lower diagrams show the binding free energy, as a function of the distance between adsorbed protein, $2R$, for highly ($\phi_{\rm p} = 0.7$, *left*) and moderately ($\phi_{\rm p} = 0.2$, *right*) charged proteins on mixed membranes with varying proportions of charged lipids; in the range $\phi = 0.05 - 0.7$. Four curves are shown for every $\phi_{\rm p}, \phi$ combination. One of these curves corresponds to the "real" case, where the lipids are allowed to demix (paying the necessary price of demixing entropy) and the adsorbed proteins interact with each other. The other three curves, shown only for comparison, were calculated with either one, or both, of these effects artificially turned off. The adsorption isotherms corresponding to the various cases are shown in the two upper diagrams.

A general conclusion from these calculations concerns the rather dramatic role of inter-protein interactions. Whether lipid demixing is allowed or arrested, for all sets of $\phi_{\rm p}, \phi$, we find that the magnitude of the adsorption free energy is steeply decreasing once the separation between adjacent protein surfaces, $2(R - R_{\rm p})$, falls below $\sim 2l_D$; that is when the counterion clouds surrounding the proteins begin to overlap. For our choice of molecular parameters this happens at $R \sim 20$ Å. At larger distances inter-protein interactions are negligible. This conclusion is in line with the calculation of Murray *at al.*, (1999) for pentalysine adsorption on mixed (frozen) membranes.

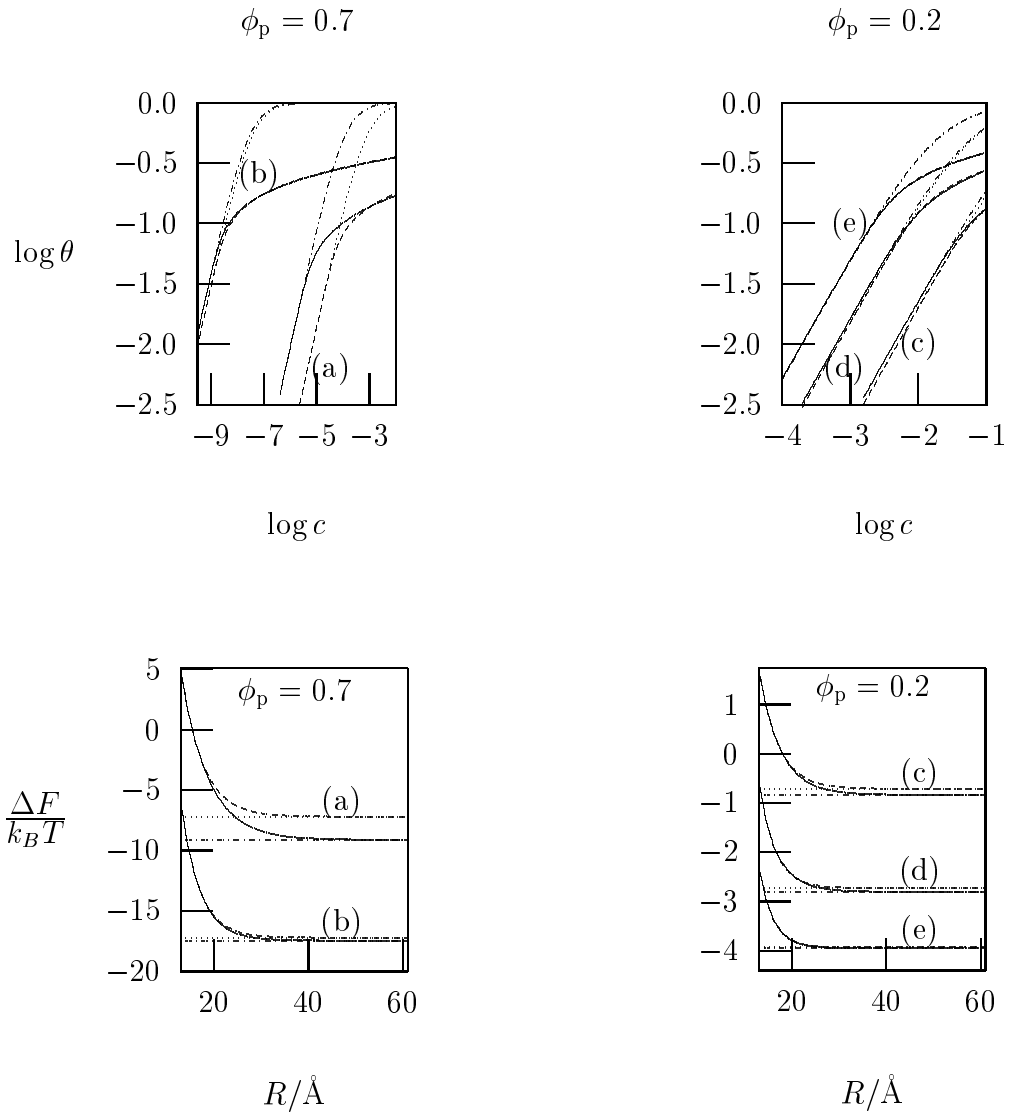

Figure 4.8: Adsorption isotherms $\theta(c)$ (top panel) and adsorption free energies $\Delta F(R)$ (bottom panel) for several combinations of protein and membrane charge densities. The two figures on the left correspond to the adsorption of highly charged proteins ($\phi_p = 0.7$) on membranes with a smaller charge density, $\phi = 0.2$ (curves marked (a)), and an equal charge density, $\phi = 0.7$ (curves marked (b)). The figures on the right are for $\phi_p = 0.2$; the curves marked (c), (d) and (e) correspond to $\phi = 0.05, 0.2$ and 0.5, respectively. In addition to the solid curves, which represent the results obtained from the full calculation, including the effects of lipid mobility (mixing) and protein-protein interactions, we also show, for comparison, three other curves, corresponding to free energies and adsorption isotherms calculated for: immobile lipids but with inter-protein electrostatic interactions (dashed curves); mobile lipids but without protein-protein interactions (dashed-dotted curves); immobile lipids and no protein-protein interactions (dotted curves). All calculations are for $h_{eq} = 3$ Å and $\tilde{\chi} = 0$.

As expected, with these interactions taken into account, the adsorption isotherms begin to saturate at much smaller values of the protein concentration in the bulk solution (c), reaching a much smaller saturation value, θ_{max}; considerably smaller than 1. These findings suggest that the simple Langmuir adsorption scheme may provide a reasonable approximate description of the adsorption equilibrium, provided the linear dimension of an adsorption site is taken as $\sim R_{\rm p} + l_D$.

Whereas the effects of inter-protein interactions become increasingly pronounced at higher surface coverage, the role of lipid mobility is mainly apparent when these interactions subside. As shown in Fig. 4.8, local demixing of the lipids in the vicinity of the adsorbed proteins can result in significant enhancement of the adsorption free energy; especially when the protein charge density is considerably higher than the average charge density of the membrane. The difference in free energy can be a substantial fraction of the total free energy. The adsorption isotherms corresponding to mobile vs. frozen lipid distributions show even greater differences because their dependence on ΔF is exponential.

4.3.3 Surface overcharging

The charges on the *apposed* faces of the membrane and the protein provide partial, possibly complete, charge neutralization, depending on the degree of surface coverage θ. In contrast, the "outer" surfaces of the proteins, those facing the aqueous solvent, hardly interact with the charged lipid surface and are not "compensated" by other "fixed" (macroion) charges. The apparent surface charge density corresponding to an adsorbing membrane, partially covered by proteins, is given by

$$\sigma_{\rm net} = \bar{\sigma} + \sigma_P A_{\rm p}/A = \bar{\sigma}(1 - 4X_{\rm c}\theta) \tag{4.8}$$

where, as before, $X_{\rm c} = -\sigma_P/\bar{\sigma}$ is the protein-membrane charge density ratio. The second equality corresponds to the special case of spherical proteins, where $A_{\rm p}/A = 4\pi R_{\rm p}^2/\pi R^2 = 4\theta$.

From the adsorption isotherms shown in Fig. 4.8 it follows that for all cases and conditions considered, *at saturation* $\sigma_{\rm net} > 0$, i.e., the total protein charge *overcompensates* the negative charge of the lipid membrane. As a specific example consider the case $\phi_{\rm p} = 0.7, \phi = 0.2, (X_{\rm c} = 3.5)$ (with mobile lipids). The saturation coverage corresponding to this case is $\theta_{\rm sat} \approx 0.16$, implying $\sigma_{\rm net} \approx -1.2\bar{\sigma}$. That is, the effective charge of the membrane, after adsorption, is approximately reversed. As qualitatively argued above, this is a consequence of the fact that only about half of the protein charges (those on the hemisphere facing the membrane) are compensated. In general, we expect $\sigma_{\rm net}/\bar{\sigma}$, to be a function of the geometry of the adsorbing particles and the charge distribution on their surface.

It should be mentioned that the phenomenon of charge overcompensation and reversal is commonplace in the adsorption of colloidal particles and polyelectrolytes on oppositely charged surfaces (Châtellier & Joanny, 1996; Joanny, 1999; Borukhov *et al.*, 1998; Park *et al.*, 1999). In fact, surface charge overcompensation (sign reversal of the apparent surface charge) has also been observed experimentally (Kékicheff *et al.*, 1993) and predicted theoretically for ordinary, especially multivalent, electrolyte solutions, (for a comprehensive discussion of these effects see Gerberg and Kjellander (1998) and references therein) . In these systems surface charge reversal is the consequence of ion-ion correlations in the bulk solution and the vicinity of the charged surfaces. Of course these correlations are not accounted for by the mean field PB theory. Nevertheless, the fact that we predict surface charge over compensation in our protein-membrane system is hardly surprising, even though our treatment of the electrolyte solution is based on PB theory. This is because in our problem the analog of the multivalent counterions in electrolyte solutions are not the small monovalent salt ions (that we treat in a mean field fashions) but, rather, the charged colloidal (protein) particles. Spatial correlations between these macro-counterions, as well as excluded volume constraints between the protein counterions and the membrane surface, are explicitly accounted for by the use of the cell model.

4.3.4 A simple model for protein-induced membrane charge polarization

Earlier in this section we have shown that the ability of a mixed fluid membrane to adjust its local charge to that of an approaching protein results in significant enhancement of the adsorption free energy. Moreover, this charge polarization tendency was found to be stronger than the entropic resistance to lipid demixing. This is reflected by the fact that ΔF is not very different from ΔF_ψ, as compared to ΔF_ϕ, see e.g., Fig. 4.5. Replacing ΔF by ΔF_ψ, i.e., omitting the (positive) demixing entropy contribution to the adsorption free energy, we can treat the membrane as a surface of constant electrostatic potential, $\psi = \psi_0$. Based on this approximation a simple, closed form, model for the adsorption of a single protein on the membrane surface, can be presented, as follows.

Suppose first that a charged and flat, say disklike, protein is approaching the membrane. The charge density on the surface of the protein, $\sigma_{\rm p} = -X_{\rm c}\bar{\sigma}$, is generally different from the average charge density on the membrane surface, $\bar{\sigma} = -\phi e/a$. Thus, the lipid composition in the contact region, $\eta = -a\sigma/e$, is no longer equal to the composition in the rest of the membrane (which can be treated as infinitely large). If the area of the protein, $A_{\rm eff}$, is large compared to the cross sectional area per lipid headgroup we can neglect edge effects and

assume that η is uniform within the contact area; η depends, of course, on the disk-surface distance h, $(\eta(h \to \infty) = \phi)$.

Within the framework of *linearized* PB theory (valid for $\psi \ll 1$) an expression for the interaction free energy between two, arbitrarily charged, planar surfaces was derived by Parsegian and Gingell (1972). Based on this expression the electrostatic free energy of our disk-membrane system is given by

$$\frac{F}{k_B T} = \frac{A_{\text{eff}}\, p_0}{a}\left[\frac{(\eta^2 + X_c^2\phi^2)\cosh(h/l_D) - 2\eta X_c \phi}{\sinh(h/l_D)} - 2\,\phi\,(\eta - \phi)\right] \tag{4.9}$$

where $p_0 = 2\pi l_B l_D/a$. To obtain the result in Eq. 4.9, we have used the expression for the reduced potential of an unperturbed membrane $\psi_0 = -2\phi p_0$ as is known from linear PB theory. The second term in this expression is the change in the electrostatic free energy in the reservoir associated with the transfer of lipids into the interaction zone. The membrane composition in the interaction zone is unknown. We find it by minimizing F with respect to η, resulting in

$$\eta = \phi\,\frac{X_c + \sinh(h/l_D)}{\cosh(h/l_D)} \tag{4.10}$$

The dependence of η on the protein-surface separation, as predicted by Eq. 4.10, is shown in Fig. 4.9 for three different values of X_c. For $h \gg l_D$ we indeed find $\eta = \phi$. Interestingly, for all X_c a maximum in η/ϕ appears at some intermediate separation. In the limit $h \to 0$, the charge density on the membrane surface becomes equal to that on the protein surface. That is, at small separations the adsorption free energy is minimal (maximal in magnitude) when the protein-membrane "complex" is *isoelecric*, at which point all the counterions (which otherwise would be confined between the surfaces) are released into the bulk solution.

The electrostatic interaction model outlined above can be extended to the case of a non-planar, e.g., spherical, protein, using a Derjaguin-like approximation (Evans & Wennerström, 1994). In this approximation, the interaction between two curved (or curved and planar) surfaces is expressed as a sum of interactions between planar and parallel area elements belonging to the two surfaces, appropriately weighted according to the curvatures of the interacting surfaces. The interaction energy between area elements is derived from the corresponding expression for infinite surfaces. The Derjaguin approximation is appropriate for moderately curved surfaces. For our problem, of a charged spherical protein interacting with a planar membrane, this requires $R_p > h$ and $R_p > l_D$.

In brief, to apply the Derjaguin approximation to the sphere-membrane problem we divide the sphere surface into circular-stripe elements, cylindrically surrounding the symmetry axis. With each such element we associate a circular shell

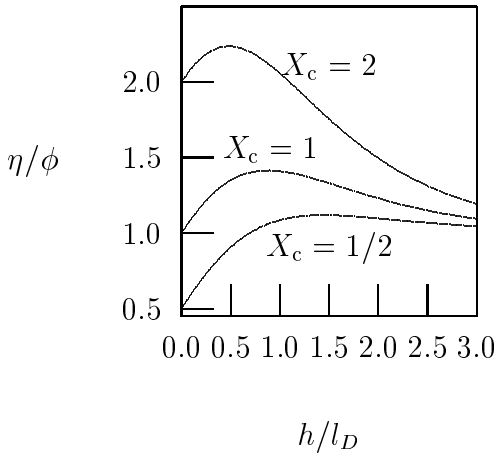

Figure 4.9: The membrane charge density in the interaction region of a "flat protein", as a function of the distance between the membrane surface and the protein. The figure shows $\eta/\phi = (X_c + \sinh h/l_D)/\cosh h/l_D$ as given by Eq. 4.10, for three representative values of the charge density ratio X_c.

of equal area on the membrane surface. The distance between the area element on the membrane (at distance r from the axis) and the corresponding area element on the sphere is $l(r) = \sqrt{(r - r_\omega)^2 + h(r_\omega)^2}$, with $h(r_\omega) = d + R_p - \sqrt{R_p^2 - r_\omega^2}$ and $r_\omega = R_p \sin\omega$ where $\omega = 2\arcsin(r/2R_p)$ is the angle between the membrane normal and the radius vector connecting the protein center with the area element on the protein surface. (The interaction range on the membrane, as measured by r, exceeds the projected radius of the protein, R_p. We let the angle ω vary over the protein hemisphere facing the membrane, *i.e.*, ω varies between 0 and $\pi/2$, implying that on the membrane the interaction zone is bounded by $r_{max} = \sqrt{2}R_p$.) Then, using Eq. 4.10, we calculate $\eta(l(r)) = \eta(r)$, the lipid composition at distance $l(r)$ from the sphere or, equivalently, at distance r from the symmetry axis, in the membrane plane. The results of these calculations are shown in Fig. 4.10 for three values of the protein-membrane charge ratio, namely, $X_c = 0.5$, $X_c = 1$, and $X_c = 2$. To ensure the validity of the Derjaguin approximation we have used here a large protein radius $R_p = 30$ Å. The other parameters in this series of calculations are $l_D = 10$ Å, $\phi = 0.1$ and $h/l_D = 0.2$. Also shown in the figure are the numerical solutions for $\eta(r)$ according to the nonlinear PB theory. The simple model in Eq. 4.10 is in good qualitative agreement with PB theory. It predicts correctly the accumulation of charged lipids near the adsorbed protein and the tendency toward charge matching at the binding site of the sphere.

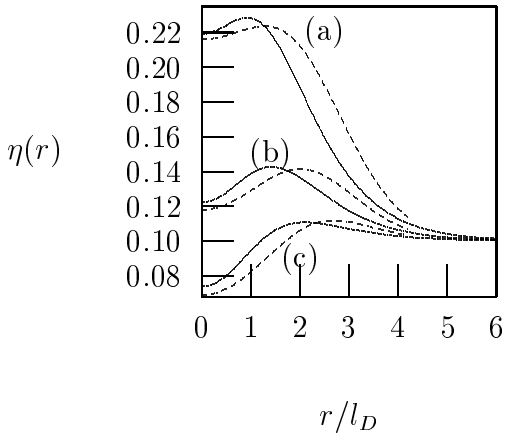

Figure 4.10: The lipid distribution $\eta(r)$ according to nonlinear PB theory (solid curves) and the Derjaguin-like approximation (dashed curves), for $l_D = 10$ Å, $\phi = 0.1$, $R_{\rm p} = 30$ Å and $h/l_D = 0.2$. Curves (a), (b) and (c) correspond to $X_{\rm c} = 2, 1$ and 0.5, respectively.

4.3.5 Non-ideal Mixing

Let us now examine the effect of a non-ideal contribution to the free energy (i.e., a non-zero $\tilde{\chi}$ value) on the migration of lipids in the vicinity of the charged protein. Fig. 4.11 shows the charge density modulation for $\tilde{\chi} = 0$ and $\tilde{\chi} = 1$, for a protein of $\phi_{\rm p} = 0.7$ and membrane with $\phi = 0.2$, for several cell sizes, R. The effect of the non-ideal mixing is apparent: the higher the value of $\tilde{\chi}$, the stronger the compositional modulations of the lipids. In fact, such a non-ideal mixing term may result in charge density modulations yet stronger than in the case of a similar surface without a non-ideal mixing contribution but with constant potential boundary condition.

It is well known (Hill, 1960) that a sufficiently large non-ideal mixing parameter will eventually render any system unstable with respect to macroscopic phase separation. The smallest value of $\tilde{\chi}$ at which this occurs is called the critical point $\tilde{\chi}_c$. Similarly for a membrane with adsorbed proteins on it, we expect the formation of lateral domains within the membrane for $\tilde{\chi} > \tilde{\chi}_c$. That is, instead of varying the composition only locally, the lipids may rearrange macroscopically to take advantage of the favorable non-ideal mixing contribution. This results in macroscopic membrane domains that do not only differ in their lipid composition but also in the density of adsorbed proteins. An interesting question is whether a protein-free membrane can be stable while the same membrane with adsorbed proteins on it would phase separate. In other words, can the adsorption of proteins onto membranes induce phase separation?

A simple qualitative illustration of this idea can be provided by the follow-

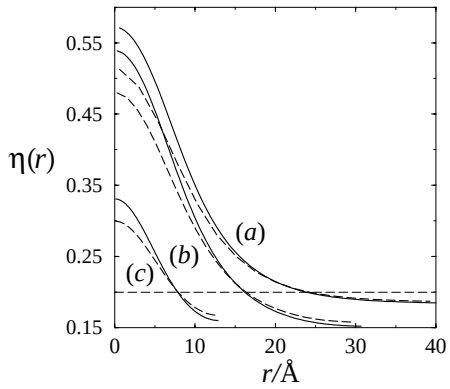

Figure 4.11: The local membrane composition, $\eta(r)$, for $\phi_{\rm p} = 0.7$, $\phi = 0.2$ for $\tilde{\chi} = 0$ (dashed) and $\tilde{\chi} = 1 k_B T$ (solid), for the cases where $R = 60$ Å (a) , $R = 31$ Å (b), and $R = 13$ Å (c).

ing model. Start with an uncharged, two-component, protein-free lipid bilayer. Within a "Bragg-Williams", mean-field approximation the free energy per lipid molecule in the membrane is $f = f_{nm}$ with

$$f_{nm} = k_B T \left[\phi \ln \phi + (1-\phi)\ln(1-\phi) + \tilde{\chi}\phi(1-\phi)\right], \tag{4.11}$$

where the first two terms correspond to the ideal "mixing" of the lipids within the membrane, and the last term represents the non-ideal mixing contribution. As is well known, Eq. 4.11 gives rise to a critical point $\tilde{\chi}_c = 2$ at $\phi = \phi_c = 0.5$ (Hill, 1960).

Consider now a two-component, protein-free lipid bilayer that has one of its components carrying an electrical charge. We account for the corresponding electrostatic free energy by adding to the molecular free energy $f = f_{nm} + f_{el}$ the term (Lekkerkerker, 1989)

$$f_{el} = 2 k_B T \phi \left[\frac{(1-q)}{p} + \ln(p+q)\right] \tag{4.12}$$

where $p = p_0 \phi$, with $p_0 = 2\pi l_B l_D / a$ and $q = \sqrt{p^2+1}$. Eq. 4.12 is the charging free energy of a homogeneously charged membrane of composition ϕ within Poisson-Boltzmann theory. Again, above a certain value $\tilde{\chi} > \tilde{\chi}_c$ appears a (chemical) instability in the membrane with respect to demixing (at the same ϕ_c) (Hill, 1960; Reichel, 1998). The value of the critical point depends on p_0 For $p_0 \ll 1$ it is $\tilde{\chi}_c = 2 + p_0$, increasing to $\tilde{\chi}_c = 2 + \sqrt{3}$ for $p_0 \gg 1$. In Fig. 4.12 (curve a), the behavior of $\tilde{\chi}_c$ is plotted as a function of p_0. The new critical value, $\tilde{\chi}_c$, is always higher than that for an uncharged membrane. The reason for this is the additional repulsion between the head group charges, which renders the mixing process more favorable.

The presence of adsorbed proteins can regain the instability. By neutralizing some (or most) of the lipids in the membrane the additional electrostatic free energy contribution is diminished. The combined protein-membrane system is then expected to display a lower critical demixing parameter $\tilde{\chi}_c$, intermediate between that of a neutral and protein-free, charged membrane. Turning to our illustrative model we adsorb onto the charged membrane proteins of charge z_p and cross-sectional area a_p with coverage θ. This will modify the molecular free energy per lipid $f = f_{nm} + f_{el} + f_{im}$. First, the charging energy f_{el} will be lowered due to the neutralizing effect of the adsorbed proteins. Second, f contains the additional contribution $f_{im} = k_B T\,(a/a_\mathrm{p})\,[\theta \ln\theta + (1-\theta)\ln(1-\theta)]$, accounting for the mixing entropy of the protein layer. While in Fig. 4.11 f_{el} was calculated based on a microscopic model, it is sufficient for our present purpose to consider a highly simplified description of f_{el}. To this end, we shall assume that each adsorbed protein lowers the charge on the membrane by an amount of z_p, without inducing charge density modulations within the membrane. That is, the membrane is treated to remain homogeneously charged, but with an effective composition $\phi^{\mathrm{eff}} = \phi - z_\mathrm{p}\theta a/a_\mathrm{p}$. Consequently, the charging energy per lipid is now given by Eq. 4.12 where ϕ is replaced by ϕ^{eff}. Clearly then, for $a_\mathrm{p}\phi = a z_\mathrm{p}\theta$ all charged lipids would be neutralized by corresponding protein charges, rendering the membrane uncharged (implying $f_{el} = 0$ and thus $\tilde{\chi}_c = 2$). This however is not what the model predicts. Rather, the demixing contribution of the adsorbed protein layer (f_{im}) provides an additional contribution opposing macroscopic phase separation which gives rise to an increase of the critical point with respect to that of a neutral membrane. In fact, the critical $\tilde{\chi}_c$ for a membrane with an adsorbed protein layer is given by the minimum of the expression (maximum of the spinodal)

$$\frac{1}{2\phi(1-\phi)} + \frac{p_0}{q + 2p_0\bar{\theta}(1-\bar{\theta})z_\mathrm{p}^2 a/a_\mathrm{p}} \tag{4.13}$$

with respect to ϕ and $\bar{\theta}$ where q is given by the expression

$$q = \sqrt{1 + p_0^2(\phi - z_\mathrm{p}\bar{\theta}a/a_\mathrm{p})^2} \tag{4.14}$$

In the derivation of Eq. 4.13 all relevant degrees of freedom must be included (Hill, 1960; Reichel, 1998). That is, the membrane is able to adjust not only its composition but also the amount of adsorbed proteins in each of its subphases. The only two conserved quantities are the average composition, ϕ, of the membrane and the bulk concentration of the proteins in solution which determines the average coverage, $\bar{\theta}$, of the protein layer. Fig. 4.12 displays $\tilde{\chi}_c$ according to Eq. 4.13 as a function of $p_0 = 2\pi l_B l_D/a$ for several choices of z_p, a_p, and a. We see that, indeed, $\tilde{\chi}_c$ is intermediate between that of a protein-free

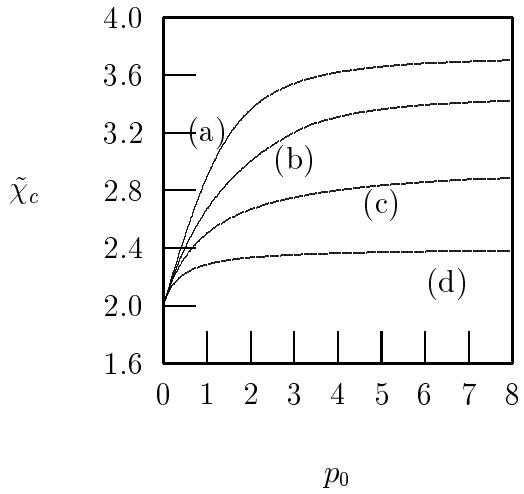

Figure 4.12: The critical point $\tilde{\chi}_c$ of a mixed membrane with an adsorbed protein layer as a function of $p_0 = 2\pi l_B l_D/a$ for no adsorbed proteins (a), $a_\mathrm{p} = a$ and $z_\mathrm{p} = 1$ (b), $a_\mathrm{p} = 2a$ and $z_\mathrm{p} = 2$ (c), and $a_\mathrm{p} = 5a$ and $z_\mathrm{p} = 5$ (d).

and fully neutralized membrane. Fig. 4.12 also suggests that large and highly charged proteins are more efficient in reducing the critical point. At this point we emphasize again the approximative nature of the model. It does not take into account any structural details of the adsorbed proteins, nor does it allow for modulations of the membrane compositions within each phase. Moreover, it neglects the electrostatic repulsion between adsorbed proteins. Thus, it cannot replace detailed numerical calculations. However, it points at a mechanism by which lipid membranes may mediate the accumulation of proteins into domains.

4.4 Concluding Remarks

4.4.1 Other theoretical models

We conclude this chapter with a short account of other theoretical models that have been previously studied. The electrostatic binding of various peptides on lipid membranes was calculated and compared to experiment by Ben-Tal *at al.*, (Ben-Tal *et al.*, 1996; Ben-Tal *et al.*, 1997; Murray *et al.*, 1999), based on solutions of the nonlinear PB equation for atomic models of the lipid bilayer and the peptides. Assuming a "frozen" lipid distribution in the mixed membrane these authors calculated peptide binding constants as a function of salt concentration, finding good agreement with experiment. Employing linear PB theory, Roth *at al.* (1998) have modeled protein-surface binding as the adsorption of a charged sphere on a uniformly charged planar surface. Analyzing the enthalpic and entropic

contributions to the adsorption free energy as a function of the protein-surface charge density ratio, they conclude that the entropic component associated with the release of mobile counterions provides the major contribution to the binding free energy. This conclusion is in line with the common notion that counterion release is the main driving force for electrostatic attraction between oppositely charged macromolecules (see e.g., (Record *et al.*, 1978; Wagner *et al.*, 2000)).

At least two theoretical models have recognized and emphasized the important role of lipid mobility and demixing in determining the protein binding free energy and adsorption isotherms. One of these models, by Densiov *at al.* (1998), has further suggested that protein-induced lipid demixing is the mechanism underlying the formation of lipid-protein domains in membranes. The domains are membrane regions (phases) characterized by a large lateral density of adsorbed proteins and "adsorbing" lipids, coexisting with other regions ("nondomains") of lower protein density. Based on Gouy-Chapman theory, these authors have calculated the adsorption free energy of pentalysine on the surface of a mixed membrane, composed of acidic and neutral lipids, and found it to increase with the mole fraction of acidic lipid in the membrane. Their calculations show that the gain in electrostatic free energy associated with the adsorption of proteins on the phase separated membrane overrides the concomitant loss in lipid mixing entropy, suggesting that domain formation is thermodynamically favorable. It should be noted, however, that this calculation does not account for two important (and coupled) effects. First, assuming uniformly smeared surface charge distributions (in both the domain and nondomain regions), the model can not account for *local* lipid demixing; i.e., for the accumulation of acidic lipids in the immediate vicinity of an adsorbed basic peptide. Second, the model assumes that the basic peptides neutralize a certain fraction of the acidic lipid charges, thus reducing the net surface charge density. The structural characteristics of the adsorbed peptides and, consequently, the lateral electrostatic repulsion between them, are not included in the model. This, direct interaction between peptides has been studied by Murray *at al.* (1999), by calculating the adsorption energy of a peptide onto a vacant membrane adsorption "site", surrounded by pre-adsorbed peptides. These authors find that the adsorption energy indeed decreases, though not to the extent predicted by models assuming uniformly smeared (lipid and protein) surface charges. However, this latter calculation does not allow for local demixing of the lipids. Qualitatively, recalling that the membrane is a 2D fluid mixture, one expects that the already adsorbed peptides will deplete the charged lipids from the vacant regions, thereby reducing the adsorption energy of an additional peptide and hence enhancing the effects of adsorbate-adsorbate repulsion.

Clearly, if lipid demixing can take place locally, i.e., in the vicinity of singly

adsorbed peptides there is no thermodynamic incentive for adsorbate aggregation. This conclusion is consistent with the general result that, at least according to PB theory, the interaction between like-charged colloidal particles is always repulsive, whether in the bulk or in the vicinity of a confining wall (Neu, 1999; Sader & Chan, 1999b; Sader & Chan, 1999a). This, in turn, suggests that protein domain formation is most likely driven by a non-electrostatic mechanism, e.g., a lipid-mediated protein attraction resulting from elastic membrane deformations (and hence line tension) around the protein-membrane interaction zone (Sperotto & Mouritsen, 1993; Gil *et al.*, 1998).

Another theoretical model allowing for lipid redistribution upon protein adsorption on mixed lipid membranes has been presented by Heimburg *at al.*, (Heimburg *et al.*, 1999; Heimburg & Marsh, 1995). Here too, the electrostatic adsorption energy is calculated using Gouy-Chapman theory, assuming that every adsorbed peptide neutralizes a certain number of charged lipids. The charged and neutral lipids are allowed to exchange, as in chemical equilibrium, between the "protein covered" and vacant regions. The equilibrium compositions in these regions are determined by the interplay between adsorption energy and mixing entropy. Then, using either van der Waals or scaled particle theory to account for *non-electrostatic* lateral interactions between the adsorbed proteins the authors derive adsorption isotherms for membranes of varying (average) lipid compositions. With appropriate choice of interaction parameters the model shows good agreement with experimental adsorption isotherms of cytochrome *c* on mixed dioleoyl phosphatidylglycerol/dioleoyl phosphatidylcholine membranes.

In both models outlined above the lipid composition in the protein adsorption domains (whether local or global) is different from that of the protein deficient regions. Both models do not allow for local variations in lipid composition, on a molecular scale, within and around the protein-membrane interaction zone, nor for the dependence of the composition profile on protein lateral density and hence on protein-protein repulsion.

4.4.2 Conclusions

Based on a general free energy expression we have analyzed the role of lipid mobility (hence demixing) and lateral adsorbate interactions, on the adsorption free energy of globular charged proteins onto mixed lipid membranes. We found that the binding energy is significantly enhanced by the ability of the charged lipids to adjust their local concentration in the vicinity of the adsorbed protein. The effects of this, lipid-mobility, degree of freedom are particularly pronounced when the protein is highly charged and the membrane is weakly charged. In this case,

the extent of local membrane charge modulation is substantial, especially at low protein densities. Inter-protein repulsions within the adsorbed layer become important, as expected, when the counterion atmospheres of neighboring proteins begin to overlap. Both the lipid demixing degree of freedom and the lateral interactions between the proteins are reflected in the calculated adsorption isotherms. Assuming that the lipid charge in the vicinity of the adsorbed protein matches the ("membrane facing") protein charge, and that the minimal distance between protein is governed by their counterion screening clouds provides an approximate scheme for calculating (Langmuir-like) adsorption isotherms.

At saturation the charges on the membrane and the protein regions facing the membrane are nearly equal. The protein charges facing the aqueous solution remain uncompensated, implying "charge reversal" of the adsorbing surface.

The addition of a non-ideal lipid mixing contribution to the free energy leads to a stronger membrane charge density modulation. Together with an energy term not considered here which depends on the gradient in charge density, this non-ideality may be at the base of the experimentally observed formation of high density protein domains in lipid membranes.

Chapter 5

Postlude

The work presented in this dissertation has focused on the electrostatic interaction of rigid macromolecules with lipid membranes. The study of such forces has always attracted interest – both experimental and theoretical. This is because it was realized early on, that electrostatic forces are fundamental and often paramount in understanding the interactions leading to formation of macromolecular assemblies of the kind so often encountered in nature.

The theoretical study of such interactions has experienced a new thrust in the past decade, due, at least in part, to the advent of computers that can perform high speed calculations. These have enabled the study of more complex systems that ultimately result in equations that are numerically harder to solve. The models suggested for the systems studied can now include a more complex and intricate picture, involving more degrees of freedom, that are relevant to the full description of the real physical system examined.

The outcome of such numerical calculations can then be compared with the results obtained from more simple models that can be solved analytically (or at least semi-analytically). Thus, we may be reassured that the underlying principles and forces in action hold even in light of complexity. In addition, new insights are also gained as to the effect of strongly coupled degrees of freedom to the systems' behavior.

Chapters 2 and 3 discussed the interaction of lipid membranes and DNA molecules. Chapter 2 has dealt with one specific ordered phase, the lamellar L_α^C phase, that may form when mixing lipids that tend to form planar membranes and DNA in an aqueous solution. Our model included the electrostatic degrees of freedom, taking into account the mixing (and demixing) of the mobile salt ions, as well as the charged and uncharged lipids in the (mixed) membrane.

An important achievement was the construction and subsequent solution of the appropriate free energy functional, leading to a modified Poisson-Boltzmann

equation with special boundary conditions, taking into account the possibility of charged lipids to demix in the presence of a charged macroion. The basic underlying mechanism for the association of charged macromolecules, i.e. counterion release, was theoretically predicted and confirmed directly through experiment. We also showed the importance of lipid demixing in the vicinity of oppositely charged DNA, tending towards charge matching.

Using the same model, the experimentally observed phase behavior of the system was also accounted for. A simple analytical model was presented, reconfirming many of the important results of the more complex model.

In Chapter 3, membrane elasticity, another important degree of freedom, was added to the electrostatic and mixing. Thus, yet more complex and rich phase behavior could be accounted for. One example is the formation of the hexagonal H_{II}^{C} phase upon softening of the lipid membrane involved in forming the L_{α}^{C} complex. Several phase diagrams were presented, pertaining to systems with typical compositions and elastic properties. The principles governing the formation of different phases were elucidated. We also showed how all the relevant degrees of freedom (electrostatic, mixing and elasticity) could all be combined self-consistently in a free energy functional. This was demonstrated in the analysis of the formation of the corrugate L_{α}^{C} complexes, where elasticity often opposes the electrostatic tendency for the membrane to bend around DNA molecules.

In Chapter 4, we turned to discuss systems where peripheral proteins, another class of rigid macromolecules, interact with lipid membranes. The coverage dependent adsorption free energy was determined, again including electrostatic and mixing contributions to the free energy. The importance of these degrees of freedom, as well as the electrostatic interaction between adsorbed proteins was demonstrated through the adsorption isotherms. Some common principles to the ones discussed in chapters 2 and 3 emerge here: the tendency towards charge matching on the membrane and protein, and the consequent membrane polarization. We also showed how membrane charges are typically over compensated by protein-charges. Finally, we argued that lipid-protein domains may be enhanced by non-ideal lipid mixing contributions.

All models presented were discussed on the level of the mean-field (Poisson-Boltzmann) theory. As presented in Chap. 1, it is also possible to harness alternative approaches, such as computer simulations (Lyubartsev & Nordenskiold, 1995; Grønbech-Jensen *et al.*, 1997). These may shed light on effects which can not be described by mean-field, PB theory. For example, Bandyopadhyay *et al.* (Bandyopadhyay *et al.*, 1999) use simulations to study lamellar DNA-lipid complexes. Their results generally agree with ours, in that they find corrugations and charge density modulations in the membrane surface due to the interac-

tion with the DNA. However, they also find other effects that are absent from our model. In particular, they find that *both* the helper and charged lipids are involved in neutralizing the anionic DNA phosphate groups. The electrostatic interactions between the CL and HL headgroups of the two lipids allow the HL headgroups to orient out of the bilayer plane, and thus interact with the DNA molecule. Albeit, as has been demonstrated throughout this work, our results, based on mean-field calculations, are consistent with most of the available experimental data. This supports our belief, based on previous works (see Sec. 1.2.1), that the most important degrees of freedom in these systems are indeed properly taken into account, and that the influence of other contributions on the system's behavior, such as correlations between mobile charges, are of secondary importance here.

Since the work presented here was wholly devoted to the interaction of *rigid* macromolecules with charged membranes, the realm of flexible polymers interacting with membranes has been left out. This would be a natural extension of this work. For example, ss-DNA is a highly flexible polymer, that would most probably behave quite differently when interacting with lipids. Recent work (Artzner *et al.*, 2000) has investigated the effect of adding other polyelectrolytes (dextran sulphate) to a system of lipoplexes. Thus, and exchange between DNA and polyelectrolyte in the lipid-polyelectrolyte mesophases was observed. This probes another important aspect: the dissolution of lipoplexes in living cells as part of the transfection process. An even more general emerging aspect is the interaction of lipids with self-assembling amphiphiles, to form other mesophases such as micellar aggregates, again reminiscent of the ones formed by the amphiphiles themselves when they are in solution (Kwak, 1998; Goddard & Ananthapadamanabhan, 1993; Diamant & Andelman, 2000).

To conclude, a self-consistent scheme, accounting for the important lipid demixing and elastic degrees of freedom has been presented. The free energy functional presented throughout this work can be extended to include other relevant effects and degrees of freedom, such as ionizable lipid headgroups (Ninham & Parsegian, 1971) and the effect of line tension due to a gradient in the lipid composition profile. It is my feeling that the strength of this self-consistent approach is evident in the studied systems presented here.

Appendix A

Solving the Poisson–Boltzmann Equation for two parallel cylinders

A.1 Introduction

The electrostatic interaction between colloidal particles and macromolecules often plays a crucial role in the stability of these systems (Israelachvili, 1992). Albeit, while the cases of two charged interacting planes and spheres has been extensively studied, (Israelachvili, 1992; Langmuir, 1938; Carnie *et al.*, 1994; Stankovich & Carnie, 1996; Palkar & Lenhoff, 1994; Warszyńsky & Adamczyk, 1997; Ledbetter *et al.*, 1981; Hoskin, 1955; Hoskin & Levine, 1955) the case of two rods has gained less attention. Thus, our goal in this appendix is to present a numerical method for calculating the electrostatic interaction between either two (infinitely long) parallel charged rods, or between a rod and a charged planar surface, in a solution containing added salt.[1]

Evaluating the electrostatic force between these model particles, even within the framework of PB theory, is a formidable task. As discussed in Chaps 1--3, to a good approximation, the interaction between two double-stranded DNA molecules can be modeled as that between infinite cylinders, since DNA is a rigid polyelectrolytes, with a typical persistence length of 50nm, much larger than the (axial) separation between neighboring charges ($\sim$0.17nm). In a similar fashion, lipid bilayers may be modeled as infinite planes or slightly curved surfaces.

Several studies of the interaction between charged rod-like particles have been

[1]The results presented in this appendix were reported in Harries (1998)

presented in the past (Ohnishi *et al.*, 1960; Brenner & McQuarry, 1972; Brenner & Parsegian, 1974; Grønbech-Jensen *et al.*, 1997; Ray & Manning, 1994). Some of these rely on the use of the linearized version of the PB equation (in the case that the cylinders are immersed in a salt solution) (Brenner & Parsegian, 1974; Brenner & McQuarry, 1972). This is an appropriate approximation in cases of low surface charge densities. However, when dealing with particles of high surface charge density, and a radius comparable to the Debye length (e.g. DNA molecules), this approximation is no longer valid. In the limit where the inter-particle distance is much smaller than their radii, the Derjaguin approximation may be employed (Israelachvili, 1992). However, no *single* approximation is expected to hold true for the whole range of inter-particle separations.

Another, alternative approach to studying the interaction between charged rods is provided by the "counterion condensation" theory (CC) (Ray & Manning, 1994). Using this theory, an attractive force was found between two interacting line charges (though the force was not evaluated continuously for the whole range of inter-particle distances). This is in contrast to the expected result from PB theory, where two equally charged rods should always repel (see sec. III). We note however, that it is was suggested that CC theory is not a preferable approximation to PB theory (Stigter, 1975).

In the case that no salt is added, an exact analytical solution exists for the force between two rods using PB theory (Ohnishi *et al.*, 1960). In a recent study, the force between two charged rods with no added salt was evaluated using Brownian-Dynamics simulations (Grønbech-Jensen *et al.*, 1997). Inter-rod attraction was found in the case corresponding to DNA in a solution of divalent-counterions.

In the past few years, several numerical procedures have been devised for calculating the double layer forces and free energies between *spherical* particles (Carnie *et al.*, 1994; Stankovich & Carnie, 1996; Palkar & Lenhoff, 1994; Warszyńsky & Adamczyk, 1997; Ledbetter *et al.*, 1981). Usually these studies involve using bispherical coordinates to transform the problem into one solvable in a closed domain, and with convenient boundary conditions. Prominent among these methods is the procedure first introduced by Carnie et al (see e.g., (Carnie *et al.*, 1994; Stankovich & Carnie, 1996); details of the general numerical scheme used to solve the PB equation can be found in (Houstis *et al.*, 1985)), which was later extended to the treatment of two spheres of arbitrary radii. In the limiting case where one radius is infinite, this corresponds to the interaction of a sphere and a plane. This numerical algorithm which uses a spline collocation scheme to solve the full PB equation, will be extended in the present study to the treatment of cylindrical particles. The method presented here is most general, and can be

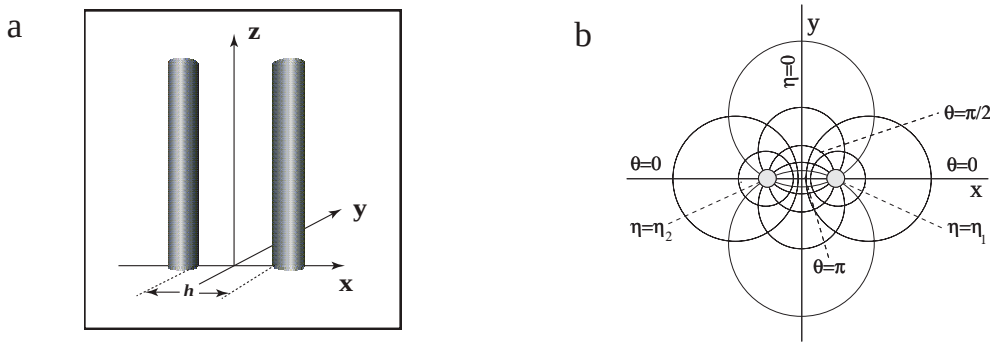

Figure A.1: a) A system of two interacting charged parallel rods. b) Traces of constant η and θ curves in the bicylinder coordinate system. The shaded areas correspond to the volume interior to the two interacting cylinders in the model system.

used to treat, for example, the interaction of various types of colloidal particles. However, the numerical examples presented below, are mainly relevant to systems containing DNA and lipid bilayers. In particular, it will be shown that the interaction between equally charged rods is always repulsive, whereas when the rods are not equally charged, an attraction may appear. Results for the case of an interacting cylinder with a wall are also presented. We find that the surface charge density modulation on the plane of constant potential, may show either an accumulation or depletion of counter charges near the cylinder (depending on the ratio between the suface charge densities on the plane and cylinder).

A.2 Method of solution

The model consists of two infinitely long cylinders of radii a_1 and a_2, immersed in a solution of 1:1 electrolyte, of bulk concentration n_0. The two cylinders are separated by a surface to surface distance h (see Fig. A.1a). In all cases considered, it is assumed that inside the particles the dielectric constant is zero. This is a common approximation when dealing with low dielectric particles, eliminating the need to solve for the potential within them.

All lengths in the system will henceforth be expressed in terms of the Debye length, $\kappa^{-1} = (\epsilon_0 \epsilon_r k_B T / 2 n_0 e^2)^{1/2}$, where ϵ_r is the dielectric constant of the solution, ϵ_0 the permittivity of vacuum, e the electronic charge, k_B is Boltzmann's constant, and T the absolute temperature. The PB equation for the scaled electrostatic potential $\psi = e\phi/k_B T$, everywhere outside the cylinders is:

$$\nabla^2 \psi = \sinh \psi \tag{A.1}$$

In a similar manner, reduced units will be used to scale the surface charge

density ($\sigma^\star = \sigma l_B/e\kappa$), force per unit length ($f^\star = f l_B/k_BT\kappa$), and free energy per unit length ($F^\star = F l_B/k_BT$), where $l_B = e^2/\epsilon_0\epsilon_r k_BT$ is the Bjerrum length.

The boundary conditions for this system can be conveniently expressed in terms of bicylinder coordinates (η, θ, z) (Moon & Spencer, 1961). The traces of the coordinate surface on the xy plane are shown in Fig A.1b. The coordinate surfaces are obtained by translating these curves along the z axis. Coordinate surfaces of constant η form nested, non-concentric cylinders whose centers lie on the x axis. The $\eta = 0$ ($x = 0$) surface corresponds to the infinite mid-plane with an infinite radius. The bicylinder coordinates relate to the rectangular ones by:

$$\begin{aligned} y &= \frac{b \sin\theta}{\cosh\eta - \cos\theta} \\ x &= \frac{b \sinh\eta}{\cosh\eta - \cos\theta} \\ z &= z \end{aligned} \tag{A.2}$$

Thus in bicylinder coordinates, the region outside the two cylinders corresponds to a rectangular domain with $0 \le \theta \le 2\pi$ and $\eta_2 \le \eta \le \eta_1$, where η_1 and η_2 correspond to the surface of the two cylinders; η_1, η_2 and b are related to κa_1, κa_2 and κh through:

$$\begin{aligned} \frac{b}{\sin\eta_1} &= \kappa a_1 \\ -\frac{b}{\sin\eta_2} &= \kappa a_2 \\ \frac{b}{\tanh\eta_1} - \frac{b}{\tanh\eta_2} &= \kappa a_1 + \kappa a_2 + \kappa h \end{aligned} \tag{A.3}$$

The use of this coordinate system is similar to the use of bispherical coordinates to study the two-sphere interaction problem (Carnie *et al.*, 1994; Stankovich & Carnie, 1996; Palkar & Lenhoff, 1994; Warszyńsky & Adamczyk, 1997; Ledbetter *et al.*, 1981; Hoskin, 1955; Hoskin & Levine, 1955). The difference can be expressed in terms of the scale factors: two in one set have the same form as the corresponding two in the other set, while the third differs (Moon & Spencer, 1961).

Noting the z-invariance of the potential, the PB equation (A.1) assumes the form:

$$\frac{(\cosh\eta - \cos\theta)^2}{b^2}\left(\frac{\partial^2\psi}{\partial\eta^2} + \frac{\partial^2\psi}{\partial\theta^2}\right) = \sinh\psi \tag{A.4}$$

Following Carnie et al. (Carnie *et al.*, 1994; Stankovich & Carnie, 1996), we solve this equation using Newton-Raphson (NR) iteration and collocation with

bicubic Hermite basis functions. All calculations of the potential were performed using a 29×29 grid. The maximum absolute difference between the final values of the potential in succeeding iterations in the NR scheme was less than 5×10^{-4}.

The boundary condition corresponding to interaction under constant surface potential is $\psi = \psi_0$ on the surface of the cylinder. For interaction under constant charge density, the boundary condition will be: $-\nabla\psi\cdot\hat{\mathbf{n}} = \sigma^\star$, on the surface of the cylinder (of constant η), where $\hat{\mathbf{n}}$ is the unit normal directed towards the particle. In cases where the surface charge density is not constant, the local charge density can be evaluated using this relation. Two additional boundary conditions arise from the symmetry of the system, and correspond to: $\partial\psi/\partial\theta = 0$, on surfaces of $\theta = 0$ and $\theta = \pi$ (see Fig. A.1).

As was previously shown (Hoskin, 1955; Hoskin & Levine, 1955), the dimensionless force (per unit length) $f^\star$ acting on one of the particles, can be found by integrating the stress tensor over a closed surface enveloping that particle. In the present case, we can choose to integrate over a closed surface consisting of a cylinder with constant $\eta < \eta_1$, and of unit (Debye) length, capped by two planer circles. We can thus find the force per unit length acting on one of the cylinders. The contribution to the integral from the end-caps vanishes, and hence:

$$\begin{aligned} f^\star &= \frac{2}{b}\int_0^\pi \left\{ \left[\frac{b^2(\cosh\psi - 1)}{(\cosh\eta - \cos\theta)^2} + \frac{1}{2}\left(\left(\frac{\partial\psi}{\partial\theta}\right)^2 - \left(\frac{\partial\psi}{\partial\eta}\right)^2 \right) \right] \times (1 - \cosh\eta\cos\theta) \right. \\ &+ \left. \frac{\partial\psi}{\partial\theta}\frac{\partial\psi}{\partial\eta}\sinh\eta\sin\theta \right\} d\theta \end{aligned} \tag{A.5}$$

For two cylinders of equal radii, it is convenient to integrate over the plane $\eta = 0$. For cylinder-plane interaction, the integration was carried out over the cylinder of $\eta = \eta_1/2$. The free energy of two interacting cylinders with respect to a state of infinite separation, $F^\star$, was then evaluated by integrating the force over the separation distance κh. We note that the free energy may also be evaluated using a spatial integration, but this was found in previous studies to yield numerically less accurate results in the corresponding case of interacting spheres (Carnie *et al.*, 1994; Stankovich & Carnie, 1996).

A.3 Results and discussion

For the sake of comparison with previous approximate solutions of the PB equation, we first consider a system of two *weakly* charged rods of equal radii. In this limit the electrostatic potential is everywhere small ($\psi \ll 1$) and the use of the linearized PB equation is valid for the single cylinder case. As previously shown

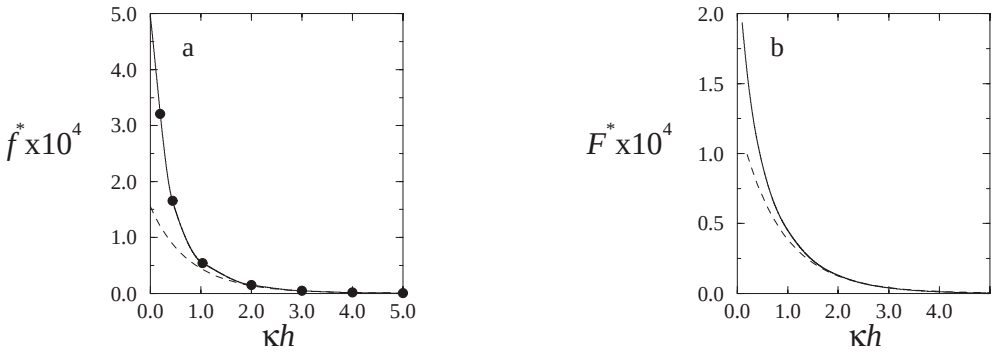

Figure A.2: a) The reduced force per unit length for two interacting cylinders as a function of separation distance, for equal radii $\kappa a = 1$ and an equal constant charge density $\sigma^\star = 0.001$. The full and dashed lines correspond to the numerical and approximate calculations respectively. The dots represent the points evaluated numerically. b) The free energy, $F^\star$, as a function of separation distance for the same system as in (a).

by Brenner et al. (Brenner & Parsegian, 1974; Brenner & McQuarry, 1972), if $h > \kappa^{-1}$, the force and interaction free energy between two cylinders can be evaluated based on the linearized PB equation and using the superposition approximation. One then finds $F(\kappa R) = CK_0(\kappa R)$, where $R = h + 2a$ is the interaxial distance, K_0 is the zero order modified Bessel function of the second kind, and C is a constant related to the charge densities on the cylinders. In Fig. A.2 we compare the interaction free energy between two weakly charged cylinders ($\kappa a_1 = \kappa a_2 = 1$, $\sigma^\star = 0.001$, $n_0 \simeq 0.065M$), as calculated by the approximate solution above, with the full numerical calculation of Eq. A.5, treating C as an adjustable parameter to be optimized. As expected, deviations are observed at small inter-cylinder separations, κh, in which regime the superposition approximation used by Brenner et al. (Brenner & Parsegian, 1974; Brenner & McQuarry, 1972) is no longer valid.

We now turn to the numerical solution of the nonlinear PB equation for the interaction between two charged cylinders of equal radii and *high* charge densities. The forces were calculated using Eq. A.5 and the free energy by integrating the force. The interaction between *two cylinders of equal radii and equal constant surface charge densities* was calculated for $\sigma^\star = -8.4$, and $\kappa a = 1$ (see Fig. A.3). For $a \simeq$1.2nm, corresponding to the radius of B-DNA, the latter condition implies $n_0 \simeq 0.065$M. Also shown in Fig. A.3 are results for the interaction between two *oppositely charged* cylinders with $\sigma^\star = \pm 8.4$. We find that in the first case the interaction is always repulsive, whereas in the second it is always attractive. Note however that the repulsion (for a given h) is always weaker than the attraction.

These results can be explained as follows. When integrating the stress tensor

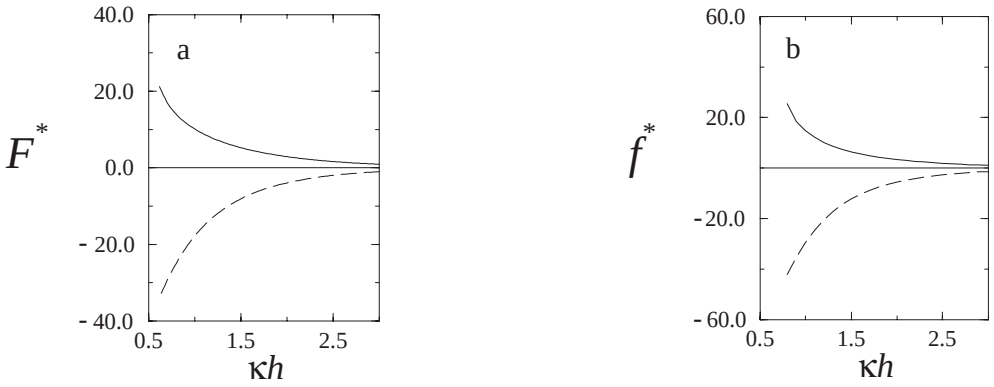

Figure A.3: a) The free energy, $F^\star$, for two interacting cylinders as a function of separation distance, for equal radii of $\kappa a = 1$ and of equal (full line) and opposite (dashed line) constant charge density of $\sigma\star = \pm 8.4$. b) The reduced force per unit length as a function of separation distance for the same systems as in (a).

over the plane of $\eta = 0$ the integrand assumes a simple form. It can be shown, using symmetry considerations alone, that the force between equally charged cylinders of equal radii (for which $\partial\psi/\partial\eta = 0$ at the mid-plane) will always be repulsive (Langmuir, 1938; Carnie *et al.*, 1994; Stankovich & Carnie, 1996; Ohnishi *et al.*, 1960). Similarly, for two cylinders of equal radii but opposite charge density (for which $\partial\psi/\partial\theta = 0$ and $\psi = 0$ at the mid-plane) it will always be attractive within the PB formulation. In the specific case studied, the difference between the repulsion and attraction forces reflects the influence of the added salt. For the equally charged cylinders (Ohnishi *et al.*, 1960), the volume between the two cylinders will contain a high concentration of ions of the opposite charge, while for the oppositely charged cylinders this volume will be low in ionic concentration for ions of both charges. This "counterion release" – the release of counterions from the confined volume between cylinders due to the mutual charge compensation of the two cylinders – is entropically favorable, contributing to the attraction. In turn, this will also result in a stronger direct interaction between the oppositely charged, unmasked rods. However, in general it might also be found in other cases that confining the ions to the inter-cylinder volume in the equally charged cylinders' case will result in a strong repulsion at small distances.

We note that for very large charge densities or surface potentials (exceeding $\sigma^\star \sim 7.0$ in the systems considered), in particular for small separation distances (say $\kappa h < 0.4$), a well converged result for the potential was not always achieved. The problem may be overcome, at least in some cases, by increasing the number of grid points (also making the calculations lengthier in time), supplying a better initial approximate guess for the potential, or solving the PB equation for the potential difference between an initial guess and the true potential, (instead of

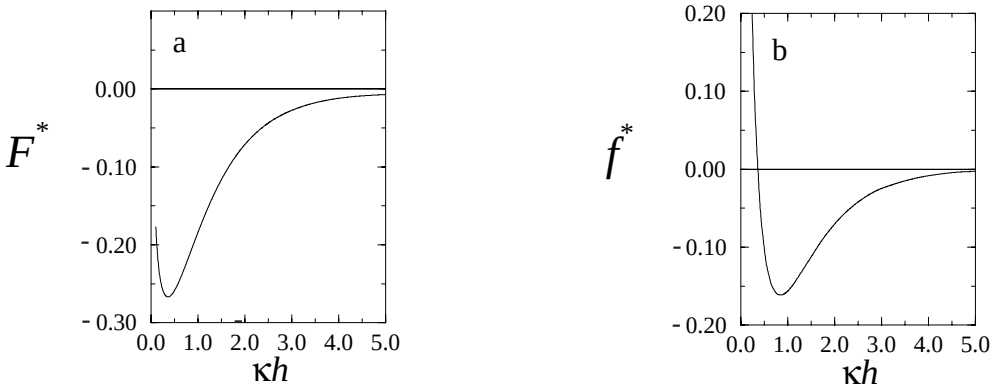

Figure A.4: a) The free energy, $F^\star$, per unit length for two interacting cylinders as a function of separation distance, for equal radii of $\kappa a = 1$ and constant charge densities $\sigma_1^\star = 1$ and $\sigma_2^\star = -2$. b) The reduced force as a function of separation distance for the same systems as in (a).

solving for the potential itself).

When the two cylinders are *oppositely charged, but not with the same surface charge density*, a minimum in both the force and free energy may appear (as is also the case with charged spheres) (Carnie *et al.*, 1994; Stankovich & Carnie, 1996; Palkar & Lenhoff, 1994). This can be seen in Fig. A.4, where the cylinders (each with the same unit radius as before), have surface charge densities of $\sigma_1^\star = 1$ and $\sigma_2^\star = -2$, respectively. Previous calculations pertaining to the interaction between *spheres* show that a similar minimum was found mainly due to an entropic contribution (Palkar & Lenhoff, 1994). In the present case, this may be explained as follows. At large enough distances, the approach of the two oppositely charged cylinders enables counterion release, which is entropically favorable. When the distance becomes small enough, the non-equal surface charge densities require that some of the counterions remain in the inter-cylinder volume, resulting in an entropically unfavorable compression of counterions which ultimately leads to repulsion.

We have also calculated the interaction free energy as a function of the distance between *a charged cylinder and an oppositely charged plane* ($\eta = 0$). In Fig. A.5a we show the interaction free energy between a cylinder of charge density $\sigma_c^\star = -6$ and a planar surface of a constant electric potential $\psi = 2$ (corresponding to $\sigma^\star \simeq 2.3$ when $\kappa h \to \infty$). This system provides a reasonable model for the interaction between a DNA rod and a lipid bilayer composed of cationic and neutral lipids, where the charged lipids are freely diffusing ($\psi = const$), so as to minimize the internal free energy. Upon approaching the plane the cylinder induces a charge modulation in the planar surface (May & Ben-Shaul, 1997; Harries, 1998). Fig. A.5b shows the charge density profile on the surface, as a

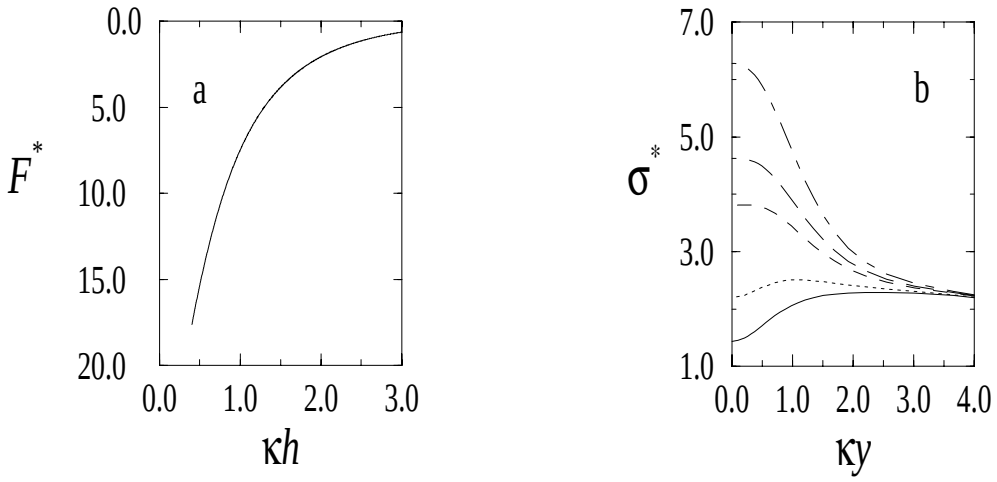

Figure A.5: a) The interaction free energy, $F^\star$, as a function of separation distance for a cylinder of radius $\kappa a = 1$ and constant charge density of $\sigma_c^\star = -6$, and a plane of constant potential $\psi^\star = 2$. b) The surface charge density on a plane of constant potential ($\psi^\star = 2$) as a function of the distance from the projection of the cylinder axis on the plane (κy). The constant cylinder-wall distance is $\kappa h = 0.4$. The cylinder radius is $\kappa a_c = 1$. The curves correspond to surface charge densities (top to bottom) of $\sigma_c^\star = -6, -4, -3, -1, 0$ on the cylinder.

function of the distance (κy) from the projection on the plane of the rod axis, for a fixed cylinder-plane separation (κh=0.4), for several different values of the rod charge density $\sigma_c^\star$. Not surprisingly, for high values of $\sigma_c^\star$ opposite charges on the "membrane" accumulate in the vicinity of the rod. On the other hand, for low charge densities on the cylinder there is a reduction of charge density on the plane near the cylinder. A qualitative explanation of this effect can be given as follows. If the cylinder is very weakly charged (say neutral), it acts as a confining wall with respect to the counterions in the gap between the rod and the plane. This leads to an excess of counterion (osmotic) pressure, which can be partly relieved by the escape of some counterions from the gap, and concomitantly, of surface charges from this region. Indeed, the onset of this reduction is observed close to the point where the charge densities on the plane and cylinder are equal.

Appendix B

Numerical method for solving the Poisson–Boltzmann Equation

In this appendix we outline the numerical proceedure we employed in solving the PB equation with special boundary conditions corresponding to the case of mobile membrane lipids.

In solving the full nonlinear Poisson-Boltzmann equation we follow previous calculations of the electrostatic potential which employed Newton-Raphson iterations of the Laplacian (Carnie *et al.*, 1994; Stankovich & Carnie, 1996). The problem is thus reduced to a sequence of linear elliptic equations of the form:

$$\nabla^2\psi_{n+1} - (\cosh\psi_n)\psi_{n+1} = \sinh\psi_n - (\cosh\psi_n)\psi_n. \tag{B.1}$$

in which ψ_n is the electrostatic potential in the n-th iteration step. (The value of the initial guess, ψ_0, can be chosen arbitrarily, and was in general set to $\psi_0 = 0$ in our calculations.) As $n \to \infty$, ψ_n converges to the solution of the full nonlinear equation. In practice, less than 50 iterations ensure $|\psi_n - \psi_{n+1}| < 10^{-3}$ for all grid points. In fact the two added terms represent a numerical gradient in the ψ solution domain. When this term is very small ψ becomes stable with respect to further iterations, and the solution is self consistent and matches the PB solution.

The linear elliptic problem was solved in each iteration by using the publicly available GENCOL routine (Houstis *et al.*, 1985). This procedure can solve the linear equation on an arbitrary (closed) domain using collocation with bi-cubic Hermite functions. In most cases, a 40×40 evenly spaced grid was used, but sometimes a variably spaced grid was also used.

For the lipid membrane, a nonlinear boundary condition (see Eq. 2.5) must be solved, stating the relation between the surface charge density, the potential ψ and the Lagrange multiplier $\lambda(\psi)$. This can be handled through the use of

a second Newton-Raphson iteration on the boundary condition, in addition to the one on the Laplacian. The two iterations can then proceed simultaneously. Writing Eq. 2.5 in the form:

$$\frac{\partial\psi}{\partial n} = g(\psi) = -\frac{\frac{1}{\beta}e^{-(\psi+\lambda)}}{\frac{1-\phi}{\phi} + e^{-(\psi+\lambda)}} \tag{B.2}$$

the Newton-Raphson iteration for the boundary condition would result in:

$$\frac{\partial\psi_{n+1}}{\partial y} - \psi_{n+1}g'(\psi_n) = g(\psi_n) - \psi_n g'(\psi_n). \tag{B.3}$$

For $g'(\psi)$ we chose a "modified" derivative:

$$g'(\psi) = -\frac{\frac{1}{\beta}\frac{1-\phi}{\phi}e^{-(\psi+\lambda)}}{\frac{1-\phi}{\phi} + e^{-(\psi+\lambda)}}. \tag{B.4}$$

In each iteration step the potential calculated in the previous step is used to evaluate λ using Eq. 2.3. This value of λ is used to determine the boundary condition for the lipid bilayer through Eq. B.3. It is then possible to solve Eq. B.1 for the current step, etc.

Once the potential is found, it now remains to evaluate the free energy of the complex due to the charging and mixing processes. In principle, f_C could be evaluated using Eq. 2.2. For numerical purposes it is more convenient to use the equivalent form:

$$\begin{aligned}\frac{f_C}{kT} &= \frac{1}{2}\int_{S_{III}}\frac{\sigma^-}{e}\psi \mathrm{d}S + \frac{1}{2a}\int_{S_V}\eta\psi \mathrm{d}S + \frac{\kappa^2}{4\pi l_B}\int_v(\frac{1}{2}\psi\sinh\psi - \cosh\psi + 1)\mathrm{d}v \\ &+ \frac{1}{a}\int_{S_V}\left[\eta\ln\frac{\eta}{\phi} + (1-\eta)\ln\frac{1-\eta}{1-\phi}\right]\mathrm{d}S + n\left[\phi\ln\phi + (1-\phi)\ln(1-\phi)\right]\end{aligned} \tag{B.5}$$

where $n = N_C/D_C$ is the number of lipid molecules in the unit cell. (The passage from Eq. 2.2 to Eq. B.5 involves using: (i) the identity $(\nabla\psi)^2 = \nabla\cdot(\psi\nabla\psi) - \psi\nabla^2\psi$, (ii) Gauss theorem to convert the volume integral of $\nabla\cdot(\psi\nabla\psi)$ to a surface integral over $\psi\nabla\psi \propto -\psi\eta$, (iii) the use of the PB equation, Eq. 2.4, for $\nabla^2\psi$ and the Boltzmann distributions: $n_\pm = n_0 exp(\mp\psi)$.) This procedure precludes the need for using the derivatives of the potential (which are prone to a larger numerical error).

References

Adamson, A. W. 1990. *Physical chemistry of surfaces*. Fifth edn. New York: Wiley.

Alberts, B., Bray, D., Lewis, J., Raff, M., Roberts, K., & Watson, J. D. 1994. *Molecular biology of the cell*. Third edn. New York and London: Garland Publishing.

Alexander, S., Chaikin, P. M., Grant, P., Morales, G. J., Pincus, P., & Hone, D. 1984. Charge renormalization, osmotic pressure, and bulk modulus of colloidal crystals: theory. *J. chem. phys.*, **80**, 5776–5781.

Andelman, D. 1995. Electrostatic properties of membranes: The Poisson-Boltzmann theory. *Section 12, pages 603–642 of:* Lipowsky, R., & Sackmann, E. (eds), *Structure and dynamics of membranes*, second edn., vol. 1. Amsterdam: Elsevier.

Andelman, D., Kozlov, M. M., & Helfrich, W. 1994. Phase transitions between vesicles and micelles driven by competing curvature. *Europhys. lett.*, **25**, 231–236.

Artzner, F., Zantl, R., Rapp, G., & Rädler, J.O. 1998. Observation of a rectangular columnar phase in condensed lamellar cationic lipid-DNA complexes. *Phys. rev. lett.*, **81**, 5015–5018.

Artzner, F., Zantl, R., & Rädler, J. O. 2000. Lipid-dna and lipid-polyelectrolyte mesophases: Structure and exchange kinetics. *Cell mol biol*, **46**, 967–978.

Bandyopadhyay, S., Tarek, M., & Klein, M. L. 1999. Molecular dynamics study of a lipid-DNA complex. *J. phys. chem. b*, **103**, 10075–10080.

Battersby, B. J., Grimm, R., Hübner, S., & Cevc, G. 1998. Evidence for three-dimensional interlayer correlations in cationic lipid-DNA complexes as observed by cryo-electron microscopy. *Biophys. biochim. acta*, **1372**, 379–383.

Bazzi, M. D., & Nelsestuen, G.L. 1990. Extensive segregation of acidic phospholipids in membranes induced by protein kinase C and related proteins. *Biochemistry*, **30**, 7961–7969.

Ben-Shaul, A. 1995. Molecular theory of chain packing, elasticity and lipid protein interaction in lipid bilayers. *Section 7, pages 359–402 of:* Lipowsky, R., & Sackmann, E. (eds), *Structure and dynamics of membranes*, vol. 1. Amsterdam: Elsevier.

Ben-Shaul, A., & Gelbart, W. M. 1994. Statistical thermodynamics of amphiphile self-assembly: Structure and phase transitions in micellar solutions. *Section 1, pages 1–104 of:* Gelbart, W. M., Ben-Shaul, A., & Roux, D. (eds), *Micelles, membranes, microemulsions, and monolayers*, first edn. New York: Springer.

Ben-Tal, N., Honig, B., Peitzsch, R. M., Denisov, G., & McLaughlin, S. 1996. Binding of small basic peptides to membranes containing acidic lipids: theoretical models and experimental results. *Biophys. j.*, **71**, 561–575.

Ben-Tal, N., Honig, B., Miller, C., & McLaughlin, S. 1997. Electrostatic binding of proteins to membranes. theoretical predictions and experimantal results with charybdotoxin and phospholipid vesicles. *Biophys. j.*, **73**, 1717–1727.

Birrell, G. B., & Griffith, O. H. 1976. Cytochrome c induced lateral separation in a diphosphatidylglycerol-steroid spin-label model membrane. *Biochemistry*, **13**, 2925–2929.

Bloomfield, V. A. 1991. Condensation of DNA by multivalent cations: considerations on mechanisms. *Biopolymers*, **31**, 1471–1481.

Bloomfield, V. A. 1996. DNA condensation. *Curr. opin. struct. biol.*, **6**, 334–341.

Boggs, J. M., Wood, D. D., Moscarello, M. A., & Papahadjopoulos, D. 1977. Lipid phase separation induced by a hydrophobic protein in phosphatidylserine–phosphatidylcholine vesicles. *Biochemistry*, **16**, 2325–2329.

Borukhov, I. 1999. *Polyelectrolytes, polyampholytes and electrolytes in solution and near surfaces.* Ph.D. thesis, Tel-Aviv University.

Borukhov, I., Andelman, D., & Orland, H. 1995. Polyelectrolyte solutions between charged surfaces. *Europhys. lett.*, **32**, 499–504.

Borukhov, I., Andelman, D., & Orland, H. 1997. Steric effects in polyelectrolytes: a modified Poisson-Boltzmann equation. *Phys. rev. lett.*, **79**, 435–438.

Borukhov, I., Andelman, D., & Orland, H. 1998. Scaling laws of polyelectrolyte adsorption. *Macromolecules*, **31**, 1665–1671.

Boukhnikachvili, T., AguerreChariol, O., Airiau, M., Lesieur, S., Ollivon, M., & Vacus, J. 1997. Structure of in-serum transfecting DNA-cationic lipid complexes. *Febs. letters*, **409**, 188–194.

Bradley, A. J., Maurer-Spurej, E., Brooks, D. E., & Devine, D. V. 1992. Unusual electrostatic effects on binding of C1q to anionic liposomes: Role of anionic phospholipid domains and their line tension. *Biochemistry*, **38**, 8112–8123.

Brenner, S. L., & McQuarry, D. A. 1972. On the theory of electrostatic interaction between parallel cylindrical polyelectrolytes. *J. colloid interface sci.*, **44**, 298–317.

Brenner, S. L., & Parsegian, V. A. 1974. A physical method for deriving the electrostatic interaction between rod-like polyions at all mutual angles. *Biophysical j.*, **14**, 327–334.

Bruinsma, R. 1998. Electrostatics of DNA-cationic lipid complexes: isoelectric instability. *Eur. phys. j. b*, **4**, 75–88.

Burak, Y., & Andelman, D. 2000. Hydration interactions: Aqueous solvent effects in electric double layers. *Phys. rev. e*, **62**, 5296–5312.

Carbone, M. A., & Macdonald, P. M. 1996. Cardioxin II segregates phosphatidylglycerol from mixtures with phosphatidylcholine: ^{31}P and ^{2}H NMR spectroscopic evidence. *Biochemistry*, **35**, 3368–3378.

Carnie, S. L., & Chan, D. Y. C. 1993. Interaction free energy between identical colloidal particles: The linearized Poisson-Boltzmann theory. *J. colloid interface sci.*, **155**, 297–312.

Carnie, S. L., Chan, D. Y. C., & Stankovich, J. 1994. Computation of forces between spherical colloidal particles: nonlinear Poisson-Boltzmann theory. *J. colloid interface sci.*, **165**, 116–128.

Chapman, D. L. 1913. A contribution to the theory of electrocapillarity. *Philos. mag.*, **25**, 475–481.

Châtellier, X., & Joanny, J.-F. 1996. Adsorption of polyelectrolyte solutions on surfaces: A debye-hückel theory. *J. physique ii (france)*, **6**, 1669–1686.

Chen, Z., & Rand, R. P. 1997. The influence of cholesterol on phospholipid membrane curvature and bending elasticity. *Biophys. j.*, **73**, 267–276.

Dan, N. 1996. Formation of ordered domains in membrane-bound DNA. *Biophys. j.*, **71**, 1267–1272.

Dan, N. 1997. Multilamellar structures of DNA complexes with cationic liposomes. *Biophys. j.*, **73**, 1842–1846.

Dan, N. 1998. The structure of DNA complexes with cationic liposomes–cylindrical or lamellar? *Biophys. biochim. acta*, **1369**, 34–38.

Das, T., Bratko, D., Bhuiyan, L. B., & Outhwaite, C. W. 1995. Polyelectrolyte solutions containing mixed valency ions in the cell model: A simulation and modified Poisson-Boltzmann study. *J. chem. phys.*, **107**, 9197–9207.

Dautzbenberg, H. 1997. Polyelectrolyte complex formation in highly aggregating systems. 1. effect of salt:polyelectrolyte complex formation in the presence of NaCl. *Macromolecules*, **30**, 7810–7815.

Davies, J. T. 1958. Adsorption of long-chain ions. i. *Proc. roy. soc. a*, **245**, 417–433.

Debye, P., & Hückel, E. 1923. Zur theorie der elektrolyte. *Physik*, **24**, 185–206.

Debye, P., & Hückel, E. 1924. Osmotische zustandsgleichung und aktivität verdünnter starker electrolyte. *Physik*, **25**, 97–107.

Denisov, G., Wanaski, S., Luan, P., Glaser, M., & McLaughlin, S. 1998. Binding of basic peptides to membranes produces lateral domains enriched in the acidic lipids phosphatidylserine and phosphatidylinositol 4,5-biphosphate: An electrostatic model and experimental results. *Biophys. j.*, **74**, 731–744.

Derjaguin, B. V., Churaev, N. V., & Muller, V. M. 1987. *Surface forces.* New York: Plenum Pub Corp.

Deserno, M., Holm, C., & May, S. 2000. The fraction of condensed counterions around a charged rod: Comparison of Poisson-Boltzmann theory and computer simulations. *Macromolecules*, **33**, 199–205.

Diamant, H., & Andelman, D. 2000. Self-assembly in mixtures of polymers and small associating molecules. *Macromolecules*, **33**, 8050–8061.

Evans, D. F., & Wennerström, H. 1994. *The colloidal domain, where physics, chemistry, and biology meet.* Second edn. VCH publishers.

Felgner, P. L. 1997. Nonviral strategies for gene therapy. *Scientific american*, **276**, 86–90.

Felgner, P. L., & Ringold, G. M. 1989. Cationic liposome mediated transfection. *Nature*, **331**, 461–462.

Felgner, P. L., Gadek, T. R., Holm, M., Roman, R., Chan, H. W., Wenz, M., Northrop, J. P., Ringold, G. M., & Danielsen, M. 1987. Lipofectin: A highly efficient, lipid-mediated DNA transfection procedure. *Proc. natl. acad. sci. u.s.a.*, **84**, 7413–7417.

Felgner, P. L., Tsai, Y. J., & Felgner, J. H. 1996. Advances in the design and application of cytofectin formulations. *Chap. 4, pages 43–56 of:* Lasic, D. D., & Barenholz, Y. (eds), *Handbook of nonmedical applications of liposomes.* FL.: CRC Press Boca Raton.

Fisher, M. E. 1994. The story of coulombic criticality. *J. stat. phys.*, **75**, 1–36.

Fisher, M. E., & Levin, Y. 1993. Criticality in ionic fluids: Debye-Hückel theory, bjerrum, and beyond. *Phys. rev. lett.*, **71**, 3826–3829.

Fogolari, F., & Briggs, J. M. 1997. On the variational approach to Poisson-Boltzmann free energies. *Chem. phys. lett.*, **281**, 135–139.

Friedmann, T. 1997. Overcoming the obsacles to gene therapy. *Sci. am.*, **276**, 80–85.

Fuoss, R. M., Katchalsky, A., & Lifson, S. 1951. The potential of an infinite rodlike molecule and the distribution of the counter ions. *Proc. natl. acad. sci.*, **37**, 579–589.

Galla, H. J., & Sackmann, E. 1975. Chemically induced lipid phase separation in model membranes containing charged lipids: a spin label study. *Biochim. biophys. acta*, **70**, 509–529.

Garidel, P., & Blume, A. 1998. Miscibility of phospholipids with identical headgroups and acyl chain lengths differing by two methylene units: effects of headgroup structure and headgroup charge. *Biochim. biophys. acta*, **1372**, 83–95.

Garidel, P., & Blume, A. 2000. Calcium induced nonideal mixing in liquid-crystalline phosphatidylcholine-phosphatidic acid bilayer membranes. *Langmuir*, **16**, 1662–1667.

Garidel, P., Johann, C., & Blume, A. 1997. Nonideal mixing and phase separation in phosphatidylcholine-phosphatidic acid mixtures as a function of acyl chain length and PH. *Biophys. j.*, **72**, 2196–2210.

Gawrisch, K., Parsegian, V. A., Hajduk, D. A., Tate, M. W., Gruner, S. M., Fuller, N. L., & Rand, R. P. 1992. Energetics of a hexagonal-lamellar-hexagonal-phase transition sequence in dioleoylphosphatidylethanolamine membranes. *Biochemistry*, **31**, 2856–2864.

Gawrisch, K., Han, K-H., Yand, J-S., Bergelson, L., & Ferretti, J. A. 1993. Interaction of peptide fragment 828-848 of the envelope glycoprotein of human immunodeficiency virus type I with lipid bilayers. *Biochemistry*, **32**, 3112–3118.

Gelbart, W. M., Bruinsma, R., Pincus, P. A., & Parsegian, V. A. 2000. DNA-inspired electrostatics. *Physics today*, **53**, 38–44.

Gershon, H., Ghirlando, R., Guttman, S. B., & Minsky, A. 1993. Mode of formation and structural features of DNA-cationic liposome complexes used for transfection. *Biochemistry*, **32**, 7143–7151.

Gil, T., Ipsen, J. H., Mouritsen, O. G., Sabra, M. C., Sperotto, M. M., & Zuckermann, M. J. 1998. Theoretical analysis of protein organization in lipid membranes. *Biophys. biochim. acta*, **1376**, 245–266.

Goddard, E. D., & Ananthapadamanabhan, K. P. (eds). 1993. *Interaction of surfactants with polymers and proteins*. Boca Raton, Fl.: CRC.

Goldberg, E. M., Borchardt, D. B., & Zidovetzki, R. 1998. Effects of histone and diolein on the structure of phosphatidylcholine/phosphatidylserine or phosphatidylcholine/phosphatidylglycerol bilayers. *Eur. j. biochem.*, **258**, 722–728.

Gouy, G. 1910. Sur la constitution de la charge electrique a la surface d'un electrolyte. *J. phys. france*, **9**, 457–468.

Greberg, H., & Kjellander, R. 1998. Charge inversion in electric double layers and effects of different sizes for counterion and coions. *J. chem. phys.*, **108**, 2940–2953.

Greberg, H., Kjellander, R., & Akesson, T. 1997. Ion-ion correlations in electric double layers from Monte Carlo simulations and integral equation calculation. *Molecular physics*, **92**, 35–48.

Grønbech-Jensen, N., Mashl, R. J., Bruinsma, R. F., & Gelbart, W. M. 1997. Counterion-induced attraction between rigid polyelectrolytes. *Phys. rev. lett.*, **78**, 2477–2480.

Grosberg, A. Yu., & Khokhlov, A. R. 1994. *Statistical physics of macromolecules.* New-York: AIP Press.

Gustafsson, J., Arvidson, G., Karlsson, G., & Almgren, M. 1995. Complexes between cationic liposomes and DNA visualized by cryo-tem. *Biophys. biochim. acta*, **1235**, 305–312.

Guttman, G. D., & Andelman, D. 1993. Electrostatic interactions in two-component membranes. *J. phys. ii (france)*, **3**, 1411–1425.

Harries, D. 1998. Solving the Poisson-Boltzmann equation for two parallel cylinders. *Langmuir*, **14**, 3149–3152.

Harries, D., May, S., Gelbart, W. M., & Ben-Shaul, A. 1998. Structure, stability and thermodynamics of lamellar DNA-lipid complexes. *Biophys. j.*, **75**, 159–173.

Harries, D., May, S., & Ben-Shaul, A. 2001. *Adsorption of charged macromolecules on mixed fluid membranes.* to be published in *Coll. Surf. A.*

Hartmann, W., Galla, H.-J., & Sackmann, E. 1977. Direct evidence of charge-induced lipid domain structure in model membranes. *Febs. lett*, **78**, 169–172.

Haverstick, D. M., & Galser, M. 1989. Infuence of proteins on the reorganization of phospholipid bilayers into large domains. *Biophys. j.*, **55**, 677–682.

Heimburg, T., & Marsh, D. 1995. Protein surface distribution and protein-protein interactions in the binding of peripheral proteins to charged lipid membranes. *Biophys. j.*, **68**, 536–546.

Heimburg, T., Angerstein, B., & Marsh, D. 1999. Binding of peripheral proteins to mixed lipid membranes: Effect of lipid demixing upon binding. *Biophys. j.*, **76**, 2575–2586.

Helfrich, W. 1973. Elastic properties of lipid bilayers: theory and possible experiments. *Z. naturforsch.*, **28**, 693–703.

Helfrich, W., & Servuss, R. M. 1984. Undulations, steric interaction and cohesion of fluid membranes. *Il nuovo cimento*, **3D**, 137–151.

Hill, T. L. 1955. Approximate calculation of the electrostatic free energy of nucleic acids and other cylindrical macromolecules. *Arch. biochem. biophys.*, **57**, 229–239.

Hill, T. L. 1960. *Introduction to statistical thermodynamics.* New-York: Addison-Wesley.

Hinderliter, A. K., Almeida, P. F. F., Biltonen, R. L., & Creutz, C. E. 1998. Membrane domain formation by calcium-dependent, lipid-binding proteins: insights from the C2 motif. *Biochem. biophys. acta*, **1448**, 227–235.

Honig, B., & Nicholls, A. 1995. Classical electrostatics in biology and chemistry. *Science*, **268**, 1144–1149.

Hoskin, N. E. 1955. The interaction of two identical spherical colloidal particles I. potential distribution. *Pil. t. roy. a*, **248**, 433–448.

Hoskin, N. E., & Levine, S. 1955. The interaction of two identical spherical colloidal particles II. the free energy. *Pil. t. roy. a*, **248**, 449–.

Houstis, E. N., Mitchell, W. F., & Rice, J. R. 1985. Collocation software for second order elliptic partial differential equations. *Acm trans. math. software*, **11**, 379–418.

Hui, S. W., Langner, M., Zhao, Y-L., Patrick, R., Hurley, E., & Chan, K. 1996. The role of helper lipids in cationic liposome-mediated gene transfer. *Biophys. j.*, **71**, 590–599.

Israelachvili, J. N. 1992. *Intermolecular and surface forces.* Second edn. Academic press.

Israelachvili, J. N., & Wennerström, H. 1990. Hydration or steric forces between between amphiphilic surfaces? *Langmuir*, **6**, 873–876.

Israelachvili, J. N., Mitchell, J., & Ninham, B. W. 1977. Theory of self-assembly of lipid bilayers and vesicles. *Biophys. biochim. acta*, **470**, 185–201.

Japas, M. L., & Sengers, J. M. H. L. 1990. Critical behavior of conduction ionic solutions near its consulate point. *J. phys. chem.*, **94**, 5361–5368.

Joanny, J.-F. 1999. Polyelectrolyte adsorption and charge inversion. *Eur. phys. j. b*, **9**, 117–122.

Jönsson, A-S., & Jönsson, B. 1996. Ultrafiltration of colloidal dispersions – a theoretical model of the concentration polarization phenomena. *J. colloid interface sci.*, **180**, 504–518.

Jönsson, B., & Stahlberg, L. 1999. The electrostatic interaction between a charged sphere and an oppositely charged planar surface and its application to protein adsorption. *Coll. surf. b*, **14**, 67–75.

Kasher, R., Oren, D. A., Barda, Y., & Gilon, C. 1999. Miniaturized proteins: the backbone cyclic proteinomimetic approach. *J. mol. biol.*, **292**, 421–429.

Kékicheff, P., Marčelja, S., Senden, T. J., & Shubin, V.E. 1993. Charge reversal seen in electrical double layer interaction of surfaces immersed in 2:1 calcium electrolyte. *J. chem. phys.*, **99**, 6098–6113.

Khokhlov, A. R., Starodubtzev, S. G., & Vasilevskaya, V. V. 1993. Conformational transitions in polymer gels - theory and experiment. *Adv. polymer. sci.*, **109**, 123–175.

Kirk, G. L., Gruner, S. M., & Stein, D. L. 1984. A thermodynamic model of the lamellar to inverted hexagonal phase transitionof lipif membrane–water system. *Biochemistry*, **23**, 1093–1102.

Koltover, I. 1998. *Structure and interactions in biomaterials based on membrane-biopolymer self-assembly.* Ph.D. thesis, university of California, Santa-Barbara.

Koltover, I., Salditt, T., Rädler, J. O., & Safinya, C. R. 1998. An inverted hexagonal phase of cationic liposome-DNA complexes related to DNA release and delivery. *Science*, **281**, 78–81.

Kornyshev, A. A., & Leikin, S. 2001. Sequence recognition in the pairing of DNA duplexes. *Phys. rev. lett*, **86**, 3666–3669.

Kozlov, M. M., Leikin, S., & Rand, R. P. 1994. Bending, hydration and intersticial energies quantitatively account for the hexagonal-lamellar-hexagonal reentrant phase transition in dioleoylphosphatidylethanolamine. *Biophys. j.*, **67**, 1603–1611.

Krylov, A. V., Kotova, E. A., Yaroslavov, A. A., & Antonenko, Y. N. 2000. Stabiliczation of O-pyromellitylgramicidin channel in bilayer lipid membranes through electrostatic interaction with polylysines of different chain lengths. *Biochem. biophys. acta*, **1509**, 373–384.

Kwak, J. C. T. (ed). 1998. *Polymer-surfactant systems.* New-York: Marcel Dekker.

Landau, L. D., & Lifshitz, E. M. 1960. *Electrodynamics of continuous media.* Oxford: Pergamon.

Langmuir, I. 1938. Repulsive forces between charged surfaces in water, and the cause of the Jones-Ray effect. *Science*, **88**, 430–432.

Lasic, D. D., Strey, H., Stuart, M. C. A., Podgornik, R., & Frederik, P. M. 1997. The structure of DNA-liposome complexes. *J. am. chem. soc.*, **119**, 832–833.

Lau, A. W. C., & Pincus, P. 1999. Binding of oppositely charged membranes and membrane reorganization. *Eur. phys. j. b*, **10**, 175–180.

Lau, A. W. C., Pincus, P., Levine, D., & Fertig, H. A. 2001. Electrostatic attraction of coupled wigner crystals: Finite temperature effects. *Phys.rev.e*, **6305**, 1604-1615.

LeBret, M., & Zimm, B. H. 1984. Distribution of counterions around a cylindrical polyelectrolyte and manning's condensation theory. *Biopolymers*, **23**, 287–312.

Ledbetter, J. E., Croxton, T. L., & McQuarrie, D. A. 1981. The interaction of two charged spheres in the Poisson-Boltzmann equation. *Can. j. chem.*, **59**, 1960-1864.

Leikin, S., Kozlov, M. M., Fuller, M. M., & Rand, R. P. 1996. Measured effects of diacylglycerol on structural and elastic properties of phospholipid membranes. *Biophys. j.*, **71**, 2623–2632.

Lekkerkerker, H. N. W. 1989. Contribution of the electric double layer to the curvature elasticity of charged amphiphilic monolayers. *Physica a.*, **159**, 319–328.

Levine, S. 1939. On the interaction of two colloidal particles, using the complete Debye-Hückle equation. *J. phys. chem.*, **7**, 831–842.

Lifson, S., & Katchalsky, A. 1954. The electrostatic free energy of polyelectrolyte solutions. ii. fully stretched macromolecules. *J. polymer sci.*, **13**, 43–55.

Lin, A. J., Slack, N .L., Ahmad, A., Koltover, I., George, C. X., Samuel, C. E., & Safinya, C. R. 2000. Structure and structure-function studies of lipid/plasmid DNA complexes. *J. drug. targeting*, **8**, 13–27.

Linse, P., & Jönsson, B. 1982. Electrostatic interactions in micellar solutions. a comparison between monte carlo simulations and solutions of the Poisson-Boltzmann equation. *J. phys. chem.*, **86**, 413–421.

Lipowsky, R., & Sackmann, E. (eds). 1995. *Structure and dynamics of membranes.* Elsevier, Amsterdam: Elsevier.

Livolant, F., & Leforestier, A. 1996. Condensed phases of dna: Structures and phase transitions. *Prog. pol. sci.*, **21**, 1115–1164.

Lyubartsev, A. P., & Nordenskiold, L. 1995. Monte-carlo simulation study of ion distribution and osmotic-pressure in hexagonally oriented DNA. *J. phys. chem*, **99**, 10373–10382.

Manning, G. S. 1969. Limiting laws and counterion condensation in polyelectrolyte solution i. colligative properties. *J. chem. phys.*, **51**, 923–933.

Manning, G. S. 1978. The molecular theory of polyelectrolyte solutions with applications to the electrostatic properties of polynucleotides. *Q. rev. biophys.*, **11**, 179–246.

Manning, G. S., & Ray, J. 1998. Counterion condensation revisited. *J. biomol. struc. dyn.*, **16**, 461–476.

Marčelja, S. 1992. Electrostatics of membrane adhesion. *Biophys. j.*, **61**, 1117–1121.

Marčelja, S. 1997. Effects of ion hydration in double layer interaction. *Coll. surf. a*, **130**, 321–326.

May, S. 1996. Curvature elasticity and thermodynamic stability of electrically charged membranes. *J.chem.phys.*, **105**, 8314–8322.

May, S., & Ben-Shaul, A. 1995. Spontaneous curvature and thermodynamic stability of mixed amphiphilic layers. *J. chem. phys.*, **103**, 3839–3848.

May, S., & Ben-Shaul, A. 1997. DNA-lipid complexes: stability of honeycomb-like and spaghetti-like structures. *Biophys. j.*, **73**, 2427–2440.

May, S., Bohbot, Y., & Ben-Shaul, A. 1997. Molecular theory of bending elasticity and branching of cylindrical micelles. *J. phys. chem. b*, **101**, 8648–8657.

May, S., Harries, D., & Ben-Shaul, A. 2000a. The phase behavior of cationic lipid-DNA complexes. *Biophys. j.*, **78**, 1681–1697.

May, S., Harries, D., & Ben-Shaul, A. 2000b. The role of lipid demixing and protein-protein interactions in the adsorption of charged proteins on mixed membranes. *Biophys. j.*, **79**, 1747–1760.

Mayer, L. D., Nelsestuen, G. L., & Brockman, H. L. 1983. Prothrombin association with phospholipid monolayers. *Biochemistry*, **22**, 316–321.

Sánches-Sánches, J. E., & Lozada-Cassou, M. 1992. Exact numerical solution to the integral equation version of the Poisson-Boltzmann equation, for two interacting spherical colloidal particles. *Chem. phys. lett.*, **190**, 202–208.

McCormack, D., Carnie, S. L., & Chan, D. Y. C. 1995. Calculations of electric double-layer force and interaction free energy between dissimilar surfaces. *J. colloid interface sci.*, **169**, 177–196.

McGahay, V., & M.Tomozawa. 1989. The origin of phase separation in silicate melts and glasses. *J. non-cryst. sol.*, **109**, 27–34.

Meidan, V. M., Cohen, J. S., Amariglio, N., Hirsch-Lerner, D., & Barenholz, Y. 2000. Interaction of oligonucleotides with cationic lipids: the relationship between electrostatics, hydration and state of aggregation. *Biochem. biophys. acta*, **1464**, 251–261.

Mitrakos, P., & Macdonald, P. M. 1996. DNA-induced lateral segregation of cationic amphiphiles in lipid bilayer membranes as detected via ^{2}H NMR. *Biochemistry*, **35**, 16714–16722.

Mok, K. W. C., & Cullis, P. R. 1997. Structural and fusogenic properties of cationic liposomes in the presence of plasmid DNA. *Biophys. j.*, **73**, 2534–2545.

Moon, P., & Spencer, D. E. 1961. *Field theory handbook.* Berlin: Springer.

Morrison, R. T., & Boyd, R. N. 1992. *Organic chemistry.* New-Jersy: Prentice Hall.

Murray, D., Arbuzova, A., Hangyás-Mihályné, G., Gambhir, A., Ben-Tal, N., Honig, B., & McLaughlin, S. 1999. Electrostatic properties of membranes containing acidic lipids and adsorbed basic peptides: Theory and experiment. *Biophys. j.*, **77**, 3176–3188.

Nardi, J., Bruinsma, R., & Sackmann, E. 1998. Adhesion-induced reorganization of charged fluid membranes. *Phys. rev .e*, **58**, 6340–6354.

Netz, R. R., & Orland, H. 1999. Field theory for charged fluids and colloids. *Europhys. lett.*, **45**, 726–732.

Netz, R. R., & Orland, H. 2000. Beyond Poisson-Boltzmann: Fluctuation effects and correlation functions. *Euro. phys. j.*, **1**, 203–214.

Neu, J. C. 1999. Wall-mediated forces between like-charged bodies in an electrolyte. *Phys. rev. lett.*, **82**, 1072–1074.

Ninham, B. W., & Parsegian, V. A. 1971. Electrostatic potential between surfaces bearing ionizable groups in ionic equilibrium with physiologic saline solutions. *J. theor. biol.*, **31**, 405–428.

Odijk, T. 1977. Polyelectrolytes near rod limit. *J. polym. sci.*, **15**, 477–483.

O'Hern, C. S., & Lubensky, T. C. 1998. Sliding columnar phase of DNA lipid complexes. *Phys. rev. lett.*, **80**, 4345–4348.

O'Hern, C. S., Lubensky, T. C., & J.Toner. 1999. Sliding phases in XY models, crystals and cationic lipid-DNA complexes. *Phys. rev. lett.*, **83**, 2745–2748.

Ohnishi, T., Imai, N., & Oosawa, F. 1960. Interaction between rod-like polyelectrolytes. *J. phys. soc. jap*, **16**, 896–905.

Olson, W. K., Babcock, M. S., Gorin, A., Liu, G., Marky, N. L., Martino, J. A., Pedersen, S. C., Srinivasan, A. R., Tobias, I., Westcott, T. P., & Zhang, P. 1995. flexing and folding double helical DNA. *Biophys. chem.*, **55**, 7–29.

Oosawa, F. 1968. Interaction between parallel rodlike macroions. *Biopolymers*, **6**, 1633–1647.

Oosawa, F. 1970. *Polyelectrolytes*. Second edn. Marcel Mecker, New-York.

Palkar, S. A., & Lenhoff, A. M. 1994. Energetic and entropic contributions to the interaction of unequal spherical double layers. *J. colloid interface sci.*, **165**, 177–194.

Park, S. Y., Bruinsma, R. F., & Gelbart, W. M. 1999. Sponteneous overcharging of macro-ion complexes. *Europhys. lett.*, **46**, 454–460.

Park, S. Y-S. 1999. *Theory of DNA condensation and complexation*. Ph.D. thesis, University of California, Los Angeles.

Parsegian, V. A., & Gingell, D. 1972. On the electrostatic interaction across a salt solution between two bodies bearing unequal charges. *Biophys. j.*, **12**, 1192–1204.

Podgornik, R., Rau, D., & Parsegian, V. A. 1989. The action of interhelical forces on the organization of DNA double helices: Fluctuation-enhanced decay of electrostatic double layer and hydration forces. *Macromolecules*, **22**, 1780–1786.

Podgornik, R., Rau, D., & Parsegian, V. A. 1994. Parameterization of direct and soft steric-undulatory forces between DNA double helical polyelectrolytes in solution of several different anions and cations. *Biophys. j.*, **66**, 962–971.

Podgornik, R., Strey, H. H., & Parsegian, V. A. 1998. Colloidal DNA. *Curr. opin. coll. intr. sci.*, **3**, 534–539.

Rädler, J. O., Koltover, I., Salditt, T., & Safinya, C. R. 1997. Structure of DNA-cationic liposome complexes: DNA intercalation in multilamellar membranes in distinct interhelical packing regimes. *Science*, **275**, 810–814.

Rädler, J. O., Koltover, I., Jamieson, A., Salditt, T., & Safinya, C. R. 1998. Structure and interfacial aspects of self-assembled cationic lipid-DNA gene carrier complexes. *Langmuir*, **14**, 4272–4283.

Rau, D. C., & Parsegian, V. A. 1992. Direct measurment of the intermolecular forces between counterion-condensed DNA double helices. *Biophys. j.*, **61**, 246–259.

Ray, J., & Manning, G. S. 1994. An attractive force between 2 rodlike polyions mediated by the sharing of condensed counterions. *Langmuir*, **10**, 2450–2461.

Record, Jr. M. T., Anderson, C. F., & Lohman, T. M. 1978. Thermodynamic analysis of ion effects on the binding and conformational equilibria of proteins and nucleic acids: the roles of ion association or release, screening, and ion effects on water activity. *Q. rev. biophys.*, **11**, 103–178.

Reichel, L. E. 1998. *A modern course in statistical physics*. Second edn. New-York: John-Wiley and sons.

Reiner, E. S., & Radke, C. J. 1990. Variational approach to the electrostatic free energy in charged colloidal suspentions: general theory for open systems. *J. chem. soc. faraday trans.*, **86**, 3901–3912.

Roth, C. M., Sader, J. E., & Lenhoff, A. M. 1998. Electrostatic contribution to the energy and entropy of protein adsorption. *J. colloid interface sci.*, **203**, 218–121.

Rouzina, I., & Bloomfield, V. A. 1996. Macroion attraction due to correlation between screening counterions. 1. mobile surface-adsorbed ions and diffuse ion cloud. *J. chem. phys*, **100**, 9977–9989.

Rytömaa, M., & Kinnunen, K. J. 1996. Dissociation of cytochrome c from liposomes by histone H1. comparison with basic peptides. *Biochemistry*, **35**, 4529–4539.

Sader, J. E., & Chan, D. Y. C. 1999a. Electrical double-layer interaction between charged particles near surfaces and in confined geometries. *J. colloid interface sci.*, **218**, 423–432.

Sader, J. E., & Chan, D. Y. C. 1999b. Long-range electrostatic attractions between identically charged particles in confined geometries: An unresolved problem. *J. colloid interface sci.*, **213**, 268–269.

Safinya, C. R., Sirota, E. B., Roux, D., & Smith, G. S. 1989. Universality in interacting membranes: The effect of cosurfactants on the interfacial rigidity. *Phys. rev. lett.*, **62**, 1134–1137.

Salditt, T., Koltover, I., Rädler, J. O., & Safinya, C. R. 1997. Two dimensional smectic ordering of linear DNA chains in self-assembled DNA-cationic liposome mixtures. *Phys. rev. lett.*, **79**, 2582–2585.

Seddon, J. M. 1990. Structure of the inverted hexagonal (H_{II}) phase, and non-lamellar phase transitions of lipids. *Biophys. biochim. acta*, **1031**, 1–69.

Seddon, J. M., & Templer, R. H. 1995. Polymorphism of lipid-water systems. *Section 3, pages 98–160 of:* Lipowsky, R., & Sackmann, E. (eds), *Structure and dynamics of membranes*, second edn., vol. 1. Amsterdam: Elsevier.

Sens, P., & Joanny, J. F. 2000. Counterion release and electrostatic adsorption. *Phys. rev. lett.*, **84**, 4862–4865.

Sharp, K. A., Friedman, R. A., Misra, V., Hecht, J., & Honig, B. 1995. Salt effects on polyelectrolyte-ligand binding - comparison of Poisson-Boltzmann, and limiting law counterion binding models. *Biopolymers*, **36**, 245–262.

Shklovskii, B. I. 1999. Wigner crystal model of counterion induced bundle formation of rodlike polyelectrolytes. *Phys. rev. lett*, **82**, 3268–3271.

Skolnick, J., & Fixman, M. 1977. electrostatic persistence length of a wormlike polyelectrolyte. *Macromolecules*, **10**, 944–948.

Sornette, D., & Ostrowsky, N. 1994. Lamellar phases: Effect of fluctuations (theory). *Section 5, pages 251–302 of:* Gelbart, W. M., Ben-Shaul, A., & Roux, D. (eds), *Micelles, membranes, microemulsions and monolayers*. New York: Springer-Verlag.

Sperotto, M. M., & Mouritsen, O. G. 1993. Lipid enrichment and selectivity of integral membrane proteins in two-component lipid bilayers. *Eur. biophys. j.*, **22**, 323–328.

Stankovich, J., & Carnie, S. L. 1996. Electrical double layer interaction between dissimilar spherical colloidal particles and between a sphere and a plate: nonlinear Poisson-Boltzmann theory. *Langmuir*, **12**, 1453–1461.

Sternberg, B. 1996. Morphology of cationic liposome/DNA complexes in relation to their chemical composition. *J. liposome res.*, **6**, 515–533.

Sternberg, B., Sorgi, F. L., & Huang, L. 1994. New structures in complex formation between DNA and cationic liposomes visualized by freeze-fracture electron microscopy. *Febs letters*, **356**, 361–366.

Stigter, D. 1975. The charged colloidal cylinder with a gouy double layer. *J. colloid interface sci.*, **53**, 296–305.

Stigter, D. 1995. Evaluation of the counterion condensation theory of polyelectrolytes. *Biophys. j.*, **69**, 380–388.

Strey, H. H., Parsegian, V. A., & Podgornik, R. 1997. Equation of state for DNA liquid crystals: fluctuation enhanced electrostatic double layer repulsion. *Phys. rev. lett.*, **78**, 895–898.

Ström, C., Jönsson, B., Söderman, O., & Hansson, P. 1999. Adsoption of a divalent cationic sufactant onto a silica surface. *Coll. and surf. a*, **159**, 109–120.

Stryer, L. 1988. *Biochemistry*. New-York: W. H. Freeman.

Szleifer, I., Kramer, D., Ben-Shaul, A., Roux, D., & Gelbart, W. M. 1988. Curvature elasticity of pure and mixed surfactant films. *Phys. rev. lett.*, **60**, 1966–1969.

Tanford, C. 1980. *The hydrophobic effect*. 2 edn. New-York: Wiley-Interscience.

Tarahovsky, Y. S., Khusainova, R. S., Gorelov, A. V., Nicolaeva, T. I., Deev, A. A., Dawson, A. K., & Ivanitsky, G. R. 1996. DNA initiates polymorphic structural transitions in lecithin. *Febs letters*, **390**, 133–136.

Templeton, N. S., Lasic, D. D., Frederik, P. M., Strey, H. H., Roberts, D. D., & Pavlakis, G. N. 1997. Improved DNA: Liposome complexes for increased systemic delivery and gene expression. *Nature biotechnology*, **15**, 647–652.

Turner, D. C., & Gruner, S. M. 1992. X-ray diffraction reconstitution of the inverted hexagonal (H_{II}) phase in lipid-water systems. *Biochemistry*, **31**, 1340–1355.

Verwey, E. J. W., & Overbeek, J. Th. G. 1948. *Theory of the stability of lyophobic colloids*. Elsevier, New York: Elsevier.

Vlachy, V. 1999. Ionic effects beyond Poisson-Boltzmann theory. *Annu. rev. phys. chem*, **50**, 145–165.

Wagner, K., Keyes, E., Kephart, T. W., & Edwards, G. 1997. Analytical Debye-Hückel model for electrostatic potentials around dissolved DNA. *Biophys. j.*, **73**, 21–30.

Wagner, K., Harries, D., May, S., Kahl, V., Rädler, J. O., & Ben-Shaul, A. 2000. Counterion release upon cationic lipid-DNA complexation. *Langmuir*, **16**, 303–306.

Warszyńsky, P., & Adamczyk, Z. 1997. Calculations of double-layer electrostatic interactions for sphere/plane geometry. *J. colloid interface sci.*, **187**, 283–295.

Watson, J. D., & Crick, F. H. C. 1953. Genetic implications of the structure of deoxyribonucleic acid. *Nature*, **171**, 737–738.

Weingärtner, H., Weingand, S., & Schröer, W. 1992. Near-critical scattering of an ionic fluid with liquid-liduid phase transition. *J. chem. phys*, **96**, 848–851.

Wennerström, H., Jönsson, B., & Linse, P. 1982. The cell model for polyelectrolyte systems. exact statistical mechanical relations, monte carlo simulations, and the Poisson-Boltzmann approximation. *J. chem. phys*, **76**, 4665–4670.

Yang, L., & Glaser, M. 1995. Membrane domains containing phosphatidylserine and substrate can be important for the activation of protein kinase C. *Biochemistry*, **34**, 1500–1506.

Zuidam, N. J., & Barenholz, Y. 1997. Electrostatic parameters of cationic liposomes commonly used for gene delivery as determined by 4-heptadecyl-7-hydroxycoumarin. *Biophys. biochim. acta*, **1329**, 211–222.

Zuidam, N. J., Lerner, D. H., Margulies, S., & Barenholz, Y. 1999. Lamellarity of cationic liposomes and mode of preparation of lipoplexes affect transfection efficiency. *Biophys. biochim. acta*, **1419**, 207–220.